

The role of histone 2B monoubiquitination (H2Bub1) in HER2-driven mammary carcinoma

Dissertation

for the award of the degree

"Doctor rerum naturalium"

of the Georg-August-Universität Göttingen

within the doctoral program

"Molecular Medicine"

of the Georg-August University School of Science (GAUSS)

submitted by

Evangelos Prokakis

from Athens, Greece

Göttingen, 2020

Thesis Committee

Dr. rer. nat. Florian Wegwitz
Laboratory for Molecular Gynecology
Department of Gynecology and Obstetrics
University Medical Center Göttingen
Göttingen, Germany

Prof. Dr. Matthias Dobbstein
Institute of Molecular Oncology
University Medical Center Göttingen
Göttingen, Germany

Prof. Dr. Jürgen Wienands
Institute for Cellular and Molecular Immunology
University Medical Center Göttingen
Göttingen, Germany

Members of the Examination Board

1st Referee: Dr. rer. nat. Florian Wegwitz, Laboratory for Molecular Gynecology,
Department of Gynecology and Obstetrics, University Medical Center Göttingen,
Göttingen, Germany

2nd Referee: Prof. Dr. Matthias Dobbstein, Institute of Molecular Oncology, University
Medical Center Göttingen, Göttingen, Germany

Further members of the Examination Board

Prof. Dr. Argyris Papanonis, Institute of Pathology, University Medical Center Göttingen,
Göttingen, Germany

Dr. Nico Posnien, Department of Developmental Biology, Georg-August-University
Göttingen, Göttingen, Germany

Dr. Ufuk Günesdogan, Department of Developmental Biology, Georg-August-University
Göttingen, Göttingen, Germany

Date of examination: 15 January, 2020

In memory of Nikos...
(1958-2012)

Contents

Abbreviations	I
List of Figures	VII
1. Summary	1
2. Introduction	3
2.1. Breast cancer	3
2.1.1. Breast cancer: the leading cancer entity in the global epidemiologic map	3
2.1.2. The importance of molecular classification in BC therapeutic management	3
2.1.3. The molecular oncology of HER2 ⁺ -BC	6
2.1.4. Current HER2-directed therapy of HER2 ⁺ -BC	7
2.1.5. Resistance mechanisms to HER2-targeted therapy necessitate the advent of novel therapeutic targets.....	9
2.2. The scope of cancer hallmarks	10
2.3. Dysregulation of actin cytoskeleton dynamics, a crucial cancer hallmark for cell survival, invasion and metastasis	14
2.3.1. Actin, the basic monomer of polymerized actin	14
2.3.2. Signaling pathways controlling actin filament dynamics	16
2.3.3. The role of actin cytoskeleton dynamics in HER2 ⁺ -BC, in other malignancies and its clinical value as a therapeutic target.....	18
2.4. Oncogene-induced proteotoxicity and augmented protein quality control as a critical cancer hallmark	19
2.4.1. The signaling pathway of UPR	20
2.4.2. UPR, a story of "life and death" in cancer progression	23
2.5. Epigenetic plasticity at the crossroad of different cancer hallmarks	25
2.5.1. Epigenetics: the long story short	26
2.5.2. Nucleosome, a chromatin packaging unit and signaling "hub", that masters gene transcription in eukaryotes	27
2.5.3. Epigenetic "writers, erasers and readers" shape the epigenetic landscape of eukaryotic gene regulation.....	28
2.5.4. Stages of transcription: initiation, elongation and termination	29
2.5.5. Epigenetic alterations in cancer: from bench to bedside.....	33
2.6. RNF20-RNF40 and USP22, the "writer" and "eraser" of H2B monoubiquitination	34
2.6.1. CDK9-WAC-RNF20/RNF40-mediated H2Bub1 drives transcriptional elongation	36
2.6.2. H2Bub1 <i>trans</i> -histone crosstalk with H3 methylation.....	39
2.6.3. H2Bub1 in transcriptional repression.....	40
2.6.4. RNF20/RNF40-mediated H2Bub1 is indispensable for genomic integrity	41
2.6.5. The RNF20/RNF40 E3 ligase complex possesses pleiotropic H2Bub1-dependent and -independent physiological functions.....	42

2.6.6. RNF20, RNF40, and H2Bub1 possess a context-specific role in tumor progression.....	43
2.7. USP22: a deubiquitinase with multiple protein targets and functions	45
2.7.1. Cellular function of DUBs	45
2.7.2. USP22 is the deubiquitinase of the SAGA complex	46
2.7.3. USP22 controls the differentiation and function of multiple cell lineages	47
2.7.4. USP22 possesses a tumor supportive role in the vast majority of cancer entities	49
3. Objectives of the study.....	52
4. Results: Manuscripts.....	53
4.1. Uncovering the biological consequence of global H2Bub1 loss in RNF40-deficient HER2⁺-BC	53
Manuscript I: The histone H2B ubiquitin ligase RNF40 is required for HER2-driven mammary tumorigenesis	54
Abstract.....	55
Introduction.....	55
Materials and methods	56
Results	59
RNF40 is highly expressed in HER2 ⁺ -BC	59
RNF40 plays a tumor-supportive function in Erbb2-driven mammary carcinoma in vivo.....	60
RNF40 loss impairs oncogenic properties of HER2 ⁺ -BC cells in vitro	61
RNF40 regulates actin-cytoskeleton-related genes in HER2 ⁺ -BC.....	63
RNF40 regulates the VAV3-ROCK-LIMK2-PFN2 axis through H2Bub1-H3K4me3 trans-histone crosstalk.....	68
Discussion	73
Acknowledgements	75
References of Manuscript I	76
Supplements	79
Supplementary References of Manuscript I.....	99
Author contribution	100
4.2. Exploring the impact of global H2Bub1 increase in USP22-deficient HER2⁺-BC	101
Manuscript II: USP22 promotes HER2-driven mammary carcinoma aggressiveness by suppressing the unfolded protein response.....	102
Abstract.....	104
Introduction.....	104
Results	105
USP22 supports HER2-driven mammary carcinogenesis <i>in vivo</i>	105
USP22 loss impairs the oncogenic properties of HER2 ⁺ -BC cells <i>in vitro</i>	108
USP22 suppresses apoptosis in HER2 ⁺ -BC cells	109

USP22 loss increases the sensitivity of HER2 ⁺ -BC to the unfolded protein response	111
USP22 suppresses UPR-induced apoptosis in HER2 ⁺ -BC by stabilizing HSPA5.....	115
Discussion	118
Materials and Methods	121
Acknowledgments	124
References of Manuscript II	124
Supplements	129
Supplementary References of Manuscript II.....	147
Author contribution	148
5. General discussion.....	149
5.1. The first <i>in vivo</i> study, unraveling the impact of H2Bub1 loss on an oncogene-induced malignancy, using a conditional <i>RNF40</i> knockout approach	149
5.2. Why MMTV- <i>ErbB2</i> mice show a heterogeneous population of RNF40 ⁺ and RNF40 ⁻ tumor cells in an <i>Rnf40</i> ^{fl/fl} -deficient state?	150
5.3. Understanding the context-dependent role of H2Bub1 in cancer disease	151
5.4. If H2Bub1 is a ubiquitous hPTM of active genes, why a fraction of genes is affected upon RNF40 loss?.....	153
5.5. How RNF40/H2Bub1 loss and actin dynamics imbalance elicits programmed cell death in HER2 ⁺ -BC?.....	155
5.6. The first conditional USP22 knockout BC model, pointing to a global H2Bub1-independent tumor-supportive mechanism	156
5.7. Our study presents a so far undescribed role of USP22 in suppressing UPR, via stabilizing HSPA5 in HER2 ⁺ -BC.....	157
5.8. USP22 plays multiple functions in protein homeostasis to prevent oncogene-induced PT	158
6. Conclusion	160
7. References	162
8. Referenced books.....	185
Acknowledgements	186
Curriculum vitae	189

Abbreviations

7SK	RNA Component Of 7SK Nuclear Ribonucleoprotein	ISR	Intergrated Stress Response
7SKsnRNP	7SK small nuclear ribonucleoprotein	JAK	Janus Kinase 2
AARS1	Alanyl-TRNA Synthetase 1	JAMM	Zn-dependent metalloprotease
AC	Actin Cytoskeleton	JNK	C-Jun N-Terminal kinase
ac	Acetylation	kDa	kilodalton
ADCC	Antibody-Dependent Cellular Cytotoxicity	KLF4	Krüppel-like factor 4
ADP	Adenosine Diphosphate	KMT2A	Lysine Methyltransferase 2A
AEF	ATP exchange Factor	KMT2B	Lysine Methyltransferase 2B
AKT	serine/threonine- specific protein kinase	KPNA2	Karyopherin Subunit Alpha 2
AR	Androgen Receptor	KSR	Kinase Suppressor Of Ras
Arg	Arginine	LIMK2	LIM Domain Kinase 2
ARP2/3	Actin Related Protein 2/3 complex	lncRNA	long non-coding RNA
ATF3	Activating Transcription Factor 3	LPA	Lysophosphatidic acid
ATF4	Activating Transcription Factor 4	Lum	Luminal
ATF6	Activating Transcription Factor 6	Lys	Lysine
ATP	Adenosine Triphosphate	MAPK	Mitogen-Activated Protein Kinase
ATXN7L3	Ataxin 7 Like 3	mDIA	mammalian homologue of Drosophila diaphanous
BAP	BiP-associated Protein	me	methylation
BC	Breast cancer	MED	Mediator
BIM	Bcl-2-like protein 11	MEF	Mouse Embryonic Fibroblasts

BiP	Binding immunoglobulin protein	MEPCE	Methylphosphate Capping Enzyme, LARP7: La Ribonucleoprotein 7
BMF	Bcl2 Modifying Factor	Met	Methionine
BMI1	BMI1 Proto-Oncogene, Polycomb Ring Finger	MET	MET proto-oncogene
BRD4	Bromodomain Containing 4	MINDY	Motif Interacting with ubiquitin containing novel DUBs
BRE1	E3 ubiquitin-protein ligase	miRNA	microRNA
bZIP	Basic Leucine Zipper Domain	MLL1/2	Lysine Methyltransferase 2A/2B
cFLIP	Cellular FLICE-Like Inhibitory Protein	MMTV	Mouse Mammary Tumor Virus
Ca2+	Calcium	mRNA	Messenger Ribonucleic Acid
CCNB1	Cyclin B1	mTORC2	Mechanistic Target Of Rapamycin Kinase Complex 2
CCND1	Cyclin D1	MYB	MYB Proto-Oncogene
CD274	Cluster of Differentiation 274	MYC	MYC Proto-Oncogene
CDC42	Cell Division Control protein 42 homolog	Myc B	Mycalolide B
CDK4/6	Cyclin Dependent Kinase 4/6	MYPT1	Myosin Phosphatase Target subunit 1
CDK7	Cyclin Dependent Kinase 7	NBD	Nucleotide-Binding Domain
CDK8	Cyclin Dependent Kinase 8	NELF	Negative Elongation Factor
CDK9	Cyclin Dependent Kinase 9	NFATC2	Nuclear Factor Of Activated T Cells 2
ChIP	Chromatin Immunoprecipitation	NGS	Next generation sequencing
CHOP	C/EBP homologous protein	OCT4	Octamer-Binding Protein 4
CNVs	Copy Number Variations	P	phosphorylation

COMPASS	Complex Proteins Associated with Set1	PAK4	p21-Activated Kinase 4
COX2	Cyclooxygenase2	PALB2	Partner And Localizer Of BRCA2
CpG	Cytosine Guanine island	PDK1	Pyruvate Dehydrogenase Kinase 1
CRE	Cre recombinase	PDL1	Programmed Death Ligand 1
CTD	C-terminal domain (of RNApol II)	PERK	PKR-Like Endoplasmic Reticulum Kinase
CTLs	Cytotoxic Lymphocytes	PFN2	Profilin 2
DDR	DNA Damage Repair	PI3K	Phosphoinositide-3-Kinase
DDX46	DEAD box Helicase 46	PIP2	Phosphatidylinositol-4, 5-bisphosphate
DNA	deoxyribonucleic acid	PIP3	Phosphatidylinositol-3, 4, 5-triphosphate
DNAJ	chaperone DnaJ	PKR	Protein kinase RNA
DNMT	DNA Methyltransferases	PP1A/B	Protein Phosphatase 1 Catalytic Subunit A/B
DOT1L	Disruptor Of Telomeric silencing 1-Like	PR	Progesterone receptor
DR5	Death Receptor 5	PT	Proteotoxicity
DSBs	Double-Strand Breaks in DNA	P-TEFb	Positive Transcription Elongation Factor b
DSIF	DRB Sensitivity Inducing Factor	PUMA	P53 Up-Regulated Modulator Of Apoptosis
DUB	Deubiquitinase	PyMT	Polyomavirus middle T-antigen
EEF1D	Eukaryotic Translation Elongation Factor 1 Delta	RASSF1A	Ras Association Domain Family Member 1
EGFR	Epidermal Growth Factor Receptor	RB1	Retinoblastoma 1
eIF2a	Eukaryotic Initiation Factor 2	RHEB	Ras Homolog Enriched In Brain
EMT	Epithelial–Mesenchymal Transition	RHO	Rhodopsin

ENY2	ENY2 Transcription And Export Complex 2 Subunit	RNA	Ribonucleic Acid
ER	Endoplasmic Reticulum	RNApol II	Ribonucleic Acid Polymerase II
ERAD	Endoplasmic Reticulum-Associated protein Degradation	RNF20	Ring Finger Protein 20
ERBB2	Erb-B2 Receptor Tyrosine Kinase 2	RNF40	Ring Finger Protein 40
ERK	Extracellular-signal-Regulated Kinase	ROCK1	Rho Associated Coiled-Coil Containing Protein Kinase 1
ERO1A	Endoplasmic Reticulum Oxidoreductase 1 Alpha	ROCKi	ROCK Inhibitor/Inhibition
ESR	Estrogen Receptor	S1/2P	Site 1/2 Protease
FA	Focal Adhesion	S1PR3	Sphingosine 1-Phosphate Receptor 3
FACT	Facilitates Chromatin Transcription	SAGA	Spt-Ada-Gcn5 Acetyltransferase
F-actin	Filamentous-actin	SBD	Substrate-Binding Domain
FAK(i)	Focal Adhesion Kinase (inhibitor)	SEL1L	Suppressor Of Lin-12-Like Protein 1
FBP1	Fructose-Bisphosphatase 1	Ser	Serine
FOXP3	Forkhead Box P3	SETD1A	SET Domain Containing 1A
G-actin	Globular-actin	SETD1B	SET Domain Containing 1B
GADD34	Growth Arrest And DNA Damage-Inducible Protein 34	SH2	Sarcoma homology 2 domain
GAP	GTPase-activating proteins	SIL1	SIL1 Nucleotide Exchange Factor
GARS1	Glycyl-TRNA Synthetase 1	SIRT1	Sirtuin 1
GCN2	General Control Nonderepressible 2	SNPs	Single Nucleotide Polymorphisms

GCN5	General Control Of Amino Acid Synthesis Protein 5	snRNA	small nuclear RNA
GDI	Guanine-nucleotide Disassociation Inhibitor	SOS	Son Of Sevenless
GDP	Guanosine Diphosphate	SOX2	SRY-Box Transcription Factor 2
GEF	Guanine nucleotide Exchange Factors	SPT	Serine Palmitoyltransferase
GEMM	Genetically Engineered Mouse Model	SSRP1	Structure Specific Recognition Protein 1
GRB2	Growth factor Receptor-Bound protein 2	STAT	Signal Transducer And Activator Of Transcription
GRP78	Glucose-Regulated Protein, 78kDa	STT3A	Subunit Of The Oligosaccharyltransferase Complex, Homolog A
GTP	Guanosine-5'-triphosphate	SUPT16H	Suppressor Of Ty 16 Homolog
H2A	Histone 2A	SWI/SNF	SWItch/ Sucrose Non-Fermentable
H2A.X	H2A Histone Family Member X	TAF	TATA-Box Binding Protein Associated Factor
H2A.Z	H2A Histone Family Member Z	TBP	TATA-Box Binding Protein
H2B	Histone 2B	TF	Transcription Factor
H2Bub1	Histone 2B monoubiquitination	TFII	Transcription Factor of RNApol II
H3	Histone 3	Thr	Threonine
H3K27ac	acetylation of lysine 27 on histone H3	TNBC	Triple-Negative Breast Cancer
H3K36me3	trimethylation of lysine 36 on histone H3	TP53	Tumor Protein 53
H3K4me3	trimethylation of lysine 4 on histone H3	TRAF2	Tumor Necrosis Factor Receptor-Associated Factor 2

H3K79me3	trimethylation of lysine 79 on histone H3	Treg	T-regulatory lymphocytes
H3K9ac	acetylation of lysine 9 on histone H3	TREX2	Three Prime Repair Exonuclease 2
H4	Histone 4	TRF1	Telomeric Repeat Binding Factor 1
HAT	Histone Acetyltransferases	tRNA	transfer RNA
HDAC	Histone Deacetylase	TSC1/2	Tuberous Sclerosis 1/2 Protein
HER2	Human Epidermal Growth Factor Receptor 2	Ub	Ubiquitination
HER3	Human Epidermal Growth Factor Receptor 3	UBE2A/B	Ubiquitin Conjugating Enzyme E2 A/B
HGFR	Hepatocyte Growth Factor Receptor	UCH	Ubiquitin C-Terminal Hydrolase
hPTM	Histone Post-Translational Modification	UPR	Unfolded Protein Response
HR	Hormone Receptor	USP22	Ubiquitin Specific Peptidase 22
HSP40	Heat Shock Protein 40	USP27x	Ubiquitin Specific Peptidase 27 X-Linked
HSP90AB1	Heat Shock Protein 90kDA Alpha, class B, Member 1	USP44	Ubiquitin Specific Peptidase 44
HSPA5	Heat Shock Protein Family A (Hsp70) Member 5	USP51	Ubiquitin Specific Peptidase 51
HSR	Heat Shock Response	VAV3	Vav Guanine Nucleotide Exchange Factor 3
IGF1R	Insulin-like growth factor 1 receptor	WAC	WW Domain Containing Adaptor With Coiled-Coil
IHC	Immunohistochemistry	WASP	Wiskott-Aldrich Syndrome Protein
IL6	Interleukin 6	WAVE	WASP-family verprolin-homologous protein

iNKT	invariant Natural killer T cell	XBP1	X-Box Binding Protein 1
INO80	INO80 Complex ATPase Subunit	XPC	Xeroderma Pigmentosum, Complementation Group C
IRE1	Inositol-Requiring Enzyme 1	γH2AX	Phosphorylated histone 2A member X
IRF3	Interferon Regulatory Factor 3		

List of Figures

1. Introduction

- **Figure 1:** Breast cancer pathogenesis and molecular subtypes.
- **Figure 2:** The HER2-driven signaling cascade leads to a plethora of tumorigenic features including cell survival, proliferation, and migration.
- **Figure 3:** The regulation of actin filament (F-actin) dynamics by the actin-binding proteins (ABPs) profilin and cofilin.
- **Figure 4:** The regulation of RHO-GTPases.
- **Figure 5:** Signaling pathways controlling actin filament dynamics.
- **Figure 6:** Schematic diagram of the UPR cascade in multicellular eukaryotes.
- **Figure 7:** Regulatory mechanism of HSPA5 during ER stress.
- **Figure 8:** Epigenetics: the long story short.
- **Figure 9:** The histone modification code.
- **Figure 10:** The epigenetic factors
- **Figure 11:** The multi-step process of RNAPol II-mediated transcription.
- **Figure 12:** The generic biochemical pathway of protein (de)ubiquitination and H2B (de)monoubiquitination.
- **Figure 13:** The biochemical pathway of H2Bub1.
- **Figure 14:** The intricate regulation of CDK9 by CDK7, PP1A/B and 7SK/HEXIM/LARP7/MEPCE complex.
- **Figure 15:** Schematic representation of the increasingly complex ubiquitin code.

2. Manuscript I: "The histone H2B ubiquitin ligase RNF40 is required for HER2-driven mammary tumorigenesis"

- **Fig.I.1:** RNF40 and H2Bub1 are maintained in HER2+-BC.

- **Fig.I.2:** RNF40 loss impairs oncogenic properties of HER2-BC cells in vitro.
- **Fig.I.3:** RNF40 loss increases apoptosis and impairs the expression of key components of the actin regulatory pathway in HER2+-BC.
- **Fig.I.4:** RNF40 controls the actin regulatory pathway to sustain the viability of HER2+-BC cells in vitro and in vivo.
- **Fig.II.5:** RNF40 regulates gene expression of important members of the RHO-ROCK axis in an H2Bub1/H3K4me3-dependent manner.
- **Fig.II.6:** RNF40 has a tumor-supportive function in HER2-driven mammary carcinoma by controlling the RHO/ROCK-dependent actin regulatory axis.
- **Fig.I.S1:** RNF40 and H2Bub1 loss are rare events and do not advantage tumor growth in HER2-positive malignancies of the breast.
- **Fig.I.S2:** RNF40 loss impairs oncogenic properties of HER2-positive BC cells in vitro.
- **Fig.I.S3:** RNF40 loss increases apoptosis and impairs the expression of important key-effectors of the actin regulatory pathway in HER2-positive BC cells.
- **Fig.I.S4:** RNF40 controls the actin regulatory pathway to sustain the viability of HER2-positive BC cells in vitro and in vivo.
- **Fig.I.S5:** RNF40 regulates gene expression of important members of the RHO-ROCK axis in a H2Bub1-H3K4me3 dependent manner.
- **Fig.I.S6:** RNF40 regulates gene expression of important members of the RHO-ROCK axis in a H2Bub1-H3K4me3 dependent manner.

3. Manuscript II: "USP22 promotes HER2-driven mammary carcinoma aggressiveness by suppressing the unfolded protein response"

- **Fig.II.1:** USP22 loss decreases the incidence and aggressiveness of HER2⁺-BC in the MMTV-*ErbB2* genetic mouse model.
- **Fig.II.2:** USP22 loss impairs oncogenic properties of HER2⁺-BC cells in vitro.
- **Fig.II.3:** Impaired USP22 expression sensitizes HER2⁺-BC cells to apoptosis.
- **Fig.II.4:** USP22 loss increases the sensitivity of HER2⁺-BC to the unfolded protein response.
- **Fig.II.5:** USP22 maintains HSPA5 stability and suppresses UPR-induced apoptosis in HER2⁺-BC.
- **Fig.II.6:** USP22 promotes HER2-driven mammary carcinoma aggressiveness by stabilizing HSPA5 and

- **Fig.II.S1:** Consequence of USP22-loss on HER2-signaling and gene expression of HER2⁺-BC cells.
- **Fig.II.S2:** USP22 loss increases the sensitivity of HER2⁺-BC to the unfolded protein response.
- **Fig.II.S3:** USP22 loss increases the sensitivity of HER2⁺-BC to the unfolded protein response.
- **Fig.II.S4:** USP22 stabilizes HSPA5 and suppresses UPR-induced apoptosis in HER2⁺-BC.

4. Discussion

- **Figure 16:** RNF40 and USP22 are indispensable for the tumorigenic behavior of HER2⁺-BC.


1. Summary

Breast cancer (BC) is the most frequent tumor entity in women worldwide with a high chance of therapeutic response in early- and non-metastatic disease stage. Despite the advent of HER2-specific targeted therapies, a considerable fraction of HER2 (Human Epidermal Growth Factor Receptor 2) positive breast cancer (HER2⁺-BC) patients become refractory or acquire resistance to these therapies. These patients show a poor prognosis, hence, necessitating a better characterization of the molecular pathology of this malignancy.

Accumulating studies indicate that cancer disease does not exclusively result from genetic alterations but can be fostered by aberrant epigenetic changes in the physiological gene expression program of a healthy tissue. Cancer cells benefit from the speed and reversible nature of these epigenetic alterations, empowering a rapid adaption to the gene expression program in response to adverse intra- or extracellular conditions. At the same time, this reversibility broadens the avenue to therapeutically interfere with acknowledged epigenetic dependencies in various malignancies.

Monoubiquitination of lysine 120 of histone 2B (H2Bub1) is a transcription-promoting histone post-translational modification (hPTM). Gradual loss of H2Bub1 has been numerous times linked to cancer progression in many malignancies including BC. Consequently, H2Bub1 was suspected to harbor universal tumor-suppressive properties. However, its biological function in BC has only been scarcely addressed *in vivo* with the help of xenograft approaches. To uncover the consequences of H2Bub1 imbalance in BC, we performed a combined approach whereby we compromised or augmented the global H2Bub1 levels by impairing the expression of RNF40 or USP22, the major E3 ligase and deubiquitinase (DUB) of this hPTM, respectively. Specifically, we leveraged the HER2⁺-BC mouse model MMTV-*ErbB2* as well as human HER2⁺-BC cell lines to shed light on the functional role of the H2Bub1 epigenetic machinery in cancer progression and to underpin its underlying mechanisms.

Against our initial expectations, we revealed that tumor-specific deletion of *Rnf40* led to a substantially decreased tumor burden in MMTV-*ErbB2* mice compared to their control counterparts. Accordingly, we identified that RNF40 silencing impairs the oncogenic properties in human HER2⁺-BC cell lines. Mechanistically, we discovered an unknown role of the RNF40-mediated H2Bub1/H3K4me3 *trans*-histone crosstalk in driving the actin cytoskeleton (AC) dynamics and the activity of the downstream focal adhesion kinase (FAK)-driven pathway. Therefore, our data strongly suggest that the RNF40/H2Bub1/H3K4me3 epigenetic axis plays a rather tumor-supportive than -suppressive role in HER2⁺-BC by controlling the AC/FAK axis to sustain the aggressive behavior of this malignancy.



In parallel, the H2Bub1-specific DUB USP22 was multiple times reported to harbor oncogenic properties, among other, in BC *in vitro*. Specifically, using the same experimental settings, we surprisingly uncovered a global H2Bub1-independent involvement of USP22 in the tumorigenic phenotype of HER2⁺-BC. Specifically, we confirmed that USP22 actively suppresses the unfolded protein response (UPR) by deubiquitinating and, thereby stabilizing, the ER-chaperone HSPA5 *in vivo* and *in vitro*. Accordingly, loss of USP22 activated the apoptotic cascade and significantly increased the efficiency of therapies targeting the ER folding capacity. Consequently, our data suggest that USP22 is not only a promising therapeutic target to combat HER2⁺-BC, but can substantially improve UPR-based therapeutic schemes that dysregulate proteostasis pathways for cell survival. Collectively, our data introduce novel functions of the RNF40/H2Bub1/H3K4me3 axis in this aggressive BC subtype by significantly updating the current knowledge we possess for the context-dependent role of this axis. Finally, this work sheds light on a new pro-tumorigenic function of USP22 in the suppression of UPR signaling and in the maintenance of the global chaperoning system that protects tumor cells from proteostasis imbalance.

2. Introduction

2.1. Breast cancer

Breast cancer (BC) is the most frequent malignancy in the female population and a quite heterogeneous disease comprising different molecular subtypes with differential treatment approach and prognosis. Before entering to the general background of our work, we will introduce you to some basic epidemiologic facts of BC, how molecular classification in early 2000s revolutionized the therapeutic management of the disease and with a special focus on a particularly aggressive BC subtype, the HER2-driven BC (HER2⁺-BC). Lastly, we will summarize the advantages and disadvantages of HER2⁺-BC-specific targeted therapies.


2.1.1. Breast cancer: the leading cancer entity in the global epidemiologic map

Cancer disease is a long-standing malady and whose first descriptions date back to ancient Egypt and Greece. Imhotep (1700 BC), a physician of Kingdom of Egypt, first described that BC was commonly found as a palpable, solid, sub-epidermal mass which was described as hard as an "unripe fruit" that was subsequently dissected by cauterization. In agreement, Hippocrates and Herodotus (470-460 BC) defined "carcinoma" (greek: καρκίνος) as sub-epidermal, epidermal, maxillary, cervical or mammary lump (Mukherjee, S. 2010, 6th edition; *The emperor of all maladies: A biography of cancer*; New York, Scribner). However, 3700 years after the first documented case of BC, this disease is still considered a global healthcare issue, showing the highest incidence and mortality rates, worldwide (Bray et al. 2018).

Approximately 2 million women were diagnosed with BC in 2018, 30% of whom ultimately succumbed to the disease (Bray et al. 2018). Since 1980, the global incidence of BC shows an escalating trend due to the increasing population and the prolonged life expectancy (Beard et al. 2016). BC mortality rate markedly varies, being highest in western countries and lowest in Asia. The vast majority of epidemiologic studies point to the fact that BC comprises 18% of all female cancers (Harbeck et al. 2019). BC is mainly multifactorial and depends on several risk factors such as genetic predisposition, lifestyle, and environmental factors. It is expected that the incidence of BC will increase to 85 per 100.000 women worldwide by 2021 (Han et al. 2013). Consequently, since BC is a global health problem, considerable advances in access to (early) diagnosis and novel drugs are necessitated.

2.1.2. The importance of molecular classification in BC therapeutic management

Cancer disease is based on an evolutionary process which in many aspects mimics species evolution. The most competitive and thriving species will survive by mutation and positive



selection on individuals. Consistently, tumor clones that evolve from tissue cells will present the same evolutionary behavior based on favorable mutations and positive selection cycles (Casás-Selves and Degregori 2011).

Like all neoplastic diseases, BC occurrence is proposed to happen based on two prevailing models, the "sporadic clonal evolution" and the "stem cell" model (Bombonati and Sgroi 2011). The first BC model suggests that any breast epithelial cell can be subjected to oncogenic mutations and only these cells, harboring advantageous genetic and epigenetic alterations, are positively selected for tumor progression. On the other hand, the stem cell BC model suggests that stem cells and progenitor cells are capable of initiating tumors via deregulation of their normal stem cell self-renewal properties, giving rise to breast tumorigenesis. Although both models try to explain how BC initiation occurs, they propose that the tumor heterogeneity arises from different initiating cells, either normal stem/progenitor cells or normal differentiated epithelial cells undergoing oncogene-induced dedifferentiating programs (Polyak 2007).

At the beginning of the previous century, all women diagnosed with BC received a uniform treatment with excessive and undesired surgical intervention (Baum 2002). However, we know today that BC is not a single disease, on the contrary, it exhibits different BC subtypes with distinct clinical outcomes, histopathologic features, molecular traits and differential treatment approach (Harbeck et al. 2019). With the advent of research studies showing the feasibility to identify molecularly distinct BC groups, clinicians and pathologists considered the exploitation of these molecular differences to optimize patient prognosis and treatment options. In addition, the identification of specific molecular BC subtypes with specific histological characteristics and different survival outcome enabled the shift from traditional clinical management to novel, molecular biology-based therapeutic strategies. A breakthrough study contributing to this direction came from Perou and Sorlie in 2000: this study described for the first time a molecular classification of BC based on differential gene expression profiles identified in four different BC subtypes: "luminal", "normal breast-like", "HER2-enriched" (HER2⁺), and "basal" (Perou et al. 2000).

The luminal subtype has been later on sub-classified into A and B subtypes, which show a good prognosis and exhibit a high expression of estrogen (ESR)- and progesterone (PR) receptor-driven gene expression profile. Luminal B BC patients also have a HER2-positive status (ESR⁺, PR⁺, HER2⁺), which generally explains the increased aggressiveness of these tumors and the slightly worse prognosis compared to luminal A BC patients (ESR⁺, PR⁺, HER2⁻). However, the overall good prognosis of Luminal A and B BC subtypes is mainly attributed to current endocrine therapies, tackling the activity of hormone receptors (selective estrogen receptor antagonists) or the estrogen- and progesterone-producing

biochemical pathways (aromatase inhibitors) (Rani et al. 2019) (Figure 1). On the other hand, Lum B BC patients frequently present resistance to endocrine therapies due to the adaptive switch from ESR/PR- to HER2-driven signaling pathway, therefore, a combination therapy against ESR/PR and HER2 activity has been proposed as a beneficial strategy (Rani et al. 2019).

On the contrary, the basal-like subtype typically lacks ESR, PR expression and HER2 gene amplification (ESR⁻, PR⁻, HER2⁻). 15-20% of BC patients suffer from this subtype which shows the worst prognosis and is the most difficult to treat among all breast cancer subtypes. The triple-negative state of basal-like BC renders this malignancy a hurdle in the path to therapeutic management, using current targeted therapies (anti-HER2 or -ESR/PR). Therefore, surgical intervention, radio- or conventional chemotherapy are the only standard therapeutic means to treat this aggressive BC subtype (Harbeck et al. 2019) (Figure 1).

Finally, HER2⁺-BC subtype is characterized by the *ERBB2* gene amplification and consequent overexpression, while it is devoid of any hormone receptor overexpression (ESR⁻, PR⁻, HER2⁺) (Callahan and Hurvitz 2011). With the advent of HER2 targeted therapies, the survival of HER2⁺-BC patients has been considerably improved (Dawood et al. 2010). Almost 15-30 % of the BC cases are HER2-positive. (Figure 1). However, as later discussed in chapter 2.1.5, refractory response to currently used anti-HER2 therapies is quite frequent, leading to tumor relapse and dissemination.

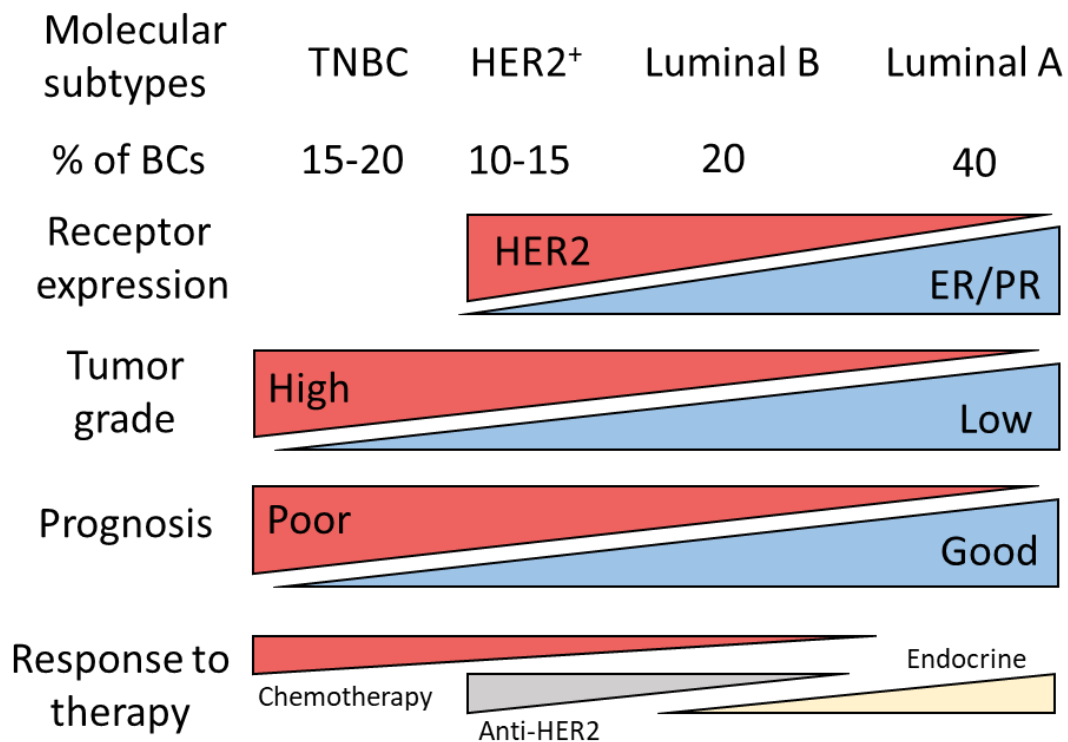


Figure 1: Breast cancer pathogenesis and molecular subtypes. Modified from Sims et al. 2007.

2.1.3. The molecular oncology of HER2⁺-BC

HER2 signaling consists multiple downstream signaling cascades with a great pathophysiological impact on BC. HER2 is a 185 kDa transmembrane receptor encoded by the *ERBB2* with a, so far, unknown ligand. The HER2 receptor is structurally and functionally similar to the family of Epidermal Growth Factor Receptors (EGFRs) (Gutierrez and Schiff 2011). HER2⁺-BC is characterized by *ERBB2* gene amplification and consequent overexpression that leads to an aberrant downstream signaling cascade. This receptor is able to homo- or heterodimerize with other EGFR family members, leading to its subsequent auto-phosphorylation in the cytoplasmic side, providing binding sites for adapter proteins to initiate downstream signaling events. HER2 receptor activates two major signaling axes, the mitogen-activated protein kinase (MAPK) and the phosphoinositide 3-kinase (PI3K)/AKT (Figure 2), both of which induce cell survival, proliferation, cell motility and anabolic processes (Serra et al. 2011).

Upon HER2 auto-phosphorylation, Growth Factor Receptor-bound protein 2 (GRB2) is recruited via its sarcoma homology 2 domain (SH2) to activate the guanine exchange factor Son of Sevenless (SOS). The latter promotes the exchange of a GDP for GTP by the small GTP-binding Rat sarcoma (RAS) protein that, in turn, becomes activated. Subsequently, RAS/GTP initiates a kinase cascade which starts with Rapid Accelerated Fibrosarcoma (RAF), mitogen-activated protein kinase (MEK), and Extracellular Signal Activated Kinase (ERK) (Lo et al. 2006). The whole phosphorylation cascade occurs via the Kinase Suppressor of Ras (KSR), which binds to all aforementioned kinases, thereby exerting a scaffolding role in a multi-kinase complex by which all MAP kinases become phosphorylated (Müller et al. 2000). Once ERK1/2 get phosphorylated, they translocate to the nucleus to phosphorylate several transcription factors promoting gene expression profiles that are necessary for cell cycle progression, DNA replication, and cell survival (Torii et al. 2006).

On the other side of the HER2-driven signaling cascade, p85, via its SH2 domain, recruits PI3K to the auto-phosphorylated HER2 or EGFR receptor. Upon binding to the receptor, p85 activates the catalytic p110 subunit of PI3K. Alternatively, active RAS/GTP is also able to activate PI3K. Subsequently, p110 phosphorylates phosphatidylinositol-4, 5-bisphosphate (PIP₂) into phosphatidylinositol-3, 4, 5-triphosphate (PIP₃). This membranous lipid becomes a docking site for pyruvate dehydrogenase lipoamide kinase 1 (PDK1) and protein kinase B (AKT) (Castellano and Downward 2011). In the next step, AKT is phosphorylated by PDK1 and mTOR complex 2 (mTORC2) at Thr308 and at Ser473, respectively, ultimately triggering cell cycle progression, anabolic processes, and cell survival (Xu et al. 2012b) (Figure 2).

Collectively, HER2 exerts a fundamental role in cell viability and fitness of HER2-overexpressing BC cells, justifiably positioning this protein as the "driving force" of this specific BC subtype.

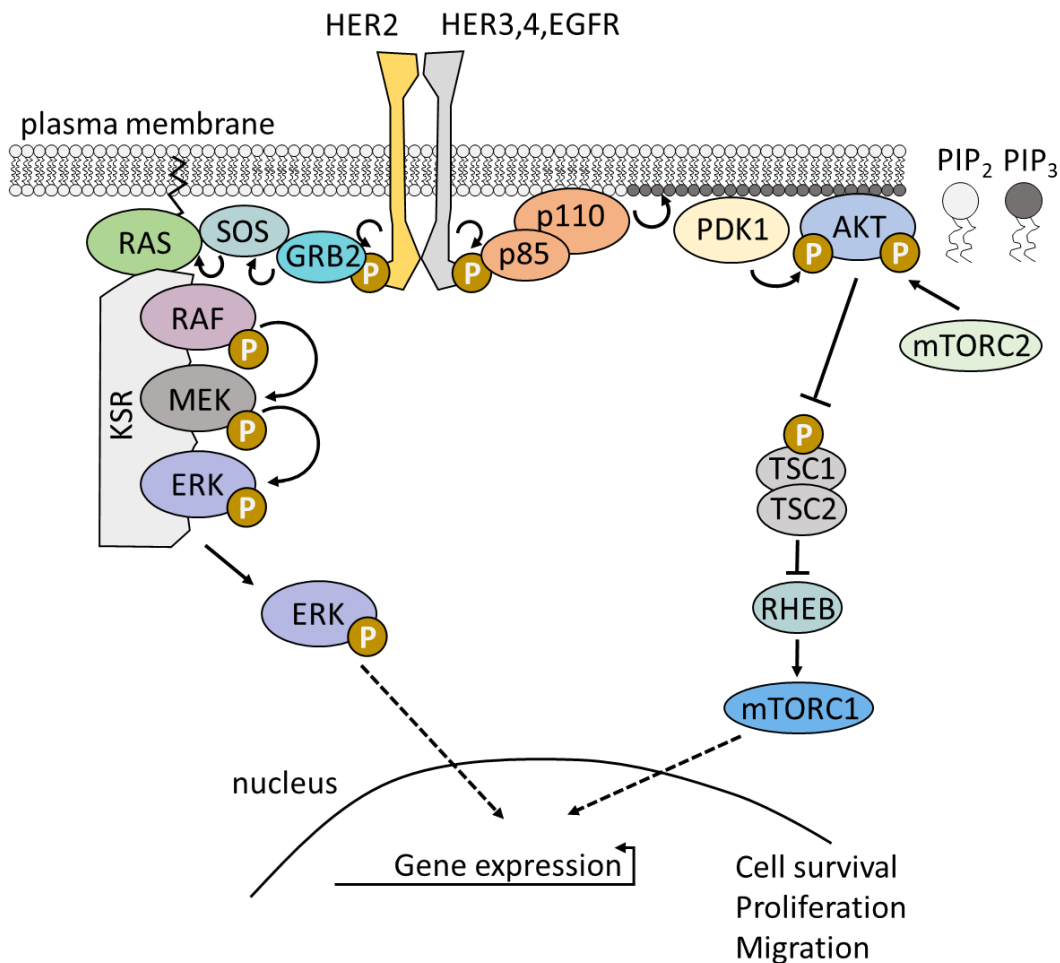



Figure 2: The HER2-driven signaling cascade leads to a plethora of tumorigenic features including cell survival, proliferation, and migration. RHEB: Ras homolog enriched in brain, TSC1/2: Tuberous Sclerosis 1/2, KSR: Kinase Suppressor of Ras
Modified from Pollock and Grandis 2015.

2.1.4. Current HER2-directed therapy of HER2⁺-BC

HER2 overexpression and gain-of-function mutations have been reported to promote tumorigenesis. Many identified mutations are localized within the kinase domain which increase the kinase activity. Moreover, the transmembrane and the extracellular domain host over 50% of all identified HER2 somatic mutations, enhancing the protein stability (Meric-Bernstam et al. 2019).

Therefore, a great number of studies in the last two decades have substantially contributed to the design of anti-HER2 agents, targeting the genetic alterations of *ERBB2* in HER2⁺-BC



patients (Wang and Xu 2019). There are three main groups of anti-HER2 therapeutic agents: monoclonal antibodies, small molecule inhibitors, and immunoconjugates.

Monoclonal antibodies

Trastuzumab was launched for the first time in 1998 under the brand name Herceptin®. It is a monoclonal IgG1 class humanized murine antibody, recognizing the extracellular part of HER2. Upon binding to HER2, Herceptin® leads to antibody-dependent cell-mediated cytotoxicity (ADCC), hence, interfering with HER2 dimerization events, leading to impaired tumorigenic signal transduction in BC cells (Spector and Blackwell 2009). It is used in adjuvant as well as advanced metastatic therapy and is administered intravenously at a body weight-based dose (Pinto et al. 2013). Furthermore, it is the first monoclonal HER2-specific antibody that was approved in combination with cytotoxic agents due to the improved therapeutic response of HER2⁺-BC patients receiving trastuzumab along with taxane or doxorubicin (Wang and Xu 2019).

Another well-known immunoglobulin used in anti-HER2 targeted therapies is pertuzumab (Perjeta®), which is a humanized recombinant monoclonal antibody, targeting the extracellular part of HER2. Its binding to HER2 prevents the heterodimerization of HER2 and HER3, thereby, impeding HER3-driven signalling and promoting ADCC (Capelan et al. 2013). Despite the modest therapeutic response that pertuzumab-treated patients showed, its greater effectiveness has been proven in cases of combinatory treatment with trastuzumab and docetaxel (Capelan et al. 2013). Noteworthy, a distinct clinical feature of this monoclonal antibody is its FDA approval in 2013 as an agent that leads to a substantial therapeutic response in neoadjuvant chemotherapy of HER2⁺-BC patients (Schneeweiss et al. 2013).

Tyrosine kinase inhibitors (TKIs)

Lapatinib with the brand name Tykerb® is a non-specific HER2 kinase inhibitor that additionally targets other EGFR family members, thereby, leading to stronger anti-proliferative effects (Burris 2004). Lapatinib potentiates stronger therapeutic response when utilized in combination with anti-HER2 monoclonal antibody therapies (Nelson and Dolder 2006). Additionally, in cases of trastuzumab resistance, lapatinib has been proven to be an appropriate choice in patients with advanced HER2⁺-BC disease (Blackwell et al. 2010).

Clinical studies have shown that the kinase inhibitor neratinib demonstrates a greater inhibitory and HER-specific effect, especially in resistance cases compared to lapatinib (Burstein et al. 2010). Currently, several advanced clinical trials are testing the efficacy of

neratinib, either as monotherapy or in combination with cytotoxic drugs e.g. paclitaxel in HER2⁺-BC patients with brain metastasis (Chan et al. 2016; Freedman et al. 2016).


Monoclonal antibody conjugates

Ado-trastuzumab emtansine (Kadcyla®) is a specially designed microtubule inhibitor-conjugated monoclonal anti-HER2 antibody. It is the first immunoconjugate that is able to deliver a cytotoxic inhibitor in a tumor-specific manner. Clinical studies have shown substantial tolerability and improved progression-free survival of Kadcyla®-treated HER2⁺-BC patients (Hurvitz et al. 2013; Lambert and Chari 2014).

2.1.5. Resistance mechanisms to HER2-targeted therapy necessitate the advent of novel therapeutic targets

Anti-HER2 therapies revolutionized the treatment of the aggressive HER2-driven BC subtype and undeniably contributed to the improved survival outcomes of HER2⁺-BC patients (Pernas and Tolaney 2019). However, a considerable fraction of HER2⁺-BC patients (40-50%) become refractory to anti-HER2 therapies by showing tumor relapse within 1.5 years and distant brain metastases with lethal implications (Lin 2015).

There is accumulating evidence that a great number of primary or acquired resistance mechanisms emerge and compensate for the inhibition of the HER2 receptor. Indeed, a number of these compensatory mechanisms lead to activation of alternative growth receptor members such as Insulin Growth Factor 1 Receptor (IGF-1R) or Hepatocyte Growth Receptor (HGFR or MET) or to gain-/loss-of-function mutations in many downstream factors of the HER2-driven signaling cascade. Hyperactivation of the PI3K/AKT/mTOR axis or activating mutations in Phosphatidylinositol-4,5-Bisphosphate 3-Kinase Catalytic Subunit Alpha (*PIK3CA* encoding the p110 subunit of PI3K) are a few representative examples of acquired resistance mechanisms to anti-HER2 therapies (Berns et al. 2007; Chandarlapaty et al. 2012; Minuti et al. 2012; Nagata et al. 2004; Nahta et al. 2005). Furthermore, the cell cycle regulatory circuit, controlling the G1-S transition in cells, has been demonstrated to mediate resistance to HER2-targeting therapies. Indeed, patient-derived xenograft approaches have shown a resensitization in anti-HER2 therapy resistant tumor biopsies by Cyclin-Dependent Kinase 4/6 (CDK4/6) inhibitors (Goel et al. 2016). Moreover, a growing number of studies point to the bidirectional cross-talk between HER2- and ESR-driven signaling. In cases where both receptors are co-expressed, ESR-driven signaling has been reported to become an escaping mechanism to overcome anti-HER2 targeted therapies (Johnston et al. 2009; Kaufman et al. 2009).



Collectively, patients suffering from HER2⁺-BC undeniably benefit from current HER2-targeted therapies. However, due to the intrinsic heterogeneity favoring the emergence of recurrent anti-HER2 resistance mechanisms (Rye et al. 2018), there is an urgent need for novel prognostic markers and molecular targets for tailored-therapies.

2.2. The scope of cancer hallmarks

The hallmarks of cancer represent a group of biological processes that are aberrantly dysregulated and predispose normal cells to cellular transformation, as well as to cancer progression. Some of these processes are necessary for the onset of this neoplastic disease while others are acquired during cancer progression and metastasis. The identification of common molecular "traits" of different cancer entities provides a consensus rationale that simplifies the complex "architecture" of this multifactorial disease. Moreover, characterization of the different cancer hallmarks enables the preclinical and clinical field to uncover druggable targets with therapeutic benefits for patients suffering from various cancer entities (Hanahan and Weinberg 2011). The following chapters will shortly introduce the basic features of all acknowledged cancer hallmarks.

Aberrant proliferation

Irrefutably, one of the most important features of cancer is the uncontrolled proliferation potential of cancer cells. Tissue-specific normal cells undergo a strict control of cell cycle progression, such as timely restricted secretion of autocrine growth factors or negative feedback loops extinguishing the initial cell-cycling signal. As a result, normal cells are controlled by a homeostatic program that contains cell number and preserves the tissue structure and function. On the contrary, cancer cells annihilate step-by-step many restrictive regulatory checkpoints that control cell cycle entry and progression, thereby, leading to an unscheduled cell division. Moreover, proto-oncogenes, playing an integral role in sustaining a plethora of cancer hallmarks (including cell cycle progression), are frequently mutated or overexpressed (e.g. *ERBB2*, *AKT* etc) to either become unresponsive to negative feedback circuits, or to strengthen cell growth stimuli, respectively (Hanahan and Weinberg 2011).

Escaping growth suppressors

Another prerequisite for tumor cells to continuously proliferate is to escape robust signaling pathways that operate as proliferation-suppressive programs. These pathways are controlled by tumor-suppressor genes that frequently undergo loss-of-function mutations or are transcriptionally silenced, hence, further augmenting the signaling transduction of uncontrolled cell cycle entry (Hanahan and Weinberg 2011). For example, *TP53* and *RB1*

represent two of the most well-known tumor-suppressor genes that are frequently mutated in cancer patients (43% and 7%, respectively) (<https://www.cbioportal.org/>, data not shown). TP53 is a major stress-sensing transcription factor that integrates a plethora of intracellular growth-inhibitory signals. For example, TP53 is able to receive signals originating from excessive DNA damage, limited amounts of nucleotides, nutrients, oxygen, thereby, leading to cell-cycle block until the stress-trigger is resolved. However, in case the cellular insult remains or becomes irreparable, TP53 can elicit a cell death program, called apoptosis [from ancient greek: ἀπόπτωσης, ἀπό=off, πτώσις=falling, meaning falling off (Galluzzi et al. 2018); see next hallmark]. Therefore, TP53 is a major factor controlling a naturally occurring cell death program that protects future cell generations from cellular "injury" and genetic defects and which is frequently dysregulated in cancer (Hanahan and Weinberg 2011).

Resistance to cell death

Apoptosis is a programmed cell death pathway functioning as a tumor-suppressive circuit that is frequently inhibited in cancer cells. Under normal condition, apoptosis exerts a homeostatic role contributing to cell clearance of aged and dysfunctional cells in order to preserve the tissue architecture and its functional role. Apoptotic signals can be intracellular or extracellular and sensed/transduced by intrinsic or extrinsic apoptotic cascades, respectively. Both apoptotic cascades, though, converge to the activation of an intracellular proteolytic cascade that is catalyzed by caspases, forming at the very end apoptotic bodies that are recognized and digested by phagocytes. In the context of cancer, tumor cells commonly harbor loss-of-function mutations in tumor-suppressor genes that are able to sense intrinsic stress signals and elicit pro-apoptotic pathways, such as *TP53*, *TNFRSF1A*, *FAS*, *FASLG*, *BCL10* etc (Hanahan and Weinberg 2011).

Alternatively, autophagy [(from ancient greek: αὐτοφαγος, αὐτό= self-, φάγος=devour, meaning self-devouring (Galluzzi et al. 2018))] is an additional normally occurring cell-death program that is active at basal levels in normal cells, but can possess context-dependent roles in cancer. Autophagy enables cells to recycle misfolded protein aggregates into amino acids, thereby, replenishing tumor cells with amino acids under nutrient deficient-states, thereby, sustaining tumor growth. On the other hand, studies have shown that loss of autophagy-decisive genes, like Beclin-1 (*Becn1*), in mice results in the spontaneous formation of neoplastic lesions, hence, serving tumor-suppressive roles (Hanahan and Weinberg 2011).

Overcoming replicative senescence or cell death

Leonard Hayflick was the first scientist to report that cancer cells are immortal. In normal cells, after every cell division cycle, the extremities of chromosomes, called telomeric DNA, are extensively shortened after a certain number of cell divisions. When reaching a critical telomere length that jeopardizes the loss of genetic information, normal cells undergo either cellular senescence or apoptotic cell death. On the contrary, cancer cells reactivate the expression of telomerase, a telomeric DNA-specific polymerase that constitutively elongates the length of the telomeric DNA, thereby, allowing cells to undergo an indefinite number of cell divisions, a state called cell immortality (Hanahan and Weinberg 2011).

Aberrant vascularization

Similar to normal tissues, tumor cells require vascularization in order to have access to oxygen and nutrients as well as to dispose metabolic byproducts and carbon dioxide. Compared to normal vascular endothelial cells, being in a quiescent state, tumor cells constantly keep endothelial cells in an angiogenic mode to continuously sprout and form new vessels within growing tumor bulks. Vascular endothelial growth factor A (VEGFA) plays a nodal role in this cancer hallmark, being expressed in response to hypoxic conditions as well as oncogenic signaling cascades (Hanahan and Weinberg 2011).

Metabolic "rewiring"

Metabolic reprogramming is a common characteristic in almost all cancer entities. The center of a growing tumor is very often confronted with limited access to nutrients and oxygen, if local angiogenesis is still inadequate to sustain the metabolic needs of tumor cells. Specifically, tumor cells can "rewire" their metabolic pathways to an oxygen-independent and glycolysis-driven ATP synthesis, a phenomenon called "Warburg effect" or aerobic glycolysis. Although aerobic glycolysis in tumor cells is 18-fold less efficient than oxidative phosphorylation in normal cells, tumor cells dramatically increase their glucose intake efficiency, providing the cells with increased amounts of glycolytic intermediates for many subsequent anabolic pathways. Metabolic reprogramming occurs also in other interconnected metabolic pathways that provide important precursor intermediates for DNA synthesis, for membrane biogenesis, as well as to scavenge reactive oxygen (generated by the dysregulated oxidative phosphorylation). Concluding, metabolic "flexibility" is critical for sustaining the bioenergetic demands as well supplying cancer cells with critical metabolites for vital cellular functions, even under hostile environmental conditions (Hanahan and Weinberg 2011).

Immune surveillance escape

For many years, the means by which tumor cells are able to establish an immune-tolerant tumor-microenvironment remained elusive. Under normal conditions, all tissues undergo an "immune-surveillance", which is responsible to clear infected or transformed cells. However, tumor bulks are frequently infiltrated by a different population of immune cells harboring immune-suppressive features, suggesting that cancer cells can actively "manipulate" the immune system. Indeed, during the last decade, we have been progressively uncovering various cancer-imposed immune tolerance mechanisms, such as cytotoxic lymphocytes (CTLs) that become inactivated via the PDL1-PD1 cancer-to-CTL crosstalk (PDL1: Programmed cell Death 1 Ligand 1) (Hanahan and Weinberg 2011).

Tumor-promoting inflammation

Although immune cell infiltration was, from the past, recognized as a histologic feature associated with a systemic anti-cancer immune response, it was later proven that certain inflammatory responses can enhance various cancer hallmarks. Specifically, tumor-associated inflammation provides tumor cells with an ideal tumor microenvironment that is supplied with growth factors, proangiogenic factors and metalloproteases favoring cell invasion and metastasis. Consequently, inflammation supports many features of other cancer hallmarks (Hanahan and Weinberg 2011).

Oncogene-induced genomic instability

A number of the abovementioned cancer hallmarks is largely dependent on genetic alterations. The oncogene-induced genomic instability is the driving force leading to a plethora of genetic alterations including copy-number variations (CNVs), single-nucleotide polymorphisms (SNPs) and aneuploidy. A certain "palette" of genetic alterations provides, therefore, the needed advantage for tumor clones to propagate and become dominant in their tumor microenvironment. The genetic contribution to cancer initiation and progression largely relies on the oncogene-induced replicative stress, which is characterized by imminent replication/transcription conflicts, provoking the formation of DNA double-strand breaks (DSBs). In normal cells, DSBs are often incompatible with cell proliferation and, normally, induce cell cycle arrest or apoptosis. However, under certain circumstances such as loss-of-function mutations of *TP53*, continuous formation of DSBs leads to genomic instability and to a heightened mutagenesis rate in the next cell generations, fostering the acquisition of further mutations that favor cancer progression (Halazonetis et al. 2008; Hanahan and Weinberg 2011).

2.3. Dysregulation of actin cytoskeleton dynamics, a crucial cancer hallmark for cell survival, invasion and metastasis

In solid cancers, acquisition of motile properties is necessary to facilitate cell invasion and metastasis, which is the major cause of mortality in this disease (Gandalovičová et al. 2017). A major intracellular machinery contributing to this invasive phenotype is the actin cytoskeleton (AC), which forms a variety of structurally distinct actin filament networks, promoting various cellular locomotion movements, including "amoeboid" or "mesenchymal" invasion. A well conserved developmental program that transcriptionally orchestrates the invasive phenotype of transformed epithelial cells and that is inextricably linked to the AC dynamics is the epithelial-to-mesenchymal transition (EMT) (Cytoskeleton-Structure, Dynamics, Function and Disease, Zhang, Xuan et al. 2017). AC dynamics is equally important for cell motility-independent phenomena in cancer. For example, the actin-regulatory network as well as actin fibers sustain the focal adhesion kinase (FAK)-dependent pro-survival pathway, thereby, actively inhibiting apoptosis and promoting anoikis resistance (from ancient greek: ἄνοικος, meaning homeless; programmed cell death due to cell-to-matrix detachment) in circulating and metastatic tumor cells (Gandalovičová et al. 2017; Hanahan and Weinberg 2011; Kümper et al. 2016; Matsubara and Bissell 2016; Puthalakath et al. 2001; Tavares et al. 2017). Finally, invasive tumor cells also secrete metalloproteinases that primarily cleave various extracellular matrix fibers to allow cellular protrusion (Hanahan and Weinberg 2011)

2.3.1. Actin, the basic monomer of polymerized actin

The AC is a very dynamic intracellular network of actin monomers coordinating vital regulatory processes such as cell motility, cytokinesis, endocytosis, and cell polarization. Spatiotemporal assembly of globular actin monomers (G-actin) to actin filaments (F-actin) and disassembly is a complex and intricate process regulated by intrinsic and extrinsic signals. Given its indispensable role in cell viability, intense research is currently ongoing to identify actin-modulating factors as therapeutic targets in various cytoskeleton-related diseases including cancer (Foerster et al. 2014; Gandalovičová et al. 2017; Nersesian et al. 2018; Patel et al. 2012; Shao et al. 2018; Stehn et al. 2013; Tavares et al. 2017).

The G-actin is an asymmetric monomer which represents a uniform orientation in a polymer-state, thereby, creating a filamentous actin (F-actin) with two structurally different ends and distinct biochemical properties. The two F-actin extremities are called the "barbed-end" (+ end) and the "pointed-end" (- end). Although both ends show a constant monomer association/dissociation equilibrium (K_{as} for association, K_{dis} for dissociation) of G-actin monomers, the respective K_{as}/K_{dis} ratio is significantly higher in the + than in - end,

conferring a higher polymerization kinetic at the + end (Molecular Biology of the Cell, 6th edition, Garland Science, 2015).

Such a high-order molecular structure is energy-demanding and dependent on the addition of ATP-bound globular actin (G-actin) to + end of F-actin. As soon as newly G-actin/ATP monomers associate with the + end, G-actin/ATP monomers subsequently hydrolyze their ATP to ADP+Pi, resulting in a - end-proximal stretch comprising only G-actin/ADP monomers (Figure 3) (Molecular Biology of the Cell, 6th edition, Garland Science, 2015).

Actin dynamics is strictly controlled by actin-binding proteins (ABPs). Actin polymerization is driven by three different ways: *de novo* nucleation, severing of pre-existing F-actin, or uncapping of the barbed end of pre-existing F-actin. Actin nucleation factors such as ARP2/3 and formins can generate new actin nuclei. In vertebrates, profilin and thymosin β 4 are able to exchange the ADP-to-ATP in the G-actin pool as well as to maintain their ATP-bound state, respectively. Therefore, the function of both ABPs favors G-actin/ATP monomers to be incorporated into the elongating F-actin (Molecular Biology of the Cell, 6th edition, Garland Science, 2015).

To keep a dynamic state of F-actin, there is a number of F-actin severing (depolymerizing) proteins maintaining the G-actin pool. The most striking example is the ADF/cofilin and its paralogues that promote F-actin disassembly. Cofilin, itself, shows a 30-80-fold higher affinity for G-actin/ADP than G-actin/ATP which allows the rapid dissociation of the former from the - end of F-actin. Moreover, cofilin hinders the nucleotide exchange (ADP-to-ATP) of G-actin, thereby depleting the G-actin/ATP monomer pool (Chen et al. 2000; Suarez and Kovar 2016, Molecular Biology of the Cell, 6th edition, Garland Science, 2015) (Figure 3).

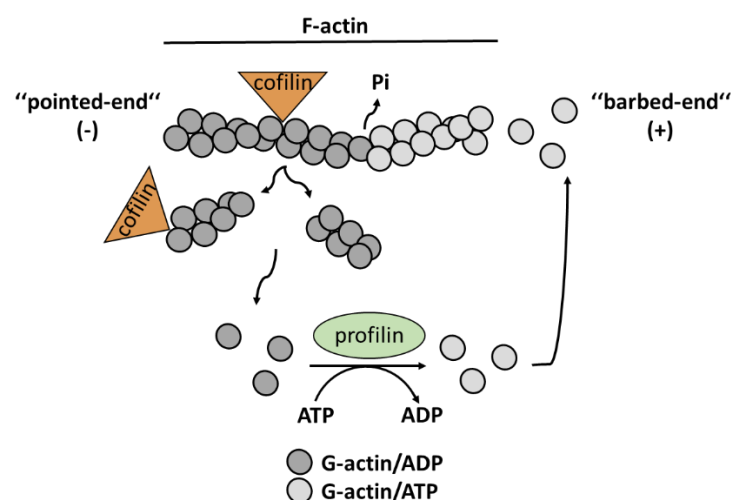


Figure 3: The regulation of actin filament (F-actin) dynamics by the actin-binding proteins (ABPs) profilin and cofilin. ATP: adenosine-triphosphate, ADP: adenosine-diphosphate, Pi: phosphate. Modified from Pontrello and Ethell 2009.

2.3.2. Signaling pathways controlling actin filament dynamics

AC turnover and actomyosin contraction are tightly regulated by RHO GTPases, functioning as "molecular switches" that dynamically change between an active GTP-bound or inactive GDP-bound state. This hydrolyzing step is strictly controlled by three different RHO-GTPase regulatory proteins: the guanine-nucleotide exchange factors (GEFs), the GTPase-activating proteins (GAPs), and the guanine-nucleotide disassociation inhibitors (GDIs). After RHO-GTPases are translated, they undergo a post-translational geranylgeranylation or farnesylation to promote their membrane translocation. GEFs are responsible for the GDP-to-GTP exchange. On the contrary, GAPs and GDIs maintain the inactive state of RHO-GTPases via induction of GTP hydrolysis or their cytoplasmic retention (in a GDP-bound form), respectively (Lin and Zheng 2015) (Figure 4).

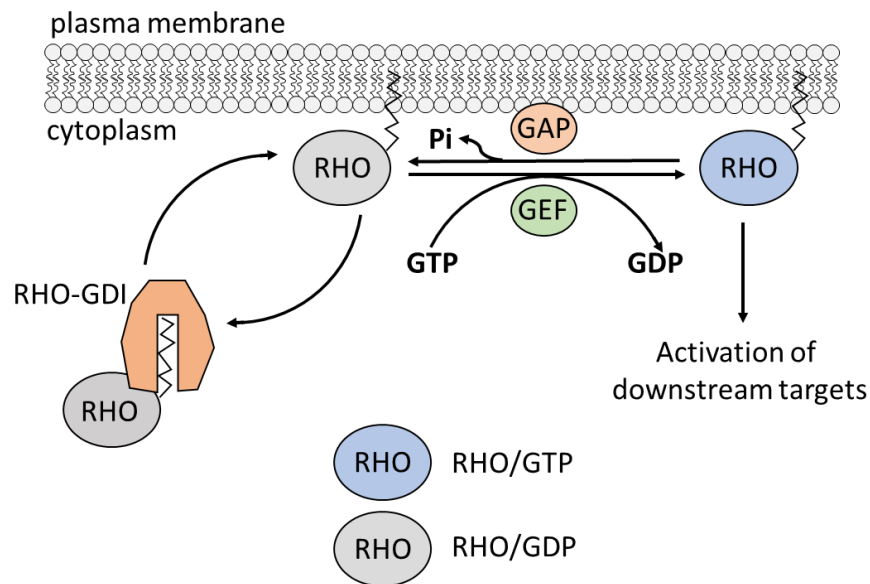


Figure 4: The regulation of RHO-GTPases. GTP: adenosine-triphosphate, GDP: adenosine-diphosphate, Pi: phosphate, GEF: Guanine-nucleotide Exchange Factor, GAP: GTPase-Activating Protein, RHO-GDI: Guanine-nucleotide Disassociation Inhibitor. Modified from Hodge and Ridley 2016.

The effects of RHO-GTPases are mediated by the conformation change they acquire, allowing a large number of downstream effectors and scaffolding proteins to be bound to them. RHO-GTPases are divided into three big protein families, the RHO, CDC42, and RAC family. RHOA (RHO member) controls the formation of a special type of F-actin, namely stress fibers, via the RHO-kinase (ROCK) members 1 and 2 which, in turn, possess multiple downstream targets. Phosphorylated LIM domain kinase (LIMK) 1 and 2 get phosphorylated and activated by ROCK1/2 which leads to cofilin phosphorylation (inactive state). As a consequence, inactive cofilin promotes F-actin abundance which favors, among other,

actomyosin contraction. ROCK1/2 phosphorylate also the myosin phosphatase (MYPT1) to inactivate it and to maintain the phosphorylation (active) status of the myosin light chain which is the most important motor protein in actomyosin contractility. Actomyosin contraction is necessary for the retraction of the "trailing" edge during cell movement. Such a retraction movement is achieved by the bipolar F-actin-bound myosin motor proteins that lead to a retrograde sliding of antiparallel actin bundles. This tension is transmitted to the focal adhesion (FA) complexes, thereby leading to a successful "trailing" edge retraction. At the end, the generated tension results not only in increased stability and maturation of FA complexes, but also in activation of the focal adhesion kinase (FAK) via autophosphorylation at Tyr397. FAK is a pivotal mechanosensor of FA complexes that drives, as a positive feedback loop, AC reorganization as well as pro-survival and cell growth pathways (Pasapera et al. 2010; Walker et al. 2016).

On the other hand, the RAC family activates plenty of downstream effectors, such as the WAVE complex, to promote F-actin formation in lamellipodia via the ARP2/3 complex. RAC and CDC42 activate the p21-activated kinase family (PAK) that can also activate LIMK kinases and promote the abundance of F-actin in lamellipodia or filopodia, respectively (Lin and Zheng 2015) (Figure 5).

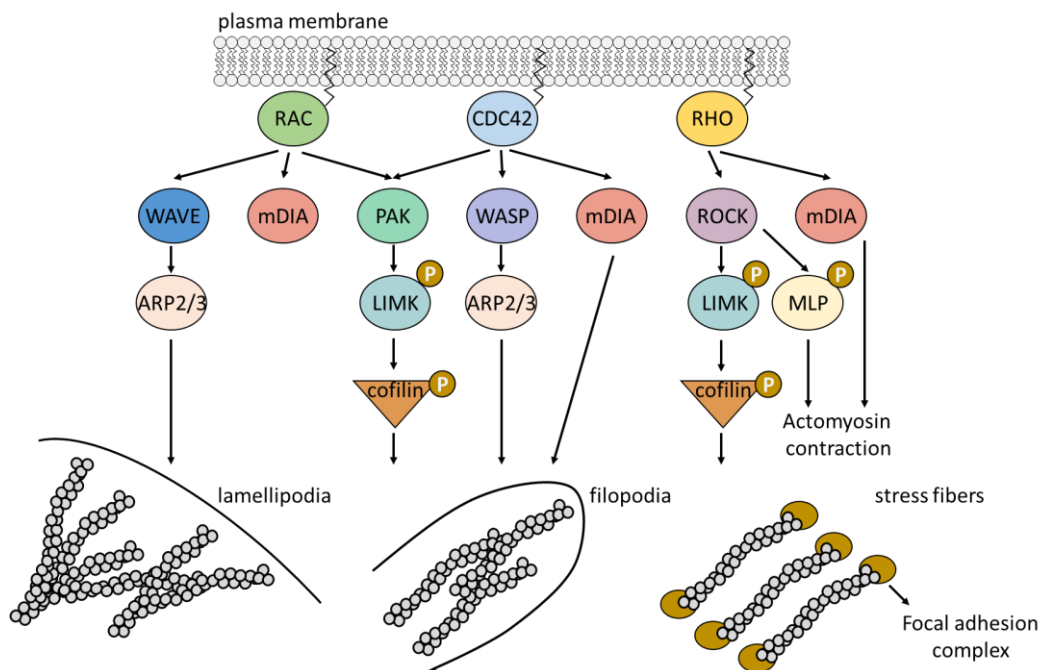



Figure 5: Signaling pathways controlling actin filament dynamics. WASP: Wiskott-Aldrich syndrome protein, WAVE: WASP-family verprolin-homologous protein, mDIA: Diaphanous Related Formin, PAK: P21 (RAC1) Activated Kinase, ROCK: RHO-associated Kinase, LIMK: Lim domain Kinase, ARP2/3: Actin Related Protein 2/3. Modified from Prudnikova et al. 2015.




Another complexity level that characterizes the spatiotemporal regulation of actin dynamics is reflected by the opposing roles and mutual negative feedback loops existing between RHO- and RAC/CDC42-GTPase families. Such an intracellular phenomenon has been reported to facilitate the mutual exclusive generation of the different F-actin structures (stress fibers, filopodia, lamellipodia), serving unique locomotion movements (cell protrusion, spreading, and cell body retraction) for a productive cell movement (Byrne et al. 2016; Nimmual et al. 2003; Sander et al. 1999).

2.3.3. The role of actin cytoskeleton dynamics in HER2⁺-BC, in other malignancies and its clinical value as a therapeutic target

Dysregulation of AC dynamics has been several times implicated in multiple tumorigenic features including cell locomotion, invasion and supporting cell viability (Gandalovičová et al. 2017; Kümper et al. 2016; Nersesian et al. 2018; Tavares et al. 2017; Trendowski et al. 2014), arguably being positioned as an essential cancer hallmark. To date, a plethora of AC-modulatory compounds has been identified as a promising group of drugs with anti-tumorigenic properties in numerous *in vitro* studies (Gandalovičová et al. 2017). Unfortunately, their heightened toxicity not only in tumors but also in normal cells has raised skepticism towards their use in the clinic (Stehn et al. 2013). However, there is an increasing number of preclinical studies, revealing novel AC-modulatory compounds with promising anti-carcinogenic potential and surprisingly low systemic toxicity (Patel et al. 2012; Stehn et al. 2013; Yu et al. 2019). To date, most promising AC-modulatory drugs with a proven therapeutic benefit are kinase inhibitors of the ROCK- or Myotonic dystrophy-related Cdc42-binding kinases (MRCK)-driven signaling cascade, showing low toxicity *in vivo* in different cancer contexts such as prostate cancer, breast cancer, melanoma and glioblastoma (Gandalovičová et al. 2017).

The expanding knowledge on the biological and clinical relevance of AC dynamics in malignancies also comes from studies focused on HER2⁺-BC. For example, ROCK1 expression has been associated with high grade, advanced stage, positive nodal metastasis, and poor survival of HER2⁺-BC patients (Lane et al. 2008; Liu et al. 2009; Tawab Osman et al. 2020). Moreover, F-actin has been shown to play a central role in HER2⁺-BC cell viability and its abundance has been associated with an advanced clinical stage (Shao et al. 2018; Wang et al. 2019b). In line, RKI-1447, a novel potent ROCK-specific inhibitor, was shown to suppress ROCK-dependent signaling cascade, anchorage-independent tumor-sphere formation, and migration. Most importantly, RKI-1447 was able to inhibit tumor growth by 87% in an MMTV-*ErbB2* mouse model mimicking HER2⁺-BC without resulting in body weight loss (Patel et al. 2012). In accordance, a novel marine



macrolide derivative called mycalolide B (Myc B) was confirmed to reduce growth and viability of HER2⁺-BC cells by impairing AC dynamics *in vitro* and *in vivo* with no signs of body weight loss in mice, as well (Nersesian et al. 2018).

Nowadays, increasing emphasis is put on optimizing conventional anti-cancer therapies in combination with novel druggable AC targets to potentiate their efficacy (Trendowski et al. 2014). Apart from the anti-metastatic and anti-invasive properties of AC drugs, they also exhibit a great anti-proliferative and anti-clonogenic effect on numerous cancer contexts, including HER2⁺-BC. Therefore, it is plausible that future therapeutic schemes containing AC drugs may enter the first clinical trials to optimize current conventional anticancer therapies (Kolber and Hill 1992; Matsubara and Bissell 2016; Tavares et al. 2017).

2.4. Oncogene-induced proteotoxicity and augmented protein quality control as a critical cancer hallmark

Besides uncontrolled cell cycle entry or evading cell death, oncogenes also reinforce multiple anabolic processes, such as increasing the protein turnover that covers the heightened proteome demands, thereby, sustaining continuous cell growth. Therefore, cancer cells rely on protein homeostasis programs, which either ensure proper protein folding or induce autophagy, whereby misfolded proteins are recycled to amino acids. Any perturbation of these homeostatic programs leads to a so-called "proteotoxicity" (PT), which results in a context-dependent cell death or in the induction of physiological and homeostatic responses supporting the global protein folding system. A well-known adaptive PT-induced adaptive response to PT is the heat shock response (HSR), which augments the folding capacity in response to accumulation of unfolded nucleus or cytosolic protein. The second homeostatic arm counteracting PT is the endoplasmic reticulum unfolded protein response (UPR or UPR^{ER}), which similarly increases the protein folding control of the endoplasmic reticulum (ER) in response to accumulating unfolded ER proteins. Recently, a similar response to accumulating mitochondrial unfolded proteins has been proposed, called mitochondrial unfolded protein response (UPR^{mt}) (Kenny et al. 2017). Importantly, both HSR and UPR have the capacity to induce autophagy or UPR^{mt}-mediated mitophagy (Dokladny et al. 2015; Papa and Germain 2014; Workman and Davies 2011). Collectively, cancer cells efficiently exploit these highly conserved homeostatic programs to dampen the oncogene-induced PT and sustain their continuous tumorigenic features.

Endoplasmic reticulum (ER) is an intracellular organelle that orchestrates the glycosylation, protein folding and cellular trafficking of proteins that reside in the Golgi apparatus, the endosome system, the lysosomes, the plasma membrane, as well as in the extracellular space (Molecular Biology of the Cell, 6th edition, Garland Science, 2015). Moreover, ER

functions as a calcium storage (Ca^{2+}) apparatus to maintain the Ca^{2+} -dependent ER-protein folding, as well as to control various Ca^{2+} -induced signaling circuits in the cytoplasm (Molecular Biology of the Cell, 6th edition, Garland Science, 2015). Imbalance of any ER-associated function, sensed by special ER-resident factors, activates UPR. UPR is a well conserved adaptive cellular response that will either promote a pro-survival, homeostatic program or cell death as soon as the cellular stress remains irreparable (Pakos-Zebrucka et al. 2016). Nowadays, the UPR-driven cascade is subjected to intense research efforts that delineate its biological and clinical relevance in human diseases including cancer.

2.4.1. The signaling pathway of UPR

UPR comprises three ER-stress sensing mediators: the PKR-Like Endoplasmic Reticulum Kinase (PERK), the Inositol-Requiring Enzyme 1 (IRE1) and the Activating Transcription Factor 6 (ATF6; Figure 6). All UPR-stress sensing factors become activated by any endoplasmic reticulum imbalance, mainly related to calcium imbalance or protein folding capacity of newly synthesized proteins. PERK is responsible for the phosphorylation of the eukaryotic transcription initiation factor 2a (eIF2a), favoring a global decrease of protein synthesis. (Pakos-Zebrucka et al. 2016). Although PERK-mediated UPR halts the cap-dependent global translation, many mRNAs escape this mechanism via a cap-independent protein synthesis. The Activating Transcription Factor 4 (ATF4) is one of the most representative examples, whose protein synthesis is initiated upon UPR induction, which later functions as a transcription factor (TF) (Guang et al. 2019). The next UPR-arm, IRE1 possesses a ribonucleolytic domain that splices, among other, the premature mRNA of XBP1 to a mature one, leading to the protein synthesis of the XBP1 that also functions as a TF (Bright et al. 2015; Tam et al. 2014). Finally, ATF6, upon UPR activation, translocates from the ER to the Golgi apparatus. As soon as ATF6 reaches the Golgi apparatus, a protease-mediated cleavage takes place to release its cytoplasmic fragment which functions as a Basic Leucine Zipper (bZIP) TF in the nucleus (Hillary and Fitzgerald 2018). The ultimate aim of UPR is to promote a homeostatic pro-survival program driven by ATF4, ATF6, and XBP1. This program initiates five major axes: inhibition of the global protein synthesis in a p-eIF2a-dependent fashion, activation of genes involved in protein folding system, induction of the endoplasmic reticulum-associated protein degradation (ERAD) system, sustaining the autophagy pathway, as well as eliciting the expression of anti-oxidant factors in response to oxidative stress. The first axis serves a number of valuable functions for the stressed cell, such as slowing down the overall cap-dependent translation, and diminishing the excess of newly synthesized proteins. Moreover, global translation inhibition allows infected cells to impede the translation of viral proteins that "highjack" the protein

synthesis machinery. Most importantly, the ISR-mediated shutdown of cap-dependent protein synthesis protects cells from the excessive accumulation of unfolded/misfolded proteins, which, otherwise, can lead to PT-induced cell death (Guang et al. 2019). The second axis increases the chaperoning capacity of partially folded proteins in order to sustain their high-order structure and function. The ERAD-axis is responsible for polyubiquitinating misfolded proteins, leading them to proteasomal degradation. Autophagy also degrades misfolded protein aggregates. Therefore, ERAD and autophagy cooperatively replenish the cells with amino acids as "building blocks" and "rewire" the metabolic program in cases of limited nutrient supply (Pakos-Zebrucka et al. 2016) (Figure 6).

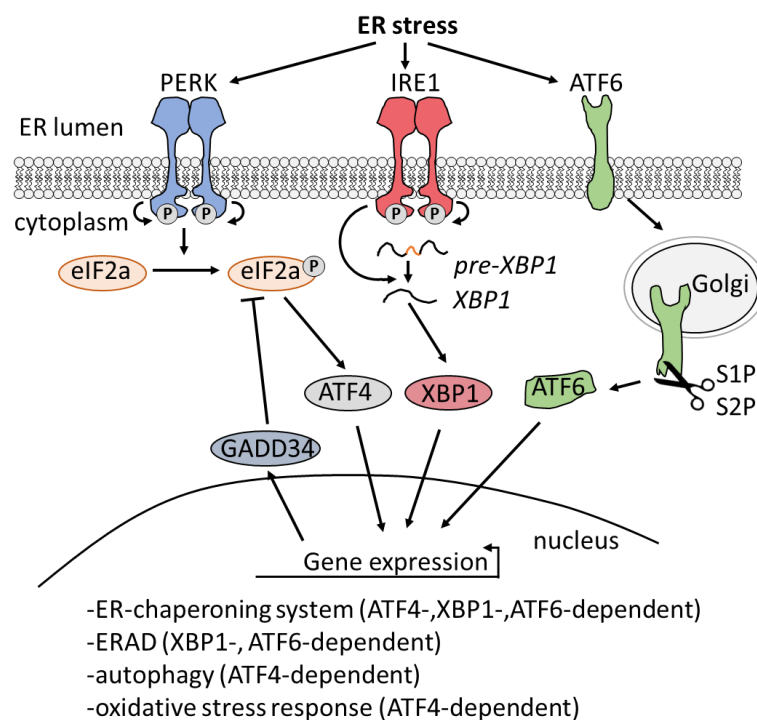


Figure 6: Schematic diagram of the UPR cascade in multicellular eukaryotes. ER stress activates PERK, IRE1 and ATF6. Upon ER stress PERK inactivates by phosphorylation of eIF2a, leading to a global translation inhibition while allowing the cap-independent translation of ATF4. IRE1 senses ER stress leading to the ribonucleolytic cleavage of pre-XBP1 to XBP1 and XBP1 translation. ATF6 also senses ER stress and translocates to the Golgi apparatus, where it is cleaved by S1P and S2P. ATF4, XBP1, and the ATF6 proteolytic product subsequently move to the nucleus to induce gene expression in response to all aforementioned stress triggers. GADD34, as one of the stress-responsive genes, functions as a negative feedback factor that dephosphorylates eIF2a. GADD34: Growth Arrest and DNA-Damage-inducible 34, UPR: unfolded protein response. Modified from Pakos-Zebrucka et al. 2016.

However, if the cellular stress is irreversible or persists, then ATF4 heterodimerizes with the C/EBP homologous protein (CHOP or *DDIT3*) and leads to a (p53-independent) pro-apoptotic gene expression program via the upregulation of *ATF3*, *PUMA*, and *BIM* (Galehdar et al. 2010; Jiang et al. 2004; Pakos-Zebrucka et al. 2016; Puthalakath et al. 2007; Sharma et al. 2018). Additionally, ATF4/CHOP heterodimer possesses cell death-promoting effects by favoring autophagy inhibition, triggering the upregulation of death receptor 5 (*DR5*) and the downregulation of Cellular FLICE-Like Inhibitory Protein (cFLIP) (Jeon et al. 2018; Lei et al. 2017). Furthermore, ATF4-CHOP dimerization leads to the induction of *ERO1a* which deteriorates the ER-oxidizing environment, hence, denaturing newly folded proteins and increasing the disequilibrium between cellular protein folding capacity and the misfolded protein load in the ER (Marciniak et al. 2004). Finally, it is noteworthy that both ATF4 and ATF3, depending on the post-translational modifications they harbor and their TF-binding partner, are able to function as tumor-supportive or tumor-suppressive TFs (Rohini et al. 2018; Wortel et al. 2017).

What is the mechanism that activates PERK, IRE1 and ATF6?

ER is a protein-folding "factory" of transmembrane and secreted proteins. Therefore, any ER-stress trigger leading to an accumulation of unfolded proteins leads to UPR. UPR-triggers derive from ER calcium disequilibrium, a dysregulated oxidizing environment, glucose deprivation, a defective protein glycosylation or folding capacity. All these potential UPR-triggers are able to physically disengage the major ER molecular chaperone, HSPA5, from PERK, IRE1, and ATF6, which in turn transduce the UPR signal to their downstream effectors (Pakos-Zebrucka et al. 2016) (Figure 7).

HSPA5 (BiP or Grp78) is the major ER chaperone that is a primary sensor and activator of the UPR and that physically attenuates the homodimerization, auto-phosphorylation and subsequent activation of PERK, IRE1, and ATF6. Many models have been described for the functional interplay between HSPA5 and the UPR-sensors in the presence of unfolded proteins and the most prevailing one suggesting a competitive binding between HSPA5-UPR sensor and HSPA5-unfolded proteins (Adams et al. 2019). HSPA5 can bind to short hydrophobic patches that are normally present in the interior side of properly folded proteins. Moreover, HSPA5 possesses an ATPase activity, and depending on the ADP- or ATP-state, this serves as a binding affinity "molecular switch" of HSPA5 for nascent unfolded proteins. During an ATP-bound state, HSPA5 promotes proper folding of its unfolded substrate. HSP40 (DNAJ) is able to bind to the HSPA5-substrate complex and to promote ATP hydrolysis, thereby, "locking" this complex conformation. BiP-associated protein (BAP or SIL1), on the contrary, can exchange ADP to ATP, causing the release of

the substrate (Figure 7). This procedure allows the unfolded substrate to become progressively folded and this chaperoning cycle can be numerous times repeated until the substrate obtains the proper conformational structure (Halperin et al. 2014).

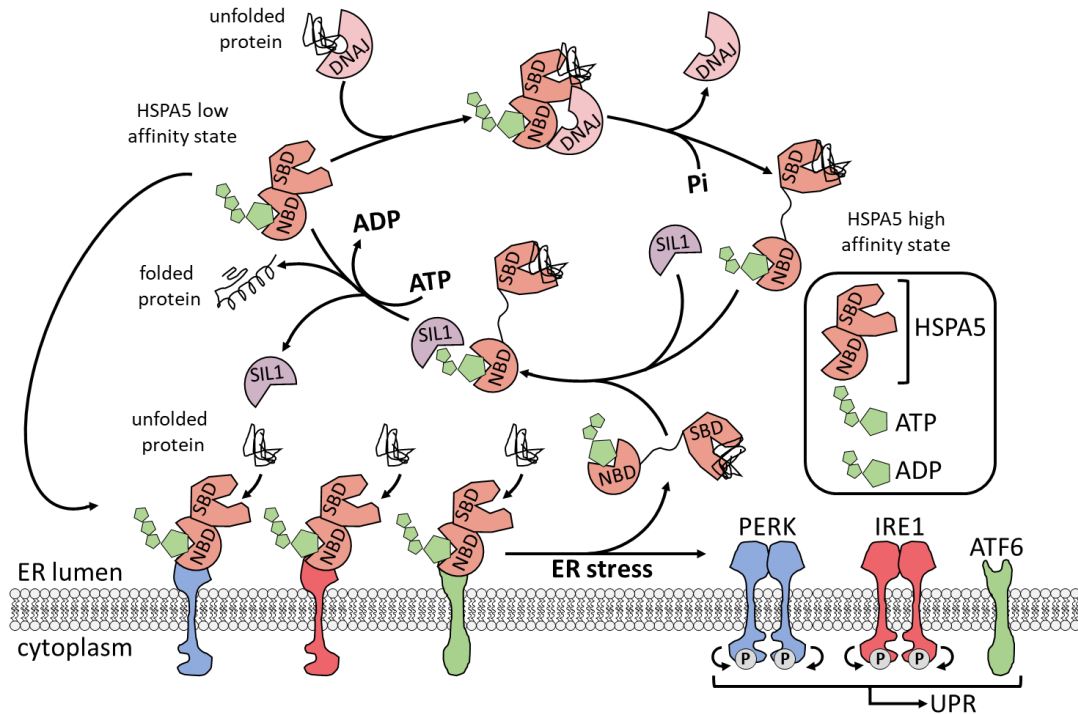



Figure 7: Regulatory mechanism of HSPA5 during ER stress. Physical disassociation of HSPA5/ATP from the UPR-mediators is favored when the former is exposed to unfolded proteins. This disengagement occurs via an allosteric conformational change on HSPA5 that subsequently allows the activation of the UPR. The substrate-binding domain (SBD) of HSPA5 shows less affinity to its substrate when bound to ADP via its nucleotide-binding domain (NBD). However, the affinity of HSPA5 to its substrate is strengthened by association of the HSPA5/ATP/substrate complex with DNAJ, a co-chaperone that induces the ATPase activity of HSPA5, thereby "locking" HSPA5 to its substrate. Finally, to prime HSPA5 for a new chaperoning cycle, SIL1 exchanges an ATP for ADP at the NBD, hence releasing the folded protein from HSPA5/ADP. Modified from Kopp et al. 2019.

2.4.2. UPR, a story of "life and death" in cancer progression

The initiation of tumor growth followed by an inadequate supply of nutrients and oxygen due to inappropriate angiogenesis may lead to a stressful microenvironment for cancer cells. Such conditions, as previously discussed, may lead to a wide range of ER-orchestrated responses either leading to a homeostatic reaction that neutralizes the initial insult or a pro-apoptotic cell death program once the insult becomes irreparable. Given the fact that UPR



signaling initially drives a pro-survival and homeostatic gene expression program, it comes as no surprise that tumor cells "hijack" this cascade for their own benefit. However, the outcome of UPR induction mainly depends on the time and intensity of cellular stress as well as on the (epi)genetic landscape which impacts the homeostasis performance of a cancer cell (Pakos-Zebrucka et al. 2016). Therefore, UPR is a highly context-dependent mechanism in cancer progression.

PERK

The PERK/p-eIF2a axis has been shown to offer various cytoprotective effects in tumor initiation and progression given the tumor-suppressive outcome of PERK deletion, ATF4 deletion, or point mutation of the phospho site of eIF2a in various cancer cell culture models experiencing chronic ER-stress (Bi et al. 2005; Cullinan et al. 2003; Harding et al. 2000; Ye et al. 2010). On the contrary, a considerable number of studies demonstrate a tumor-suppressive function of the PERK/p-eIF2a axis in different *in vitro* settings and mouse models mimicking HER2⁺-BC and prostate cancer (Dai et al. 2019; Darini et al. 2019; Donzé et al. 1995; Jo et al. 2019; Ma et al. 2018; Ranganathan et al. 2008; Sequeira et al. 2007; Zou et al. 2017). Therefore, this bivalent nature of the PERK-mediated UPR raises skepticism about its use as a pan-cancer therapeutic target.

IRE1

Similar to PERK, the role of the IRE1/XBP1-axis is also highly context-dependent. For instance, XBP1 was shown to promote, among other, therapeutic resistance in TNBC via controlling the HIF1a pathway and inducing the IL6/JAK/STAT signaling in oropharyngeal carcinoma (Chen et al. 2014; Dadey et al. 2018; Hu et al. 2015; Lyu et al. 2019; Salaroglio et al. 2017). In stark contrast, the IRE1/XBP1 axis was shown to lead to autophagic cell death in gastric cancer and to impede the metastatic potential of colon cancer cells by inhibiting the SRC/FAK/RHO signaling cascade (Kim et al. 2018b; Xie et al. 2019). Additionally, IRE1 was shown to recruit the adaptor protein tumor necrosis factor receptor-associated factor-2 (TRAF2), thereby activating the c-jun N-terminal kinase (JNK) that leads to a caspase-12-dependent cell death (Yoneda et al. 2001). Consequently, IRE1 is an ER-stress sensor that unleashes tumor supportive or suppressive effects depending on the studied cancer entity.

ATF6

In the case of the ATF6-mediated UPR, the primary effects of this cascade are less opposing and in their vast majority cytoprotective. For instance, ATF6 is responsible for the

transcription of *XBP1* and of various ER molecular chaperones to sustain the heightened protein folding capacity of cancer cells (Pakos-Zebrucka et al. 2016). In line, ATF6 was reported to function as a pro-survival factor in chemotherapy resistance and metastatic relapse via the Ras homolog enriched in brain (RHEB) and the mammalian target of rapamycin (mTOR) in epidermoid carcinoma (Schewe and Aguirre-Ghiso 2008).


HSPA5

HSPA5 expression is positively regulated by PERK, IRE1, and ATF6 as its promoter contains ER stress response binding elements (ERSE) which include ATF4, XBP1, and ATF6 binding motifs (Adams et al. 2019; Luo et al. 2003). Given the context-dependent tumor supportive role of the UPR and the convergent *HSPA5* regulation by UPR-mediators, many studies are currently engaged in unravelling the tumor supportive functions of this protein chaperone.

The global tumor supportive role of HSPA5 derives from numerous preclinical and clinical studies. In hepatocellular carcinoma, HSPA5 along with ATF6 and XBP1 were associated with increasing histological grading (Shuda et al. 2003). Accordingly, HSPA5 protein levels were massively higher in malignant forms of breast and prostate cancer compared to benign lesions, whereas HSPA5^{high} patients, receiving conventional therapies, presented a higher risk for tumor relapse (Daneshmand et al. 2007; Fernandez et al. 2000; Lee et al. 2006). In alignment, MMTV-PyT mice (a TNBC mouse model), harboring a BC tissue-specific heterozygous deletion of *Hspa5*, showed reduced tumor burden, higher levels of CHOP and caspases, and impaired tumor angiogenesis compared to the wild type counterparts (Dong et al. 2008). Collectively, the implication of HSPA5 in various cancer aspects such as proliferation, chemotherapeutic resistance and metastasis (Casas 2017), positions this molecular chaperone an ideal therapeutic target.

2.5. Epigenetic plasticity at the crossroad of different cancer hallmarks

Epigenetics is a physiological process that functions over the genetically encoded information to instruct a cell lineage-specific gene expression program in multicellular eukaryotes. The epigenetic machinery is able to integrate various extra- and intracellular cues that direct gene expression programs, thereby influencing cellular identity and function (Dupont et al. 2009). Given its responsiveness to intrinsic and extrinsic signals, oncogenic signals can give rise to multiple permissive chromatin states, augmenting the expression of tumor-supportive genes. On the contrary, oncogenic signals may lead to restrictive chromatin states, at which tumor-suppressive genes are repressed. In any case, if these chromatin states contribute to cellular "fitness", they are positively selected for in the



subsequent generations, conferring additional carcinogenic features. Such an epigenetic "switch" is reversible and can happen faster than a genetic mutation in response to a stimulus. This contributes to a rapid phenotypic plasticity that allows cancer cells to adapt to oncogenic or stressful cues (Flavahan et al. 2017; Gómez-Schiavon and Buchler 2019). Concluding, epigenetic plasticity is able to control a number of carcinogenic processes and can thereby significantly influence most of the other cancer hallmarks.

2.5.1. Epigenetics: the long story short

Conrad Hal Waddington (birth date: 8 November 1905/death date: 29 September 1975) was the first life scientist to introduce the foundations of epigenetics and the "epigenetic landscape" (EL) in order to describe the various developmental routes that an eukaryotic cell coordinately takes during embryonic development. As shown in Figure 8A, the "EL" model is illustrated as a ball rolling down a path with several branching routes (Baedke 2013). The greek prefix *epi-* [modern greek: επιγενετική, επί=over, outside of, around and γενετική=genetics (Rubin; 2001)] in epigenetics indicates that this mechanism enacts over the well-known genetic mechanism of inheritance. Moreover, C. H. Waddington acknowledged the root term "epigenesis" (ancient greek: ἐπιγένεσις=over/around genetics) which dates back to Aristotle's work "*On the Generation of Animals*" describing the development of individual body organs derived from a fertilized egg (Rubin, 2001; Henry, D. 2018).

Nowadays, it is known that the "EL" is a dynamic state of gene regulation enacted on different levels. These include DNA methylation (e.g CpG islands), histone post-translational modifications (hPTMs), nucleosome repositioning/remodeling, long-non-coding RNA (lncRNA), RNA editing, RNA methylation and miRNA expression. DNA methylation (Figure 8B) on CpG islets establishes a restrictive chromatin state for gene activation and transcription. hPTMs, nucleosome remodeling and lncRNAs modulate the chromatin openness that determines the accessibility of replication, transcription, and DNA repair machineries (Figure 8B). Finally, miRNAs, RNA methylation and RNA editing regulate gene expression on a post-transcriptional level (Frías-Lasserre and Villagra 2017; Holubekova et al. 2017; Zoghbi and Beaudet 2016).

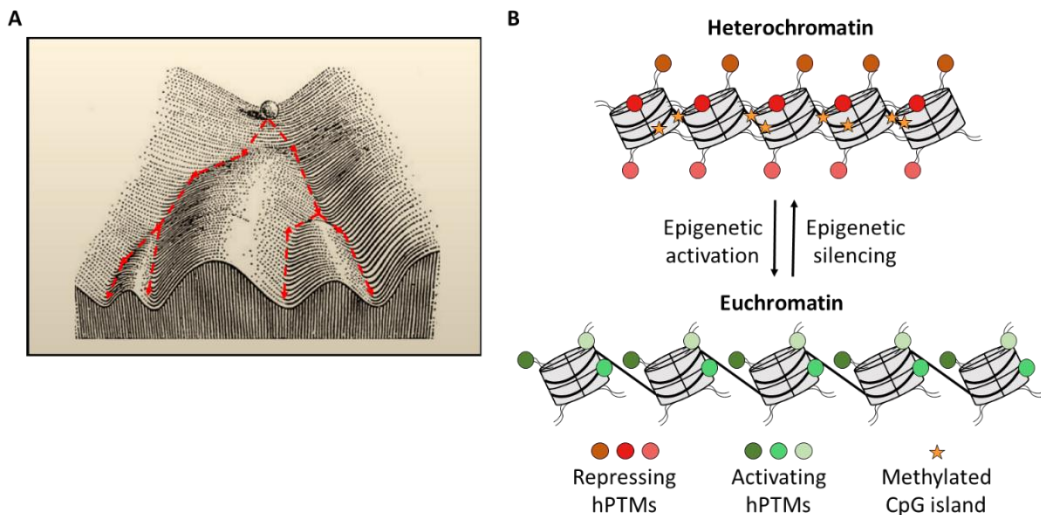


Figure 8: Epigenetics: the long story short. **A)** The epigenetic landscape model proposed by Conrad Hal Waddington in 1940 to describe the various developmental routes a eukaryotic cell takes during embryonic development. **B)** The current state-of-knowledge of epigenetic regulatory marks, repressing or activating gene expression. These marks are mainly histone post-translational modifications (hPTMs) and methylation of CpG islands in the DNA. Modified from Baedke 2013; Ohtani and Dimmeler 2011.

2.5.2. Nucleosome, a chromatin packaging unit and signaling "hub", that masters gene transcription in eukaryotes

Two histone copies of H2A, H2B, H3, and H4 form the octameric nucleosome complex responsible for the chromatin compaction in eukaryotes. Histones undergo a plethora of reversible hPTMs, thereby controlling the access of numerous DNA-binding factors, cofactors, chromosome remodelers, and of the transcriptional machinery to *cis*-regulatory regions and protein-coding genes. The degree of accessibility depends on the nature of the hPTMs. Histones undergo acetylation, methylation, phosphorylation, ubiquitination, sumoylation, glycosylation, and ribosylation. Since hPTMs enact opposing roles in chromatin compaction and accessibility, they are able to direct transcriptional activation or suppression of genes (GENES, 8th edition, B.Lewin, 2004; Figure 9).

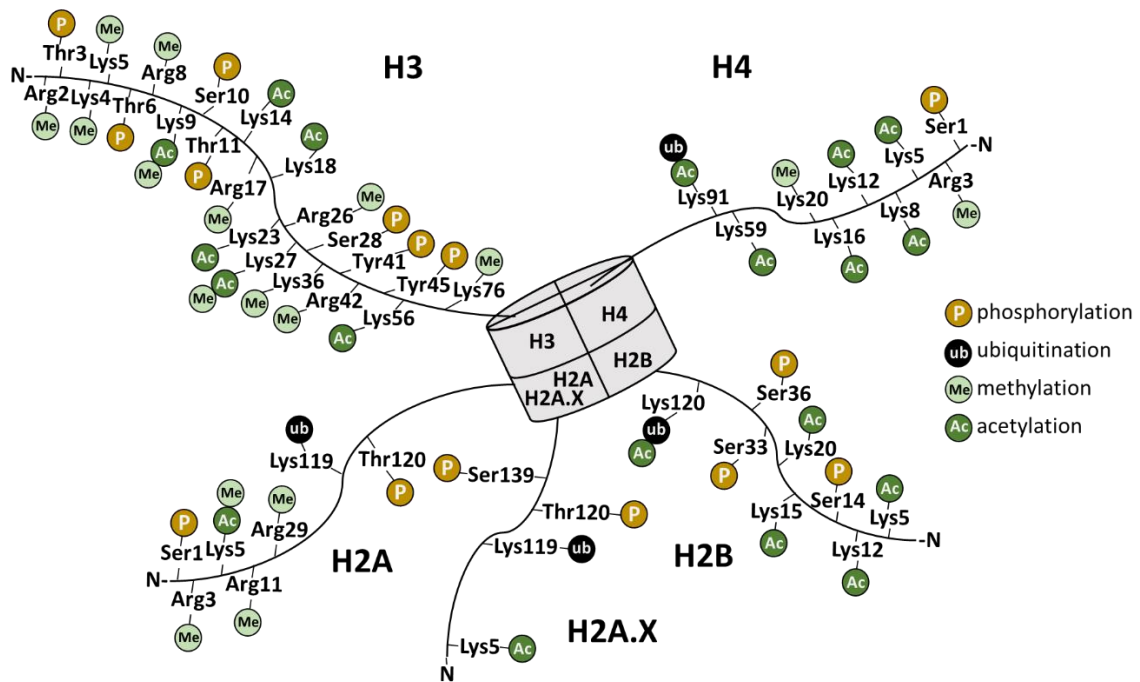


Figure 9: The histone modification code. These modifications impact gene expression by directly increasing or decreasing chromatin accessibility, by recruiting different factors or by influencing the addition/removal of another hPTM. hPTMs mediate numerous events including transcription, replication, DNA damage repair, and chromatin relaxation or compaction. Modified from Genetics, Histone Code, StatPearls Publishing, 2020.

2.5.3. Epigenetic "writers, erasers and readers" shape the epigenetic landscape of eukaryotic gene regulation

As previously mentioned, the "EL" is a dynamic gene regulatory mechanism that is finely tuned by upstream signaling pathway cascades. To achieve such an extensive interplay between signaling cues and the downstream epigenetic events, some epigenetic factors control the abundance of hPTMs (Fagnocchi et al. 2016). These epigenetic factors can be divided into three groups. The first group is the "writers" that catalyze the addition of hPTMs and the second group is the "erasers" that remove hPTMs. Finally, the third group is comprised of "readers" that recognize hPTMs to subsequently influence chromosomal accessibility, either by directly modulating nucleosome positioning/assembly or subsequently recruiting transcription coactivators or corepressors (Längst and Manelyte 2015) (Figure 10).

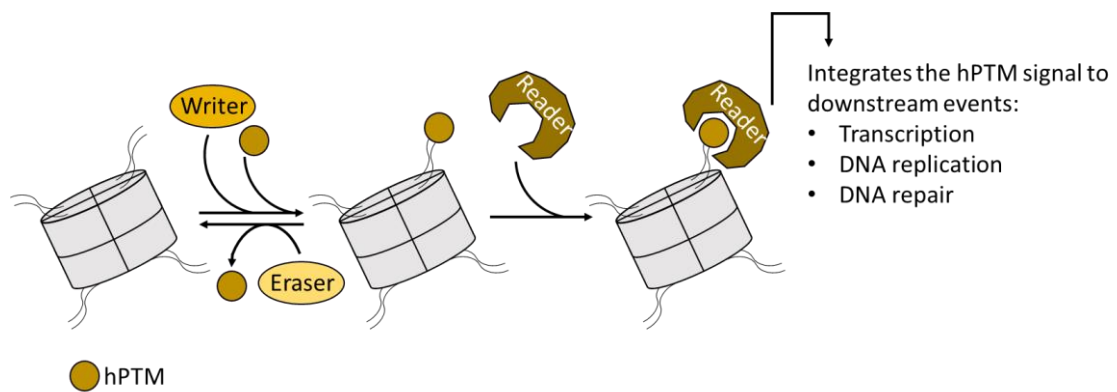



Figure 10: The epigenetic factors: "Writers" and "Erasers" regulate the abundance of histone post-translational modifications (hPTMs), while "Readers" integrate their signal to downstream chromatin-associated events. Modified from Simō-Riudalbas and Esteller 2015.

2.5.4. Stages of transcription: initiation, elongation and termination

Transcription is the first step of the central dogma in molecular biology, where a genetically encoded information is transferred from DNA to a complementary RNA that encodes a protein for a specific cellular function. Eukaryotic transcription is a multistep process, engaging numerous transcriptional complexes that ensure a controlled gene expression rate. This process is commonly instructed by the spatial distribution and abundance of various hPTMs that exert an active or inhibitory role in gene transcription. Therefore, dysregulation of any of the abovementioned transcription regulatory steps, may predispose cells to an aberrant gene expression program, leading to various pathological conditions, including cancer (Bradner et al. 2017). Successful transcription involves three sequential steps: initiation, elongation, and termination (Molecular Biology of the Cell, 6th edition, Garland Science, 2015).

Initiation

RNA polymerase II (RNAPol II) is the eukaryotic polymerase type that transcribes protein-encoding genes as well as non-coding genes including small nuclear RNAs (snRNAs) and micro RNAs (miRNAs). Its structure lacks a DNA-binding domain, therefore RNAPol II is recruited by general transcription factors to the starting point of RNA synthesis, called promoter. For example, the TATA-binding protein (TBP) as part of the TFIID complex shows a specific binding affinity for TATA motifs (within the promoter region) approx. 10-30 bp upstream from the transcriptional start site (TSS), thereby recruiting the RNAPol II/TFIIF complex. TFIID is also responsible for integrating signals, stemming from the nearby "EL" which dictates the time and rate of the transcriptional output. This process is mediated by




various subunits of the TFIID complex that can recognize various activating hPTMs. Collectively, TFIID is a general transcription factor that facilitates the recruitment of RNApol II as well as the integration of numerous upstream signals that modulate the transcriptional activity of RNApol II (Greber and Nogales 2019). Once RNApol II is recruited to the promoter, TFIIIB also binds to TBP and RNApol II to allosterically induce the latter for RNA synthesis and to establish the RNApol II binding orientation to the DNA template (Cramer 2019a). Moreover, the RNApol II-bound TFIIF is responsible for stabilizing the interactions of the polymerase with TFIID and to recruit other general transcription factors, including TFIIE and TFIIH (Molecular Biology of the Cell, 6th edition, Garland Science, 2015) (Figure 11).

Further general transcription factors are subsequently required not only for RNApol II recruitment to chromatin but also for DNA unwinding ("melting") which licenses transcriptional initiation. The TFIIH complex plays a major role in the "melting" of DNA during transcription initiation, which is achieved via its ATP-dependent helicase activity and is further allosterically induced by TFIIE. After the "melting" of DNA, the DNA template strand leads to *de novo* RNA synthesis of the first 10 bases of RNA (nascent RNA) without the use of a priming oligonucleotide. The multimodal role of TFIIH is also reflected by its additional kinase activity which is mediated by the cyclin-dependent kinase 7 (CDK7). CDK7 phosphorylates Ser5 (Ser5-P) and Ser7 (Ser7-P) on the RNApol II C-terminal domain (CTD), facilitating the transition to the transcriptional elongation phase. Furthermore, Ser5-P on the CTD becomes a docking site for enzymes that 5' cap the nascent RNA to protect it from RNase degradation (Core and Adelman 2019). Finally, the mediator complex (MED) contacts RNApol II with TFIIIB and TFIIH to stimulate the CDK7-mediated phosphorylation of the CTD of RNApol II (Kornberg 2005). Consequently, the pre-initiation complex (PIC) (including TFIIA-B, D-F, and TFIIH), and the MED complex is a prerequisite super-sized multi-subunit complex that allows RNApol II recruitment, positioning to the TSS-proximal promoter region, and DNA unwinding leading to RNApol II-mediated nascent RNA synthesis (Figure 11).

Elongation

Similar to the initiation phase of transcription, the elongation phase undergoes a multi-layered regulation. When RNApol II successfully initiates and shifts from the PIC phase, RNApol II often pauses +50 bp downstream from the TSS, a phenomenon called promoter-proximal RNApol II-pausing. This step is highly regulated by various co-activators, co-repressors, or even hPTMs such as H2Bub1, H3K4me3, and H3K9ac (Fuchs et al. 2014; Gates et al. 2017; Xie et al. 2017). To release RNApol II from the TSS-proximal region and to initiate a productive RNA synthesis, phosphorylation of Ser2 (Ser2-P) of the CTD needs



to be catalyzed by the cyclin-dependent kinase 9 (CDK9) kinase which is part of the P-TEFb complex (the regulation and biological consequence of Ser2-P on CTD will be thoroughly discussed in chapter 2.6.1). CDK9 is also known to phosphorylate the negative elongation factor (NELF), triggering its disengagement from RNAPol II, thereby eliciting the RNAPol II promoter-proximal pausing-release (for more details, see chapter 2.6.1) (Cramer 2019b; Wu et al. 2003; Figure 11).

P-TEFb, NELF and DSIF are major modulatory factors during the transcription elongation, thereby termed as "regulatory" factors of RNAPol II pausing-release. Additionally, physical barriers that impede the elongation processivity of RNAPol II, such as TSS-downstream stable or non-sliding nucleosomes, belong to the "intrinsic" or "ubiquitous" RNAPol II pausing. The transcribing RNAPol II can bypass the "intrinsic" nucleosomal barrier with the help of numerous chromosomal remodelers (Teves et al. 2014). For instance, the chromodomain helicase DNA-binding 1 (CHD1) remodeler is associated with RNAPol II during transcription elongation in yeast and mammalian cells to remodel nucleosomes downstream from the upcoming polymerase (Marfella and Imbalzano 2007; van Vugt et al. 2007). Accordingly, the FACT (facilitates chromatin transcription) remodeler is an important histone chaperone that mediates immense changes in chromatin accessibility during transcriptional elongation as well as in replication and DNA damage repair (Hsieh et al. 2013; Winkler and Luger 2011). Collectively, the transcriptional elongation phase necessitates considerable chromatin architecture changes that ensure the passage of the transcribing RNAPol II through the gene body.

Termination

When coming close to the transcription termination phase, the RNAPol II CTD recruits the cleavage, the polyadenylation specificity factor (CPSF) and the cleavage stimulation factor (CSTF) to recognize the poly-A-priming signal (AAUAA) at which RNA cleavage and release occurs. Finally, the 3'-tail is post-transcriptionally elongated by a poly-A-polymerase (approximately 200 bp in length), an event that characterizes RNAPol II-transcribed genes (GENES, 8th edition, B. Lewin, 2004; Huang, Nayak, Jankowitz, Davidson, & Oesterreich, 2011) (Figure 11).

Upon release of RNA from the transcriptional complex, RNAPol II continues transcribing for the next hundred or thousand bases until it is disengaged from the DNA. For this transcription termination event, there are two prevalent and non-mutual exclusive models, the "allosteric" and the "torpedo" model. Based on the "allosteric" model, after transcribing the poly-A-priming signal, RNAPol II undergoes a conformational change due to its (dis)association with different proteins, predisposing the transcribing polymerase to detach

from the DNA (Molecular Biology of the Cell, 6th edition, Garland Science, 2015). On the other hand, the "torpedo" model suggests that upon release of poly-A-primed RNA, the still elongating RNA starts to be cleaved by an exonuclease until it reaches the polymerase machinery, whereby it dislocates the whole transcribing polymerase from the DNA (Luo et al. 2006).

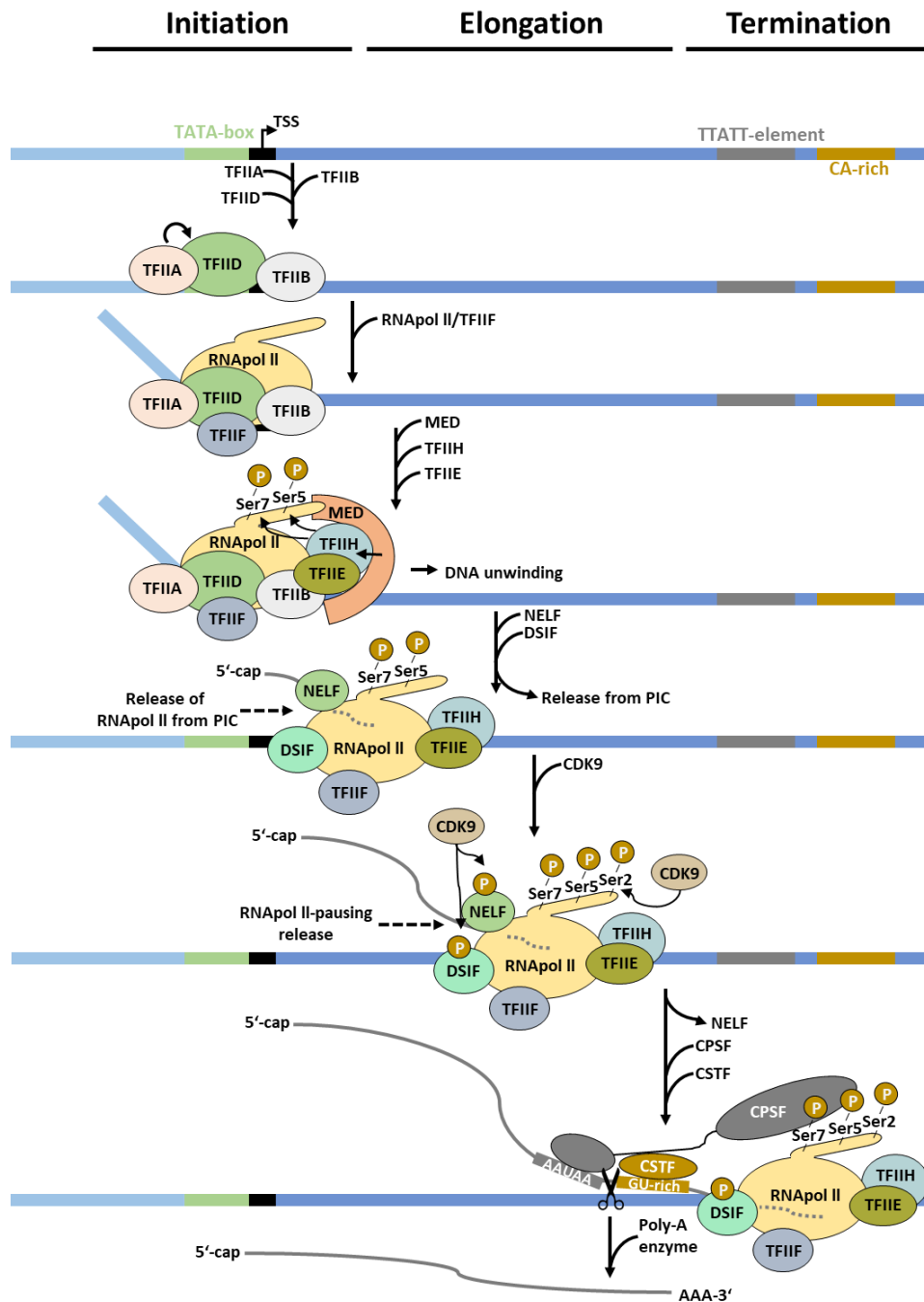


Figure 11: The multi-step process of RNAPol II-mediated transcription. Modified from Molecular Biology of the Cell, 6th edition, Garland Science, 2015.

2.5.5. Epigenetic alterations in cancer: from bench to bedside

Cancer is a genetic disease with accumulating genetic mutations accompanied by epigenetic alterations that can sustain a pro-oncogenic gene expression profile. However, "hijacking" of the epigenetic machinery offers a greater advantage to cancer cells due to the plasticity of epigenetic alterations which allow for a rapid shift in gene expression upon stimuli. Given the reversible nature of epigenetic alterations in cancer cells, pharmacological compounds that target epigenetic factors are increasingly becoming an attractive therapeutic strategy (Citron and Fabris 2020; Lu et al. 2020). Therefore, a large cohort of epigenetic factors (writers, erasers, and readers) are intensively investigated to identify druggable candidates with therapeutic potential for various malignancies (Miranda Furtado et al. 2019).

As previously discussed in chapter 2.1.4, the overall survival of HER2⁺-BC patients has been greatly improved with the advent of anti-HER2 therapies. Nevertheless, development of resistance and tumor relapse is deleterious to the patients' prognosis. Almost 50% of metastatic HER2⁺-BC patients, fail to respond to anti-HER2 targeted therapies (Slamon et al. 2001). To date, only a few preclinical and clinical studies are involved in the therapeutic management of HER2⁺-BC using modulatory agents of the epigenetic machinery, including enzymatic inhibitors of the DNA methylation or HDAC-specific inhibitors. For example, a study from Palomeras et al. found that the global methylation status is increased in trastuzumab-resistant HER2⁺-BC cells compared to parental cells, thereby leading to an extensive epigenetic silencing of numerous tumor-suppressor genes (Palomeras et al. 2019). As a proof-of-principle, specific delivery of siRNAs targeting DNA methyltransferases (DNMTs) to HER2-enriched BC cells promoted a global DNA demethylation and restored the expression of the *RASSF1A* tumor-suppressor gene (Dou et al. 2012). Also, DNMT inhibitors, such as azacytidine or decitabine, provided synergistic effects when combined with traditional chemotherapeutics in HER2⁺-BC patients (Flis et al. 2009). In another study, treatment of HER2-amplified BC cells with panobinostat (pan-HDAC inhibitor) increased the expression of various miRNAs targeting HER2 and HER3 mRNAs (Wang et al. 2013b). Accordingly, a clinical trial of phase 1 and 2 reported that HER2⁺-BC patients with metastatic or locally recurrent HER2⁺-BC showed a therapeutic benefit from the combined treatment of lapatinib with vorinostat (class I and II HDAC inhibitor), compared to lapatinib alone (Goldstein et al. 2017).

Concluding, therapeutic compounds targeting the epigenetic dependencies of BC are, to date, scarce and only limited to a specific panel of epigenetic targets. Moreover, due to the increasing number of preclinical studies, tackling various epigenetic alterations in *in vivo*

malignancies (Miranda Furtado et al. 2019), there is an urgent need to update the panel of therapeutic options in the clinics.

2.6. RNF20-RNF40 and USP22, the "writer" and "eraser" of H2B monoubiquitination

H2B monoubiquitination (H2Bub1) is one of the most intensively studied hPTMs in cell biology and related diseases, given that 47% of all H2Bub1-based studies have been published during the last five years (source from <https://www.ncbi.nlm.nih.gov/>). Nonetheless, to date, only a scarce amount of reports (Kosinsky et al. 2020; Kosinsky et al. 2019a; Melo-Cardenas et al. 2018; Tarcic et al. 2016) has performed a combined *in vivo/in vitro* study to decipher the biological consequence of global H2Bub1 dysregulation (increase or decrease), especially in a genetically engineered mouse model (GEMM) that mimics an oncogene-induced cancer. The apparently increasing interest of this hPTM mainly relies on its strong involvement in different tissue-specific differentiation programs and its pathological implications in cancer. Specifically, H2Bub1 and its obligate heterodimer E3 ligase complex, RNF20-RNF40, were found to be a critical epigenetic axis in various differentiation programs, which is consistent with the gradual loss of this histone mark in a set of human malignancies (Marsh and Dickson 2019). However, during the last years, an equal number of studies proposed a tumor-supportive role of H2Bub1, reflecting the context-dependent role of this epigenetic mark in cancer (Eckhardt et al. 2018; Gao et al. 2011; Garrido Castro et al. 2018; Jaaskelainen et al. 2012; Kosinsky et al. 2019a; Schneider et al. 2019; Wang et al. 2013a).

Protein ubiquitination is a post-translational modification, which consists of the covalent addition of a 76-amino acid moiety to a lysine residue of a protein target. Ubiquitinated proteins can be tagged by ubiquitin polymers or monoubiquitinated. Polyubiquitinated proteins are frequently recognized by the proteasome system where they undergo a proteolytic cleavage. However, other variants of ubiquitin polymers as well as monoubiquitination may confer various functional properties to the modified protein, such as differential subcellular localization, altered affinity to binding partners or allosteric regulation of their regulatory or enzymatic activity (Xu and Jaffrey 2011).

Like all other ubiquitin-based post-translational modifications, H2B monoubiquitination (H2Bub1) is catalyzed by an ATP-dependent enzymatic cascade consisting of the ubiquitin-activating enzyme (E1), the ubiquitin-conjugating enzyme (E2), and the RING finger ubiquitin ligase (E3). As a result, these enzymes mediate the addition of a ubiquitin moiety to the C-terminus of H2B at Lys123 or Lys120 in yeasts and mammals, respectively (Hwang et al. 2003; Kim and Roeder 2009). In brief, the E1 enzyme adenylates the C-terminus of the 76 amino acids ubiquitin, thereby, "activating" it to form a thioester-link with a cysteine

residue of the same enzyme. Subsequently, "active" ubiquitin is transferred to a cysteine residue of an E2 enzyme. Finally, the ubiquitin "activated" E2 is either recruited to the lysine residue of target proteins via the substrate-specific binding of E3 ligase. Alternatively, a thioester bond between the ubiquitin and the E3 ligase takes place, which, in turn, drives the addition of the ubiquitin moiety to the substrate (Figure 12) (Callis 2014).

The monoubiquitination reaction of H2B was first described in yeast studies, where Rad6 and Bre1 were the responsible E2 and E3 ligases for this histone mark, respectively (Hwang et al. 2003; Robzyk et al. 2000; Wood et al. 2003). In line, mammals possess two Bre1 homologs, RNF20 and RNF40 (E3 ligases) and two Rad6 homologs, the UBE2A and UBE2B (E2 ligases) (Foglizzo et al. 2016) (Figure 12). As it was shown in both yeast and mammals-based studies, depletion of any of them impacts the genome-wide levels of H2Bub1 (Gallego et al. 2020; Gallego et al. 2016; Hwang et al. 2003; Turco et al. 2015).

Similar to all histone modifications, H2Bub1 is reversely regulated by various epigenetic "erasers" identified in different studies. The yeast homolog Ubp8 (USP22 in mammals) subunit of the Spt-Ada-Gcn5 acetyltransferase (SAGA) co-activator complex was the first identified deubiquitinase (DUB) of H2Bub1 (Daniel et al. 2004; Henry et al. 2003; Figure 12). However, numerous subsequent studies revealed that other SAGA-dependent DUBs such as USP51, USP27X, and the SAGA-independent USP44 and USP3 are able to deubiquitinate H2Bub1, therefore, being considered as alternative DUBs for this hPTM (Atanassov et al. 2016; Lan et al. 2016).

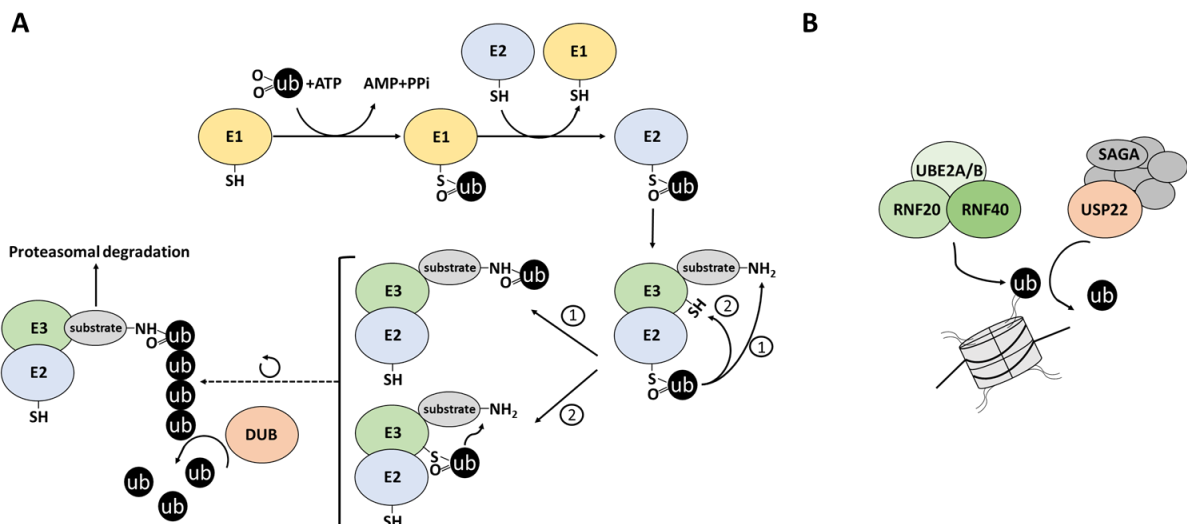


Figure 12: The generic biochemical pathway of protein (de)ubiquitination and H2B (de)monoubiquitination. A) The generic biochemical pathway of protein (de)ubiquitination. **B)** The H2Bub1-specific epigenetic "writer" complex RNF20-RNF40-

UBE2A/B and "eraser" SAGA-containing USP22. ATP: Adenosine-triphosphate, AMP: Adenosine-monophosphate, PPi: Diphosphate, DUB: deubiquitinase, ub: ubiquitin, RNF20: Ring Finger Protein 20, RNF40: Ring Finger Protein 40, UBE2A/B: Ubiquitin Conjugating Enzyme E2 A/B, USP22: Ubiquitin Specific Protease 22, SAGA: Spt-Ada-Gcn5 acetyltransferase. Modified from Maupin-Furlow 2012.

2.6.1. CDK9-WAC-RNF20/RNF40-mediated H2Bub1 drives transcriptional elongation

The intricate regulation of CDK9 activity

CDK9 is the central kinase that licenses the transition of RNApol II from the initiation to the elongation phase by catalyzing Ser2-P of the RNApol II CTD. Providing the significant co-localization of RNApol II/Ser2-P and H2Bub1 that was initially discovered in various RNF20/RNF40 dependent genes (Gomes et al. 2006; Minsky et al. 2008a), a strong mechanistic link was hypothesized for these two markers. Indeed, consequent studies showed that CDK9-mediated RNApol II/Ser2-P is indispensable for the catalysis of H2Bub1 (Bowman and Kelly 2014; Pirngruber et al. 2009). Additionally, it was reported that Ser2-P of the RNApol II CTD becomes a docking site for the WW-domain, containing adaptor with coiled-coil protein (WAC). WAC recruits the RNF20/RNF40 E3 ligase complex via its C-terminal coiled-coil region while the N-terminal WW domain recognizes the Ser2-P of the CTD of RNApol II. Hence, WAC enables the coupling of RNApol II-driven transcription with the H2Bub1-machinery at actively transcribed genes (Zhang and Yu 2011; Figure 13).

As previously mentioned, CDK9 is the central promoter-proximal pausing release factor. Due to its major role in promoting a productive transcriptional elongation, its activity is tightly regulated by various upstream factors. Upon recruitment of CDK7, which is the kinase subunit of the TFIIH complex, it phosphorylates and activates CDK9 (CDK9-P^{T186}) (Larochelle et al. 2012). Alternatively, CDK9-P^{T186} was shown to physically interact with the bromodomain protein 4 (BRD4), an epigenetic "reader" recognizing acetylated histone tails, which favors P-TEFb-dependent transcriptional elongation (Mbonye et al. 2013; Moon et al. 2005; Yang et al. 2005). In concordance with the transcription elongating role of the CDK9/Ser2-P axis, BRD4 was shown to promote transcription processivity throughout the gene bodies while loss of BRD4 led to a global decrease of Ser2-P and H2Bub1 (Nagarajan et al. 2014).

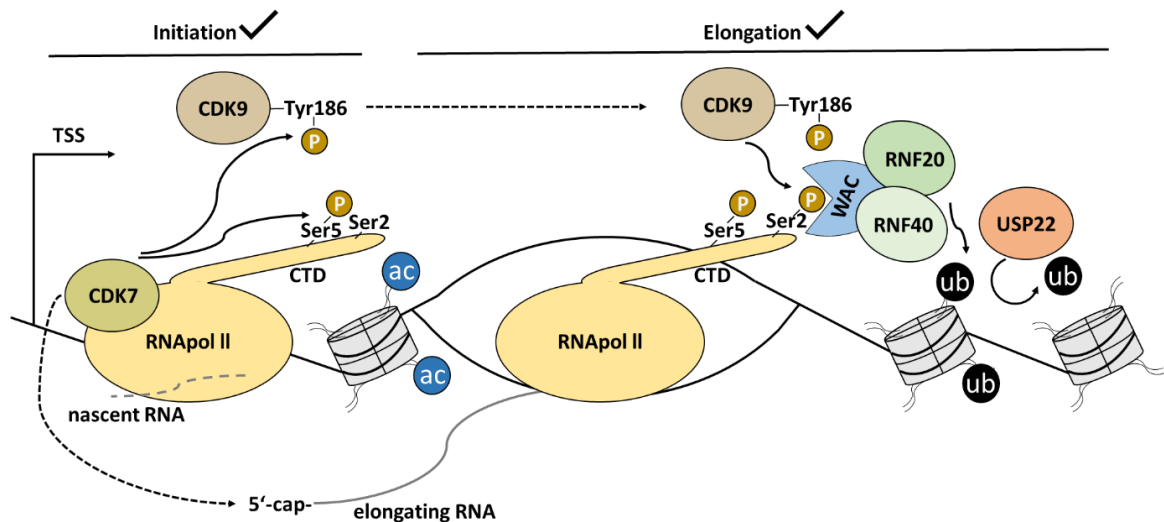


Figure 13: The CDK9-driven biochemical pathway of H2Bub1. The CDK7/Ser-5 axis is responsible for licensing transcriptional initiation while the CDK9/Ser2-P/WAC/RNF20-RNF40 axis leads to ubiquitination of H2B transcriptional elongation. UBE2A and UBE2B are not shown. TSS: Transcription initiation site. CTD: C-terminal domain of RNA Pol II, ub: H2B monoubiquitination, ac: acetylated histone, RNF20: Ring Finger Protein 20, RNF40: Ring Finger Protein 40, UBE2A/B: Ubiquitin Conjugating Enzyme E2 A/B, USP22: Ubiquitin Specific Protease 22.

The intricate regulation of CDK9 activity is illustrated by numerous studies. The P-TEFb complex is normally bound to the 7SKsnRNP (RiboNucleotide Protein) complex, which sequesters P-TEFb from the paused RNAPol II. Paradoxically, this sequestration seems to be dependent on the same CDK7-dependent CDK9 activation (CDK9-P^{T186}). Dephosphorylation of CDK9 is mainly catalyzed by the PP1A and PP1B phosphatases, thereby, disengaging P-TEFb from the 7SKsnRNP complex and increasing the availability of CDK9 for a new CDK7-driven (Figure 14) or BRD4-dependent CDK9 recruitment to the paused RNAPol II (Chen et al. 2008) .

Finally, the ultimate transcription stimulatory function of CDK9 is not limited to the CTD of RNAPol II. To further facilitate the promoter-proximal pausing release of RNAPol II, CDK9 phosphorylates and inhibits two negative transcriptional elongation factors, the negative elongation factor (NELF) and the DRB Sensitivity-Inducing Factor (DSIF). As a consequence, phosphorylated NELF and DSIF allow the paused RNAPol II to continue into transcription elongation (Zhou and Yik 2006; Figure 14).

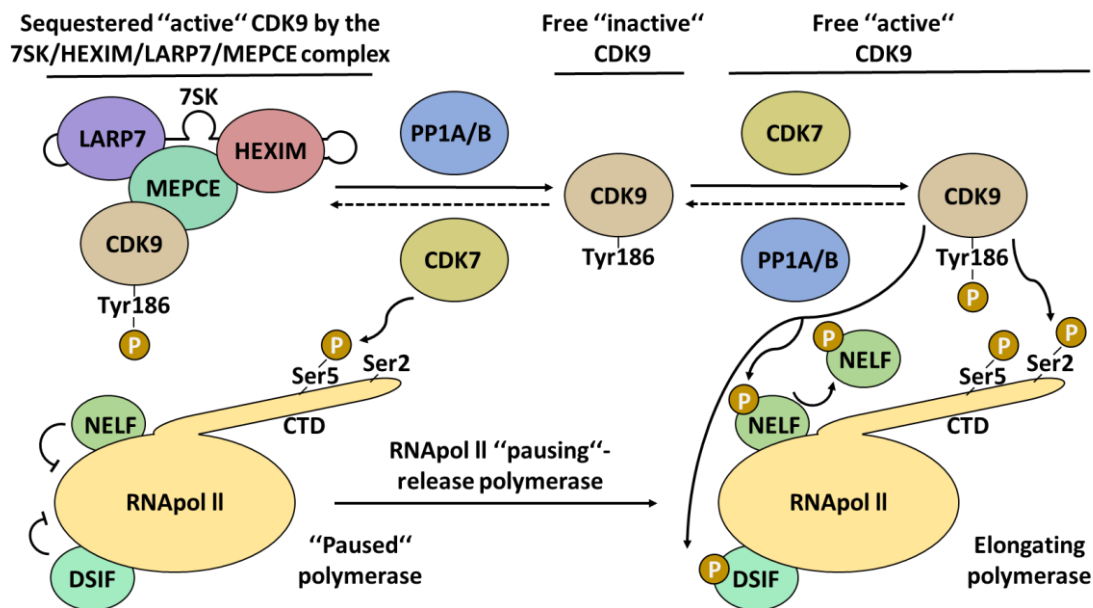



Figure 14: The intricate regulation of CDK9 by CDK7, PP1A/B and 7SK/HEXIM/LARP7/MEPCE complex. HEXIM: Hexamethylene Bis-Acetamide-Inducible Protein, MEPCE: Methylphosphate Capping Enzyme, LARP7: La Ribonucleoprotein 7, 7SK: RNA Component Of 7SK Nuclear Ribonucleoprotein, NELF: Negative Elongation Factor, DSIF: DRB Sensitivity Inducing Factor, PP1A/B: Phosphatase 1A/B, CTD: C-terminal domain of RNApol II, BRD4: Bromodomain containing protein 4.

H2Bub1 leads to transcriptional elongation

The involvement of H2Bub1 in transcriptional regulation was first reported in yeast and later on in mammalian studies showing a transcription-activating role of this hPTM (Fuchs et al. 2014; Sansó et al. 2012; Sen et al. 2013; Song and Ahn 2010; Wozniak and Strahl 2014). H2Bub1 levels have been numerous times related to transcriptional rate and gene expression output (Johnsen 2012; Xie et al. 2017). Specifically, and as later explained in chapter 2.6.5, H2Bub1 was shown to mediate different tissue-specific differentiation programs (Karpiuk et al. 2012; Liang et al. 2018; Liang et al. 2020; Najafova et al. 2020; Robson et al. 2019; Wüst et al. 2020) as well as to sustain the expression of tumor-supportive or –suppressive genes in a context-specific manner (Garrido Castro et al. 2018; Jaaskelainen et al. 2012; Jing et al. 2020; Kosinsky et al. 2019a; Prenzel et al. 2011; Schneider et al. 2019; Wang et al. 2013a).

The role of H2Bub1 in releasing RNApol II from the promoter-proximal state has been several times reported during the last decade (Fuchs et al. 2014; Laroche et al. 2012; Minsky et al. 2008b; Sansó et al. 2012; Xie et al. 2020; Xie et al. 2017). The duration of RNApol II pausing is mainly determined by two promoter-proximal elongation "barriers" which are in part resolved throughout the CDK9/Ser2-PWAC/RNF20-RNF40/H2Bub1-




epigenetic axis and its downstream *trans*-histone crosstalk (see next chapter). The "regulated pausing" relies on two CDK9 targets, NELF and DSIF which exert an inhibitory effect on the elongation licensing of RNApol II (see chapter 2.5.4). Moreover, RNApol II should overcome the nucleosomal barrier that impedes the transcriptional processivity of RNApol II, which is an additional "pausing" layer called "intrinsic pausing" (see chapter 2.5.4; Core and Adelman 2019).

Currently, there are two prevailing, non-mutual exclusive models, proposing the mechanistic role of H2Bub1 in the resolution of the "intrinsic pausing". Based on the first model, Kari et al. reported that loss of H2Bub1 via RNF40 silencing led to a decrease of chromatin-bound SUPT16H and SSRP1 which are the basic subunits of the FACT nucleosome remodeler (Kari et al. 2011). FACT is a histone chaperone that promotes DNA uncoiling from histone octamers, hence the authors hypothesized that transcribing RNApol II can overcome the nucleosomal barrier in a FACT-dependent fashion to maintain transcriptional processivity (Hsieh et al. 2013). On the other hand, the second model suggests that H2Bub1 itself interferes with chromatin compaction and leads to a biochemically accessible fiber conformation due to a plausible steric hindrance between sequential H2B monoubiquitinated nucleosomes (Fierz et al. 2011).

Collectively, in the vast majority of published studies, H2Bub1 mainly exerts an active role in transcriptional elongation via the CDK9/Ser2-P/WAC/RNF20-RNF40 axis. Nevertheless, and as explained later in chapter 2.6.3, there are a few reports pointing to a transcription-repressive role of H2Bub1 in certain contexts. Therefore, further investigation is necessitated to uncover the mechanistic involvement of H2Bub1 and its major catalytic E3 ligase complex, RNF20-RNF40, in transcriptional elongation.

2.6.2. H2Bub1 *trans*-histone crosstalk with H3 methylation

Normally, hPTMs act as docking sites for epigenetic "readers" (e.g bromodomain proteins, recognizing acetylated histones), which in turn exert several biological functions (Chiu et al. 2017; Lam et al. 2020; Maruyama et al. 2002; Oza et al. 2016; Sanchez and Zhou 2009; Yap and Zhou 2011; Zhou et al. 2018). Surprisingly, several hPTMs may affect the addition or removal of other hPTMs *in cis* (within the same histone) or *in trans* (on another histone) (Kirmizis et al. 2007; Nakanishi et al. 2009). The most representative *trans*-histone crosstalk that has been studied extensively is the one between H2Bub1 and H3K4me3 or H3K79me3 in yeasts and mammals (Shilatifard 2006). H3K4me3 is a gene-activating hPTM, extending from the promoter downstream into the gene body, where it promotes a plethora of transcription-associated processes such as RNA splicing and sustained transcriptional elongation of genes (Chen et al. 2015; Davie et al. 2015; Khan et al. 2016;



Xie et al. 2017; Zhang et al. 2016). Furthermore, H3K79me3 has been associated with transcriptional activity but also with other functions such as silencing of telomeric genes and of the DNA damage response (Valencia-Sánchez et al. 2019).


H3K4me3 is catalyzed by the complex proteins associated with set 1 (COMPASS), encompassing variable enzymatic subunits such as SETD1A, SETD1B, KMT2A, and KMT2B (Shilatifard 2012). On the other hand, H3K79me_{1,2,3} is catalyzed by the disruptor of telomeric silencing 1-like (DOT1L) (Chen and Zhu 2016). The integral role of H2Bub1 in these two different *trans*-histone crosstalks was initially uncovered in yeast-based studies showing that depletion of Bre1 or the monoubiquitination H2B mutant (H2BLys123Arg) led to a global pronounced decrease of H3K4me3 and H3K79me3. Inversely, depletion of the H2Bub1-specific DUBs caused a global increase of these hPTMs, strongly supporting the role of H2Bub1 in the *in trans* catalysis of these histone marks (Daniel et al. 2004; Gardner et al. 2005; Henry et al. 2003).

Currently, there are two prevailing models whereby H2Bub1 facilitates the *in trans* histone modification of H3K4me3 and H3K79me3. Based on the "wedge" model, ubiquitin may act as a moiety, providing steric hindrance between nucleosomes, thereby allowing the access of the COMPASS or DOT1L enzymes. The second model, the so-called "bridging" model, proposes that H2Bub1 may function as a docking site for the COMPASS and DOT1L enzymes (Sun and Allis 2002). Based on recent cryo-EM structures, it seems that DOT1L follows the "bridging" model. Specifically, DOT1L is able to bind to the H2A/H2B acidic patch of the nucleosome and the hydrophobic patch of the ubiquitin, including the Ile36, Leu71, and Leu73 residues, the latter two being associated with the activation of the catalytic activity of DOT1L (Holt et al. 2015; Worden et al. 2019).

In agreement, a very recent study from Evan J. Worden et al. showed that the COMPASS complex can interact with the histone octamer core via the Swd1 subunit. Simultaneously, the RxxxRR-containing helix (R=Arg) of Set1 bridges the nucleosome acidic patch with the hydrophobic Ile36, Leu71, and Leu73 residues of the ubiquitin moiety (similar to DOT1L) that are critical for a ubiquitin-dependent COMPASS activity (Holt et al. 2015). However, given the variable enzymatic composition of the mammalian COMPASS complex, it remains unclear whether all H3K4me3-catalyzing enzymes or a fraction of them are dependent on the H2Bub1-mediated *trans*-histone crosstalk.

2.6.3. H2Bub1 in transcriptional repression

In stark contrast to numerous studies pointing to a transcription activating role of H2Bub1, a few studies are proposing a transcription suppressive role for this histone mark. For example, RNF20 was shown to repress a fraction of genes by hindering the recruitment of



the transcription elongation factor S-II (TFIIS) to RNAPol II (Shema et al. 2011). In line, a yeast-based study reported that H2Bub1 facilitates an efficient nucleosomal disassembly in cooperation with the Spt16 subunit of the FACT complex during transcriptional elongation. Also, loss of H2Bub1 led to chromatin structure changes allowing the passage of the transcribing RNAPol II (Fleming et al. 2008). Inversely, another study observed that RNF20/RNF40 overexpression augmented the H2Bub1-mediated stability of the H2A.Z histone variant which in turn impaired the INO80-mediated chromatin remodeling of inducible enhancers (Chandrasekharan et al. 2009; Segala et al. 2016). Finally, a recent study from Men-Ying Wu et al. demonstrated that H2Bub1 and the Anti-Silencing Function 1A Histone Chaperone (Asf1) coordinately promote transcriptional silencing of yeast telomeres, hence, increasing local chromatin stability (Wu et al. 2017a). Collectively, the transcriptional suppressive role of H2Bub1 is context-specific and only reported in a few cases. Therefore, further studies should delineate the opposing function of H2Bub1 in other experimental settings.

2.6.4. RNF20/RNF40-mediated H2Bub1 is indispensable for genomic integrity

H2Bub1 has been numerous times associated with the maintenance of genomic integrity of yeast and mammalian cells. A very elegant study from Evangelista et al. nicely showed that the global H2Bub1 homeostatic machinery is critical for the DNA damage repair pathway. Specifically, H2Bub1 is indispensable for efficient homologous recombination (HR) DNA damage repair (DDR) upon the induction of DNA lesions while coordinated removal of H2Bub1 is equally vital to terminate any unscheduled cycle of HR (Evangelista et al. 2018). Many studies suggested various mechanistic modes where H2Bub1 loss elicits genomic instability. For example, our group has shown that H2Bub1 loss renders DNA damage repair inefficient, thereby leading to an unresolved DNA damage response accompanied by sustained levels of the DDR-marker γ H2AX. Surprisingly, the same study identified that this effect was phenocopied by the loss of the H2Bub1-associated chromosomal remodeler FACT, concluding that H2Bub1 may synergize with FACT to induce dynamic chromatin changes in DNA double-strand breaks (DSBs) (Kari et al. 2011). Indeed, a very recent yeast study confirmed that H2Bub1 is indispensable for histone eviction at DSBs, allowing the access of the HR DNA repair machinery to the nucleosome-free chromatin (Zheng et al. 2018a). In concordance, the Rad6/Bre1/H2Bub1 axis was uncovered to be involved in the maintenance of telomeric length via the HR pathway in yeasts (Wu et al. 2017b). Moreover, the importance of H2Bub1 in HR is strongly reflected by the fact that RNF20-mediated H2Bub1 promotes chromatin relaxation and HR during meiotic recombination, which is indispensable for fertility in sexually reproducing species (Xu et al. 2016).

To sum up, the RNF20/RNF40/H2Bub1 axis is a pathway with a wide range of implications not only in transcription but also in the maintenance of genomic integrity.

2.6.5. The RNF20/RNF40 E3 ligase complex possesses pleiotropic H2Bub1-dependent and -independent physiological functions

The development of multicellular organisms is a complex process involving transcriptomic programs, characterized by a spatiotemporal control of gene expression that results in a plethora of cell lineages. Despite the same genetic information shared among numerous cell types in our body, the emergence of tissue-specific epigenetic changes is the driving mechanism that dictates the tissue-specific gene expression program throughout different cell lineages (Skinner 2011). In this context, H2Bub1 function is associated with a number of differentiation programs.

The RNF20/RNF40 E3 ligase complex has been shown to be implicated in the differentiation program of multiple cell lineages such as adipocytes, astrocytes, heart muscle cells, multipotent stem cells, Schwann cells and osteoblasts in an H2Bub1-dependent manner (Table 1). Moreover, the RNF20/RNF40 complex has been tightly linked to multiple H2Bub1-mediated intracellular regulatory functions characteristic for specific cell types (Table 1). Exceptionally, though, the RNF20/RNF40 complex has been reported to be involved in differentiation programs in an H2Bub1-independent fashion (Table 1). For instance, RNF20 was shown to polyubiquitinate FOXP3, a T-regulatory (T-reg) lymphocyte-specific transcription factor, thereby, promoting its proteasomal degradation and interfering with the differentiation of this lymphocyte population (Cortez et al. 2020).

Concluding, the heterodimeric RNF20/RNF40 complex possesses an extensive role in multiple cell lineage-specific differentiation programs and facilitates different cell-type-specific functions in an H2Bub1-dependent or -independent mode.

Table 1: List of cell type-specific differentiation programs and functions that are dependent on the RNF20/RNF40 E3 ligase complex.

Function	H2Bub1-	Reference
<i>Adipocyte differentiation</i>	independent	(Jeon et al. 2020)
<i>Adipocyte differentiation</i>	dependent	(Liang et al. 2020)
<i>Astrocytic differentiation in the brain</i>	dependent	(Liang et al. 2018)
<i>Autophagy</i>	dependent	(Chen et al. 2017)
<i>Ferroptosis</i>	dependent	(Wang et al. 2019a)

<i>Heart differentiation</i>	dependent	(Robson et al. 2019)
<i>Heat shock response</i>	independent	(In et al. 2019)
<i>Hepatic lipogenesis</i>	independent	(Lee et al. 2014)
<i>Insulin secretion in B-cells</i>	dependent	(Wade et al. 2019)
<i>Multipotent stem cell differentiation</i>	dependent	(Karpiuk et al. 2012)
<i>Myelination of Schwann cells</i>	dependent	(Wüst et al. 2020)
<i>Differentiation of neural precursor cells</i>	dependent	(Ishino et al. 2014)
<i>Neurotransmission</i>	dependent	(Lai et al. 2018)
<i>Neurotransmission</i>	independent	(Chin et al. 2002)
<i>Osteoblast differentiation</i>	dependent	(Najafova et al. 2020)
<i>Somatic cell dedifferentiation</i>	dependent	(Xie et al. 2020)
<i>Stem cell differentiation</i>	dependent	(Fuchs et al. 2014)
<i>Treg cell dedifferentiation</i>	independent	(Cortez et al. 2020)

2.6.6. RNF20, RNF40, and H2Bub1 possess a context-specific role in tumor progression

As previously described, H2Bub1 homeostasis is a prerequisite to facilitate DNA-repair and control context-specific gene expression programs via RNAPol II promoter-proximal pause release. Consequently, imbalance of global H2Bub1 levels was frequently associated with cancer.

For instance, H2Bub1 was shown to behave as a tumor-suppressive epigenetic mark due to its gradual loss in advanced stages of breast, colorectal, serous ovarian, lung, as well as parathyroid cancer (Table 2). Based on numerous studies confirming H2Bub1 as indispensable for the differentiation of various stem or progenitor cells (see previous chapter and Table 1), it has been proposed that the RNF20/RNF40-H2Bub1 axis may block dedifferentiation, thereby, protecting differentiated cells from cell transformation and cancer occurrence (Cole et al. 2015; Reavis and Drapkin 2020; Sethi et al. 2018).

Contrariwise, our group has recently shown that RNF40-deficient mouse embryonic fibroblasts (MEFs) lose the capacity to dedifferentiate into pluripotent stem cells when transduced with the Yamanaka factors (Myc, Sox2, Klf4, Oct4) (Xie et al. 2020). Consistent with a cancer-promoting role, an increasing number of studies highlight unforeseen tumor-supportive functions of the RNF20/RNF40-H2Bub1 axis in a great number of cancer entities (Table 2). A number of these tumor-supportive H2Bub1-dependent functions mainly promote the transcriptomic program of signaling cascades that are intrinsically important for

the studied cancer entity. For instance, loss of the RNF20/H2Bub1 axis leads to an impaired tumorigenic phenotype of MLL-rearranged leukemia (Mixed Lineage Leukemia). MLL2 (KMT2B) is the major H3K4me3 catalytic MLL-fusion enzyme in this cancer entity, hence, the authors observed that RNF20 loss interferes with the H2Bub1-H3K4me3 *trans*-histone crosstalk that drives nodal gene expression programs in this cancer (Wang et al. 2013a). Likewise, blocking the catalysis of H2Bub1 was shown to affect the estrogen-receptor (ESR) and androgen receptor (AR)-responsive transcriptomic profile in ESR-driven BC (Luminal A subtype) and AR-dependent prostate cancer, respectively (Jaaskelainen et al. 2012; Prenzel et al. 2011). Additionally, our group has recently unraveled a novel tumor-supportive role of the RNF40-H2Bub1 axis, sustaining the expression of numerous anti-apoptotic genes in colorectal cancer (Schneider et al. 2019). Consequently, the RNF20/RNF40-H2Bub1 axis demonstrates a very context-dependent role in various cancer entities.

Table 2: List of cancer types where the RNF20/RNF40 E3 ligase complex shows a context-specific role. na=not applicable.

Cancer type	Role in tumor biology	H2Bub1-	Reference
<i>Acute lymphoblastic leukemia</i>	supportive	dependent	(Garrido Castro et al. 2018)
<i>Cervical cancer</i>	supportive	na	(Eckhardt et al. 2018)
<i>Colorectal cancer</i>	supportive	dependent	(Kosinsky et al. 2019a)
<i>Colorectal cancer</i>	suppressive	dependent	(Tarcic et al. 2016)
<i>Colorectal cancer</i>	supportive	dependent	(Schneider et al. 2019)
<i>Glioma</i>	supportive	dependent	(Gao et al. 2011)
<i>Hepatocellular carcinoma</i>	supportive	na	(Zheng et al. 2018b)
<i>Kidney cancer</i>	suppressive	na	(Lee et al. 2017)
<i>Lum A breast cancer</i>	suppressive	dependent	(Prenzel et al. 2011)

<i>Lum A breast and ovarian cancer</i>	supportive	dependent	(Cole et al. 2020)
<i>Luminal A breast cancer</i>	supportive	independent	(Duan et al. 2016)
<i>Luminal A breast cancer/TNBC</i>	supportive/suppressive	dependent	(Tarcic et al. 2017)
<i>Lung cancer</i>	suppressive	dependent	(Jing et al. 2020)
<i>Lung cancer</i>	suppressive	dependent	(Zhang et al. 2017)
<i>MLL-rearranged leukemia</i>	supportive	dependent	(Wang et al. 2013a)
<i>Nodal negative colorectal cancer</i>	suppressive	dependent	(Melling et al. 2016)
<i>Ovarian cancer</i>	suppressive	dependent	(Hooda et al. 2019)
<i>Ovarian cancer</i>	suppressive	dependent	(Dickson et al. 2016)
<i>Parathyroid cancer</i>	suppressive	dependent	(Hahn et al. 2012)
<i>Prostate cancer</i>	supportive	dependent	(Jaaskelainen et al. 2012)

2.7. USP22: a deubiquitinase with multiple protein targets and functions

2.7.1. Cellular function of DUBs

As mentioned in chapter 2.6, ubiquitin-based post-translational modifications (PTMs) are catalyzed by a biochemical cascade including the E1, E2, and E3 ligases. All PTMs are in principle reversible, including protein ubiquitination. The removal of ubiquitin moieties can be performed by deubiquitinases (DUBs), thereby contributing to the homeostasis of free ubiquitin levels within the cells. There are five structurally classified DUB families: the ubiquitin-specific proteases (USPs), the ubiquitin C-terminal hydrolases (UCHs), the Josephin family, the motif interacting with ubiquitin containing novel DUBs (MINDYs), and the Zn-dependent JAB1/MPN/MOV34 metalloprotease DUBs (JAMMs) (Mevisen and Komander 2017).

The biological function of DUBs is pleiotropic and very important for different cellular processes, controlling chromatin accessibility and epigenetic regulation, DNA damage

repair, and signaling transduction. One of the major functions of DUBs is to maintain the stability of various proteins via cleaving the ubiquitin polymers and, hence, protecting poly-ubiquitinated proteins from degradation by the 26S proteasome system. Ubiquitin polymers exert a plethora of additional roles, which greatly depends on their lysine (Lys) linkage-type (Figure 15). For example, the Lys48 "homotypic" ubiquitin polymer is responsible for marking misfolded proteins for proteasomal degradation while the Lys63 variant possesses scaffold properties for a number of signaling pathways such as the NF- κ B pathway (Mevisen and Komander 2017). Furthermore, ubiquitin polymers may contain multiple linkage types following a linear or a branched pattern ("heterotypic" ubiquitin polymer) and whose function is still elusive in cell biology. Finally, the simplest ubiquitin-based PTM is the monoubiquitination of histone (e.g H2Aub1, H2Bub1) and non-histone proteins, a modification that frequently alters the functional properties of the target protein rather than affecting its overall stability (see chapter 2.6; Figure 15). Therefore, depending on the protein target marked by either mono- or polyubiquitination, DUBs can exert different biological functions. Consequently, deregulation of their enzymatic activity is a potential cause of many pathophysiological conditions, including cancer (Mevisen and Komander 2017).

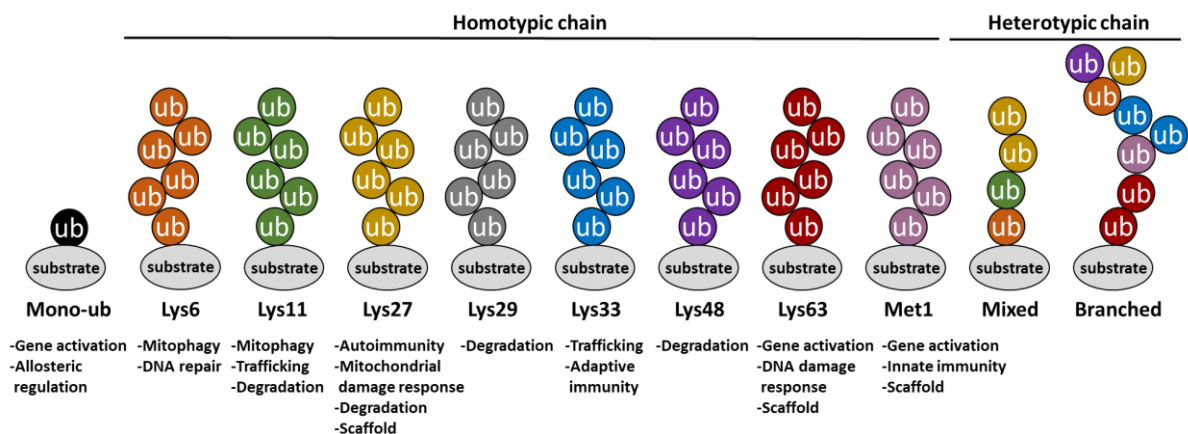



Figure 15: Schematic representation of the increasingly complex ubiquitin code. Monoubiquitination, the least complex modification, can be extended on lysine residues, giving rise to eight homotypic polyubiquitin chains. Heterotypic chains contain more than one linkage type in mixed or branched polymers. ub: ubiquitin. Lys: lysine, Met: methionine. Modified from Mevisen and Komander 2017.

2.7.2. USP22 is the deubiquitinase of the SAGA complex

Ubiquitin-specific protein 22 (USP22) is a member of the USP family with various non-histone and histone targets. In an early study at the beginning of this century, Glinsky et al. confirmed USP22 as a member of the so-called "death-from-cancer" signature. This



signature was shown to possess a strong prognostic power of a short time interval to distant metastasis and high chance of tumor relapse after therapy in several cancer types (Glinsky et al. 2005) (see chapter 2.7.4). Moreover, the role of USP22 has also been characterized in various physiological processes such as cell lineage-specific differentiation programs and cell type-specific functions (see chapter 2.7.3).

USP22 is part of the Spt-Ada-Gcn5 acetyltransferase (SAGA) complex, which is organized into the deubiquitinase module (DUBm), the histone acetyltransferase module (HATm), the SPT (SPTm) and the TAF (TAFm) modules, the latter two involved in modulating the activity of the transcriptional machinery (Wang and Dent 2014). The best characterized enzymatic modules of the SAGA complex are the DUBm and HATm whose catalytic activity are based on USP22 and GCN5, respectively. The DUBm is responsible for the deubiquitination of H2A (H2Aub1) at Lys119 and of H2B (H2Bub1) at Lys120, while GCN5 acetylates H3 at Lys9 (H3K9ac). Due to its complex composition with multiple transcription-regulatory subunits and its dual enzymatic activity, the SAGA complex exerts multiple roles that are tightly linked to chromatin architecture. For example, as shortly mentioned in chapter 2.6.4, the DUBm of the SAGA complex restores the DNA lesion-specific increase of H2Bub1 to basal levels upon a complete cycle of DNA repair (Evangelista et al. 2018). Moreover, many studies point to a functional interplay between the SAGA complex and the transcription and export complex-2 (TREX2) to connect the ongoing transcription with the nuclear pore complex (NPC) for consequent RNA export (García-Oliver et al. 2012). Finally, it was reported that the TAFm of the SAGA complex and the DEAD-Box Helicase 46 (DDX46) control the timing of transcriptional elongation and pre-spliceosomal assembly (Shao et al. 2020).

2.7.3. USP22 controls the differentiation and function of multiple cell lineages

Accumulating evidence points to a pleiotropic nature of USP22 in cell-type-specific differentiation programs, DNA repair and immunity. These documented functions are partly dependent on USP22's DUB activity exerted on monoubiquitination-based hPTMs (H2Aub1, H2Bub1), thereby, modulating the downstream tissue-specific gene expression program (Atanassov et al. 2011). For instance, USP22 deubiquitinates the transcription-suppressive H2Aub1 histone mark in invariant natural killer cells (iNKTs) to promote the expression of genes, necessary for their terminal differentiation (Zhang et al. 2020). In addition, USP22-deficient mice showed an impaired differentiation phenotype of intestine epithelial cells and of the cortical area of the brain (Ji et al. 2019; Kosinsky et al. 2015a). Moreover, it has been shown that B-lymphocyte-specific loss of USP22 in mice interferes

with the antibody class switch recombination by deubiquitinating H2Bub1, leading to inefficient non-homologous end-joining (NHEJ) DNA repair (Li et al. 2018).

Alternatively, USP22 has been numerous times reported to deubiquitinate various non-histone proteins to mainly promote protein stability (Table 3-4). As such, USP22 was found to deubiquitinate and stabilize FOXP3 which is responsible for the differentiation of T-regulatory (Treg) lymphocytes, thereby sustaining the immune tolerance of USP22-proficient mice (Cortez et al. 2020). Furthermore, USP22 can positively regulate the innate immune response of cells upon viral infection via stabilizing karyopherin subunit alpha 2 (KPNA2), the nuclear importin of the interferon responsive factor 3 (IRF3) (Cai et al. 2020). Collectively, USP22 not only is able to orchestrate various cell type-specific differentiation programs but also to exert a few immune-regulatory functions in an epigenetic and non-epigenetic dependent manner (Table 3).

Table 3: List of cell type-specific differentiation programs and functions that are dependent on USP22. na=not applicable

Function	protein target	Reference
<i>Antibody class switch recombination via NHEJ DNA repair</i>	na	(Li et al. 2018)
<i>Co-activates nuclear receptors and counteracts heterochromatin state</i>	H2Aub1/H2Bub1	(Zhao et al. 2008)
<i>Differentiation of iNKT immune cells</i>	H2Ab1	(Zhang et al. 2020)
<i>Differentiation of intestinal epithelial cells</i>	na	(Ji et al. 2019; Kosinsky et al. 2015b)
<i>Differentiation of T-reg cells</i>	Foxp3	(Cortez et al. 2020)
<i>Differentiation of vasculature in the placenta</i>	na	(Koutelou et al. 2019)
<i>Neuronal differentiation</i>	Hes1	(Kobayashi et al. 2015)
<i>Nuclear import of IRF3 to assist interferon response</i>	IRF3	(Cai et al. 2020)
<i>Promotes differentiation of embryonic stem cells</i>	H2Bub1	(Kobayashi et al. 2015)
<i>Regulation of hepatic β-oxidation and oxidative phosphorylation</i>	SIRT1	(Kim et al. 2018a)
<i>Regulation of oxidative environment and inflammation in podocytes</i>	na	(Shi et al. 2016)

2.7.4. USP22 possesses a tumor supportive role in the vast majority of cancer entities

As previously discussed in chapter 2.7.2, USP22 is part of the "death-from-cancer" gene signature which possesses a strong prognostic value to predict tumor relapse, distant metastasis, and overall poor survival of cancer patients (Glinsky et al. 2005). An increasing number of studies have confirmed that USP22 behaves as a tumor-supportive DUB in the majority of cancer types (Table 4). In accordance, USP22 was found to be increased in mRNA and protein levels in different cancer types compared to normal adjacent tissues and was positively associated with the proliferation index of tumor cells. USP22 has been extensively shown to exert multiple oncogenic functions in an epigenetic or a non-epigenetic dependent manner (Melo-Cardenas et al. 2016) (Table 4).

As a basic catalytic subunit of the DUBm of the SAGA complex, USP22 deubiquitinates H2Bub1 and H2Aub1, thereby controlling various tumor supportive transcriptomic programs and modulating chromatin architecture in different contexts. For example, our group has recently showed that USP22 is indispensable for driving the gene expression of the molecular chaperone HSP90AB1 in breast and colorectal cancer. Therefore, patients, suffering from USP22-dependent malignancies may benefit from currently available HSP90-specific pharmacologic inhibitors (Kosinsky et al. 2019b). Also, USP22-driven H2Aub1 deubiquitination was reported to be pivotal for γ H2AX-mediated DNA damage repair and cisplatin resistance in lung adenocarcinoma (Wang et al. 2017).

Apart from regulating the monoubiquitination status of H2A and H2B (Daniel et al. 2004; Henry et al. 2003; Zhang et al. 2008; Zhao et al. 2008), USP22 can deubiquitinate non-histone targets to prolong their protein stabilization and protecting them from the proteasomal degradation. Even more striking is the fact that the vast majority of all acknowledged USP22 non-histone targets possess a well-known tumor supportive role in cancer initiation and progression. For example, USP22 was shown to deubiquitinate MYC in various human breast cancer lines to sustain different carcinogenic features (Kim et al. 2017). Also, a very recent study demonstrated that USP22 deubiquitinates and protects the estrogen-receptor α (ESR α) of luminal A BC cells from proteasomal degradation, hence, confirming the multimodal role of this DUB in a single cancer type (Wang et al. 2020a). Additionally, many studies have shown that USP22 is able to exert its deubiquitinating and protective function on further non-histone tumor-supportive factors (e.g SIRT1, BMI1, CD274, COX2, and CCND1) in various cancer entities (Table 4), strongly arguing for a global role of this DUB in various malignancies.

Apart from the fact that USP22 is directly related to a panel of oncogenic features in cancer cells, it is also able to control immunomodulatory functions. For instance, USP22 was reported in two different cancer entities to prolong the protein stability of CD274, an immune inhibitory receptor ligand that allows the tumor to bypass the immune surveillance and to establish an immune-tolerant tumor microenvironment (Huang et al. 2019; Wang et al. 2020b).

To summarize, USP22 is able to mediate deubiquitination of H2Aub1 and H2Bub1 to directly control transcription and DNA repair, however, its functional versatility has been shown to extend to non-histone targets with numerous implications in cancer disease.

Table 4: List of cancer types where USP22 shows a context-specific role. na=not applicable.

Cancer type	Role in tumor biology	Protein target	Reference
<i>B cell lymphoma</i>	supportive	H2Bub1	(Ramachandran et al. 2016)
<i>Breast cancer</i>	supportive	MYC	(Kim et al. 2017)
<i>Breast cancer (Luminal A)</i>	supportive	ERa	(Wang et al. 2020a)
<i>Cervical cancer</i>	supportive	na	(Gong et al. 2018; J et al. 2019)
<i>Colorectal cancer</i>	suppressive	H2Bub1	(Kosinsky et al. 2020; Kosinsky et al. 2019b)
	supportive	H2Bub1	(Wang et al. 2015)
	supportive	CCNB1	(Lin et al. 2015)
	supportive	SIRT1	(Ao et al. 2014)
<i>Gastric cancer</i>	supportive	SOS	(Lim et al. 2020)
	supportive	BMI1	(Ma et al. 2017)
<i>Glioma</i>	supportive	BMI1	(Qiu et al. 2018)
	supportive	KDM1A	(Zhou et al. 2016)
	supportive	CD274	(Huang et al. 2019)
<i>Hepatocellular carcinoma</i>	supportive	COX2	(Xiong et al. 2017a)
	supportive	SIRT1	(Ling et al. 2017; Xiong et al. 2017b)
	supportive	CCND1	(Pan et al. 2021)
	suppressive	PU.1	(Melo-Cardenas et al. 2018)
<i>Leukemia</i>	supportive	CD274	(Wang et al. 2020b)
	supportive	PALB2	(Nardi et al. 2020)
<i>Lung cancer</i>	supportive	EGFR	(Zhang et al. 2018)
	supportive	H2Aub1,	(Wang et al. 2017)
	supportive	SIRT1	(Xu et al. 2018)
	supportive	COX2	(Xiao et al. 2015)

	supportive	XPC	(McCann et al. 2020)
	supportive	NFATC2	(Gao et al. 2014)
<i>Prostate cancer</i>	supportive	CCND1	(Gennaro et al. 2018)
<i>T cell lymphoma</i>	supportive	RCAN1	(Hong et al. 2015)
<i>Various cancer types</i>	supportive	FBP1	(Atanassov and Dent 2011)

3. Objectives of the study

H2Bub1 is a multifaceted, gene-activating hPTM with numerous physiological and pathological roles in cell biology, hence, it has drawn lots of attention in the cancer epigenetics field. Due to its documented gradual loss in various malignancies (including BC), H2Bub1 was initially thought to function as a universal tumor-suppressive marker (Cole et al. 2015; Reavis and Drapkin 2020; Sethi et al. 2018). However, several other studies have recently reported a tumor-supportive role for this hPTM, revealing its context-dependent role in cancer (see Table 4).

To date, the impact of global H2Bub1 imbalance on BC development, using a GEMM, has been elusive. In addition, the *in vivo* outcome of global H2Bub1 loss has been only ascertained in Lum A BC and TNBC, showing subtype-specific roles in tumor BC progression (Prenzel et al. 2011; Tarcic et al. 2017). On the contrary, the consequence of H2Bub1 homeostasis dysregulation has been so far not described in HER2⁺-BC *in vivo*. Based on the widely supported tumor-suppressive role of H2Bub1 (Marsh et al. 2020; Marsh and Dickson 2019), we do hypothesize that global H2Bub1 loss will aggravate, while global H2Bub1 increase will impede the tumorigenic phenotype of HER2⁺-BC, *in vivo*. To fill these critical gaps, we decided to explore the effect of global H2Bub1 loss or increase in the MMTV-*ErbB2* GEMM for HER2⁺-BC (Rennhack et al. 2019; Taneja et al. 2009). To accomplish that, we genetically deleted *Rnf40* or *Usp22*, the respective major E3 ligase and DUB of H2Bub1, in a mammary tissue-specific manner (Hwang et al. 2003).

Concluding, with this dual study, we expect to unravel the phenotypic, as well as the epigenetic consequences of global H2Bub1 disequilibrium in HER2⁺-BC and to finally picture the context-dependent role of this hPTM in the whole spectrum of BC subtypes.

4. Results: Manuscripts

4.1. Uncovering the biological consequence of global H2Bub1 loss in RNF40-deficient HER2⁺-BC

The 1st part of this work laid the ground for uncovering the role of H2Bub1 and its major E3 ligase, RNF40, in the tumorigenic behavior of an aggressive mammary malignancy, namely HER2⁺-BC. To delineate the biological impact of global H2Bub1 loss in this aggressive malignancy, we employed MMTV-*ErbB2* mice, a conditional *Rnf40* knockout GEMM (mammary tissue-specific) that mimics HER2⁺-BC. Moreover, to solidify the validity of our findings, we applied functional assays and NGS approaches to understand the phenotypic impact and the epigenetic/transcriptomic alterations elicited upon RNF40 loss, using human cell culture models of HER2⁺-BC. Finally, we took advantage of human publically available NGS data and tumor biopsies to further reinforce the translational value of our preclinical findings.

Despite the growing evidence that H2Bub1, as well as its major E3 ligase complex RNF20-RNF40 play a context-dependent role in cancer, several reports associated this epigenetic axis with a tumor-suppressive role in various cancers (Marsh and Dickson 2019; Table 2). Concluding, we speculated that RNF40 and H2Bub1 loss would accentuate the aggressive behavior of HER2⁺-BC, whereas the expression of this markers would associate with a favorable prognosis for HER2⁺-BC patients.

Manuscript I: The histone H2B ubiquitin ligase RNF40 is required for HER2-driven mammary tumorigenesis

Florian Wegwitz^{1,5,*}, **Evangelos Prokakis^{1,*}**, Anastasija Pejkovska¹, Robyn Laura Kosinsky¹, Markus Glatzel², Klaus Pantel³, Harriet Wikman³, Steven A. Johnsen^{1,3,4,#}

¹Department of General, Visceral and Pediatric Surgery, University Medical Center Göttingen, Göttingen, Germany

²Institute for Neuropathology, University of Hamburg-Eppendorf, Hamburg, Germany

³Institute of Tumor Biology, University Medical Center Hamburg-Eppendorf, Hamburg, Germany

⁴Gene Regulatory Mechanisms and Molecular Epigenetics Lab, Division of Gastroenterology and Hepatology, Mayo Clinic, Rochester, MN, USA

⁵Department of Gynecology and Obstetrics, University Medical Center Göttingen, Göttingen, Germany

***These authors contributed equally to this work**

#Address correspondence to johnsen.steven@mayo.edu (S.A.J.)

Running title

RNF40 controls HER2-driven breast cancer

Keywords

RNF40, H2Bub1, actin, ROCK1, cancer

This work was supported by funding from the Deutsche Krebshilfe to S.A.J. (1352320), and to H.W. and K.P. (Priority Program "Translational Oncology"; 70112507).

CORRESPONDING AUTHOR INFORMATION

Steven A. Johnsen, Ph.D.

Division of Gastroenterology and Hepatology

Mayo Clinic

200 First St SW

Rochester, MN 55902

Tel.: +1 507 255-6138

Fax: +1 507 255-6318

Email: johnsen.steven@mayo.edu

Conflict of interest

F.W., E.P., A.P., R.L.K., K.P., H.W., M.G. and S.A.J. declare no conflict of interest.


Abstract

The HER2-driven breast cancer subtype (HER2⁺-BC) displays a particularly aggressive behavior. Anti-HER2 therapies have significantly improved the survival of patients with HER2⁺-BC. However, a large number of patients become refractory to these targeted therapies, necessitating the development of new strategies for advanced disease treatment. Alterations of the epigenome are common in cancers and represent attractive novel molecular therapeutic targets. Monoubiquitination of histone 2B (H2Bub1) by its obligate heterodimeric E3 ubiquitin ligase complex RNF20/RNF40 has been described to have tumor suppressor functions and loss of H2Bub1 has been associated with cancer progression. In this study, we utilized human tumor samples, cell culture models, and a mammary carcinoma mouse model with tissue-specific *Rnf40* deletion and identified an unexpected tumor-supportive role of RNF40 in HER2⁺-BC. We demonstrate that RNF40-driven H2B monoubiquitination is essential for transcriptional activation of the RHO/ROCK/LIMK pathway components and proper actin cytoskeleton dynamics through a trans-histone crosstalk with histone 3 lysine 4 trimethylation (H3K4me3). Collectively, this work demonstrates a previously unknown essential role of RNF40 in HER2⁺-BC, revealing the H2B monoubiquitination axis as a possible tumor context-dependent therapeutic target in breast cancer.

Introduction

Breast cancer (BC) is the most common form of cancer in the female population¹. The survival rates of BC vary greatly and strongly depend on both early detection as well as the molecular subtype². Notably, the HER2-positive breast cancer subtype (HER2⁺-BC) is particularly invasive and displays a poorer prognosis compared to hormone receptor-positive (ER+ or/and PR+) BC³. Importantly, while current anti-HER2 therapies are initially highly effective for many BC patients with HER2⁺-tumors, a significant number of patient tumors develop therapy resistance, tumor relapse, and disease progression⁴. Thus, new approaches are necessary to combat HER2⁺-BC.

Precision oncology approaches aim to utilize or develop novel targeted therapies that exploit tumor-specific dependencies and/or vulnerabilities based on specific molecular alterations present in a given tumor or molecular subtype⁵. Similar to genetic alterations, epigenetic alterations play an important role in tumorigenesis and tumor progression, resulting in altered patterns of DNA methylation, post-translational histone modifications, and changes in chromatin accessibility or chromatin architecture. Due to the reversible nature of many of these changes, numerous substances targeting epigenetic factors are



currently in various stages of preclinical and clinical testing to determine their efficacy as anticancer therapies⁶.

Previous work from our lab and others revealed a particular importance of histone 2B monoubiquitination (H2Bub1) in controlling cellular differentiation⁷⁻¹⁰ and demonstrated that H2Bub1 levels are decreased in ER-positive BC compared to normal adjacent epithelium^{11,12}. These findings have led to the hypothesis that H2Bub1, catalyzed by the obligate heterodimeric Ring Finger Protein 20 and 40 (RNF20/RNF40) E3 ubiquitin ligase complex, has a tumor-suppressive function. This hypothesis has been further supported by studies investigating the function of RNF20 and RNF40¹³⁻¹⁷, while we and others have uncovered tumor-supportive roles of RNF20 and RNF40 in colorectal cancer^{18,19} and androgen-dependent prostate cancer²⁰, suggesting that RNF20/RNF40-driven H2B monoubiquitination plays a context-dependent role in cancer.

H2Bub1 is localized across the body of active genes²¹ and is closely coupled to transcriptional elongation²²⁻²⁵. Studies in both yeast and human cells have revealed a coupling of H2Bub1 and the trimethylation of lysines 4 and 79 of histone 3 (H3K4me3 and H3K79me3, respectively) near the transcriptional start site and transcribed regions of active genes, respectively^{22,26-30}. Interestingly, past studies demonstrated that H3K4me3 extends into the transcribed region of genes displaying a particularly high transcriptional elongation rate³¹. Consistent with H2Bub1 being closely linked to transcriptional elongation²³, we recently demonstrated that loss of RNF40-mediated H2B monoubiquitination results in the narrowing of H3K4me3 domains near the transcriptional start sites (TSS) of important cell fate-determining genes displaying high elongation rates^{10,22,32}.

In this study, we sought to examine the role of RNF40-mediated H2B monoubiquitination in HER2⁺-BC. Our studies using a tissue-specific transgenic and gene ablation approach demonstrate for the first time that RNF40 exerts a profound tumor-supportive function in HER2-driven mammary carcinoma. In support of these *in vivo* findings, we show that RNF40 silencing leads to decreased cell proliferation and specific transcriptional and epigenetic changes in human HER2⁺-BC cell lines. Finally, we unveil a previously undescribed role of RNF40-mediated H2B monoubiquitination in driving the expression of specific genes regulating actin-cytoskeleton dynamics and downstream signaling.

Materials and methods

Animal handling and mouse model generation

Animals were housed under specific pathogen-free (SPF) conditions in accordance with the animal rights laws and regulations of Lower-Saxony (LAVES, registration number #15/1754). See also Supplementary Data for more details.

Histology of human and murine tissues and publically available dataset analyses

Tissue microarrays of human primary and metastatic breast cancer were generated at the University Medical Center Hamburg Eppendorf, Germany (local ethical committee approval number: OB/V/03 and MC-267/13, respectively) in accordance with the ethical standards of the 1964 Declaration of Helsinki. RNF40 and H2Bub1 scoring were established based on the staining intensity (null = no detectable staining, low = weak staining intensity, high = strong staining intensity). Detailed staining procedures and antibodies used for immunohistochemical staining are provided in Supplementary Information.

Publically available datasets

The Kaplan–Meier plotter (kmplot.com) and The Cancer Genome Atlas (<https://portal.gdc.cancer.gov/>)-derived publically available datasets were used to examine the association of RNF40 expression with Relapse-Free Survival (RFS) or Overall Survival (OS) of HER2⁺-BC patients. Parameters for BC subtype classification are given in Supplementary Information. Publically available ChIP-seq datasets for HCC1954 cells (GSE85158 and GSE72956) were downloaded from Gene Expression Omnibus (www.ncbi.nlm.nih.gov/geo/)^{33,34}.

Cell culture, transfections, and functional assays

HCC1954 (CRL-2338™) and SKBR3 (HTB-30™) cells were purchased from the American Type Culture Collection (ATCC®). siRNA transfections were performed using Lipofectamine® RNAiMAX (Invitrogen) according to the manufacturer's guidelines. Proliferation kinetics and tumorspheres were recorded using Celigo® S imaging cytometer (Nexcelom Bioscience LLC) and IncuCyte® Live Cell Analysis System (Sartorius AG). Colonies and migrated cells from transwell assay were washed with PBS, fixed, stained and scanned with an Epson Perfection V700 Photo. Further details are available in Supplementary Data.

Immunofluorescence microscopy

Cells were plated and transfected on coverslips and grown for another 72 h. Cells were then washed with PBS, cross-linked with 4% paraformaldehyde and permeabilized with 1% Triton X-100 in PBS or TBS for 10 min, blocked for 1 h and incubated with the primary antibody overnight. Coverslips were washed and secondary anti-body was applied with DAPI for 1 h at room temperature. Coverslips were washed and mounted on microscope slides. A detailed protocol and a list of antibodies are available in Supplementary Data.

Microscopy

Immunohistochemistry (IHC) pictures were taken with a Zeiss Axio Scope A1. Bright-field images of cultured cells were taken with a Nikon Eclipse S100 inverted microscope and immunofluorescence pictures with a Zeiss LSM 510 Meta confocal microscope. Fluorescence intensity was quantified using the ImageJ software. Image analysis workflow is described in the Supplementary Data.

Annexin and caspase 3/7 activity assay

For annexin V staining, cells were trypsinized and resuspended in binding buffer at 72 h post-transfection and incubated with Annexin-V-FITC (Southern Biotech) and propidium iodide (Sigma–Aldrich) for 15 min at room temperature. Samples were analyzed using a Guava EasyCyte Plus flow cytometer (Guava Technologies).

The kinetic apoptosis assay for caspase 3/7 activity was performed according to the manufacturer's instructions (CS1-V0002(3)-1, ViaStain™ Live Caspase 3/7 Detection Kit, Nexcelom). Scanning was performed 24, 48, and 72 h post-transfection using a Celigo® S imaging cytometer (Nexcelom Bioscience LLC). For detailed proto-cols, please refer to the Supplementary Data.

ChIP library preparation and data analysis

Chromatin immunoprecipitation was performed as described previously³⁵ 72 h after transfection with control or RNF40 siRNAs using antibodies against H2Bub1 (Cat. No. 5546 S, Cell Signaling Technology) and H3K4me3 (Cat. No. C15410003-50, Diagenode). Next-generation sequencing libraries were prepared using the Microplex Library Preparation kit v2 (Diagenode, Cat.No. C05010011) according to manufacturer's instructions and samples were sequenced (single-end 50 bp) on a HiSeq4000 (Illumina) at the NGS Integrative Genomics Core Unit (NIG) at the University Medical Center Göttingen (ArrayExpress accession E-MTAB-9234). Processing of sequencing data was performed in the Galaxy environment (galaxy.gwdg.de). Briefly, ChIP-seq reads were mapped to the hg19 reference genome assembly using Bowtie2 (version 2.3.2.2). PCR duplicates were removed using the RmDup tool (version 2.0.1). The deeptools suite (version 3.2.0.0.1) was utilized to generate normalized coverage files (bamCoverage), call peak changes (bigwigCompare), and to generate aggregate plots and heatmaps (computeMatrix and plotHeatmap). Occupancy profiles were visualized using the Integrative Genomics Viewer (IGV 2.4.8). A detailed analysis work-flow is available in Supplementary Data.

RNA library preparation and data analysis

RNA sequencing libraries were generated from HCC1954 cells at 72 h post-transfection with the NEXTFLEX® Rapid Directional RNA-Seq Kit (Bio Scientific, Catalog #NOVA-5138-07) according to the manufacturer's instructions and samples were sequenced (single-end 50 bp) on a HiSeq4000 (Illumina) at the NIG (ArrayExpress accession E-MTAB-9234). RNA-seq data were processed in the Galaxy environment. Raw reads were trimmed (FASTQ Trimmer), mapped to the reference genome hg19 using TopHat (version 2.1.1) and read counts per gene were calculated with featureCounts. Finally, differential gene expression analysis and normalized counts were obtained using DESeq2. A detailed analysis workflow is available in Supplementary Data.

Results

RNF40 is highly expressed in HER2⁺-BC

While we and others have uncovered potential opposing tumor-supportive or tumor-suppressive roles of H2Bub1 and its E3 ligases RNF20 and RNF40 in ER-positive and triple-negative BC^{11,12,16}, the role of this epigenetic pathway in HER2⁺-BC is currently unclear. Therefore, we investigated RNF40 expression and H2Bub1 levels by immunohistochemical staining of tissue microarrays containing 21 primary HER2⁺-BC samples and 38 brain metastases. Interestingly, all analyzed HER2⁺-BC samples expressed detectable levels of both RNF40 and H2Bub1 (Fig.I.1A–C and Fig.I.S1A). Notably, high levels of RNF40 expression were more frequently detected in HER2⁺ brain metastases compared to primary tumors (Fig.I.1A, B, Fig.I.S1B). We, therefore, examined the relationship between RNF40 mRNA levels and survival in HER2⁺-BC patients using publicly available data (TCGA, KM plotter) and observed that high levels of RNF40 expression were associated with reduced overall, relapse-free and distant metastasis-free survival (Fig.I.1D, E and Fig.I.S1C). Unfortunately, due to the limited number of primary HER2⁺-BC samples analyzed in this study, we were not able to detect any correlation of H2Bub1 or RNF40 levels to tumor grade (Fig.I.S1D). Interestingly, RNF40 expression was found to be significantly higher in HER2⁺-BC tissues compared to normal mammary tissues in the TCGA dataset (Fig.I.S1E). In summary, these data demonstrate that RNF40 expression is not lost in metastatic HER2⁺-BC and that its expression correlates with poor prognosis in these patients.

RNF40 plays a tumor-supportive function in *ErbB2*-driven mammary carcinoma in vivo

Since RNF40 expression and activity were largely maintained in human HER2⁺-BC, we hypothesized that a loss of RNF40 may impair HER2-driven tumorigenesis. To test this hypothesis, we utilized the MMTV-*ErbB2* genetic mouse model³⁶ to generate a tri-transgenic MMTV-*ErbB2*; MMTV-Cre; *Rnf40*^{fl^{ox}} mouse line with mammary tissue-specific co-expression of HER2 and Cre recombinase, and a floxed *Rnf40* allele. This approach enabled us to achieve a simultaneous HER2 over-expression and mammary epithelium-specific ablation of *Rnf40*^{18,22}. Consistent with our findings in human HER2⁺-BC, MMTV-*ErbB2*; *Rnf40*^{wt/wt} tumors did not display a loss of either RNF40 or H2Bub1 when compared to the adjacent normal mammary epithelium (Fig.I.S1F). Moreover, immunohistochemical analyses confirmed that HER2 expression was unaffected by *Rnf40* deletion (Fig.I.1F). However, both heterozygous (*Rnf40*^{wt/fl}), and especially homozygous loss of *Rnf40* (*Rnf40*^{fl/fl}) resulted in a pronounced increase of tumor-free survival of MMTV-*ErbB2* animals (Fig.I.1G). Remarkably, despite the high tumor incidence in this mouse model (100% of *Rnf40*^{wt/wt} mice developed tumors within 220 days), 2 out of 14 *Rnf40*^{fl/fl} animals (14%) never developed tumors within 18 months (Fig.I.1G). Moreover, *Rnf40*^{fl/fl} mice developed significantly fewer tumors than *Rnf40*^{wt/wt} (Fig.I.1H) and displayed strongly reduced tumor growth kinetics (Fig.I.1I). Notably, *Rnf40* loss did not induce morphological changes, as visible in H&E staining of the *Rnf40*^{wt/wt} and *Rnf40*^{fl/fl} tumors (Fig.I.S1H). To estimate the efficiency of *Rnf40* deletion in this model, we performed qRT-PCRs and immunohistochemical staining in *Rnf40*^{wt/wt} and *Rnf40*^{fl/fl} tumors (Fig.I.1J and I.S1G). Consistent with the lack of a complete block in tumor incidence and growth, *Rnf40*^{fl/fl} lesions displayed a heterogeneous pattern of RNF40 expression, suggesting that the few tumors that did develop in this model were largely caused by an incomplete deletion of the *Rnf40* allele. Consistently, similar effects have been reported in several other tumor types and with various Cre models, where rare tumors that appeared consistently retained some expression of the essential floxed gene^{37,38}. This is further supported by the observation that both H2Bub1, as well as the proliferation marker Ki67, displayed a similar heterogeneous expression pattern as RNF40 (Fig.I.1J, I.1.K and Fig.I.S1I). Taken together, these results demonstrate that RNF40 plays an essential role in HER2-driven mammary tumor initiation and progression.

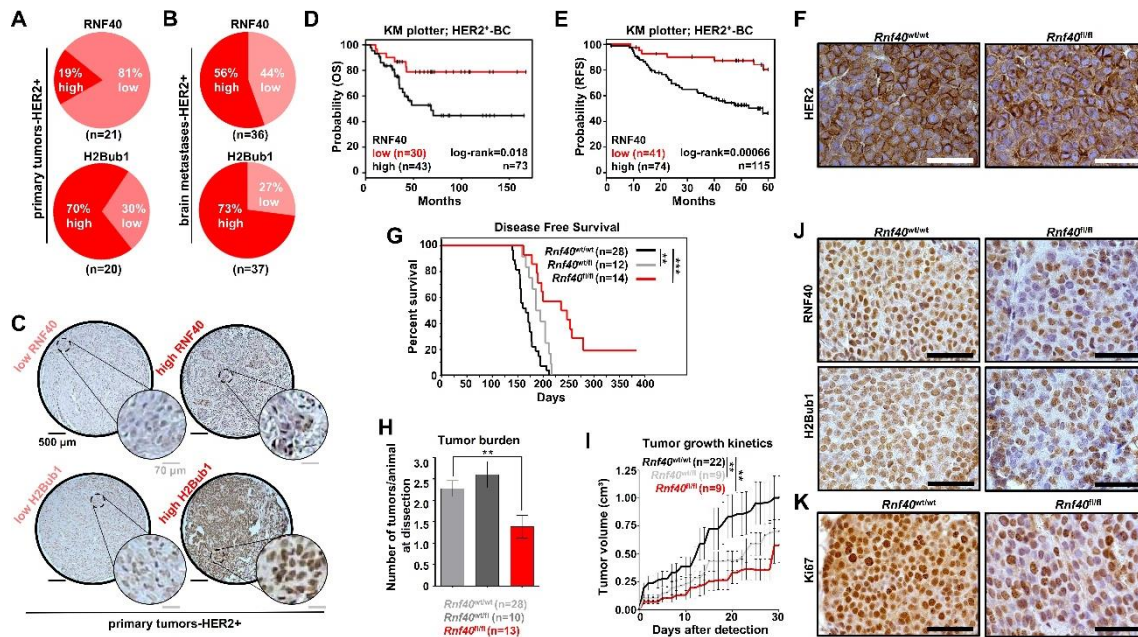


Fig.I.1 RNF40 and H2Bub1 are maintained in HER2⁺-BC. **A, B** TMAs with HER2-positive primary BC (n = 21) and brain metastases (n = 37) were stained for RNF40 and H2Bub1 by IHC. Distribution of RNF40 and H2Bub1 staining intensity in HER2-positive primary BCs (**A**) and brain metastases (**B**). **C** Representative images of low and high H2Bub1 and RNF40 staining intensity in primary HER2-BC specimens. **D, E** Overall survival (OS) (**D**) and relapse-free survival (RFS) plots (**E**) of HER2-BC patients with low and high gene expression of RNF40, using the online tool kmplot.com. Log-rank test. **F** Representative immunohistochemical staining of HER2 in the *Rnf40*^{wt/wt} and *Rnf40*^{fl/fl} mammary carcinomas. **G** Disease-free survival of *Rnf40*^{wt/wt} compared to *Rnf40*^{wt/fl} or *Rnf40*^{fl/fl} mice. Log-rank test. **H** Bar graph depicting the average number of observed tumors per animal in each transgenic mouse cohort. **I** Tumor growth kinetics of all transgenic mouse cohorts. **J, K** Immunohistochemical detection of RNF40, H2Bub1 (**J**) and Ki67 (**K**) in the *Rnf40*^{wt/wt} and *Rnf40*^{fl/fl} mammary carcinomas. Scale bars: 100 μ m. **H, I** One-way ANOVA test. **p < 0.01, ***p < 0.005. Error bars: standard error of the mean (SEM).

RNF40 loss impairs oncogenic properties of HER2⁺-BC cells in vitro

We next sought to investigate the underlying molecular mechanisms determining the dependence of HER2⁺-BC on RNF40. For this purpose, we selected two different human HER2⁺-BC cell lines (HCC1954, SKBR3) and assessed different parameters related to their tumorigenic properties following siRNA-mediated RNF40 knockdown. RNF40 depletion and concomitant loss of H2Bub1 in both cell lines (Fig.I.2A, Fig.I.S2A–B) resulted in reduced cellular confluency compared to control transfected cells (Fig.I.2B). Furthermore, growth kinetics (Fig.I.2C and supplementary video), clonogenic capacity (Fig.I.2D) and

tumorsphere formation (Fig.I.2E, Fig.I.S2C) were strongly impaired upon RNF40 loss in HER2⁺-BC cell lines. In support of these results, an analysis of gene essentiality data from the DepMap portal (<https://depmap.org/>), revealed that HER2⁺-BC cell lines are strongly dependent on RNF40 expression (Fig.I.S2D). Consistently, the levels of the proliferation marker Ki67 were markedly reduced in both HER2⁺-BC cell lines upon RNF40 depletion (Fig.I.2F). Finally, we also tested the migration potential of HCC1954 cells upon RNF40 depletion in a transwell migration (Fig.I.2G) and a gap closure assay (Fig.I.S2E). Both approaches revealed impaired cellular motility upon RNF40 loss. Together with our *in vivo* observations, these findings support that RNF40 expression is essential for maintaining tumorigenic properties of HER2⁺-BC cells *in vitro* and *in vivo*.

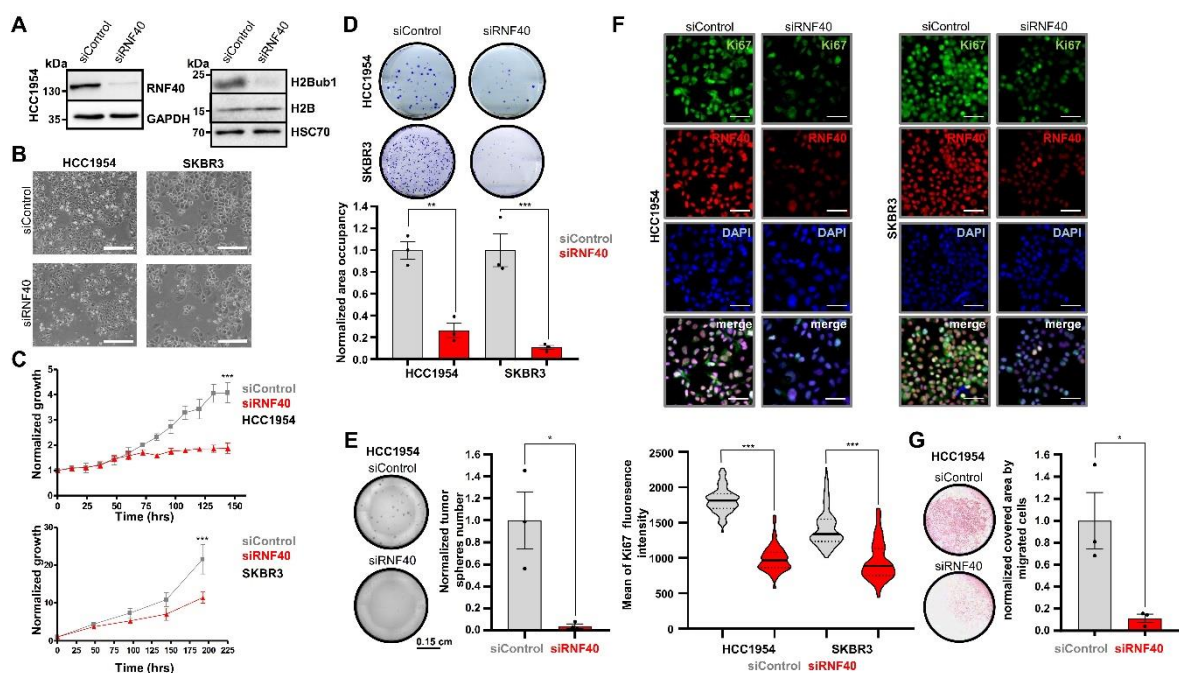


Fig.I.2 RNF40 loss impairs oncogenic properties of HER2-BC cells *in vitro*. **A** Western blot validation of RNF40 knockdown efficiency and decreased H2Bub1 levels in HCC1954 cells. **B** Representative bright-field pictures of control and RNF40 siRNA-transfected HCC1954 and SKBR3 cells. Scale bars (white): 500 μm. **C, D** Proliferation curves (**C**) and clonogenic assays (**D**) of control and RNF40-depleted HCC1954 and SKBR3 cells. Quantification of the occupied area in clonogenic assays is shown for both cell lines (**D**, lower panel). Student t-test. **E** Tumorsphere formation assay of control and RNF40-depleted HCC1954 cells (left panel). Quantification of the tumorsphere number normalized to the control condition (right panel). Student t-test. **F** Representative pictures from immunofluorescence detection of RNF40 and the proliferation marker Ki67 in control and RNF40-depleted HCC1954 and SKBR3 cells (upper panel). Scale bars = 60 μm. Quantification of the Ki67 immunofluorescence intensity of single nuclei in control and RNF40-depleted HCC1954 and

SKBR3 cells (lower panel). The median intensity values of the respective groups are provided as green bars. Mann–Whitney test. **G** Transwell migration assay of control and RNF40-depleted HCC1954 cells with representative results (left panel) and the corresponding quantification (right panel). * $p < 0.05$, ** $p < 0.01$, *** $p < 0.005$. All experiments were performed in biological triplicates. Error bars: SEM.

RNF40 regulates actin-cytoskeleton-related genes in HER2⁺-BC

To understand the underlying mechanism underlying the anti-proliferative effects of RNF40 loss, we tested whether the activity of the signaling cascade downstream of HER2 may be directly affected by RNF40 loss. However, while the HER2 inhibitor lapatinib (lap) significantly blocked ERK and AKT phosphorylation, we could not observe any impairment of the two pathways following RNF40 depletion in either HCC1954 or SKBR3 cells, suggesting that the observed RNF40-dependent effects are not due to alterations in HER2 signaling (Fig.I.3A, Fig.I.S3A). Therefore, given the transcriptional regulatory role of H2Bub1, we performed mRNA-sequencing (mRNA-seq) analyses of HCC1954 cells following RNF40 depletion and identified 360 up- and 324 downregulated genes ($|\log_2 \text{fold change}| > 0.6$; $p < 0.05$) (Fig.I.3B). Consistent with our previous findings in colorectal cancer¹⁹, Gene Set Enrichment Analysis (GSEA) identified a significant enrichment of the “HALLMARK_APOPTOSIS” signature, potentially explaining the reduced oncogenic properties (Fig.I.3C, Fig.I.S3B). In accordance, stratifying HER2⁺-BC patients from The Cancer Genome Atlas (<https://portal.gdc.cancer.gov/>) according to RNF40 expression levels using publically available mRNA-seq data, we observed that RNF40^{low} tumors are also enriched for the same “HALLMARK_APOPTOSIS” gene set (Fig.I.3C, Fig.I.S3C). Increased apoptosis was confirmed by microscopic time-lapse analyses (see supplementary videos), higher levels of cleaved caspase 3 and cleaved PARP in Western blot (Fig.I.3D, Fig.I.S3D) and an increase in Annexin-V-positive cells (Fig.I.3E). Given the fact that RNF40 depletion resulted in decreased cell number and cell migration, we performed additional gene ontology analyses and identified an actin-cytoskeleton regulatory pathway signature as being downregulated following RNF40 depletion ($\log_2 \text{FC} \leq -0.6$, $p < 0.05$) (Fig.I.3F and I.S3E). The downregulation of Vav Guanine Nucleotide Exchange Factor 3 (VAV3), Rho-Associated Coiled-Coil Containing Protein Kinase 1 (ROCK1), LIM Domain Kinase 2 (LIMK2), and Profilin 2 (PFN2), which directly control filamentous actin dynamics, was confirmed in both siRNF40-depleted cell lines at the mRNA (Fig.I.3G and Fig.I.S3F) and protein levels (ROCK1, VAV3; Fig.I.3H, Fig I.S3G).

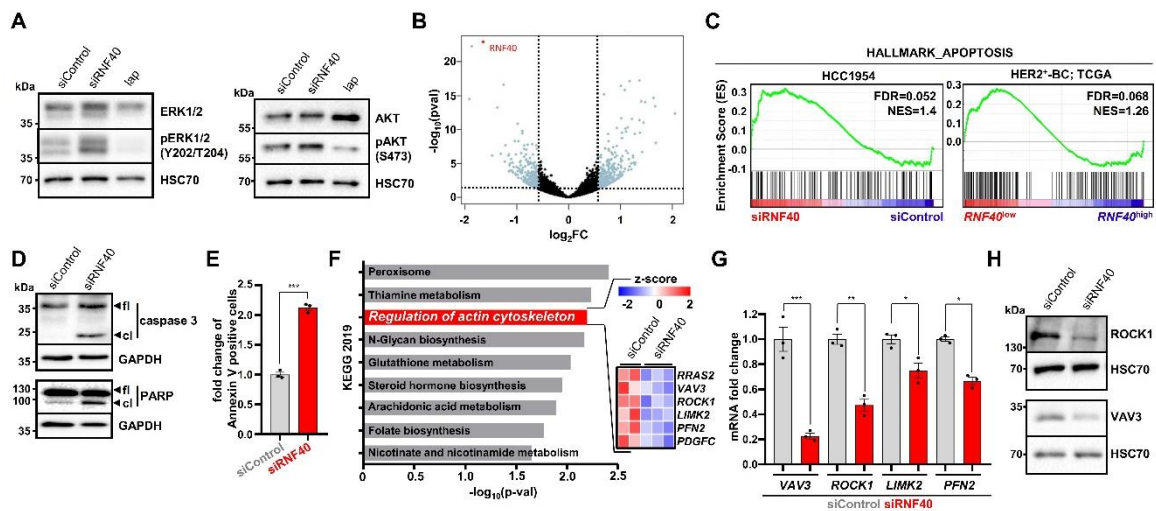



Fig.1.3 RNF40 loss increases apoptosis and impairs the expression of key components of the actin regulatory pathway in HER2⁺ BC. **A** Western blot analysis of the total and phosphorylated forms of ERK1/2 and AKT in control and RNF40-depleted HCC1954 cells. 1 μ M Lapatinib (lap) was applied for 12 h as a positive control. **B** Volcano plot displaying gene expression changes occurring in HCC1954 cells upon RNF40 depletion and measured by mRNA sequencing. **C** Gene Set Enrichment Analysis (GSEA) of the mRNA-sequencing data identified the “HALLMARK_APOPTOSIS” geneset as being significantly enriched in the RNF40-depleted HCC1954 cells and in RNF40^{low}-expressing HER2⁺ BC patients (TCGA). NES normalized enrichment score. **D** Western blot analysis showing that the markers of apoptosis, the cleaved forms of caspase 3 and PARP, are increased in RNF40-depleted HCC1954 cells compared to the control condition. **E** Annexin-V-based flow cytometric analysis of control and RNF40-depleted HCC1954 cells. **F** Pathway enrichment analysis (Enrichr tool; <https://amp.pharm.mssm.edu/Enrichr/>) showing that genes significantly downregulated upon RNF40 knockdown ($\log_2FC \leq -0.6$, $p < 0.05$) are enriched for the KEGG 2019 signature “Regulation of actin cytoskeleton”. A heatmap depicting the differential expression of genes extracted from this signature is shown in the right panel. **G, H** The identified signature was validated via qRT-PCR (**G**) and western blot (**H**) for selected genes in HCC1954 cells. Student t-test. * $p < 0.05$, ** $p < 0.01$, *** $p < 0.005$. All experiments were performed in biological triplicates. Error bars: SEM.

Phosphorylation of the cofilin protein by LIMK downstream of ROCK1 plays an important role in controlling actin-cytoskeleton dynamics³⁹. In its active unphosphorylated form, cofilin destabilizes filamentous actin (F-actin) and leads to actin depolymerization. Interestingly, cofilin phosphorylation (p-cofilin) levels were strongly reduced in RNF40-depleted HCC1954 cells (Fig.1.4A). Phalloidin staining confirmed impaired F-actin formation upon




RNF40 depletion in HCC1954 (Fig.I.4B) and SKBR3 cells (Fig.I.S4A) and these effects could be phenocopied by ROCK1 inhibition (Fig.I.4A, B) and VAV3 knockdown (Fig.I.4C). To exclude a bi-directional regulation between RNF40 and ROCK1, we verified that RNF40 protein levels remained unchanged upon ROCK1 inhibition (Fig.I.S4B). Importantly, cofilin phosphorylation was also markedly decreased in murine Rnf40^{fl/fl} tumors compared to wild type counterparts and significantly associated with H2Bub1 levels (Fig.I.4D). Together, these data confirm the in vitro and in vivo importance of the RNF40/H2Bub1 axis in controlling actin cytoskeletal dynamics in HER2⁺-BC.

The role of the ROCK1 pathway is not limited to the control of actin cytoskeletal dynamics, but also plays a central role in suppressing apoptosis, potentiating cell survival and is significantly associated with poor prognosis in HER2⁺-BC patients⁴⁰⁻⁴⁴. Thus, we hypothesized that the dysregulation of the ROCK1-dependent actin regulatory pathway may be responsible for the apoptotic phenotype induced by RNF40 loss. Indeed, inhibition of ROCK1 by RKI-1447 led to impaired HCC1954 cell proliferation (Fig.I.S4C) and increased caspase 3 cleavage (Fig.I.4E).

Cell-to-substrate focal adhesion complexes are tightly coupled to the actin cytoskeleton and significantly contribute to preserving antiapoptotic pathways via the Focal Adhesion Kinase (FAK)^{42,45}. Thus, we hypothesized that RNF40 depletion may impair focal adhesion signaling by interfering with actin dynamics. To test this hypothesis, we examined if RNF40 loss influences the size of focal adhesions by performing immunofluorescence staining for vinculin, one of the molecules bridging focal adhesion complexes and F-actin. Indeed, the focal adhesion area was substantially decreased upon RNF40 depletion and these effects were phenocopied by VAV3 depletion (Fig.I.4F). Furthermore, both RNF40 depletion and ROCK inhibition reduced the levels of active phosphorylated FAK (p-FAK) (Fig.I.4G). Moreover, consistent with these findings, direct inhibition of FAK led to a significant decrease of HCC1954 cell growth (Fig.I.S4D). Together, our data suggest that RNF40 sustains the tumorigenic phenotype of HER2⁺-BC cells by maintaining actin dynamics and FAK-activity in a ROCK1-dependent manner.

To confirm a role for the actin regulatory pathway in the impaired tumorigenic phenotype of HCC1954 cells upon RNF40 loss, we examined the effects of restoring this signaling cascade. For this purpose, we treated HCC1954 cells with an allosteric sphingosine 1-phosphate receptor-3 agonist (CYM-5441), which was shown to activate actin polymerization as well as increase cancer stem cell expansion in BC^{46,47}. Treatment of RNF40-depleted HCC1954 cells with CYM-5441 significantly rescued apoptosis as measured by Annexin V staining (Fig.I.4H) and caspase 3/7 activity (Fig.I.S4E). Additionally, treatment with either CYM-5441 (Fig.I.4I) or lysophosphatidic acid (Fig.I.S4F),



which has also been shown to activate this pathway⁴⁸, partially rescued the impaired proliferation of HCC1954 cells following RNF40 depletion. Notably, this rescue was prevented by treatment with RKI-1447 (Fig.I.S4G-H), confirming that partial restoration of the actin regulatory pathway is central to the observed partial rescue.

Finally, to verify our findings in human HER2⁺-BC samples, we performed GSEA analyses on publically available mRNA-seq data from The Cancer Genome Atlas (TCGA; <https://portal.gdc.cancer.gov/>) stratifying patients based on RNF40 expression. In addition to H2Bub1-related gene signatures, RNF40^{high} tumors were also significantly enriched for gene sets characteristic for actin filament dynamics and cell adhesion. Similarly, RNF40^{low} tumors were enriched for apoptotic gene signatures (Fig.I.4J, Fig.I.S4I, J). In accordance, like RNF40 (Fig.I.S1B), higher VAV3, ROCK1 and LIMK2 expression is associated with distant metastasis and poor survival outcome in HER2⁺-BC patients (Fig.I.4K).

Collectively, these findings establish the RNF40/ H2Bub1 axis as an important regulator of HER2⁺-BC cell viability by controlling actin regulatory dynamics and focal adhesion signaling via the VAV3-ROCK1-LIMK2-PFN2 cascade.

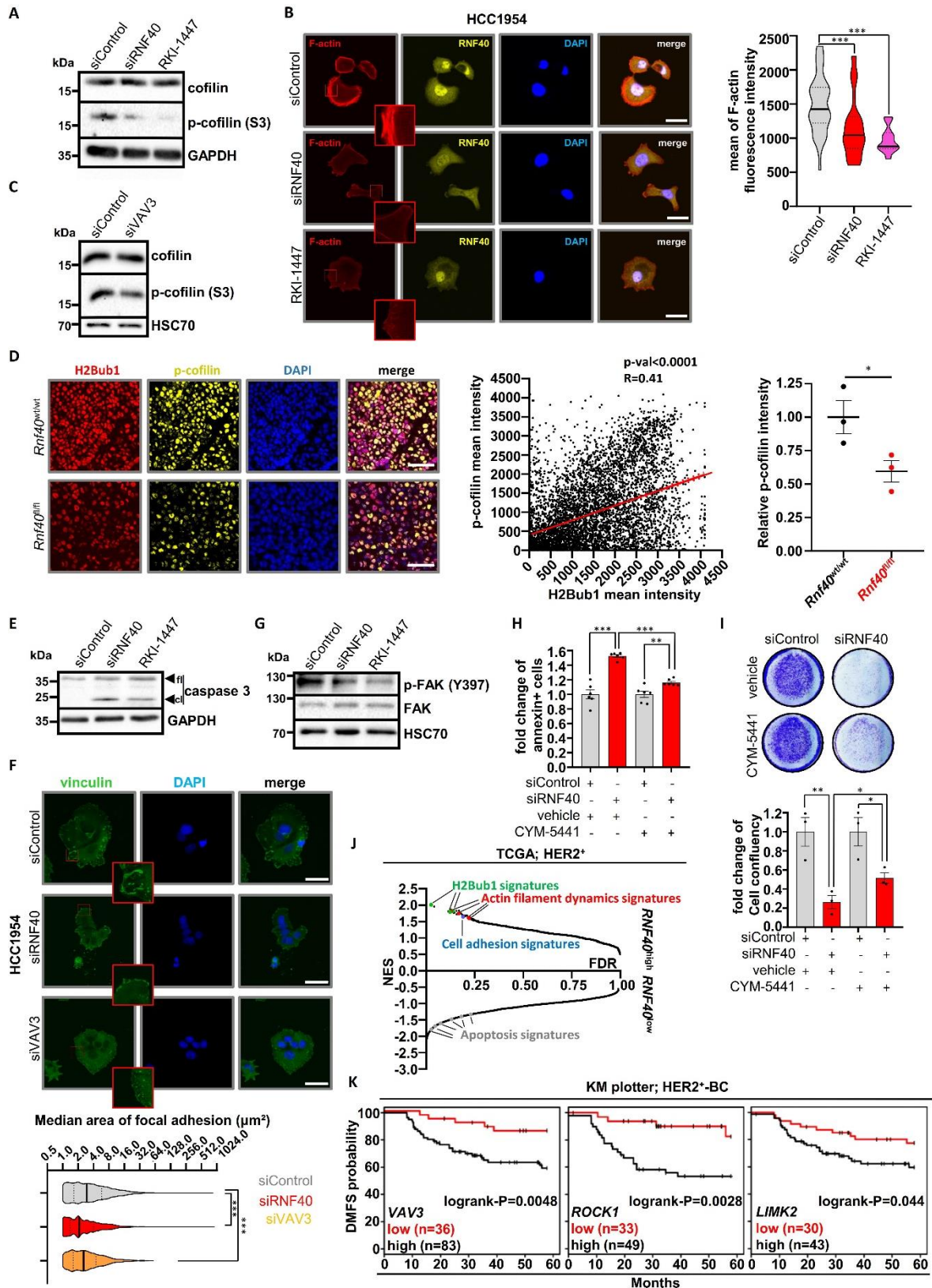



Fig.1.4 RNF40 controls the actin regulatory pathway to sustain the viability of HER2⁺-BC cells in vitro and in vivo. A Western blot analysis showing a reduction of phosphorylated cofilin (p-cofilin) upon RNF40 knockdown and ROCK inhibitor treatment

(RKI-1447, 16 μ M) in HCC1954 cells. **B** Representative pictures of immunofluorescence staining for F-actin in control, RNF40-depleted and RKI-1447-treated (16 μ M) HCC1954 cells (right panel). Quantification of F-actin intensity in the respective conditions (left panel). Scale bars (white) = 50 μ m. ANOVA one-way (Kruskal–Wallis test). **C** Western blot analysis showing a reduction of phosphorylated cofilin in VAV3-depleted HCC1954 cells. **D** Representative pictures of p-cofilin detected by immunofluorescence (left panel), scatter plot showing a correlation of H2Bub1 and p-cofilin intensity in the single tumor cells (middle panel) and quantification of the relative p-cofilin intensity in Rnf40^{wt/wt} and Rnf40^{fl/fl} tumors (right panel, Student t-test). **E** Western blot analysis assessing cleaved caspase 3 levels (cl cleaved, fl full length) in control, RNF40-depleted and RKI-1447-treated HCC1954 cells. **F** Representative immunofluorescence pictures of vinculin in control, RNF40-depleted and VAV3-depleted HCC1954 cells (right panel). Bar graph displaying the median focal adhesion area in the respective conditions (left panel). Scale bars = 50 μ m. ANOVA one-way (Kruskal–Wallis test). **G** Western blot analysis assessing phosphorylated and total FAK levels of control, RNF40-depleted and RKI-1447-treated (16 μ M) HCC1954 cells. **H, I** Annexin V assay (**H**) and proliferation assay (**I**) of control and RNF40-depleted HCC1954 cells with and without the S1PR₃ agonist CYM-5441 (10 μ M). Quantification of cell confluency (lower panel). Student t-test. **J** Graphical representation of all gene sets (C5_GO_Biological_Process) enriched in RNF40^{high}- and RNF40^{low}-expressing HER2⁺-BC biopsies in GSEA analyses. Normalized gene expression data were retrieved from the TCGA portal (<https://portal.gdc.cancer.gov/>). **K** Distant Metastasis-Free Survival (DMFS) based on the expression of VAV3, ROCK1, and LIMK2 in HER2⁺-BC patients. Data were retrieved from the online tool KM plotter (kmplot.com). *p < 0.05, **p < 0.01, ***p < 0.005. All experiments were performed in biological triplicates. Error bars: SEM.

RNF40 regulates the VAV3-ROCK-LIMK2-PFN2 axis through H2Bub1-H3K4me3 trans-histone crosstalk


Cyclin-dependent kinase 9 (CDK9) is a critical upstream regulator of H2B monoubiquitination that functions to recruit the WAC/RNF20/RNF40 complex by phosphorylating the carboxy-terminal domain (CTD) of RNA Pol II, thereby directly coupling H2B monoubiquitination to transcriptional elongation^{7,24}. Thus, we hypothesized that inhibition of CDK9 would phenocopy the effects of RNF40 loss without impairing RNF40 protein expression levels, thereby providing further support for the role of H2Bub1 in the observed effects. Indeed, treatment of HCC1954 cells with a CDK9-specific inhibitor (BAY-1251152; CDK9i, 120 nM) led to a pronounced reduction of H2Bub1 and impaired the expression of all RNF40-dependent actin regulatory genes (Fig.I.5A and I.S5A). Furthermore, CDK9 inhibition phenocopied the proliferative defects and the F-actin



impairment of RNF40-depleted cells, without impairing RNF40 protein expression (Fig.I.S5B-C). Conversely, overexpression of CDK9 in HCC1954 cells significantly increased the expression of RNF40-dependent actin regulatory genes (Fig.I.S5D). Together, these results support a central function of RNF40-mediated H2B monoubiquitination in regulating the expression of central actin regulatory factors.

Previous studies described a crosstalk between H2Bub1 and H3K4 trimethylation (H3K4me3) both in yeast and human systems^{26,29,30}. Moreover, we recently demonstrated that RNF40-mediated H2B monoubiquitination governs the broadening of H3K4me3 from the transcriptional start site (TSS) into the transcribed region to facilitate transcriptional elongation of many moderately H2Bub1-marked genes in mouse embryo fibroblasts (MEFs) and osteoblasts^{10,22}. To examine if RNF40 controls the expression of genes of the actin regulatory network by modulating H2Bub1 and H3K4me3 levels, we performed chromatin immunoprecipitation sequencing (ChIP-seq) analyses (Fig.I.S5E). Strikingly, consistent with our previous findings²², RNF40-dependent genes showed lower levels of H2Bub1 occupancy compared to unregulated genes or genes upregulated following RNF40 depletion (Fig.I.5B). Given our previous finding that H3K4me3 “peak narrowing” is a distinct epigenetic feature involved in the regulation of RNF40-dependent genes, we identified regions with an increase or a global or partial (3’ narrowing) decrease of H3K4me3 occupancy upon RNF40 silencing (Fig.I.5C). The identified regions were then used for differential binding (DiffBind) analyses. Interestingly, the majority of the regions influenced by RNF40 depletion markedly lost H3K4me3 (8518 regions), whereas only a few regions gained H3K4me3 occupancy (351 regions) (Fig.I.5D and Fig.I.5E). Most of the regions showing decreased H3K4me3 (Fig.I.5D) were located near TSS regions (Fig.I.S5F). Moreover, regions displaying no changes in H3K4me3 occupancy displayed only a mild peak narrowing, while regions displaying a significant loss of H3K4me3 occupancy exhibit a stronger peak narrowing upon RNF40 depletion (Fig.I.5E and I.S5G). Importantly, consistent with our gene expression analyses, TSS-associated regions displaying decreased H3K4me3 occupancy following RNF40 depletion included genes associated with the actin regulatory pathway signature (Fig.I.S5H).

We next investigated changes of H3K4me3 occupancy at TSS of robustly down-, up-, and unregulated genes under control or RNF40-depleted conditions. Genes downregulated upon RNF40 silencing displayed the most pronounced decrease in H3K4me3 occupancy in the gene body (the 3’ end of the peak) compared to unregulated or upregulated genes (Fig.I.5F-G). Importantly, a significant fraction of downregulated genes (162 out of 324, $\log_2FC \leq -0.6$, $p < 0.05$) showed a concomitant decrease in H3K4me3 near the TSS (“Group A” in Fig.I.5H). Moreover, this group was enriched for genes involved in controlling




actin dynamics. We validated the decrease in H3K4me3 spreading into the gene body of the ROCK1, LIMK2 and VAV3 genes by ChIP-qPCR (Fig.I.S5I).

As a control, we identified a group of genes with a similar size, similar expression range and comparable H3K4me3 peak width as Group A (Group C), whose expression was not affected by RNF40 knockdown but was characterized by a reduction of H3K4me3 occupancy (Fig.I.5I and I.S6A). We tested the sensitivity of this control group to H2Bub1 loss by verifying the regulation of randomly selected Group C members upon CDK9i treatment. Strikingly, none of the four tested genes were found to be regulated, confirming the validity of our approach (Fig.I.S6B). Under control conditions, Group A genes harbored lower H2Bub1 levels than Group C genes, but comparable H3K4me3 levels and peak height (Fig.I.5J and Fig.I.S6C). However, Group A genes presented a more profound H3K4me3 peak narrowing upon RNF40 depletion compared to Group C (Fig.I.5K and Fig.I.S6D). The 162 genes found to be downregulated at the mRNA level, but not showing any H3K4me3 loss (Group B), displayed overall lower expression values, smaller H3K4me3 regions and displayed only negligible levels of H2Bub1 across their gene body (Fig.I.5H–K, Fig.I.S6A). We, therefore, concluded that the genes within Group B may be indirect downstream targets of RNF40-dependent regulation. Together, these findings support the hypothesis that the actin regulatory gene network is dependent on direct epigenetic regulation by RNF40 through modulation of H2Bub1 and a trans-histone crosstalk with H3K4me3 in HER2⁺-BC cells.

To further investigate the importance of H3K4me3 driving the expression of the actin regulatory genes, we treated HCC1954 cells with OICR9429, which impairs COMPASS-dependent H3K4 methylation by inhibiting WDR5, a common subunit of the SETD1A/B- and MLL1/2-containing methyltransferase complexes⁴⁹. Consistent with our hypothesis, all identified RNF40-dependent actin regulatory genes were downregulated upon treatment, confirming the central role of H2Bub1-dependent H3K4 trimethylation in activating these genes (Fig.I.S6E). Moreover, given the close connection between H3K4me3 spreading and transcriptional elongation at specific genes³¹, we hypothesized that interfering with the negative elongation factor (NELF) might rescue the expression of the actin regulatory genes upon RNF40 loss. Consistently, depletion of NELF-E partially restored the expression of all RNF40-dependent actin regulatory genes in the absence of RNF40 (Fig.I.S6F). This further supports our findings with CDK9 inhibition and further suggests an intimate connection between RNA Pol II elongation, H2Bub1, and H3K4me3 in controlling genes in the actin-cytoskeleton network.

To finally characterize the epigenetic landscape distinguishing Group A and C, and which may further help to explain the RNF40-dependency of Group A genes, we analyzed ChIP-



seq data for several other histone modifications in HCC1954 cells^{33,34}. These analyses revealed that the occupancy of the active histone marks H3K27ac and H3K9ac was slightly higher near the TSS of Group C genes in comparison to Group A, while the elongation-associated modifications, H3K36me3 and H3K79me2, were dramatically higher in the gene body of Group C. Accordingly, RNA Pol II occupancy was also higher on genes in Group C compared to the other groups (Fig.I.S6G). Together, when compared to the genes within Groups A and B, genes within Group C display a more pronounced occupancy of epigenetic marks associated with active gene transcription⁵⁰. Thus, these additional epigenetic modifications may help to compensate for the loss of H2Bub1 following RNF40 depletion, whereas lower levels of these active marks on Group A genes may render them to be more sensitive to changes in H2Bub1/ H3K4me3 occupancy.

In summary, we conclude that RNF40 is a major epi-genetic regulator of the actin regulatory gene network in HER2⁺-BC cells via H2B monoubiquitination and the downstream trans-histone control of H3K4me3 occupancy in the transcribed region.

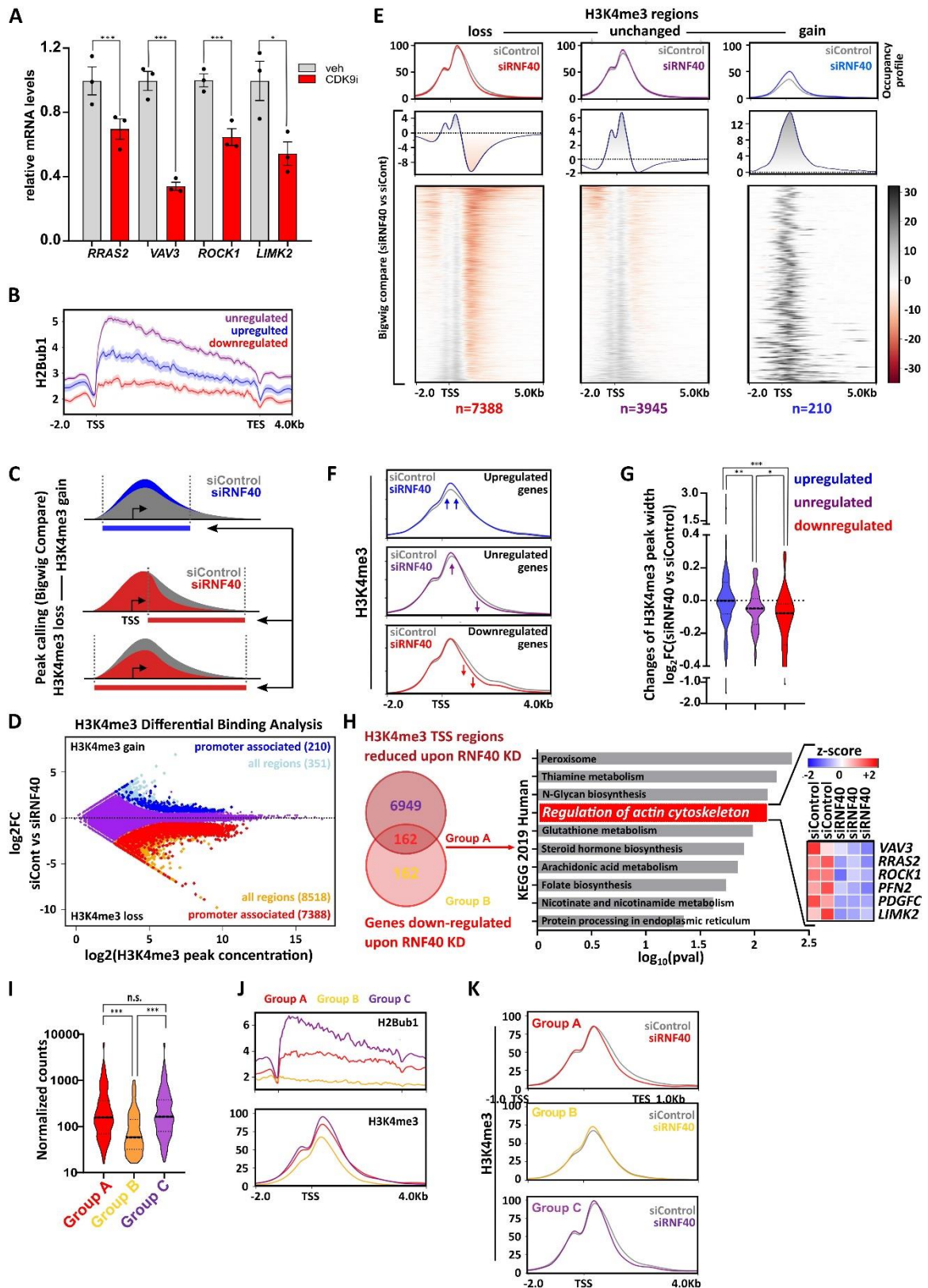



Fig.I.5 RNF40 regulates gene expression of important members of the RHO-ROCK axis in an H2Bub1/H3K4me3-dependent manner. A Expression levels of RNF40-dependent actin regulatory genes in DMSO- and CDK9i-treated (BAY-1251152) HCC1954

cells (120 nM, 6 h) assessed by qRT-PCR. Student t-test. **B** H2Bub1 occupancy profiles at gene body of down-, up-, and unregulated genes upon RNF40 depletion (regulated genes $|\log_2FC| \geq 0.6$, $p < 0.05$, unregulated genes $|\log_2FC| \leq 0.1$, $p > 0.95$). **C** Schematic workflow showing the procedure utilized to identify regions losing or gaining H3K4me3 occupancy upon RNF40 depletion. **D** Differential Binding Analysis results showing H3K4me3 regulated ($|\log_2FC| \geq 0.7$, $FDR < 0.05$) and unregulated regions (in purple). **E** Heatmaps and respective aggregate profiles depicting changes of H3K4me3 occupancy in the identified gained ($\log_2FC \geq 0.7$, $FDR < 0.05$, peak concentration ≥ 6.2), lost ($\log_2FC \leq -0.7$, $FDR < 0.05$, peak concentration ≥ 6.2) or unregulated ($|\log_2FC| \leq 0.2$, $FDR > 0.1$, peak concentration ≥ 6.2) regions upon RNF40 depletion based on the DiffBind analysis results in C. **F** Aggregate plots showing changes of H3K4me3 occupancy at TSS-associated regions of genes identified in RNA-seq analysis as robustly down-, up- ($|\log_2FC| \geq 0.8$, $p < 0.05$), and unregulated ($|\log_2FC| \leq 0.1$, $p > 0.95$) following RNF40 depletion. **G** Quantification of changes in H3K4me3 peak width upon RNF40 depletion in regulated and unregulated genes. ANOVA one-way (Kruskal–Wallis test). **H** Left panel: classification of genes influenced by RNF40 depletion into Group A (simultaneous downregulation and H3K4me3 loss at TSS region), Group B (downregulation without H3K4me3 loss). Right Panel: Group A genes were analyzed for pathway enrichment using the online Enrichr web tool (<https://amp.pharm.mssm.edu/Enrichr3/>). **I** Violin plot providing the median of normalized counts of the three gene groups (Group A, B, and C). ANOVA one-way (Kruskal–Wallis test). **J** Aggregate plots of H2Bub1 and H3K4me3 at basal state in Group A, B, and C genes. **K** Changes in H3K4me3 occupancy at TSS-regions of group A, B, and C genes. H3K4me3 and H2Bub1 ChIP-seq experiments were performed in biological triplicates or duplicates, respectively. * $p < 0.05$, ** $p < 0.01$, *** $p < 0.005$.

Discussion


H2B monoubiquitination has previously been reported to serve a tumor-suppressive function with its levels gradually decreasing during cancer progression. Interestingly, the role of RNF20, a subunit of the obligate heterodimeric RNF20/RNF40 E3 ubiquitin ligase complex catalyzing the deposition of H2Bub1, is more contradictory and has been reported to exert opposing functions depending on cancer type or subtype^{16,17}. To date, only few studies examined RNF40 expression in cancer. Upon examination of a cohort of both primary BC and brain metastases, we identified the loss of RNF40 expression and H2Bub1 as rare events in primary and metastatic HER2⁺-BC lesions. Publically available data-sets corroborate our results, showing only a very low rate of genetic alterations (<1%) causing loss of RNF40 function in BC (cbioportal.org, data not shown). Interestingly, the same



datasets report a much higher frequency of RNF40 locus amplification in malignancies of the breast (4–6%) accompanied by increased RNF40 expression levels in tumors compared to normal tissues (TCGA dataset). Additionally, high expression levels of RNF40 were associated with an unfavorable outcome in HER2⁺-BC patients. Finally, the genetic model for Rnf40 loss in endogenous HER2-driven mammary carcinomas used in this study supported the human patient data, arguing for a tumor-supporting role for RNF40 in HER2-dependent BC. Together, our data do not support a general tumor-suppressive function of RNF40 and H2Bub1.

Upon investigating the transcriptional and molecular epigenetic mechanisms rendering HER2⁺-BC cells critically dependent upon RNF40, we observed that loss of RNF40 had a profound impact on the pattern of occupancy of H3K4me3 leading to a significant “peak narrowing” in the transcribed region downstream of the TSS on regulated genes. The crosstalk between H2Bub1 and H3K4me3 has been intensively studied in the past and has been attributed to the trans-regulation of the histone methyltransferase activity of the COMPASS family of H3K4 methyltransferases by H2Bub1^{7,10,22,24}. Our previous work revealed that RNF40 promotes the expression of a specific subset of genes displaying a high elongation rate via modulation of H3K4me3 peak broadening. Our new integrated datasets in HER2⁺-BC not only support a role for RNF40 in maintaining transcriptional elongation-associated spreading of H3K4me3, but also show that these genes display a less pronounced accumulation of various activating epigenetic marks compared to RNF40-independent genes. Interestingly, RNF40-dependent genes also displayed lower H3K79me2 levels, another histone mark that was shown to function downstream of H2Bub1 to epigenetically regulate gene expression, implying that an additional epigenetic layer helps to control the transcriptional output of RNF40/H2Bub1-independent genes²⁸. We therefore hypothesized that this specific group of genes is rendered particularly sensitive to H2Bub1 loss upon RNF40 depletion due to their overall less active chromatin status.

Strikingly, many genes identified in this study as being RNF40-dependent are well-known effectors of the actin regulatory pathway. In addition to the reported implication of RNF40 in the DNA damage response⁵¹, replication stress¹⁴, microtubule spindle organization⁵², inflammation¹⁸, and regulation of hormone receptor activity^{12,20}, the discovery that the maintenance of actin dynamics critically depends upon RNF40 in HER2⁺-BC is both new and of significant interest. Notably, HER2⁺-BC cells were previously shown to heavily rely on intact actin dynamics for cancer cell viability, motility and metas-tasis^{43,53}. Importantly, we specifically identified VAV3, ROCK1, LIMK2, and PFN2 as RNF40-dependent genes and confirmed the functional consequence of their impaired expression, which resulted in decreased cofilin phosphorylation both in vitro and in vivo, and decreased F-actin



abundance and impaired actin dynamics. Importantly, we identified the ROCK1 kinase as a central RNF40-regulated factor controlling the actin regulatory pathway. Consistently, inhibition of ROCK activity using the specific inhibitor RKI-1447 phenocopied the impaired tumorigenic phenotype caused by RNF40 loss. Interestingly, activation of the actin-cytoskeleton signaling pathway by treating RNF40-depleted cells with an S1PR₃ agonist partially rescued these effects. Therefore, these data strongly suggest that the imbalance in the control of actin dynamics in RNF40-depleted cells is largely dependent on the loss of ROCK1 activity.

In addition to the central role of actin-cytoskeleton dynamics in controlling cellular migration, ROCK1, F-actin and the focal adhesion kinase signaling pathway also have critical functions in suppressing apoptosis and are strongly associated with BC progression including HER2⁺-BC^{41,44,54–57}. While we previously identified a role for RNF40 in suppressing apoptosis in colorectal cancer cells via expression of antiapoptotic members of the BCL2 family of proteins¹⁹, our current results suggest that RNF40 supports HER2⁺-BC tumor viability and tumorigenic features in a distinct manner via maintenance of ROCK-dependent focal adhesion kinase signaling. Our data suggest that RNF40-driven H2B monoubiquitination plays a decisive, context-specific function in HER2⁺-BC by controlling the actin regulatory circuit and down-stream signaling to maintain antiapoptotic signaling and promote cellular migration in cancer cells. It is therefore attractive to speculate that simultaneous inhibition of the RNF20/RNF40 E3 ubiquitin ligase activity, or upstream regulatory components such as CDK9, together with inhibition of either ROCK1 or FAK might provide synergistic effects in the treatment of HER2⁺-BC.

Together, our data support a context-dependent role of RNF40 and H2B monoubiquitination in breast carcinogenesis and suggest that the RNF20/RNF40 E3 ubiquitin ligase and/or its upstream regulators or downstream targets may serve as attractive targets for the development of new anticancer strategies in HER2⁺-BC (Fig.I.6).

Acknowledgements

We would like to thank S. Bolte, N. Molitor, and the staff of the European Neuroscience Institute Göttingen for assistance in the animal handling administration, F. Alves (Translational Molecular Imaging, Max Planck Institute for Experimental Medicine, Göttingen) for access to the IncuCyte[®] Live Cell Analysis System (Sartorius AG), S. Lutz (Institute of Pharmacology and Toxicology, University Medical Center Göttingen, Göttingen) for providing the vinculin antibody, and M. Dobbstein for reagents for measuring caspase 3/7 activity (Department of Molecular Oncology, Göttingen). Also, we want to thank our colleagues Ana Patricia Kutchat and Xin Wang for their productive input. This work was

supported by funding from the Deutsche Krebshilfe to S. A.J. (1352320), and to H.W. and K.P. (Priority Program “Translational Oncology”; 70112507). Open Access funding enabled and organized by Projekt DEAL.

Author details

¹Department of General, Visceral and Pediatric Surgery, University Medical Center Göttingen, Göttingen, Germany. ²Department of Gynecology and Obstetrics, University Medical Center Göttingen, Göttingen, Germany. ³Institute for Neuropathology, University of Hamburg-Eppendorf, Hamburg, Germany.

⁴Institute of Tumor Biology, University Medical Center Hamburg-Eppendorf, Hamburg, Germany. ⁵Gene Regulatory Mechanisms and Molecular Epigenetics Lab, Division of Gastroenterology and Hepatology, Mayo Clinic, Rochester, MN, USA

Conflict of interest

The authors declare that they have no conflict of interest.

Publisher's note

Springer Nature remains neutral with regard to jurisdictional claims in published maps and institutional affiliations.

Supplementary Information accompanies this paper at (<https://doi.org/10.1038/s41419-020-03081-w>).

Received: 23 June 2020 Revised: 18 September 2020 Accepted: 21 September 2020

References of Manuscript I

1. Bray, F. et al. Global cancer statistics 2018: GLOBOCAN estimates of incidence and mortality worldwide for 36 cancers in 185 countries. *CA Cancer J. Clin.* 68, 394–424 (2018).
2. Coleman, M. P. et al. Cancer survival in five continents: a worldwide population-based study (CONCORD). *Lancet Oncol.* 9, 730–756 (2008).
3. Perou, C. M. et al. Molecular portraits of human breast tumours. *Nature* 406, 747–752 (2000).
4. Nahta, R., Yu, D., Hung, M.-C., Hortobagyi, G. N. & Esteva, F. J. Mechanisms of disease: understanding resistance to HER2-targeted therapy in human breast cancer. *Nat. Clin. Pract. Oncol.* 3, 269–280 (2006).
5. Hanahan, D. & Weinberg, R. A. A. Hallmarks of cancer: the next generation. *Cell* 144, 646–674 (2011).
6. Mohammad, H. P., Barbash, O. & Creasy, C. L. Targeting epigenetic modifications in cancer therapy: erasing the roadmap to cancer. *Nat. Med.* 25, 403–418 (2019).
7. Karpiuk, O. et al. The histone H2B monoubiquitination regulatory pathway is required for differentiation of multipotent stem cells. *Mol. Cell* 46, 705–713 (2012).
8. Fuchs, G. et al. RNF20 and USP44 regulate stem cell differentiation by modulating H2B monoubiquitination. *Mol. Cell* 46, 662–673 (2012).

9. Chen, S., Li, J., Wang, D.-L. L. & Sun, F.-L. L. Histone H2B lysine 120 monoubiquitination is required for embryonic stem cell differentiation. *Cell Res.* 22, 1402–1405 (2012).
10. Najafova, Z. et al. RNF40 exerts stage-dependent functions in differentiating osteoblasts and is essential for bone cell crosstalk. *Cell Death Differ.* <https://doi.org/10.1038/s41418-020-00614-w> (2020).
11. Bedi, U. et al. SUPT6H controls estrogen receptor activity and cellular differentiation by multiple epigenomic mechanisms. *Oncogene* 34, 465–473 (2015).
12. Prenzel, T. et al. Estrogen-dependent gene transcription in human breast cancer cells relies upon proteasome-dependent monoubiquitination of histone H2B. *Cancer Res.* 71, 5739–5753 (2011).
13. Zhang, K. et al. Loss of H2B monoubiquitination is associated with poor-differentiation and enhanced malignancy of lung adenocarcinoma. *Int. J. Cancer* 141, 766–777 (2017).
14. Chernikova, S. B. et al. Deficiency in mammalian histone H2B ubiquitin ligase Bre1 (Rnf20/Rnf40) leads to replication stress and chromosomal instability. *Cancer Res.* 72, 2111–2119 (2012).
15. Tarcic, O. et al. RNF20 Links Histone H2B Ubiquitylation with Inflammation and Inflammation-Associated Cancer. *Cell Rep.* 14, 1462–1476 (2016).
16. Tarcic, O. et al. RNF20 and histone H2B ubiquitylation exert opposing effects in Basal-Like versus luminal breast cancer. *Cell Death Differ.* 24, 694–704 (2017).
17. Johnsen, S. A. The enigmatic role of H2Bub1 in cancer. *FEBS Lett.* 586, 1592–1601 (2012).
18. Kosinsky, R. L. et al. Loss of RNF40 decreases NF- κ B activity in colorectal cancer cells and reduces colitis burden in mice. *J. Crohn's Colitis* 13, 362–373 (2019).
19. Schneider, D. et al. The E3 ubiquitin ligase RNF40 suppresses apoptosis in colorectal cancer cells. *Clin. Epigenetics* 11, 98 (2019).
20. Jaaskelainen, T. et al. Histone H2B ubiquitin ligases RNF20 and RNF40 in androgen signaling and prostate cancer cell growth. *Mol. Cell. Endocrinol.* 350, 87–98 (2012).
21. Minsky, N. et al. Monoubiquitinated H2B is associated with the transcribed region of highly expressed genes in human cells. *Nat. Cell Biol.* 10, 483–488 (2008).
22. Xie, W. et al. RNF40 regulates gene expression in an epigenetic context-dependent manner. *Genome Biol.* 18, 32 (2017).
23. Fuchs, G., Hollander, D., Voicheck, Y., Ast, G. & Oren, M. Cotranscriptional histone H2B monoubiquitylation is tightly coupled with RNA polymerase II elongation rate. *Genome Res.* 24, 1572–1583 (2014).
24. Pirngruber, J. et al. CDK9 directs H2B monoubiquitination and controls replication-dependent histone mRNA 3'-end processing. *EMBO Rep.* 10, 894–900 (2009).
25. Pavri, R. et al. Histone H2B monoubiquitination functions cooperatively with FACT to regulate elongation by RNA polymerase II. *Cell* 125, 703–717 (2006).
26. Sun, Z.-W. W. & Allis, C. D. Ubiquitination of histone H2B regulates H3 methylation and gene silencing in yeast. *Nature* 418, 104–108 (2002).
27. Ng, H. H., Xu, R.-M. M., Zhang, Y. & Struhl, K. Ubiquitination of histone H2B by Rad6 is required for efficient Dot1-mediated methylation of histone H3 lysine 79. *J. Biol. Chem.* 277, 34655–34657 (2002).
28. Valencia-Sánchez, M. I. et al. Structural basis of Dot1L stimulation by histone H2B lysine 120 ubiquitination. *Mol. Cell* 74, 1010–1019 (2019). e6.

29. Kim, J. et al. RAD6-mediated transcription-coupled H2B ubiquitylation directly stimulates H3K4 methylation in human. *Cells* 137, 459–471 (2009).
30. Kim, J., Hake, S. B. & Roeder, R. G. The human homolog of yeast BRE1 functions as a transcriptional coactivator through direct activator interactions. *Mol. Cell* 20, 759–770 (2005).
31. Chen, K. et al. Broad H3K4me3 is associated with increased transcription elongation and enhancer activity at tumor-suppressor genes. *Nat. Genet.* 47, 1149–1157 (2015).
32. Xie, W., Miehe, M., Laufer, S. & Johnsen, S. A. The H2B ubiquitin-protein ligase RNF40 is required for somatic cell reprogramming. *Cell Death Dis.* 11, 287 (2020).
33. Franco, H. L. et al. Enhancer transcription reveals subtype-specific gene expression programs controlling breast cancer pathogenesis. *Genome Res.* 28, 159–170 (2018).
34. Malladi, S. et al. Metastatic latency and immune evasion through autocrine inhibition of WNT. *Cell* 165, 45–60 (2016).
35. Hamdan, F. H. & Johnsen, S. A. DeltaNp63-dependent super enhancers define molecular identity in pancreatic cancer by an interconnected transcription factor network. *Proc. Natl Acad. Sci. USA* 115, E12343–E12352 (2018).
36. Guy, C. T. et al. Expression of the neu protooncogene in the mammary epithelium of transgenic mice induces metastatic disease. *Proc. Natl Acad. Sci. USA* 89, 10578–10582 (1992).
37. Miao, R. Y. et al. MYB is essential for mammary tumorigenesis. *Cancer Res.* 71, 7029–7037 (2011).
38. Costa, T. D. F. et al. PAK4 suppresses RELB to prevent senescence-like growth arrest in breast cancer. *Nat. Commun.* 10, 3589 (2019).
39. Maciver, S. K. & Hussey, P. J. The ADF/cofilin family: actin-remodeling proteins. *Genome Biol.* 3, reviews3007.1–3007.12. <https://genomebiology.biomedcentral.com/articles/10.1186/gb-2002-3-5-reviews3007>. (2002).
40. Desouza, M., Gunning, P. W. & Stehn, J. R. The actin cytoskeleton as a sensor and mediator of apoptosis. *Bioarchitecture* 2, 75–87 (2012).
41. Patel, R. A. et al. RKI-1447 is a potent inhibitor of the Rho-associated ROCK kinases with anti-invasive and antitumor activities in breast cancer. *Cancer Res.* 72, 5025–5034 (2012).
42. Chrzanowska-Wodnicka, M. & Burridge, K. Rho-stimulated contractility drives the formation of stress fibers and focal adhesions. *J. Cell Biol.* 133, 1403–1415 (1996).
43. Tavares, S. et al. Actin stress fiber organization promotes cell stiffening and proliferation of pre-invasive breast cancer cells. *Nat. Commun.* 8, 15237 (2017).
44. Tawab Osman, N., Khalaf, M. & Ibraheem, S. Assessment of CIP2A and ROCK-I expression and their prognostic value in breast cancer. *Pol. J. Pathol.* 71, 87–98 (2020).
45. Choong, G., Liu, Y. & Templeton, D. M. Cadmium affects focal adhesion kinase (FAK) in mesangial cells: involvement of CaMK-II and the actin cytoskeleton. *J. Cell. Biochem.* 114, 1832–1842 (2013).
46. Donati, C. & Bruni, P. Sphingosine 1-phosphate regulates cytoskeleton dynamics: implications in its biological response. *Biochim. Biophys. Acta* 1758, 2037–2048 (2006).
47. Wang, Y. C. et al. Benzyl butyl phthalate promotes breast cancer stem cell expansion via SPHK1/S1P/S1PR3 signaling. *Oncotarget* 7, 29563–29576 (2016).
48. Yung, Y. C., Stoddard, N. C. & Chun, J. LPA receptor signaling: pharmacology, physiology, and pathophysiology. *J. Lipid Res.* 55, 1192–1214 (2014).

49. Lu, K., Tao, H., Si, X. & Chen, Q. The histone H3 lysine 4 presenter WDR5 as an oncogenic protein and novel epigenetic target in cancer. *Front. Oncol.* 8, 502 (2018).
50. Zhang, T., Cooper, S. & Brockdorff, N. The interplay of histone modifications—writers that read. *EMBO Rep.* 16, 1467–1481 (2015).
51. Kari, V., Shchebet, A., Neumann, H. & Johnsen, S. A. The H2B ubiquitin ligase RNF40 cooperates with SUPT16H to induce dynamic changes in chromatin structure during DNA double-strand break repair. *Cell Cycle* 10, 3495–3504 (2011).
52. Duan, Y. et al. Ubiquitin ligase RNF20/40 facilitates spindle assembly and promotes breast carcinogenesis through stabilizing motor protein Eg5. *Nat. Commun.* 7, 12648 (2016).
53. Nersesian, S. et al. Effects of modulating actin dynamics on HER2 cancer cell motility and metastasis. *Sci. Rep.* 8, 17243 (2018).
54. Walker, S. et al. Oncogenic activation of FAK drives apoptosis suppression in a 3D-culture model of breast cancer initiation. *Oncotarget* 7, 70336–70352 (2016).
55. Al-Juboori, S. I. K. et al. PYK2 promotes HER2-positive breast cancer invasion. *J. Exp. Clin. Cancer Res.* 38, 210 (2019).
56. Wang, Z. et al. GPER stabilizes F-actin cytoskeleton and activates TAZ via PLC β -PKC and Rho/ROCK-LIMK-Cofilin pathway. *Biochem. Biophys. Res. Commun.* 516, 976–982 (2019).
57. Shao, J., Zhang, H. & Wang, Z. Coronin 1c and F-actin promote metastasis of breast cancer. *Med. Sci. Monit.* 24, 5980–5987 (2018).

Supplements

Supplementary Figures

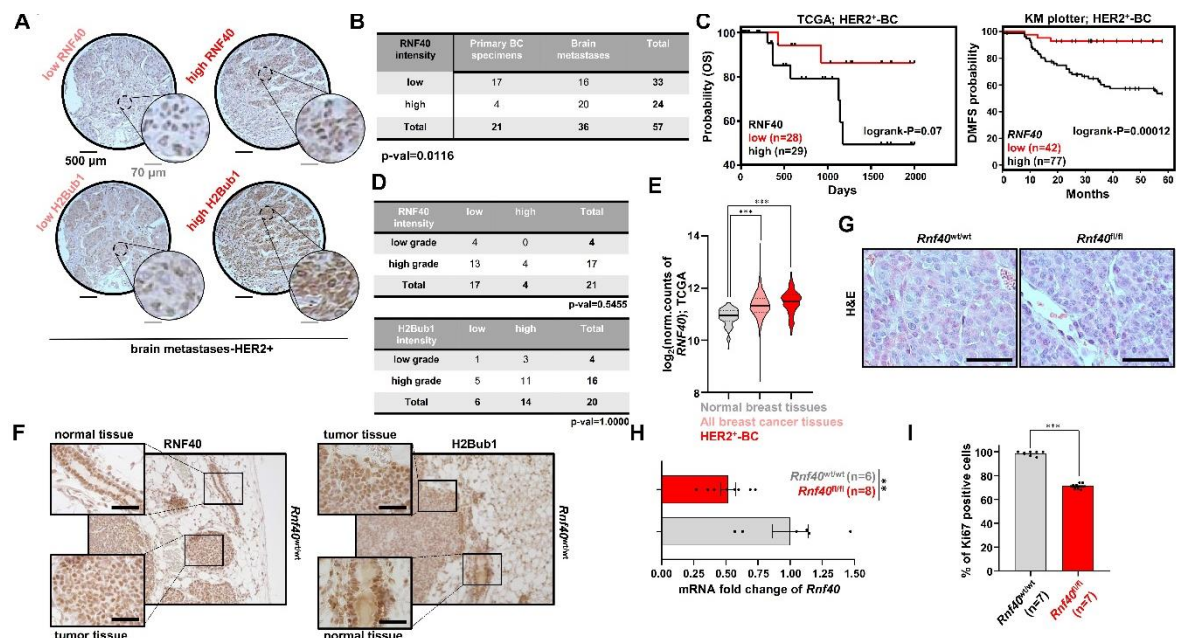


Fig.I.S1 RNF40 and H2Bub1 loss are rare events and do not advantage tumor growth in HER2-positive malignancies of the breast. A: Representative pictures of low and high H2Bub1 and RNF40 staining in HER2-positive brain metastases TMA specimens. **B:** 2x2

contingency table of RNF40^{low}- and RNF40^{high}-expressing primary tumors and brain metastases biopsies. Fisher exact test. **C:** Overall survival (OS) and Distant Metastasis-Free Survival (DMFS) analysis of RNF40^{low}- and RNF40^{high}-expressing HER2-positive BC patients, retrieved from TCGA (<https://xenabrowser.net/>) and KM-plotter (kmplot.com), respectively. **D:** 2x2 contingency table of RNF40^{low}-, RNF40^{high}-, H2Bub1^{low}- and H2Bub1^{high}-expressing primary tumors compared to their respective tumor grade. Fisher exact test. **E:** RNF40 expression is in overall higher in breast tumor tissues (n=6470) and in the HER2-enriched BC subtype (n=82), than in their normal healthy counterparts (n=101) (log₂normalized counts, source=TCGA BRCA dataset). One-way ANOVA (Kruskal-Wallis-test). **F:** Representative pictures of RNF40 and H2Bub1 immunohistochemical staining on Rnf40^{wt/wt} normal mammary epithelial tissues adjacent to growing tumors. Scale bar: 100 μm. **G:** Representative pictures of hematoxyline-and-eosin (H&E) stained Rnf40^{wt/wt} and Rnf40^{fl/fl} tumors. Scale bar: 100 μm. **H:** RT-qPCR validation of the Rnf40 knockout efficiency in murine primary tumor tissues at the gene expression level. **I:** Quantification of Ki67 positive cells in IHC stained paraffin sections of Rnf40^{wt/wt} and Rnf40^{fl/fl} tumors (n=7 tumors per mouse cohort, n=2 analyzed pictures per tumor). **p-val<0.01, ***p-val<0.005. Student t-test. **H** and **I:** error bars= SEM.

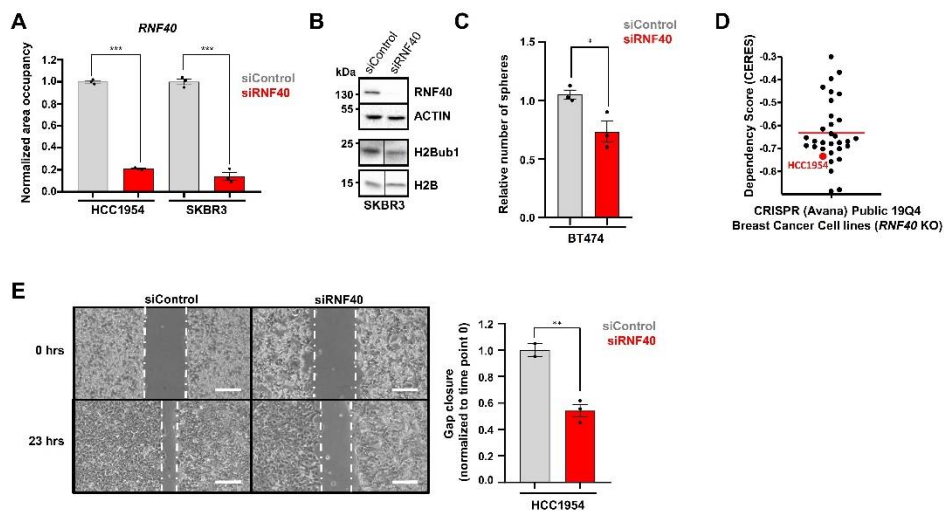


Fig.I.S2: RNF40 loss impairs oncogenic properties of HER2-positive BC cells *in vitro*.

A: Validation of the RNF40 silencing in HCC1954 and SKBR3 cells using qRT-PCR. **B:** Validation of the RNF40 silencing and H2Bub1 decrease in siRNF40-treated SKBR3 cells by western blot analysis. **C:** Tumor sphere formation assay of siControl- and siRNF40-treated BT474 cells. Student t-test. **D:** Essentiality of RNF40 in various breast cancer cell lines, as assessed in the CRISPR-Cas9 screen Avana 19Q4 (<https://depmap.org>) **E:** Representative pictures (left panel) and quantification (right panel) of a gap closure assay from siControl- and siRNF40-transfected HCC1954 cells. Error bars: SEM. Student t-test.

p-val<0.01, *p-val<0.005. White scale bars: 500 μ m. All experiments were performed in biological triplicates. Error bars: SEM.

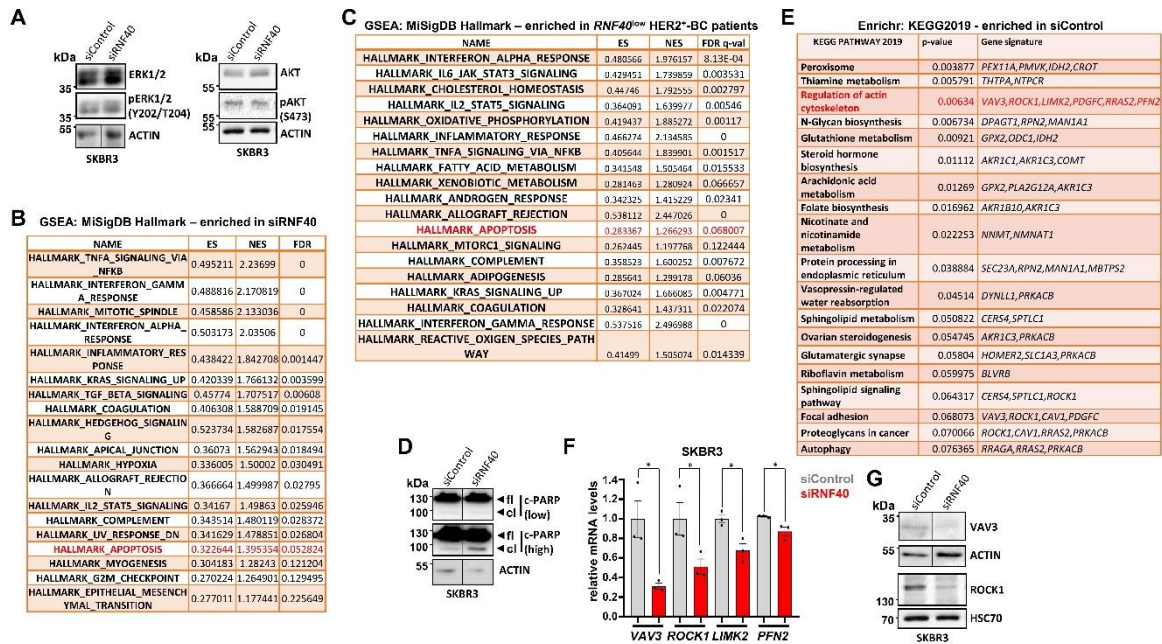


Fig.I.S3: RNF40 loss increases apoptosis and impairs the expression of important key-effectors of the actin regulatory pathway in HER2-positive BC cells. A: Western blot analysis of ERK1/2, pERK1/2, AKT, pAKT levels in siControl- and siRN40-treated SKBR3 cells. **B-C:** List of gene signatures enriched (FDR < 0.25) in siRN40-treated HCC1954 (**B**) as well as in *RNF40^{ow}*-expressing HER2⁺-BC biopsies (**C**) (normalized sequencing data were retrieved from TCGA portal; GSEA analysis, HALLMARK gene sets). **D:** Western blot analysis of cl-PARP (cleaved PARP) and fl-PARP (full-length PARP) levels in siControl- and siRN40-treated SKBR3 cells. **E:** List of enriched gene signatures in HCC1954 cells upon siControl-treatment (Enrichr analysis, KEGG 2019 database). **F:** Validation of the *VAV3*, *ROCK1*, *LIMK2* and *PFN2* downregulation in siRN40-treated SKBR3 cells via qRT-PCR. **G:** Western blot analysis of ROCK1 and VAV3 protein levels in siControl- and siRN40-treated SKBR3 cells. All qRT-PCRs and western blot analyses were performed in biological triplicates. Student t-test. *p-val<0.05. Error bars: SEM.

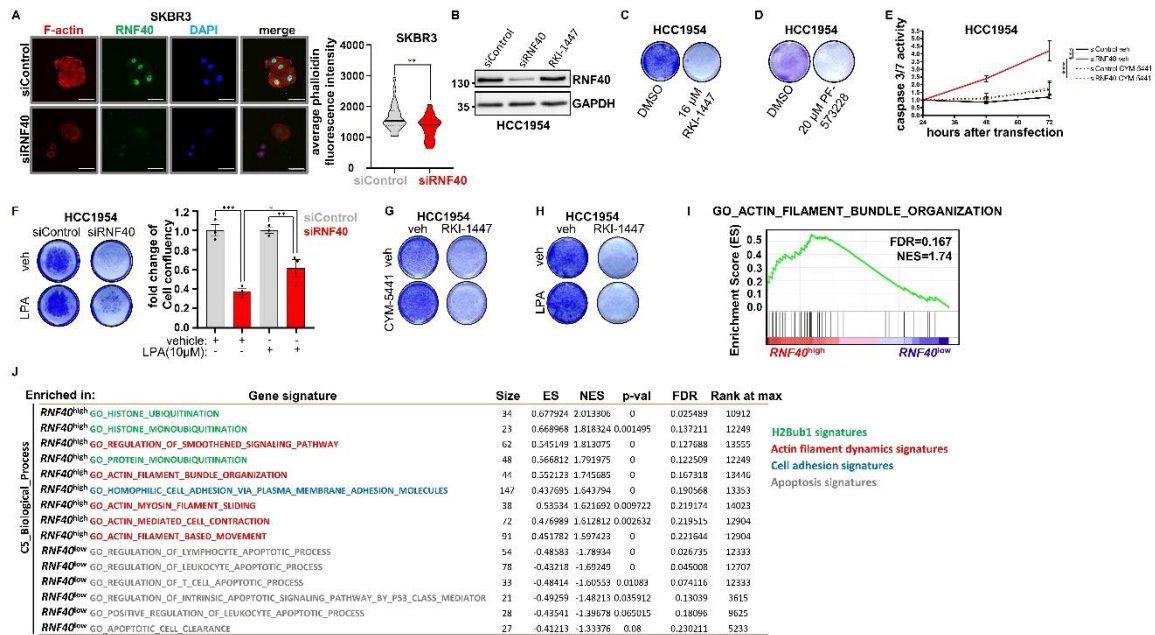


Fig.I.S4: RNF40 controls the actin regulatory pathway to sustain the viability of HER2-positive BC cells *in vitro* and *in vivo*. **A:** Representative pictures of immunofluorescence staining of F-actin (phalloidin) in siControl- and siRNF40-treated SKBR3 cells (left panel). Scale bars (red) = 50 μ m. Quantification of F-actin intensity in the respective conditions (right panel). Mann-Whitney test. **B:** Western blot analysis of RNF40 levels in siControl-, siRNF40- and RKI-1447-treated HCC1954 cells (16 μ M, ROCK inhibitor). **C-D:** Crystal violet staining of HCC1954 cells showing a loss of confluency upon RKI-1447 (16 μ M, ROCK inhibitor) (C) or PF-373228 (20 μ M, FAK inhibitor) treatment (D) compared to DMSO control. **E:** Cleaved caspase 3 and 7 activity kinetics measurement in siControl- and siRNF40 treated HCC1954 cells with and without S1PR₃ agonist treatment. **F:** Crystal violet staining of siControl- and siRNF40-treated HCC1954 cells with and without rescue through 10 μ M LPA treatment. Quantification of cell confluency (right panel). Student t-test. **G-H:** Crystal violet staining of vehicle and RKI-1447 (16 μ M) treated HCC1954 cells with and without 10 μ M S1PR₃ (G) agonist or 10 μ M LPA (H) treatment. **I-J:** GSEA profile of the “GO_ACTIN_FILAMENT_BUNDLE_ORGANISATION” gene set enriched in *RNF40*^{high}-expressing HER2⁺-BC biopsies (I). Table of all significantly enriched (FDR<0.25) gene sets associated with H2Bub1, actin dynamics, focal adhesion and apoptosis (J). Data were retrieved from TCGA (<https://portal.gdc.cancer.gov/>). **E** and **F:** Student t-test *p-val<0.05, **p-val<0.01, ***p-val<0.005. All experiments were performed in biological triplicates. Error bars: SEM.

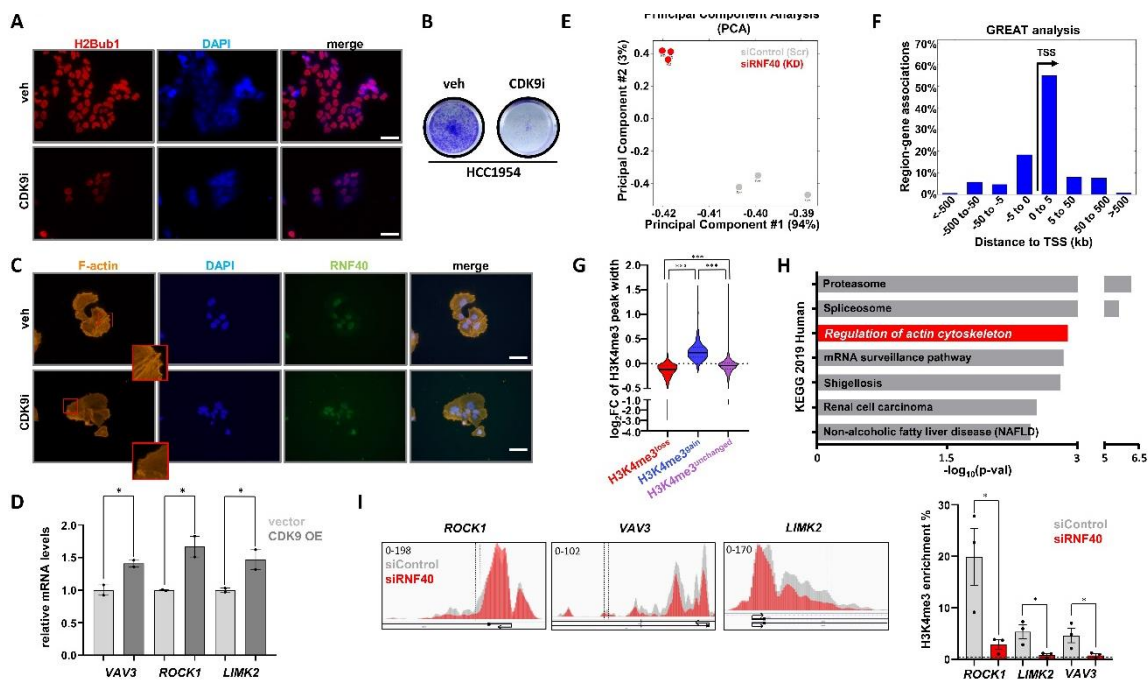


Fig.I.S5: RNF40 regulates gene expression of important members of the RHO-ROCK axis in a H2Bub1-H3K4me3 dependent manner. **A:** Immunofluorescence staining of H2Bub1 in DMSO- and CDK9i-treated HCC1954 cells (BAY-1251152, 120 nM, 48 hours). Scale bar: 100 μ m. **B:** Crystal violet staining of HCC1954 cells treated with DMSO- or CDK9i (BAY-1251152, 120 nM, 5 days). **C:** Immunofluorescence staining of F-actin and RNF40 in DMSO- and CDK9i-treated HCC1954 cells (BAY-1251152, 120nM, 48 hours). Scale bar: 100 μ m. **D:** qRT-PCR of the actin regulatory genes in empty vector- and CDK9-overexpressing HCC1954 cells. Student t-test. **E:** Principal component analysis from Differential Binding Analysis results on H3K4me3 occupied regions in siControl- and siRNF40-treated HCC1954 cells. **F:** “GREAT” cis-regulatory region analysis showing the genomic distribution of H3K4me3 loss regions upon RNF40 silencing. **G:** H3K4me3 peak width change upon RNF40 silencing of regulated and unchanged regions identified with a DiffBind analysis. One-way ANOVA (Kruskal-Wallis-test). **H:** Pathway enrichment analysis with the web-based Enrichr tool for all genomic regions losing H3K4me3. **I:** ChIP-qRT-PCR validating the loss of H3K4me3 occupancy at the 3'-prime end of *ROCK1*, *LIMK2* and *VAV3* peaks (right panel). Integrative genomic viewer (IGV) tracks of H3K4me3 in siControl- and siRNF40-treated HCC1954 cells. Dotted lines represent the used ChIP-qRT-PCR primers to confirm the H3K4me3 narrowing (left panel). All qRT-PCRs were performed in biological triplicates. Student t-test. Error bars: SEM. *p-val<0.05, ***p-val<0.005.

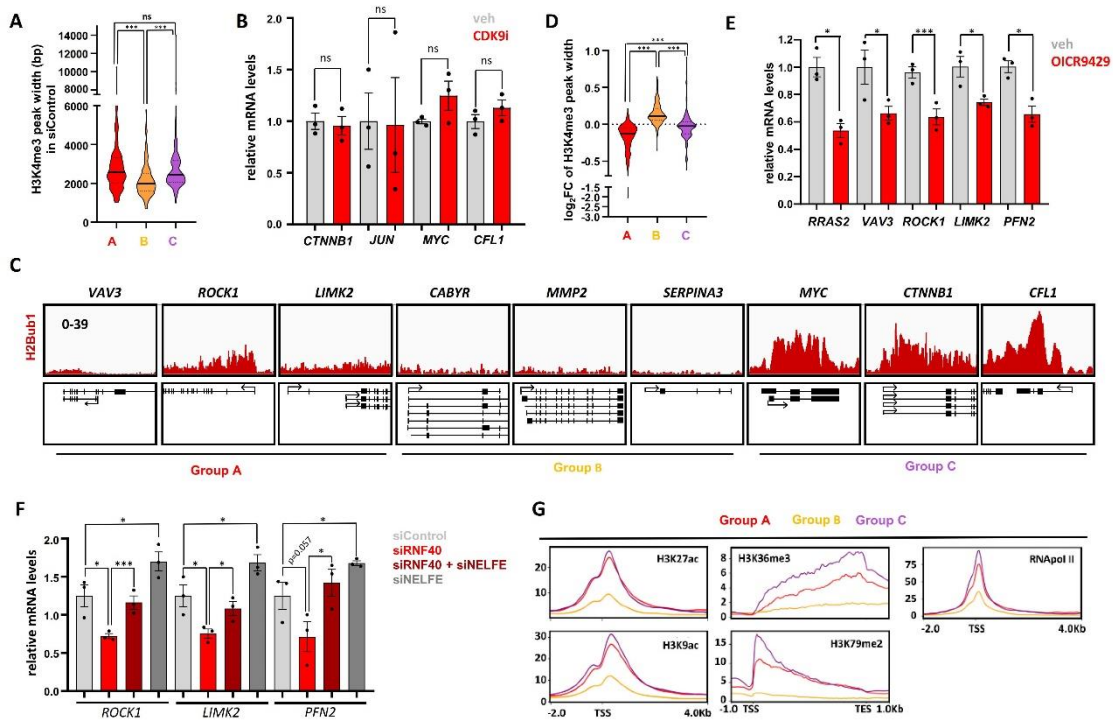


Fig.I.S6: RNF40 regulates gene expression of important members of the RHO-ROCK axis in a H2Bub1-H3K4me3 dependent manner. **A:** Violin plot showing the median of H3K4me3 peak width in basal condition at the TSS of Groups A, B and C genes. One-way Anova (Kruskal-Wallis test). **B:** qRT-PCR of some representative Group C genes in DMSO- or CDK9i-treated (BAY-1251152, 120 nM, 6 hours) HCC1954 cells. Student t-test. **C:** Integrative Genomic Viewer (IGV) tracks of H2Bub1, H3K27ac, H3K79me2, H3K36me3 and H3K9ac at Group A, Group B and Group C genes. **D:** Violin plot showing the median of the H3K3me3 peak width change of Group A, B and C genes. One-way Anova (Kruskal-Wallis test). **E:** qRT-PCR of *RRAS2*, *VAV3*, *ROCK1*, *LIMK2* and *PFN2* in DMSO- and OICR9429-treated (WDR5-specific inhibitor) HCC1954 cells (5 μ M, 5 days). Student t-test. **F:** qRT-PCR of actin regulatory genes in siControl-, siRNF40-, siNELFE, siRNF40+siNELFE-treated HCC1954 cells. Student t-test. **G:** Aggregate plots of H3K79me2, H3K36me3, H3K27ac, H3K9ac or RNAPol II occupancy at TSS of group A, B and C* genes in control HCC1954 cells (Accession number: GSE85158, GSE72956). Error bars: SEM: ns=not significant, * p-val<0.05, *** p-val<0.005. All qRT-PCRs were performed in biological triplicates.

Supplementary Tables

Table S1: cell lines used in this study.

Human cell line	HCC1954	SKBR3	BT474
Tissue of origin	43 years old, female, mammary gland, adenocarcinoma	61 years old, female, ductal carcinoma	60 years adult, female, ductal carcinoma
Morphology and growth properties	epithelial, monolayer, adherent	epithelial, monolayer, adherent	epithelial, patchy
Supplier	ATCC	ATCC	ATCC
Recommended medium	RPMI 1640. GlutaMAX™ (Thermofisher Scientific)	DMEM/F12- Dulbecco's Modified Eagle's Medium: Nutrient Mixture F-12 (Thermofisher Scientific)	DMEM/F12- Dulbecco's Modified Eagle's Medium: Nutrient Mixture F-12 (Thermofisher Scientific)
HER2 amplification status	+	+	+
ER/PR status	-/-	-/-	-/+
p53 status	mutated (Y136C)	mutated (R175H)	Mutated (E285K)

Table S2: siRNAs used in this study.

Gene	siRNA
Non-Targeting #5	UGGUUUACAUGUCGACUAA
<i>RNF40</i>	#1 GAGAUGCGCCACCUGAUUA
	#2 GAUGCCAACUUUAAGCUAA
	#3 GAUCAAGGCCAACCCAGAUU
	#4 CAACGAGUCUCUGCAAGUG
<i>VAV3</i>	#1 GCAGAGACCGAACUUUAUUA
	#2 GCAAAGCACAUCAAGAUUU
	#3 AGACCGAACUUUAUUAAUAG
	#4 GUAUGCAGCCCUCGUGUAA
<i>NELFE</i>	#1 ATGGAGTCAGCAGATCAGTTCAAGAGACTGATCTGCTGACTCCATC TTTTT
	#2 GATCAAAAAGATGGAGTCAGCAGATCAGTCTCTTGAAGTACTGATCTGC TGACTCCATCA

Table S3: qRT-PCR primers used in this study.

Gene name	Forward (5'-3')	Reverse (5'-3')	Species	Reference
<i>RPLP0</i>	GATTGGCTACCCA ACTGTTG	CAGGGGCAGCAGCCAC AAA	Human	(1)
<i>Rplp0</i>	GATTCGGGATATGCTGTT GG	GCCTGGAAGAAGGAGG TCTT	Mouse	This study
<i>RNF40</i>	AGTACAAGGCGCGGTTG A	GAAGCAGAAAACGTGG AAGC	Human	(2)
<i>Rnf40</i>	GGCCCAGCTGGATGAAA CTGT	ACTGAGAGGGGCTCGA AACT	Mouse	This study
<i>VAV3</i>	CCAATGGACTGCGAAGA ACT	GTAAAGGGGGTCTTCA TGC	Human	This study
<i>ROCK1</i>	CTGCAACTGGA ACTCAA CCA	GCCAACTGCATCTGAAG CTC	Human	This study
<i>LIMK2</i>	AGTCCCGGCTTACTTCA CCT	CCCAA ACTTCCCCCAGT AGT	Human	This study
<i>PFN2</i>	CCAAGAGTCAAACCGTT GGT	GGGCGTCTTTCAGAGCA TTA	Human	This study
<i>RRAS2</i>	CGGATTATGATCCAACCA TTG	TGTTCTCTCATGGCTCC AAAC	Human	This study
<i>CTNNB1</i>	TGGATACCTCCCAAGTC CTG	CTGAGCTCGAGTCATTG CAT	Human	This study
<i>MYC</i>	GGACGACGAGACCTTCA T	GCCGCTCCACATACAGT C	Human	This study
<i>CFL1</i>	GCAAGAAGGAGGATCTG GTG	CCTTGGAGCTGGCATAA ATC	Human	This study

Table S4: ChIP-qPCR primers used in this study.

Gene name	Forward (5'-3')	Reverse (5'-3')	Species	Reference
Control primers				
<i>GAPDH</i> (gene body)	CCGGGAGAAGCTGAGTCATG	TTTGCGGTGGAATGTCCTT	Human	(3)
<i>HNRNPK</i> (TSS proximal region)	TCCACGAGGTCCCTAGTTCC	GCCATTTCCCTGAGCGTGTA	Human	This study
H3K4me3 narrowing assessment				
<i>VAV3</i> (TSS proximal region)	CCGGAGAGGAAACTTGTCAC	CCACCCTCCATCAGAGAAAA	Human	This study
<i>ROCK1</i> (TSS proximal region)	GGAGCTAAATCGCAAAAAGG	TTTGTTGAATGGCGATCGTA	Human	This study

LIMK2 (TSS proximal region)	GAACCTTTAAGGGCCAGACC	AGGGGCAAGAAGATCAGGTT	Human	This study
------------------------------------	----------------------	----------------------	-------	------------

Table S5: List of primary antibodies.

	WB (dilutions)	IHC (dilutions)	IF (dilutions)	ChIP (dilutions)	cat.number/ company
HSC70	(1:100)				sc-1050, Santa Cruz
GAPDH	(1:2000)				OTI2D9, Origene
ACTIN	(1:200)				sc-1616 (1- 19), Santa Cruz
HER2		(1:500,EDTA buffer)			2165, Cell Signaling
RNF40		(1:100,EDTA buffer)			ab191309, Abcam
RNF40	(1:1000)				D2R20, Cell Signaling
RNF40			(1:500)		R9029, Sigma Aldrich
H2Bub1	(1:50)	(1:100,EDTA buffer)			home-made
H2Bub1			(1:500,citric buffer)	1 µg/sample	5546, Cell Signaling
H2B	(1:500)				07-371, Millipore
Ki67		(1:1000,citric buffer)			home-made (rabbit)
H3K4me3				1 µg/sample	003050, Diagenode
PARP	(1:500)				9542, Cell Signaling
caspase-3	(1:500)				9662, Cell Signaling
p-ERK Y202/T204	(1:200)				sc-7383, Santa Cruz
ERK1	(1:200)				sc-94, Santa Cruz
p-AKT S473	(1:500)				736 E11, Cell Signaling
AKT	(1:500)				9272, Cell Signaling
ROCK1	(1:200)				sc-17764, Santa Cruz

VAV3	(1:100)				CSB-PA006523-100, Cusabio
p-cofilin S3	(1:1000)		(1:100,citric buffer)		77G2, Cell Signaling
cofilin	(1:1000)				D3F9, Cell Signaling
vinculin			(1:200)		V9131, Sigma Aldrich

Table S6: List of secondary antibodies.

	WB (Dilution)	IHC (Dilution)	IF (Dilution)	Cat.number, company
HRP-anti-rabbit IgG	(1:10.000)			211-032-171, Dianova
HRP-anti-mouse IgG	(1:10.000)			115-035-174, Dianova
Alexa 555-anti-rabbit IgG			(1:400)	A-21429, Molecular Probes
Alexa 488-anti-mouse IgG			(1:400)	A-21202, Molecular Probes
DyLight 649-anti-rabbit IgG			(1:400)	711-495-152, Dianova
Alexa 555-anti-mouse IgG			(1:400)	A-31570, Molecular Probes
biotin-anti-rabbit IgG		(1:200)		711-065-152, Dianova
biotin-anti-mouse IgG		(1:200)		711-065-150, Dianova

Table S7: Average ChIP-seq library size.

sample	Average library size	Accession number
H3K4me3_siControl (replicate 1)	326 bp	
H3K4_siRNF40 (replicate 1)	334 bp	
H3K4me3_siControl (replicate 2)	300 bp	
H3K4_siRNF40 (replicate 2)	330 bp	
H3K4me3_siControl (replicate 3)	394 bp	
H3K4_siRNF40 (replicate 2)	285 bp	
H2Bub1_siControl (replicate 1)	299 bp	
H2Bub1_siControl (replicate 2)	274 bp	

Input_siControl (replicate 1)	280 bp	
Input_siRNF40 (replicate 1)	267 bp	

Supplementary Materials and Methods


Animal handling and mouse model generation

Animals were housed in the animal facility of the European Neuroscience Institute (ENI) of Göttingen under specific pathogen-free (SPF) conditions. The generation of mice harboring a conditional *Rnf40* allele was previously described by our group (2). All mice had a FVB/N background. Specifically, the *Rnf40*^{oxP} mice were crossed with MMTV-Cre and MMTV-ErbB2 mice to allow co-expression of the Cre-recombinase and of the rat *ErbB2* proto-oncogene in mammary epithelial cells (4,5). Tumors animals were monitored twice a week. Growing tumors were detected by palpation and size was measured with a caliper. The measurements were performed in a blinded way by two independent investigators. Three cohorts of animals were analyzed in this study: n=28 *Rnf40*^{wt/wt}, n=12 *Rnf40*^{fl/wt} and n=14 *Rnf40*^{fl/fl} animals. To avoid bias caused by short tumor monitoring time, the number of animals included in “tumor burden” and “tumor growth kinetics” analyses was reduced (n=10 *Rnf40*^{fl/wt}; n=13 *Rnf40*^{fl/fl}, and n=22 *Rnf40*^{wt/wt}; n=9 *Rnf40*^{fl/wt}; n=9 *Rnf40*^{fl/fl}, respectively).

Histology of human tissue microarrays (TMAs) and murine tumors

176 primary mammary tumors and 78 brain metastases samples of known subtype on two TMAs, kindly provided by Prof. Harriet Wikman-Kocher, Prof. Klaus Pantel (Tumor Biology Institute, University of Hamburg-Eppendorf) and Prof. Markus Glatzel (Institute for Neuropathology, University of Hamburg-Eppendorf, Hamburg, Germany), were successfully stained for RNF40 and H2Bub1 using IHC.

Paraffin-embedded tissue microarrays as well murine tumors were deparaffinized in xylol for 20 min and rehydrated with subsequent incubations in 50% isopropanol/50% xylol, 100% isopropanol, 100%, 90% and 70% ethanol, and finally tap water for 5 min each. For hematoxylin and eosin (H&E) staining, nuclei were stained with hematoxylin solution (Carl Roth GmbH) for 1 min. Excess dye was removed using running tap water for 5 min. Counterstaining with eosin (Carl Roth GmbH) was performed for 5-10 min. For immunohistochemical staining (IHC), upon rehydration, antigen retrieval was performed by boiling slides in EDTA buffer (1 mM EDTA, pH 8, 0.1% Tween 20) or citric buffer (10 mM citric acid, pH 6, 0.1% Tween 20) for 10 min in a pressure cooker. After allowing tissue sections to cool slowly, endogenous peroxidase was inactivated with 3% hydrogen



superoxide in PBS for 45 min and unspecific antigen binding was blocked with 5% bovine serum albumin (BSA, Merck) and 1% donkey serum (Dianova GmbH) in PBS (blocking solution) for 1 hour at room temperature in a humid chamber. Afterwards, primary antibodies were diluted in blocking solution and sections were incubated overnight in the humid chamber at 4 °C. Sections were next washed twice with 0.1% Tween 20 in PBS (PBS-T) and incubated with biotinylated secondary antibodies blocking solution (1:200 dilution) for 1 hour in the humid chamber at room temperature. After a wash step with PBS-T, Avidin-Peroxidase conjugate (Sigma-Aldrich) diluted in PBS (1:1000) was applied on the sections for 90 min at room temperature in the humid chamber. Finally, staining was developed using 3,3'-diaminobenzidin-tetrahydrochloride (DAB) with 1% hydrogen superoxide in PBS and counterstained using hematoxylin. Slides were washed under running tap water for 5 min and dehydrated in increasing concentrations of ethanol, isopropanol, xylol and mounted with Roti®-Histokitt mounting medium (Carl Roth GmbH). Table S5 and S6 list the antibodies, dilutions and corresponding antigen retrieval buffers used in this study.

For the evaluation of the TMAs staining, two independent blinded observers monitored the staining intensity (0 = negative, 1 = very weak staining, 2 = weak staining, 3 = moderate staining and 4 = strong staining). The score was determined based on the 25% most intensively stained tumor cells. The two evaluations were finally compared and reevaluated if a discrepancy was identified. Because of the relatively low number of HER2⁺-BC, we classified the samples as RNF40^{low} (staining scores 1 and 2) and RNF40^{high} (staining scores 3 and 4) in our analyses. Samples were classified along their intrinsic subtypes based on published procedure (6): luminal A: ER-positive/PR-positive/HER2-score 0, luminal B: ER-positive/PR-positive/HER2-score 1-3, HER2-positive: ER-negative/PR-negative/HER2-score 1-3, TNBC: ER-negative/PR-negative/HER2-score 0.

Analysis of publically available patient datasets

Kaplan-Meier Plotter

The Kaplan-Meier Plotter (<http://kmplot.com>) platform was used to study the relapse-free survival (RFS) of HER2-positive patients with low or high expression of *RNF40* (7). Following settings were used here:

RFS: Affymetrix probe identity number for *RNF40* gene expression 206845_s_at; auto-select best cutoff mode; HER2-positive BC patients selection criteria: ER-negative, PR-negative, HER2-positive.

OS: Affymetrix probe identity number for *RNF40* gene expression 239801_at; auto-select best cutoff mode; HER2-positive BC patients selection criteria: HER2-positive intrinsic subtype.

DMFS: Affymetrix probe identity number for *RNF40*, *VAV3*, *ROCK1*, *LIMK2* gene expression are 206845_at, 218806_s_at, 235854_x_at and 202193_at, respectively; auto-select best cutoff mode; HER2-positive BC patients selection criteria: intrinsic subtype

TCGA

The TCGA-derived BReast AdenoCarcinoma (BRCA) dataset was retrieved from the Xena browser (<https://xenabrowser.net>) (8) online platform to analyze the impact of *RNF40* expression level on the OS of HER2-positive BC patients (classified along the PAM50). A cutoff of 11.53 normalized reads counts was selected to discriminate low and high *RNF40*-expressing patients. The results were finally plotted with Graphpad Prism v8.01. TCGA normalized expression levels of *RNF40* in normal mammary tissues and breast adenocarcinoma was extracted from the same platform.

DepMap

The CERES scores for the genetic essentiality of all screened HER2-positive breast cancer cell lines were performed by Meyers et al. (9) and are publically available at the DepMap portal (<https://depmap.org/portal/>) under the dataset name "CRISPR (Avana) Public 19Q4". CERES score values were plotted as a scatter plot using Graphpad Prism v8.01.

Cell culture

HCC1954 and SKBR3 cells were purchased from ATCC company (following Table S1) and cultivated using the recommended medium supplemented with 10% fetal bovine serum (FBS) and 1% penicillin/streptomycin at 37°C and 5% CO₂.

siRNA transfections

Transfections were performed using Lipofectamine® RNAiMAX (Invitrogen) according to the manufacturer's guidelines. siGENOME SMARTpool siRNA (Dharmacon) are shown in Table S2.

Plasmid transfections

Transfections were performed using TrasiT-2020 (Mirus) according to the manufacturer's instructions. An overexpressing vector harboring CDK9 cDNA in the pSG5 backbone was utilized to overexpress CDK9 in HCC1954 cells. The empty vector was used as a control. Briefly, 240,000 cells per well in a 6-well plate were seeded and the following day the

plasmid transfection was performed. At 88 hours post-transfections, cells were harvested for RNA extraction.

Proliferation, colony and sphere formation assay

All experiments were performed in biological triplicates.

HCC1954 cells:

Proliferation assay: 24 hours post-transfection, 1,000 cells were seeded in a 96-well plate. Cell confluency was recorded every 12 hours for 6 days using an IncuCyte® Live Cell Analysis System (Sartorius AG). *Clonogenic and tumor sphere formation assay:* 24 hours post-transfection, 500 (for colony formation assay) and 1000 (for tumor sphere formation assay) cells were seeded in a 6-well and 96-well low adherent plate, respectively. 15 days after seeding, colonies were washed with PBS, fixed with methanol for 10 min and stained with 1% crystal violet in 20% ethanol for 20 min. After a final wash in water, stained colonies were scanned using EPSON perfection V700 PHOTO scanner. 20 days after seeding, spheres were scanned using a Celigo® S imaging cytometer (Nexcelom Bioscience LLC) and quantified. Number of colonies or spheres was assessed using ImageJ.

SKBR3 cells:

Proliferation and clonogenic assay: 220,000 cells were reverse transfected in biological triplicates in a 6-well plate and re-transfected 96 hours after the first transfection. 24 hours later, 1,000 cells (for proliferation assay) and 500 cells (for colony formation assay) were seeded on a 96-well (adherent) and a 6-well plate, respectively. Proliferating cells were scanned every 2 days using a Celigo® S imaging cytometer (Nexcelom Bioscience LLC). 15 days after seeding, colonies were washed, fixed, stained, scanned and analysed as previously described.

BT474 cells:

Tumor sphere formation assay: 220,000 cells were reverse transfected in biological triplicates in a 6-well plate and re-transfected 96 hours after the first transfection. 24 hours later, 500 cells per well were seeded in a low adherent 96-well plate. and the culture medium was supplemented with B27 supplements (Gibco, cat.11530536) based on manufacturer's instructions. 9 days after seeding, tumor spheres were scanned using a Celigo® S imaging cytometer (Nexcelom Bioscience LLC) and quantified.

ROCK and FAK inhibition: 30,000 and 220,000 HCC1954 cells were seeded in 12-well (proliferation assay) and 6-well plates (protein extraction), respectively. The following day, medium was replaced with fresh one including 16 μ M RKI-1447 (CAS 1342278-01-6, Toronto Research Chemicals) or 20 μ M PF-573228 (14924, Cayman Chemical). Cells for protein isolation were harvested after 12 hours of treatment while cells for proliferation

assay were grown for 5 days. Finally, plates were fixed, stained, scanned and analysed as previously described.

WDR5 inhibition: 50,000 cells per well in a 12-well plate were seeded. The following day, HCC1954 cells were treated with DMSO or 5 μ M of the WDR5-specific inhibitor OICR-9429 (Selleckhem) for 5 days to subsequently perform RNA extraction.

Rescue experiments: upon RNF40 silencing, 30,000 and 220,000 HCC1954 cells were reverse transfected in biological triplicates in a 12-well (proliferation assay) and 6-well plate (protein isolation), respectively. 24 hours after transfection, medium was replaced with fresh one including 10 μ M CYM-5441 (S1PR₃ agonist, SML0680, Sigma-Aldrich) or 10 μ M lysophosphatidic acid (LPA, CAS 325465-93-38, Santa Cruz). For protein isolation, cells were protein harvested 72 hours post-transfection while cells for proliferation assay were grown for 5 days.

Co-treatment of S1PR₃ agonist- or LPA-induced with ROCK inhibition: 30,000 HCC1954 cells were seeded in a 12-well plate. The following day, medium was replaced with fresh one including 10 μ M CYM-5441 or 10 μ M LPA plus 16 μ M RKI-1447 and cells were grown for 5 days. Finally, plates were fixed, stained, scanned and analysed as previously described.

Annexin V and caspase 3/7 activity assay

Annexin V assay (modified from (10)): 72 hours post-transfection, cells were washed with PBS and resuspended in 1x Binding buffer (10 mM HEPES, 0.14 M NaCl, 2.5 mM CaCl₂ pH: 7.4) at a concentration of 10⁶ cells/ml. 100 μ l of the cell suspensions were transferred to sterile tubes, 5 μ l of Annexin V-FITC (Southern Biotech) and 1 μ l of propidium iodide (1mg/ml, Sigma Aldrich) was added in each sample and suspension was incubated for 15 min at room temperature in the dark. Finally, 400 μ l of 1x Binding buffer was added to each tube and samples were analysed using a Guava EasyCyte Plus flow cytometer from Guava Technologies.

Caspase 3/7 activity assay: 24 hours post-transfection, 1,000 cells were seeded on a 96-well plate containing in each well 100 μ l medium containing caspase 3/7 fluorescent substrate (CS1-V0002-1, ViaStain™ Live Caspase 3/7 Detection Kit) and Hoechst 33342, according to the manufacturer's instructions (CS1-V0002(3)-1, ViaStain™ Live Caspase 3/7 Detection Kit) and supplemented with either 10 μ M CYM-5441 or vehicle. Scanning was carried out with a Celigo® S imaging cytometer (Nexcelom Bioscience LLC). Output data were normalized to the first day of scanning for each condition.

Migration assays

Trans-well migration assay: 120,000 HCC1954 cells were reverse transfected in biological triplicates, and re-transfected 96 hours later. The following day, cells were serum starved for 8 hours and then collected, counted using trypan blue and 50,000 viable cells were seeded on each trans-well inserts (Corning, 24-well insert, 8 μ m pore) while normally supplemented medium was added beneath the inserts. 48 hours after seeding, the inserts were washed with PBS and cells that have not migrated through the membrane were removed with a cotton Q-tip. Migrated cells were then fixed with methanol for 10 min, stained with crystal violet, scanned and analysed as previously described (see method for proliferation assay).

Gap-closure assay: 120,000 HCC1954 cells were reverse transfected in biological triplicates, and re-transfected 96 hours later. Cells were collected, counted using trypan blue and 70,000 viable cells were seeded on each silicone insert (ibidi, 2-well μ -Dish 35 mm). Once cells became adherent, silicone chambers were removed and photos were taken using a Nikon Eclipse TS100 inverted microscope at time point 0 and 23 hours after silicone insert removal. Gap closure was measured using ImageJ and normalized to time point 0 hours.

Immunofluorescence microscopy

10-15,000 cells were reverse transfected on coverslips in biological triplicates in a 6-well plate as previously described. 72 hours post-transfection cells were washed with PBS and fixed with 4% paraformaldehyde in PBS for 20 min. Thereafter, cells were permeabilized with 1% Triton X-100 in TBS for 10 min, washed once with TBS and blocked with blocking solution (3% BSA in TBS-T) for 1 hour in a humid chamber. The primary antibody was diluted in blocking solution and applied on the coverslips for overnight incubation in a dark humid chamber at 4°C. The following day, coverslips were washed three times with TBS-T and incubated with fluorophore-conjugated secondary antibodies and DAPI (1:1000 dilution) dissolved in blocking solution, for 1 hour in a dark humid chamber. For F-actin staining, Alexa555 conjugated to phalloidin (Abnova) was added to the secondary antibody solution at 1:400 dilution. Coverslips were washed three times with TBS-T. Finally, coverslips were mounted on microscope slides. Pictures were taken with a Zeiss LSM 510 Meta confocal microscope. Fluorescence intensity was quantified using ImageJ.

Fluorescence intensity quantification: photographed areas were processed in ImageJ. To quantify Ki67 (*in vitro*) as well p-cofilin (*in vivo*) staining, the DAPI channel was utilized as reference to determine cell nuclei regions. Finally, Ki67 or p-cofilin staining intensity was measured for every nucleus. To quantify F-actin staining intensity, the area covered by cells

was determined based on the phalloidin channel. The average F-Actin staining intensity was determined in this area for each picture.

To quantify the focal adhesion area and their staining intensity, a particle analysis was performed on the vinculin channel. Used antibodies are listed at Tables S5 and S6.

Protein isolation and western blot analysis

Protein isolation: Radioimmunoprecipitation Assay Buffer (RIPA; 10 mM Tris-Cl pH 8, 1 mM EDTA, 1% v/v Triton X-100, 0.1% sodium deoxycholate, 0.1% SDS, 140 mM NaCl) supplemented with protease and phosphatase inhibitors was used (1 μ M activated orthovanadate, 10 mM β -glycerophosphate disodium salt hydrate, 10 mM Pefablock, 10 mM N-Ethylmaleimide, 1 mM Aprotinin/Leupeptinin, 1 μ M NaF, 1 μ M iodoacetic acid). Cells were washed once with PBS and 200 μ l of RIPA buffer was added to each well (6 well plate). After 10 min incubation on ice, cells were scraped and lysates were sonicated for three cycles 30s on/off each using a Bioruptor (Diagenode). Laemmli buffer (375 mM Tris/HCl, 10% SDS, 30% glycerol, 0.02% bromophenol blue, 9.3% DTT) was added to each lysate and cooked at 95°C for 5 min before protein separation with a 10 to 12% polyacrylamide gel. Proteins were transferred to nitrocellulose membrane (0.45 μ m pore, Immobilon, Millipore), blocked with 5% skimmed milk in TBS-T for 1 hour and incubated with primary antibody overnight at 4°C. The day after, membrane was washed with TBS-T, incubated 1 hour with secondary antibody at room temperature. After a final wash step, protein detection was achieved with the Millipore substrate in a BioRad ChemiDoc™ imager. Used primary antibodies are listed at Table S5 and S6.

RNA isolation and quantitative RT-PCR (qRT-PCR)

RNA isolation and quantitative RT-PCR were performed as previously described (11,12). Briefly, 72 hours post-transfection, cells were washed with PBS and lysed in 500 μ l Qiazol (Qiagen). For RNA extraction from tissues, 50-100 mg frozen tissue was homogenized with 0.5-1 ml Qiazol with three cycles of 10-15 sec/2,000 rpm in a PowerLyzer24 (MoBio Laboratories). Lysates were then collected and RNA was extracted, as previously described (11,12). Reverse transcription of 1 μ g RNA was performed using M-MuLV reverse transcriptase (NEB) with random primers according to the manufacturer's instructions. Expression of specific genes was finally estimated by quantitative real-time PCR using a CFX Connect™ Real-Time System (Bio-Rad). Gene expression levels were normalized relative to the *RPLP0* house keeping gene. qRT-PCR program: 1x 2 min-95°C, 40x 10 sec-95°C followed by 1x 30 sec-60°C. Primers (Table S3) were designed using the design tool

(http://biotools.umassmed.edu/bioapps/primer3_www.cgi) and were ordered from Sigma-Aldrich (Germany).

Chromatin Immunoprecipitation (ChIP)

72 hours post-transfection, cells were crosslinked with 1% formaldehyde for 20 minutes and quenched by glycine (125mM final concentration) at room temperature for 5 min. Subsequently, fixed cells were scraped and nuclear pellets were collected and washed with Nelson buffer (150 mM NaCl, 20 mM EDTA, 50 mM Tris-HCl (pH 7.5), 0.5% v/v NP-40, 1% v/v Triton-X-100, 20 mM NaF). Nuclei were then sonicated in Gomes lysis buffer (150mM NaCl, 20 mM EDTA, 50 mM Tris-HCl (pH: 8), 1% v/v NP-40, 0.5% v/v sodium deoxycholate, 20 mM NaF, 0.1% SDS) for 20 cycles using a Bioruptor Pico (Diagenode) with each cycle setup of 30 s on/off. After performing shearing check, samples were precleared by incubation with 50% slurry of sepharose beads (GE Healthcare), centrifuged and supernatants were incubated with H2Bub1, H3K4me3 antibody or control rabbit IgG (1 μ g, C15410206, Diagenode) overnight. Protein A-sepharose beads were added to samples and incubated for 2 hours at 4°C, then washed [1 time with Gomes lysis buffer, 2 times with Gomes wash buffer (0.5 M LiCl, 0.02 M EDTA, 0.1 M Tris-EDTA, 1% NP-40, 0.02 M NaF, 1% sodium deoxycholate) and two times again with Gomes lysis buffer]. DNA-beads complexes were washed once more with 1 mM Tris and 10 mM EDTA buffer (TE) before DNA was extracted. Samples were run in three biological replicates per condition. For ChIP antibodies, please refer to Table S5. H2Bub1 and H3K4me3 ChIP efficiency was validated via ChIP-qPCR for genomic regions known to be H2Bub1 positive (body region of *GAPDH*) or H3K4me3 positive (TSS-proximal region of *HNRNPK*). The signal was normalized to input DNA and presented as percent input for triplicates in each condition. The validation of H3K4me3 regulated regions was performed by ChIP-qPCR following the same procedure. Primer list available in Table S4.

Library preparation for RNA and ChIP-seq and next generation sequencing

RNA sequencing libraries were generated with the NEXTflex™ Rapid Illumina Directional Kit (Biooscientific, Catalog #NOVA-5138-07) according to the manufacturer's instructions. RNA library underwent amplification in a thermal cycler using the following program: 1 cycle of 37°C-30 min, 98 °C-2 min and 15 cycles of [98 °C-30 sec, 1x 65 °C-30 sec, 1x 72 °C-60 sec] and one cycle of 72 °C-4 min.

ChIP libraries were generated with the Microplex Library Preparation kit v2 (Diagenode, C05010011) and were amplified using the following program: 1 cycle of [72 °C-3 min, 85 °C-2 min, 1x 98 °C-2 min], 4 cycles of [98 °C-20 sec, 67 °C-20 sec, 72 °C-40 sec] and 16 (H3K4me3, input) or 17 cycles (H2Bub1) of [98 °C-20 sec and 72 °C-50 sec].

The quality and size of the libraries was examined using the high sensitivity DNA kit (Agilent) on the Agilent Bioanalyzer 2100 (Table S7). Finally, the concentration of the mRNA- and ChIP libraries was estimated with a Qbit (Invitrogen), multiplexed in 2 nM pooled libraries and sequenced (single-end, 50 bp) on a HiSeq4000 (Illumina) in the Transcriptome and Genome Analysis Laboratory (TAL) at the University Medical Center of Göttingen.

Bioinformatic analysis of mRNA-sequencing data

Fastq files were uploaded and processed in the Galaxy environment (<https://galaxy.gwdg.de>). Qualitative of the sequencing data was assessed using FastQC (version 0.72)(13). Fastq files were trimmed for the first 11 bp using the FASTQ Trimmer tool (version 1.0.0) (14). Output data were aligned to the human reference genome hg19 (downloaded from www.ensembl.org) using the TopHat Gapped-read mapper (version 2.1.1)(15). Aligned reads were then assigned to the respective genomic features using featureCounts (version 1.4.6.p5) and, finally, DESeq2 (version 2.11.39) was used to identify significantly differentially regulated genes (16).

Matrix visualisation of actin cytoskeleton gene signatures in Fig.I.3F and I.5F were created using the Morpheus tool (<https://software.broadinstitute.org/morpheus/>). Gene Set Enrichment Analyses (GSEA) were performed with normalized counts of siControl and siRNF40 conditions using following specific settings: 1,000 permutations, type: gene set and a maximum size of sets of 1,000) (17). Pathway enrichment analysis for all RNF40-dependent genes was performed using the online tool Enrichr (18).

mRNA-seq data (in FPKM) from HER2+ BC patients were retrieved from the Genomic Data Commons Data Portal (GDC). FPKM count tables were sorted along RNF40 expression ($RNF40^{low}=27$, $RNF40^{high}=29$) in a common count table and subsequently subjected to GSEA analysis. Volcano plot of normalized enrichment score and FDR of all gene ontology signatures of biological processes (GO_BP) were plotted using Graphpad Prism v8.01.

Bioinformatic analysis of ChIP-sequencing data

Fastq files were uploaded and processed in the Galaxy environment (<https://galaxy.gwdg.de>). Qualitative of the sequencing data was assessed using FastQC (version 0.72) (13). Respective reads were aligned to the human reference genome hg19 using Bowtie2 (version 2.3.2.2) (19) using the “very sensitive end-to-end” mapping mode. Output bam files were filtered using the “Filter SAM or BAM” tool (version 1.1.2) (20) using a minimum MAPQ quality score of 5. Subsequently, PCR duplicates were removed using the “RmDup” tool (version 2.0.1) (20). BigWig files of the H3K4me3 and H2Bub1 tracks

were created using the "bamCoverage" (version 2.5.1.1.0 and version 3.0.1.0, respectively, (21)) (normalisation to reads per kilobase per million; RPKM) from Deeptools in the Galaxy environment. Reads in this step were extended using the average fragment size of each sample calculated from the library quality screening step (Table S7). A minimum mapping quality was set at 5 while a black list chromatin region hg19-based file, downloaded from <https://sites.google.com/site/anshulkundaje/projects/blacklists>, was used to exclude regions with anomalous signal. For peak calling of H2Bub1 and H3K4me3 data, "MACS2 callpeak" (version 2.1.1.20160309.5, (22)) was used with the respective input files as background (settings: FDR<0.05, broad regions, cut-off for broad regions at 0.05). Finally, to generate heatmaps and aggregate plot profiles from the given regions, "computeMatrix", "plotHeatmap" and "plotProfile" (version 3.2.0.0.0) from the DeepTools suite were used, respectively.

To identify and call more precisely H3K4me3-regions regulated upon RNF40 silencing, we used the "bigwigCompare" (version 3.2.0.0.0) from DeepTools of the Galaxy environment to compute the fold change values between siRNF40 and siControl conditions (bin size = 50 bp). Bins with read density over 5 and |fold change| ≥0.8 (regulated regions) or |fold change| <0.8 (for unregulated) were kept and merged using the "MergeBed" (version 2.27.1) from DeepTools with a maximum distance of 250 bp. Subsequently, the output region file underwent differential binding analysis as well principal component analysis using R-studio Bioconductor R package (Diffbind, (23)) run on R version 3.3.1 according to the instructions. We limited our analyses to promoter associated regions and assigned significantly differentially regulated H3K4me3 regions to the respective genes. Visualisation of those regions was performed using a volcano plot script from the bioconductor website (<https://www.bioconductor.org>) run on R version 3.3.1.

For the aggregate profile of H3K4me3 peak width changes in Fig.I.S5C, I.5F and I.S5F, the peak width was calculated using the following equation and expressed in log2scale:

$$\text{Peak width (bp)} = \frac{\text{siRNF40 (peak end-peak start)}}{\text{siControl (peak end-peak start)}}$$

For the region-gene association of all "Diffbind"-defined regions with loss of H3K4me3 (Fig.I.S5B), the online Genomic Region Enrichment Analysis Tool (GREAT, (24)) was used with human reference genome hg19 and 1kb upstream and 5kb downstream from the nearest TSS as presets. For visualisation of the BigWig files across the human reference genome, Integrative Genomics Viewer tool (version 2.4.8, (25)) was used. For performing pathway enrichment analysis for genomic regions with loss of H3K4me3 upon RNF40 silencing, the online tool Enrichr was used (18).

Supplementary References of Manuscript I

1. Karpiuk, O. *et al.* The Histone H2B Monoubiquitination Regulatory Pathway Is Required for Differentiation of Multipotent Stem Cells. *Mol. Cell* **46**, 705–713 (2012).
2. Xie, W. *et al.* RNF40 regulates gene expression in an epigenetic context-dependent manner. *Genome Biol.* **18**, 32 (2017).
3. Najafova, Z. *et al.* RNF40 exerts stage-dependent functions in differentiating osteoblasts and is essential for bone cell crosstalk. *Cell Death Differ.* 1–15 (2020). doi:10.1038/s41418-020-00614-w
4. Shema, E. *et al.* The histone H2B-specific ubiquitin ligase RNF20/hBRE1 acts as a putative tumor suppressor through selective regulation of gene expression. *Genes Dev.* **22**, 2664–2676 (2008).
5. Guy, C. T. *et al.* Expression of the neu protooncogene in the mammary epithelium of transgenic mice induces metastatic disease. *Proc. Natl. Acad. Sci. U. S. A.* **89**, 10578–82 (1992).
6. Wagner, K. U. *et al.* Cre-mediated gene deletion in the mammary gland. *Nucleic Acids Res.* **25**, 4323–4330 (1997).
7. Tang, P. & Tse, G. M. Immunohistochemical Surrogates for Molecular Classification of Breast Carcinoma: A 2015 Update. *Arch. Pathol. Lab. Med.* **140**, 806–14 (2016).
8. Györfy, B. *et al.* An online survival analysis tool to rapidly assess the effect of 22,277 genes on breast cancer prognosis using microarray data of 1,809 patients. *Breast Cancer Res. Treat.* **123**, 725–31 (2010).
9. Goldman, M. *et al.* The UCSC Xena Platform for cancer genomics data visualization and interpretation. Preprint at <https://www.biorxiv.org/content/10.1101/326470v6>
10. Meyers, R. M. *et al.* Computational correction of copy number effect improves specificity of CRISPR-Cas9 essentiality screens in cancer cells. *Nat. Genet.* **49**, 1779–1784 (2017).
11. Lakshmanan, I. & Batra, S. Protocol for Apoptosis Assay by Flow Cytometry Using Annexin V Staining Method. *BIO-PROTOCOL* **3**, (2013).
12. Prenzel, T. *et al.* Estrogen-dependent gene transcription in human breast cancer cells relies upon proteasome-dependent monoubiquitination of histone H2B. *Cancer Res.* **71**, 5739–5753 (2011).
13. Mishra, V. K. *et al.* Histone deacetylase class-I inhibition promotes epithelial gene expression in pancreatic cancer cells in a BRD4- and MYC-dependent manner. *Nucleic Acids Res.* **45**, 6334–6349 (2017).
14. Blankenberg, D. *et al.* Manipulation of FASTQ data with Galaxy. *Bioinformatics* **26**, 1783–1785 (2010).
15. Conway, E., Healy, E. & Bracken, A. P. PRC2 mediated H3K27 methylations in cellular identity and cancer. *Curr. Opin. Cell Biol.* **37**, 42–48 (2015).
16. Trapnell, C., Pachter, L. & Salzberg, S. L. TopHat: Discovering splice junctions with RNA-Seq. *Bioinformatics* **25**, 1105–1111 (2009).
17. Love, M. I., Huber, W. & Anders, S. Moderated estimation of fold change and dispersion for RNA-seq data with DESeq2. *Genome Biol.* **15**, (2014).
18. Subramanian, A. *et al.* Gene set enrichment analysis: A knowledge-based approach for interpreting genome-wide expression profiles. *Proc. Natl. Acad. Sci. U. S. A.* **102**, 15545–15550 (2005).

19. Kuleshov, M. V. *et al.* Enrichr: a comprehensive gene set enrichment analysis web server 2016 update. *Nucleic Acids Res.* **44**, W90–W97 (2016).
20. Langmead, B. & Salzberg, S. L. Fast gapped-read alignment with Bowtie 2. *Nat. Methods* **9**, 357–359 (2012).
21. Li, H. *et al.* The Sequence Alignment/Map format and SAMtools. *Bioinformatics* **25**, 2078–2079 (2009).
22. Ramírez, F. *et al.* deepTools2: a next generation web server for deep-sequencing data analysis. *Nucleic Acids Res.* **44**, W160-5 (2016).
23. Feng, J., Liu, T., Qin, B., Zhang, Y. & Liu, X. S. Identifying ChIP-seq enrichment using MACS. *Nat. Protoc.* **7**, 1728–1740 (2012).
24. Ross-Innes, C. S. *et al.* Differential oestrogen receptor binding is associated with clinical outcome in breast cancer. *Nature* **481**, 389–393 (2012).
25. McLean, C. Y. *et al.* GREAT improves functional interpretation of cis-regulatory regions. *Nat. Biotechnol.* **28**, 495–501 (2010).
26. Robinson, J. T. *et al.* Integrative genomics viewer. *Nat. Biotechnol.* **29**, 24–26 (2011).

Author contribution

Author Full Name:	Specification of Contribution to the Manuscript:
Florian Wegwitz	Study design, cell culture experiments and molecular analyses, mRNA-seq library preparation, ChIP-seq library preparation and data analysis, mouse experiments, histological analyses, preparation, drafting and revision of manuscript
Evangelos Prokakis	Study design, cell culture experiments and molecular analyses, mRNA-seq library preparation and data analysis, histological analyses, ChIP-seq library preparation and data analysis, preparation, drafting and revision of manuscript
Anastasija Pejkovska	Cell culture methods and molecular biology experiments, manuscript proof reading
Robyn Laura Kosinsky	Mouse experiments, manuscript proof reading
Markus Glatzel	Generation of the brain metastases TMA, manuscript proof reading
Klaus Pantel	Generation of the primary tumors TMA, manuscript proof reading
Harriet Wikman	Generation of the primary tumors TMA, IHC score validation, manuscript proof reading
Steven A. Johnsen	Study design and conception, preparation, drafting and revision of manuscript

4.2. Exploring the impact of global H2Bub1 increase in USP22-deficient HER2⁺-BC

The 2nd part of the current work sought to investigate the biological outcome of global H2Bub1 increase in HER2⁺-BC via genetically deleting *Usp22* in a GEMM for HER2⁺-BC. To translate our findings to the human situation, similar to the 1st part of this work, we used functional assays in cell culture models that resemble to this mammary malignancy. Since SAGA-containing USP22 is strongly involved in transcription-regulatory processes, we applied a combined RNA-seq approach in both models to track the gene expression alterations occurring upon USP22 loss. Finally, to align our preclinical findings to the patient's situation, we made use of publically available NGS data.

Given the oftentimes reported tumor-supportive role of USP22 in a plethora of cancer entities (Glinsky et al. 2005; Table 4), we expected to observe a strongly impaired tumorigenic phenotype in USP22-deficient HER2⁺-BC, *in vivo* and *in vitro*. In line, we also hypothesized that USP22 expression was a strong prognostic marker for poor survival outcome in HER2⁺-BC patients.

Manuscript II: USP22 promotes HER2-driven mammary carcinoma aggressiveness by suppressing the unfolded protein response.

Evangelos Prokakis¹, Anna Dyas^{1,2}, Regina Grün¹, Sonja Fritzsche^{1,5}, Upasana Bedi³, Zahra B. Kazerouni¹, Robyn L. Kosinsky^{1,4}, Steven A. Johnsen^{1,4#}, Florian Wegwitz^{1,5#}

¹Department of General, Visceral and Pediatric Surgery, University Medical Center Göttingen, Göttingen, Germany

²MRC Cancer Unit, University of Cambridge, Hutchison/MRC Research Centre, Box 197, Cambridge Biomedical Campus, Cambridge, CB2 0XZ, UK

³Chromatin Remodeling Laboratory, School of Life Sciences, Jawaharlal Nehru University, New Delhi, India - 110067

⁴Gene Regulatory Mechanisms and Molecular Epigenetics Lab, Division of Gastroenterology and Hepatology, Mayo Clinic, 200 First St SW, Rochester, MN 55905, USA

⁵Department of Gynecology and Obstetrics, University Medical Center Göttingen, Göttingen, Germany

#Address correspondence to fwegwit@gwdg.de (F.W.) or johnsen.steven@mayo.edu (S.A.J.)

Running title

USP22 stabilizes HSPA5 in HER2⁺ breast cancer

Keywords

USP22, HSPA5, HER2, ER, cancer

This work was supported by a grant from the German Cancer Aid to S.A.J. (111600)

CORRESPONDING AUTHOR INFORMATION

Florian Wegwitz, Dr. rer. nat.

Molecular Gynecology


Department of Gynecology and Obstetrics

Robert-Koch-Straße 40

Göttingen, 37075

Tel.: +49 551 39 69811

Email: fwegwit@gwdg.de



Steven A. Johnsen, Ph.D.

Division of Gastroenterology and Hepatology

Mayo Clinic

200 First St SW

Rochester, MN 55902

Tel.: +1 507 255-6138

Fax: +1 507 255-6318

Email: johnsen.steven@mayo.edu


Abstract

The Ubiquitin-Specific Protease 22 (USP22) is a deubiquitinating subunit of the mammalian SAGA transcriptional co-activating complex. USP22 was identified as a member of the so-called “death-from-cancer” signature predicting therapy failure in cancer patients. However, the importance and functional role of USP22 in different types and subtypes of cancer remain largely unknown. In the present study, we leveraged human cell lines and genetic mouse models to investigate the role of USP22 in HER2-driven breast cancer (HER2⁺-BC) and demonstrate for the first time that USP22 is required for tumorigenic properties in murine and human HER2⁺-BC models. To get insight into the underlying mechanisms, we performed transcriptome-wide gene expression analyses and identified the Unfolded Protein Response (UPR) as a pathway deregulated upon USP22 loss. The UPR is normally induced upon extrinsic or intrinsic stresses that can promote cell survival and recovery if shortly activated or programmed cell death if activated for an extended period. Strikingly, we found that USP22 actively suppresses UPR induction in HER2⁺-BC cells by stabilizing the major endoplasmic reticulum (ER) chaperone HSPA5. Consistently, loss of USP22 renders tumor cells more sensitive to apoptosis and significantly increases the efficiency of therapies targeting the ER folding capacity. Together, our data suggest that therapeutic strategies targeting USP22 activity may sensitize tumor cells to UPR induction and could provide a novel, effective approach to treat HER2⁺-BC.

Introduction

HER2-positive breast cancer (HER2⁺-BC) is characterized by the overexpression and/or amplification of the *ERBB2* gene encoding the epidermal growth factor receptor 2, which occurs in approximately 15-20 % of all breast cancers (BC) (1,2). Abnormally high levels of HER2 at the plasma membrane of breast epithelial cells promote sustained intracellular signaling and stimulate aberrant cell division and tumor formation. The emergence of therapeutic strategies specifically targeting the HER2 receptor and its downstream signaling two decades ago dramatically improved the prognosis of HER2⁺-BC patients (3,4). Despite this progress, numerous patients do not respond to the therapy or develop resistant recurrences, and ultimately succumb to the disease (5). Thus, a better understanding of the molecular specific dependencies of HER2⁺-BC may uncover novel therapeutic targets that have the potential to enhance the efficacy of existing therapies or provide alternative treatment approaches for this aggressive disease.

The Ubiquitin Specific Peptidase 22 (USP22) is a deubiquitinating enzyme that was identified as a member of an 11 gene “death-from-cancer” signature which correlates with cancer stem cell characteristics and predicts disease recurrence, metastasis and poor response to therapy in malignancies of various origins including breast cancer (6). USP22



is a conserved subunit of the deubiquitination module (DUBm) of the Spt-Ada-Gcn5 acetyltransferase (SAGA) complex, a large multimeric complex that plays an important role in gene regulation (7,8). Specifically, USP22 is the catalytic subunit of the SAGA DUBm and functions to modulate gene transcription via removal of monoubiquitination from histones H2A and H2B (9). Noteworthy, USP22 also modulates the stability and function of multiple non-histone targets associated with cancer progression and poor prognostic outcome including c-Myc, Cyclin D1, Cyclin B1, EGFR, SOS, SIRT1, COX2, XPC, KDM1A, ERa (10–18) as well as nodal immunologic factors (19–21). Our previous studies demonstrated a function for USP22 in intestine epithelial cell differentiation *in vivo* and a surprising tumor-suppressive function for USP22 in colorectal cancer (22,23). Importantly, while loss of USP22 potentiated colorectal tumorigenesis via activation of the mTOR pathway, USP22-deficient tumors also displayed a particular vulnerability to either mTOR or HSP90 inhibitors (23,24). Together, these studies suggest an ambiguous and context-dependent role of USP22 where it can have either tumor supportive or tumor-suppressive functions.


The Unfolded Protein Response (UPR) pathway has been shown to play a decisive role in HER2⁺-BC aggressiveness (25). Aberrant activation of oncogenes including HER2 results in increased protein synthesis (26). The consequent induction of endoplasmic reticulum (ER) stress due to the abnormal accumulation of misfolded proteins leads to the activation of the three signaling branches of the UPR controlled by PERK, IRE1 α , and ATF6, respectively. Although low UPR activation has been shown to support the oncogenic transformation and tumor progression, higher and prolonged UPR signaling levels elicit a switch to anti-tumor, p53-independent pro-apoptotic signaling (26). Consequently, sustained UPR activation is associated with better outcomes in HER2⁺-BC (25,27–29).

In this study, we utilized both *in vitro* cell culture and an *in vivo* genetic mouse model to identify the ER-chaperone HSPA5 (also known as GRP78 or BiP) as an important deubiquitination target of USP22. This mechanism is required for the tumorigenic properties of HER2⁺-BC cells whereby USP22 inhibits UPR signaling and suppresses PERK-mediated programmed cell death via stabilization of HSPA5.

Results

USP22 supports HER2-driven mammary carcinogenesis *in vivo*.

A positive correlation between USP22 expression and cancer disease progression has been frequently reported in the past. Indeed, analysis of HER2⁺-BC patients within the TCGA breast cancer cohort confirms that patients with tumors displaying high *USP22* expression show a particularly poor prognosis (Fig. II.1A). However, to date, *in vivo* genetic mouse model studies examining the role of USP22 in cancer have been limited to prostate,



leukemia, and colorectal malignancies (16,24,37). To investigate the consequences of *Usp22* loss in HER2-driven mammary carcinomas, we utilized a transgenic mouse model in which the gene encoding HER2 (*ErbB2*) was expressed under the mammary specific MMTV promoter (MMTV-*ErbB2*). The additional mammary specific deletion of *Usp22* was achieved by crossing a mouse line containing a floxed *Usp22* allele (*Usp22^{flox}*) with the mammary-specific deletion line MMTV-Cre (Fig. II.1B) (24). Subsequent monitoring of tumor occurrence revealed a strong increase of disease-free survival in animals with tissue-specific *Usp22* knockout (median survival: 335 days) compared to *Usp22^{wt/wt}* animals (median survival: 166 days, see II. Fig.1C). Remarkably, 12.5% of *Usp22^{fl/fl}* mice never developed the disease, pointing at a critical role of *Usp22* in HER2-driven BC. Interestingly, heterozygous *Usp22* deletion in mammary carcinoma cells was sufficient to significantly increase disease-free survival of MMTV-*ErbB2* animals (median survival: 209 days), implying that the reduction of USP22 levels is sufficient to impair the oncogenic properties of HER2⁺-BC. Further analyses demonstrated that *Usp22* loss not only delayed tumor growth but also strongly reduced tumor burden as reflected by the decreased number of tumors per animal and slower tumor growth kinetics (Fig. II.1D-E). We confirmed the efficiency of the knockout in *Usp22^{fl/fl}* tumors via qRT-PCR (Fig. II.1F). Interestingly, neither the morphology nor the monoubiquitination of H2B (H2Bub1) levels of the growing tumors were affected by *Usp22* deletion. Additionally, immunohistochemical analyses confirmed that the expression of HER2, the driving oncogene in this tumor model, was not affected by *Usp22* deletion (Fig. II.1G). Our findings, therefore, demonstrate a critical tumor-promoting role of USP22 in HER2-driven BC.

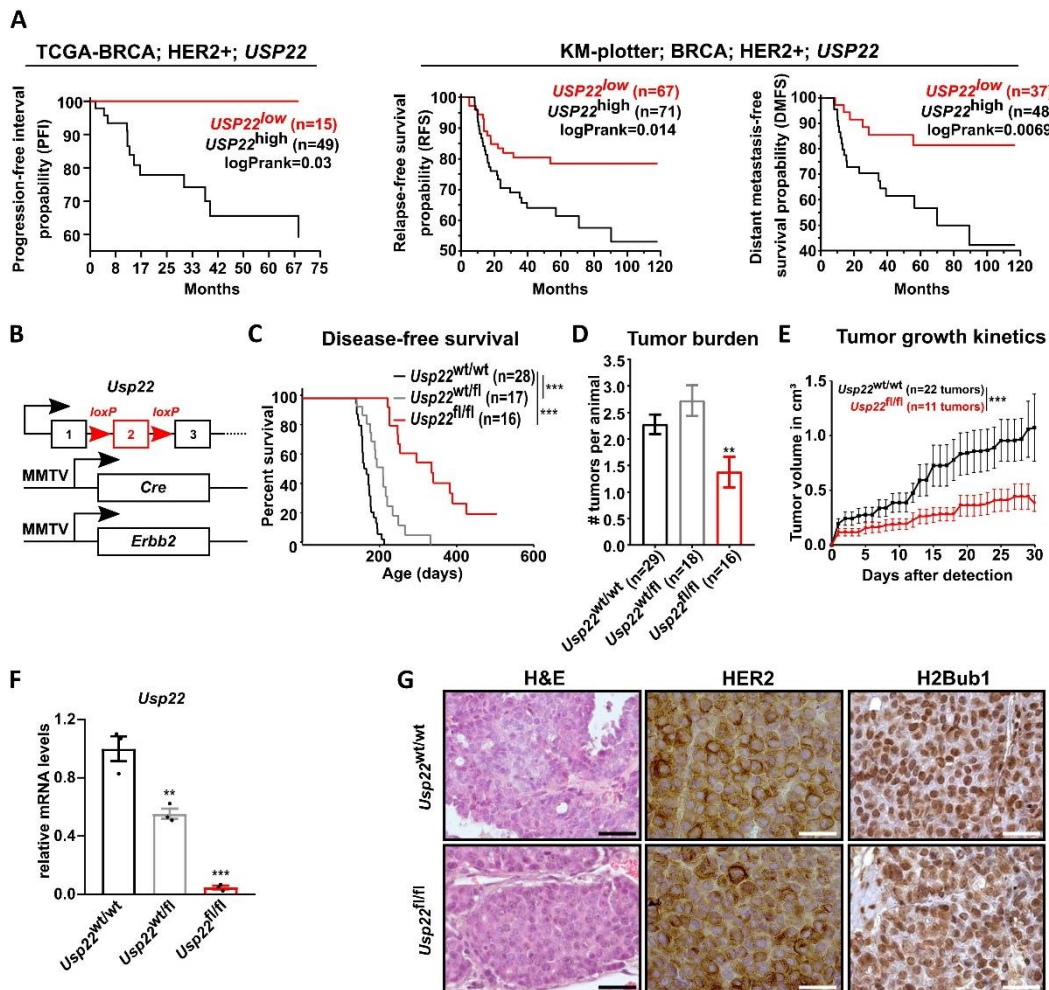


Fig.II.1: USP22 loss decreases the incidence and aggressiveness of HER2⁺-BC in the MMTV-*ErbB2* genetic mouse model. A) Progression-free interval (PFI), relapse-free survival (RFS), and distant metastasis-free survival (DMFS) plot of low- and high-*USP22* expressing HER2⁺-BC patients. Survival data were retrieved from TCGA-BRCA (xenabrowser.net) and KM-plotter derived. LogPrank test. **B)** Schematic representation of the three transgenes of the MMTV-*ErbB2*; MMTV-cre; *Usp22*flox mouse model. **C)** Disease-free survival analysis of *Usp22*^{wt/wt} (n=28); *Usp22*^{fl/wt} (n=17) and *Usp22*^{fl/fl} (n=16) animals. Log-rank test. **D)** Average number of tumors per animals in *Usp22*^{wt/wt} (n=29); *Usp22*^{fl/wt} (n=18) and *Usp22*^{fl/fl} (n=16) animals. One-way Anova test. **E)** Tumor growth kinetics of n=22 *Usp22*^{wt/wt} and n=11 *Usp22*^{fl/fl} tumors. Student t-test on the area under the curve (AUC). **F)** Validation of *Usp22* deletion efficiency in *Usp22*^{wt/wt}, *Usp22*^{fl/wt} and *Usp22*^{fl/fl} tumors (n=5 per group) via RT-qPCR. One-way ANOVA test. **G)** Representative H&E, HER2, and H2Bub1 staining on *Usp22*^{wt/wt} and *Usp22*^{fl/fl} tumors section. Black scale bar: 50 μ m. White scale bar: 25 μ m. ** p-val<0.01, *** p-val<0.005. Error bars: standard error of the mean (SEM).

USP22 loss impairs the oncogenic properties of HER2⁺-BC cells *in vitro*

To extend our observations to the human disease, we utilized two HER2⁺ human BC cell lines (HCC1954 and SKBR3) and first investigated the effect of USP22 depletion on their oncogenic properties. Loss of USP22 (Fig. II.2A-B) led to a pronounced reduction of cell number, clonogenic growth, and migratory properties of both cell lines (Fig. II.2C-E). To evaluate whether the loss of USP22 affects the HER2-signaling cascade, we examined the phosphorylation of ERK1/2 and AKT, two major downstream molecular targets of HER2 following USP22 depletion (26). Notably, in contrast to treatment with the HER2 inhibitor lapatinib, which led to a prominent reduction of both pERK1/2 and pAKT (Fig. II.1F), we did not observe notable changes in the signal transduction downstream of HER2 following USP22 depletion in HCC1954 (Fig. II.2F) and SKBR3 cells (Fig. II.S1A). Consistent with the observed effect on proliferation, the PCNA expression was strongly reduced upon USP22 silencing in HCC1954 cells compared to control transfected cells (Fig. II.2G). Taken together, loss of USP22 interferes with the tumorigenicity of HER2⁺-BC cells *in vitro* and *in vivo* without affecting HER2 expression or its canonical downstream signaling cascade.

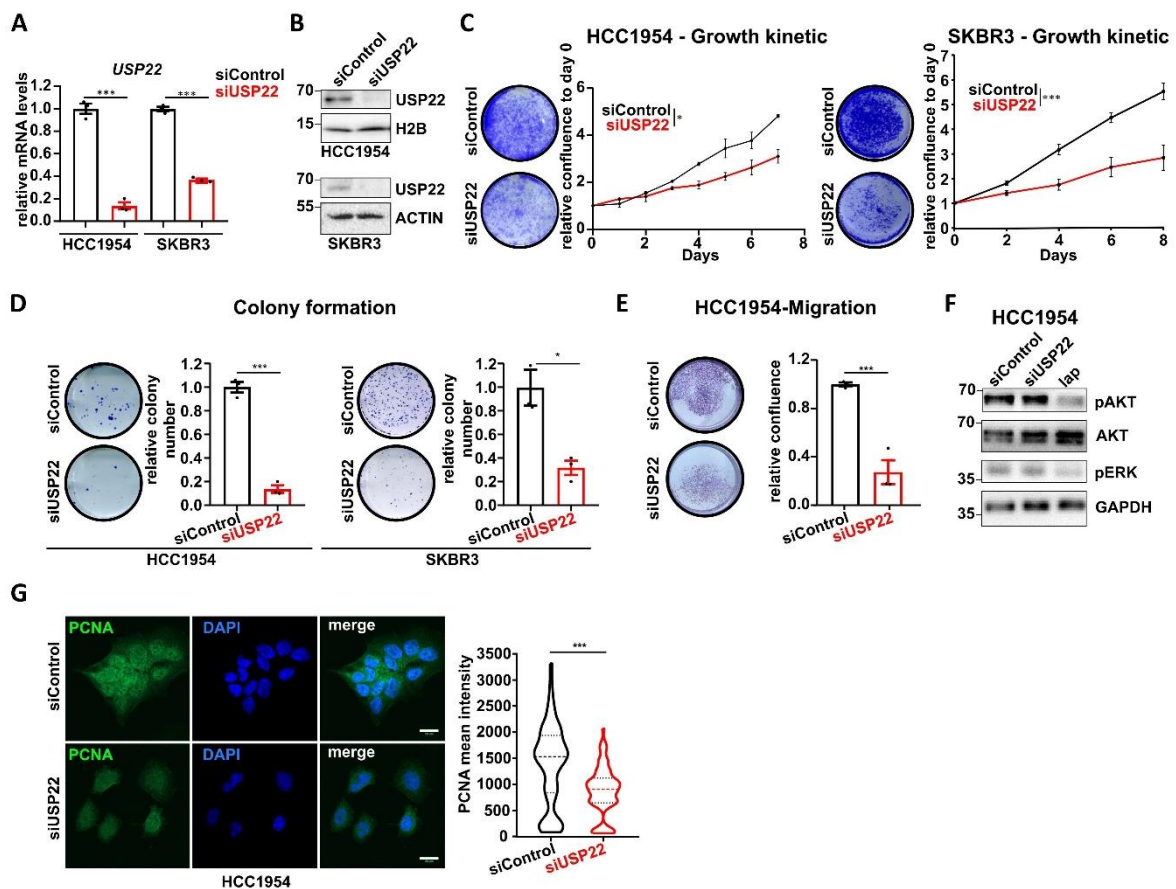


Fig.II.2: USP22 loss impairs oncogenic properties of HER2⁺-BC cells *in vitro*. A-B) Validation of USP22 knockdown efficiency via qRT-PCR (**A**) and western blot analysis (**B**) in HCC1954 and SKBR3 cells. **C-D)** Representative crystal violet staining (left panels) and quantifications (right panels) of cell confluency (**C**) and colony formation assay (**D**) of siControl- and siUSP22-treated HCC1954 and SKBR3 cells. **E)** Trans-well migration assay of HCC1954 cells with or without USP22 knockdown. Left panel: representative crystal violet; right panel: quantification. **F)** Western blot analyses showing no loss of pAKT and pERK upon USP22 silencing. Lapatinib was used as a positive control (lap; 1 μ M, 12 hours treatment). **G)** Representative pictures of PCNA and DAPI immunofluorescence staining in siUSP22- and siControl-treated HCC1954 cells. Quantification of average PCNA intensity is provided in the right panel (n=5 pictures per replicate). All experiments were performed in biological triplicates. Error bars: standard error of the mean (SEM). Statistical analyses: **A, C, D,** and **E:** Student t-test (for the growth kinetic assays, the area under the curve was used to calculate the statistic difference); **G:** Mann-Whitney test. . * p < 0.05, *** p-val<0.005.

USP22 suppresses apoptosis in HER2⁺-BC cells

To understand the USP22-dependent signaling pathways underlying its oncogenic properties, we performed transcriptome-wide analyses in murine HER2⁺-BC tumors and HCC1954 cells by mRNA-sequencing (mRNA-seq) following genetic *Usp22* deletion or siRNA-mediated USP22 depletion, respectively. We identified 1,141 differentially regulated genes upon *Usp22* loss in the murine tumors, and 496 differentially regulated genes upon USP22 knockdown in HCC1954 cells (Fig.II.3A). Interestingly, the overlap of genes regulated in murine and human tumor cells was rather low (Fig II.S1B and II.C). However, as USP22 governs similar oncogenic features in both *in vitro* and *in vivo* systems, we hypothesized that, despite the scarce overlap of regulated genes, the underlying molecular mechanisms are likely the same in both human and murine tumors. We, therefore, investigated commonly regulated pathways in the USP22-deficient condition by using Gene Set Enrichment Analysis (GSEA) and subsequently intersecting the *in vitro* and *in vivo* results. We observed that the majority of significantly enriched gene sets (FDR < 0.25) upon impairment of USP22 in HCC1954 and HER2-driven murine tumors substantially overlapped (Fig.II.3B). Interestingly, HER2⁺-BC tumor cells lacking USP22 showed enrichment for gene signatures associated with stress-induced signaling pathways (e.g. hypoxia, p53 pathway) as well apoptosis (Fig.II.3B-C). To assess whether USP22 loss indeed induces apoptosis in HER2⁺-BC cells, we first examined cell morphology following USP22 knockdown and observed an increase of membrane blebbing and cytoplasmic vacuolization, characteristics of programmed cell death (38) (Fig.II.3D). The induction of

apoptosis was further confirmed by assessing the levels of cleaved PARP as well as through flow cytometry-based annexin V assay (Fig.II.3E-F). In agreement, the levels of the apoptosis inducer Casp3 as well as its active cleaved form were elevated in *Usp22^{fl/fl}* mammary carcinomas measured by RT-qPCR and IHC staining (Fig.II.3G-I). Finally, we reasoned that if a higher rate of apoptosis is responsible for the reduced tumorigenic properties observed upon USP22 loss in HER2⁺-BC, the inhibition of caspase activity should, at least partially, rescue the impaired phenotype. Strikingly, treatment with the pan-caspase inhibitor Z-VAD almost fully restored cellular viability of USP22-deficient HCC1954 cells (Fig.II.3J). Together, for the first time, these findings demonstrate that USP22 is essential for suppressing apoptosis in HER2⁺-BC cells *in vivo* and *in vitro*.

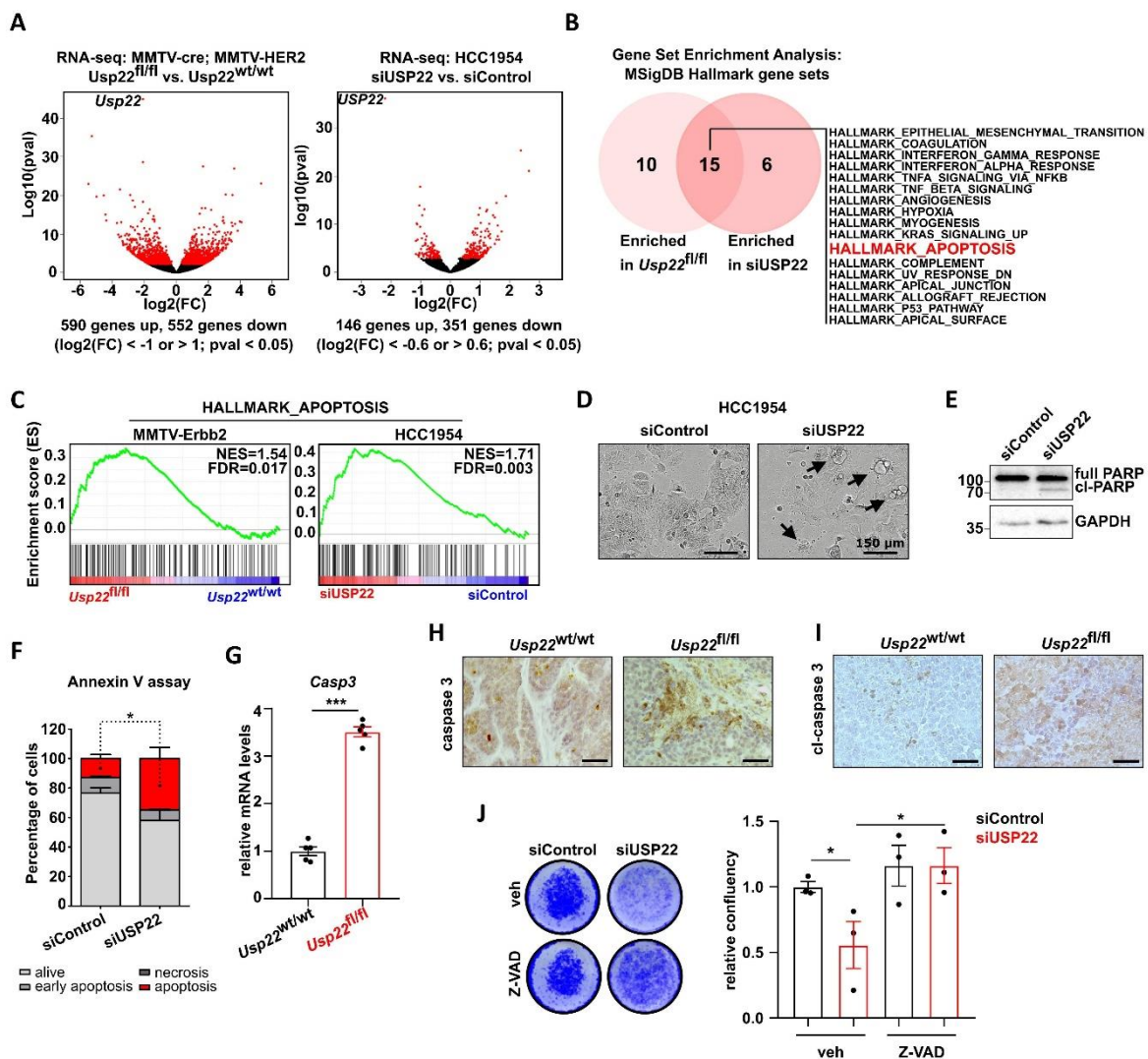


Fig.II.3: Impaired USP22 expression sensitizes HER2⁺-BC cells to apoptosis. **A)** Volcano plots showing differentially regulated genes in *Usp22^{fl/fl}* (n=4) versus *Usp22^{wt/wt}* (n=4) tumors (left panel) and in HCC1954 cells treated with siUSP22 (n=3) versus siControl (n=2) (right panel). **B)** Venn diagram showing gene sets of the MSigDB “HALLMARK” gene


sets collection commonly enriched upon USP22 loss in murine HER2⁺-mammary carcinomas and human HCC1954 cells. **C)** GSEA profiles: both mouse and human HER2⁺-tumor cells significantly enrich the “HALLMARK_APOPTOSIS” gene signature upon USP22 loss. **D-F)** HCC1954 cells strongly induce apoptosis upon USP22-knockdown, as shown in representative phase-contrast pictures (**D**), western blot analysis of cleaved PARP (**E**) and FACS-based Annexin V assay (**F**). **G)** Measurement of *Casp3* levels via RT-qPCR in *Usp22*^{wt/wt} and *Usp22*^{fl/fl} tumors (n=5 tumors per group). **H-I)** Immunohistochemical staining of full (**H**) and cleaved (**I**) caspase 3 in *Usp22*^{wt/wt}- and *Usp22*^{fl/fl}-tumors. Black scale bar=50 μm. **J)** Proliferation assay of siControl- and siUSP22-treated HCC1954 cells, co-treated with Z-VAD (80 μM). Statistical analyses: Student t-test (**F, G and J**): * p-val<0.05, *** p-val < 0.005, ns=not significant. All experiments were performed in biological triplicates or more (specified where applicable). Error bars: standard error of the mean (SEM). NES: Normalized Enrichment Score.

USP22 loss increases the sensitivity of HER2⁺-BC to the unfolded protein response

To elucidate the molecular mechanisms underlying increased apoptosis in USP22-deficient HER2⁺-BC cells, we focused on the genes of the “HALLMARK_APOPTOSIS” signature that were commonly up-regulated *in vitro* and *in vivo*. As a highly ranked gene in both HER2⁺-BC systems, the pro-apoptotic *Activating Transcription Factor 3 (ATF3)* gene particularly drew our attention (Fig.II.4A, Fig.II.S2A-B). The increased mRNA levels of *ATF3* and another pro-apoptotic factor *BCL10*, another member of the same signature, were validated via qRT-PCR in the HER2-driven murine tumors and HCC1954 cells (Fig.II.4B). Accordingly, IHC staining revealed pronounced increased levels of ATF3 in *Usp22*^{fl/fl} tumors compared to their wild-type counterpart (Fig.II.4C). To determine whether elevated ATF3 levels underlie the transcriptional changes mediated by USP22 loss, we evaluated the “regulatory target gene sets” MSigDB collection. Indeed, a significant enrichment of upregulated genes harboring at least one ATF3 binding site in their promoter was observed in both siUSP22 and *Usp22*^{fl/fl} tumor cells (Fig.II.4D). Of note, ATF3 also belongs to the previously identified significantly upregulated genes of the “HALLMARK_HYPOXIA” signature enriched in both HER2⁺-BC models (Fig.II.3B, Fig.II.S2B). ATF3 is a well-known transcription factor frequently activated upon various cellular stress conditions including hypoxia and endoplasmic reticulum (ER) stress caused by calcium imbalance, oxidizing environment, or impaired protein chaperoning capacity (39–41). To identify the processes underlying *ATF3* stimulation upon USP22 loss, we performed further mining of the GSEA results obtained from the MSigDB “gene ontology” collection. The enrichment of numerous signatures characteristic for UPR-signaling particularly drew our attention. Interestingly, the

"GO_PERK_MEDIATED_UNFOLDED_PROTEIN_RESPONSE" gene signature was significantly regulated in both *in vivo* and *in vitro* HER2⁺-BC models upon USP22 loss (Fig. II.4E, Fig. II.S2C). Therefore, we hypothesized that the increased *ATF3* expression levels upon USP22 reduction result from sustained ER stress.

The activation of the UPR-signaling is mediated by three major transmembrane receptors in the ER-membrane with stress-sensing functions, IRE1 α , PERK, and ATF6 α (26). Upon activation, the serine/threonine kinase PERK catalyzes the phosphorylation of the eukaryotic initiation factor 2 alpha (eIF2 α), thereby temporarily impeding the global protein synthesis and promoting the cap-independent translation of, among others, *Activating Transcription Factor 4 (ATF4)* that in turn stimulates *ATF3* transcription. This cascade of events has been shown to promote cellular recovery in adverse intra- or extracellular conditions (39). However, sustained activation of the PERK/ATF4/ATF3 axis of the UPR can stimulate the expression of a panel of pro-apoptotic genes including *CHOP* (alias *DDIT3*), *PMAIP* and *GADD34* (alias *PPP1R15A*) that subsequently lead to the induction of an efficient p53-independent programmed cell death if cellular stress becomes irreparable (42–44). To test if the higher levels of *ATF3* and the impaired tumor phenotype upon loss of USP22 in HER2⁺-BC are caused by sustained activation of the UPR, we analyzed several known markers and genes regulated by this pathway. Strikingly, levels of phosphorylated eIF2 α (p-eIF2 α) and *ATF4* were elevated in siUSP22-treated HCC1954 cells (Fig. II.4F). *In vivo*, *ATF4* protein levels were also markedly increased in *Usp22*^{fl/fl} tumors compared to the wild-type tumors (Fig. II.4G). Additionally, many UPR- and *ATF3*-responsive genes including *PPP1R15A*, *DDIT3*, *PPP2R5B*, *CREB5*, *CDKN2B*, and *KLF13* were found to be upregulated in siUSP22-treated HCC1954 cells (Fig. II.S2D). In agreement, GSEA of human HER2⁺-BC whole transcriptome datasets (TCGA BRCA dataset) demonstrated that *USP22*^{low} lesions also have elevated UPR-signaling compared to *USP22*^{high} tumors (Fig. II.4H). Accordingly, a significant negative correlation between *USP22* expression and several UPR-responsive genes including *ATF3*, *PPP1R15A*, *DDIT3*, and *BCL2L1* was observed in HER2⁺-BC patients (Fig. II.S2E). Furthermore, higher expression levels of *ATF3*, *PPP1R15A*, *PPP2R5B*, *DDIT3*, and *BCL10* are associated with better prognosis in HER2⁺-BC patients, suggesting an overall tumor-suppressive role of the UPR-driven signaling cascade (Fig. II.S2F). Interestingly, the regulation of UPR by USP22 might not be limited to the HER2⁺-BC subtype, as an enrichment of UPR-specific gene signatures was also observed in mRNA-seq datasets of normal immortalized mammary epithelial cells (MCF10A) and prostate carcinoma cells (LNCaP) upon USP22 knockdown (Fig. II.S3A, Fig. II.S3B). Taken together, our results support a negative regulatory role of USP22 in controlling UPR signaling.



As described above, PERK plays a central role in the activation of the UPR. Based on our findings that both p-eIF2A and ATF4 levels were increased upon USP22 loss, together with an enrichment of a PERK-mediated UPR gene expression signature in both *in vivo* and *in vitro* models, we postulated that USP22 might suppress PERK activation to maintain low UPR levels in cancer cells. To test this hypothesis, we depleted USP22 in HCC1954 and SKBR3 cells and examined the effects of treatment with the PERK inhibitor (PERKi) GSK2606414. Strikingly, PERK inhibition not only reversed the activation of UPR-responsive genes (Fig. II.4I, Fig. II.S3C) but also efficiently rescued apoptosis-associated PARP cleavage caused by USP22 depletion (Fig. II.4J) and cell viability of both cell lines (Fig. II.4K-L). To confirm that activation of the UPR downstream of PERK impairs HER2⁺-BC cell growth, we treated HCC1954 cells with the PERK activator CCT020312 (2.5 μM) alone or in combination with USP22 knockdown. Indeed, PERK activation alone markedly reduced HCC1954 proliferation and significantly potentiated the anti-proliferative effects of USP22 depletion (Fig. II.S3E). Taken together, our findings demonstrate that USP22 supports the tumorigenic phenotype and reduces the apoptotic rate of HER2⁺-BC cells by maintaining low UPR-signaling.

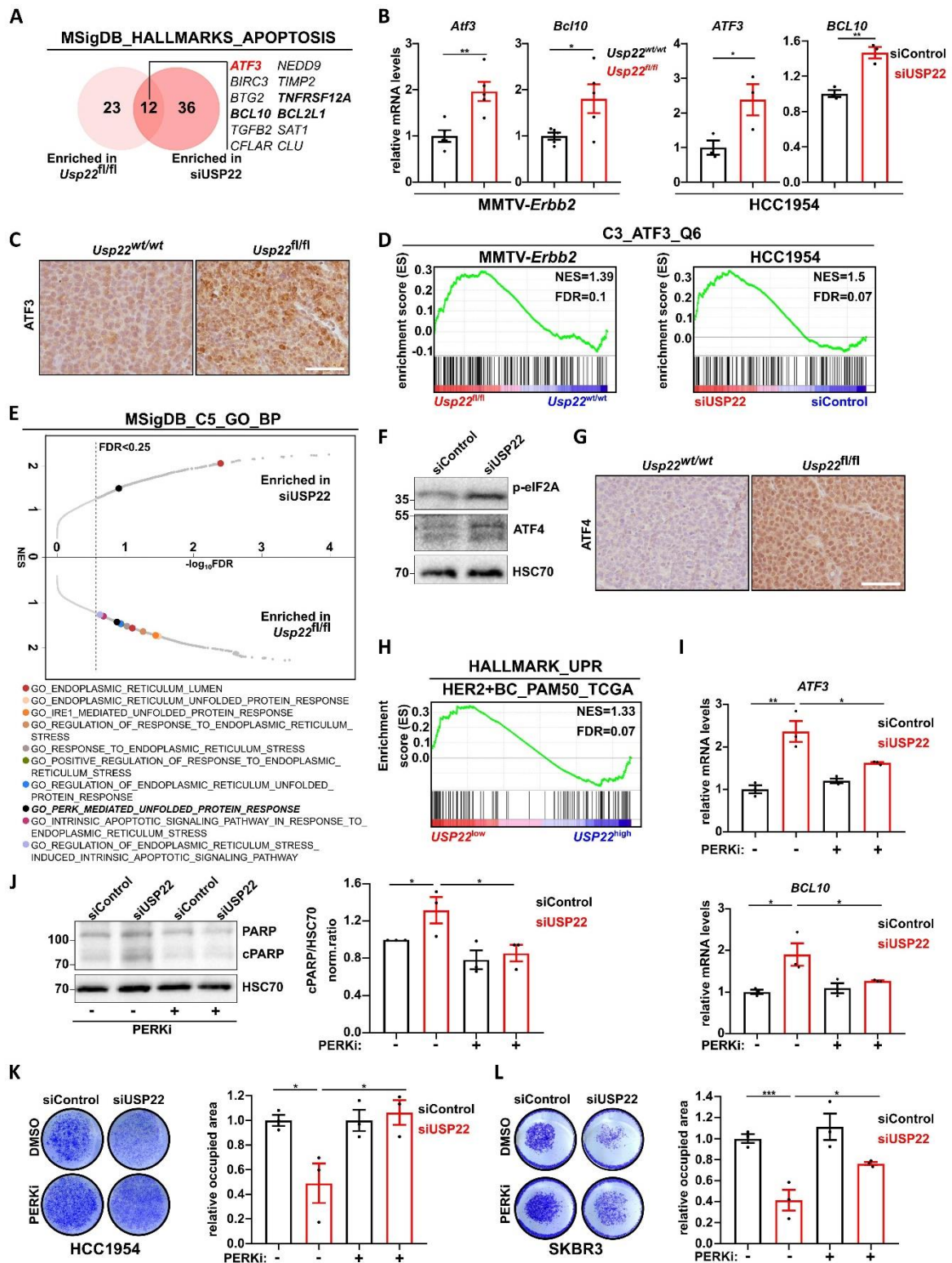



Fig.II.4: USP22 loss increases the sensitivity of HER2⁺-BC to the unfolded protein response. **A)** Venn diagram of co-regulated genes of the MSigDB “HALLMARK_APOPTOSIS” in both murine and human HER2⁺-BC models. **B)** RT-qPCR validation of the increased *ATF3* and *BCL10* expression levels in *Usp22^{fl/fl}* tumors (n=5

tumors per group) and siUSP22-treated HCC1954 cells compared to the respective control conditions. **C)** Representative pictures of immunohistochemical detection of ATF3 levels in *Usp22^{wt/wt}* and *Usp22^{fl/fl}* tumors. Scale bar: 50 μ m. **D)** Gene set enrichment analysis in murine tumor cells and HCC1954 cell line showing an enrichment for genes harboring at least one ATF3 binding site in their regulatory region ("ATF3_Q6") upon USP22 loss. **E)** Graphical integration of the GSEA analysis results from HCC1954 and MMTV-*ErbB2* tumor cells upon USP22 loss utilizing the MSigDB "GO gene sets" collection. **F)** Western blot analysis showing an increase of p-eIF2 α and ATF4 protein levels upon siUSP22-treatment in HCC1954. **G)** Representative pictures of immunohistochemical detection of ATF4 in *Usp22^{wt/wt}* and *Usp22^{fl/fl}* tumors. Scale bar: 50 μ m. **H)** GSEA analysis of HER2⁺-BC patients data (TCGA-BRCA dataset) showing a significant enrichment of the "HALLMARK_UNFOLDED_PROTEIN_RESPONSE" gene signature in *USP22^{low}* tumors (*USP22^{low}*: FPKM value \leq 29.56, *USP22^{high}*: FPKM value \geq 38.46). **I)** PERK inhibition in HCC1954 cells (GSK2606414, 8 μ M, 24h) inhibits the induction of *ATF3* and *BCL10* upon USP22 knockdown, as assessed by RT-qPCR. **J)** PERK inhibitor treatment of HCC1954 cells (GSK2606414, 8 μ M, 24h) reverses the induction of apoptosis upon USP22 loss, as assessed by western blot for cleaved PARP. **K-L)** PERK inhibition (GSK2606414, 8 μ M) rescues the proliferation of HCC1954 (**K**) and SKBR3 cells (**L**) upon siRNA mediated knockdown of *USP22*. Left panels: representative crystal violet staining, right panels: quantification, respectively. Statistical analyses: Student t-test (**B**), One-way Anova (**I-L**). * p-val<0.05, ** p-val<0.01. All experiments were performed in biological triplicates or more (specified where applicable). Error bars: standard error of the mean (SEM). NES: Normalized Enrichment Score.

USP22 suppresses UPR-induced apoptosis in HER2⁺-BC by stabilizing HSPA5

In addition to its function in epigenetic regulation, USP22 has been shown to deubiquitinate several other cellular proteins. Notably, a recent ubiquitinome-wide analysis identified the heat shock 70 kDa protein 5 (HSPA5, also known as BiP or GRP78) as a target of USP22-mediated deubiquitination in prostate cancer cells (16). Given the fact that HSPA5 is a major regulator of PERK activity, we hypothesized that USP22 may function to suppress UPR activation by deubiquitinating and stabilizing this ER-residing chaperone. To test this, we first examined the impact of USP22 loss on the RNA and protein levels of HSPA5 in the murine and human HER2⁺-BC models. Consistent with our hypothesis, USP22-silencing specifically affected HSPA5 protein levels without affecting *HSPA5* mRNA expression in both human HER2⁺-BC cell lines (Fig. II.5A and II.B). Similarly, although *Usp22^{fl/fl}* tumors exhibit a significant increase in *Hspa5* gene expression compared to wild-type tumors,



immunohistochemistry staining showed a strong decrease in HSPA5 protein levels (Fig. II.5C, D and II.S4A). To further confirm that USP22 directly regulates HSPA5, we performed co-immunoprecipitation to examine whether USP22 and HSPA5 physically interact in cells. Indeed, immunoprecipitation of USP22 resulted in the co-precipitation of HSPA5 (Fig. II.5E). Importantly, treatment of HCC1954 cells with the proteasome inhibitor bortezomib restored HSPA5 levels following USP22 depletion, further confirming a central role of USP22 in stabilizing HSPA5 by preventing its degradation by the ubiquitin-proteasome system (Fig. II.5F). Consistently, cycloheximide chase analyses demonstrated that HSPA5 stability was significantly shorter upon USP22 loss compared to control transfected cells (Fig. II.5G). Taken together, these results demonstrate a previously unknown role of USP22 in stabilizing HSPA5 in HER2⁺-BC.

HER2⁺-BC patients with HSPA5^{high}-expressing lesions have a poor survival outcome compared to their HSPA5^{low} counterparts (Fig. II.S4B). We, therefore, tested whether the impairment of HSPA5 activity could phenocopy the loss of USP22 and induce the UPR. Indeed, inhibition of HSPA5 using the specific inhibitor HA15 led to a pronounced activation of UPR signaling as measured by the induction of *ATF3*, *PPP1R15A*, *DDIT3*, *BCL10* and *CREB5* gene expression in HCC1954 and SKBR3 cells (Fig. II.5H, Fig. II.S4C). Furthermore, HA15 treatment also increased the apoptosis rate of HCC1954 cells (Fig. II.5I). Consistently, either HSPA5 inhibition or depletion significantly reduced HER2⁺-BC cell viability (Fig. II.5J, Fig. II.S4D) and these effects could be potentiated by USP22 depletion (Fig. II.5K, Fig. II.S4E). Together, our study reveals a previously unknown role of USP22 in suppressing activation of UPR signaling by stabilizing the major ER-resident molecular chaperone HSPA5. Our results further reveal a vulnerability of HER2⁺-BC cells expressing low levels of USP22 to UPR induction. This may provide a novel therapeutic approach for innovative HER2⁺-BC treatment strategies based on USP22 expression and/or inhibition.

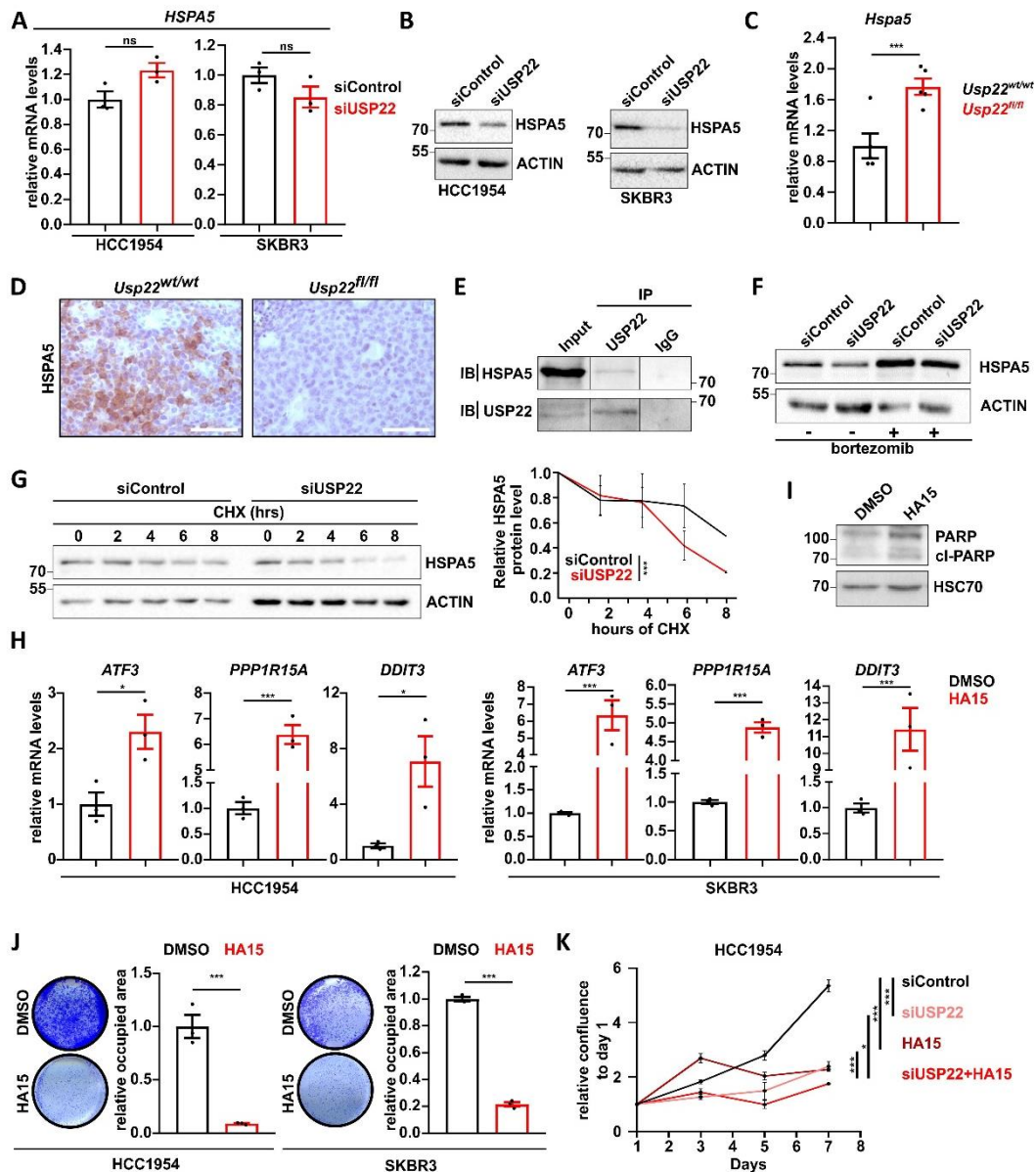


Fig.II.5: USP22 maintains HSPA5 stability and suppresses UPR-induced apoptosis in HER2⁺-BC. A-B) RT-qPCR (A) and western blot analysis (B) assessing HSPA5 mRNA and protein levels in siControl- and siUSP22-treated HCC1954 and SKBR3 cells, respectively. C-D) RT-qPCR (C) and immunohistochemical detection (D) assessing HSPA5 mRNA and protein levels in *Usp22^{wt/wt}* and *Usp22^{fl/fl}* tumors, respectively. N=5 tumors per group. E) Co-immunoprecipitation analysis of USP22 and HSPA5 in HCC1954 cells. IP: immunoprecipitation. IB: immunoblot. F) Proteasome inhibition (bortezomib, 20 nM, 12 hours) rescues loss of HSPA5 protein levels upon USP22 knockdown in HCC1954 cells, as assessed by western blot. G) Cycloheximide chase assay (50 μ M) showing a reduction of HSPA5 protein stability upon USP22 knockdown in HCC1954 cells. Left panel: representative HSPA5 western blot; right panel: densitometric quantification of HSPA5 protein levels over time and normalized to the respective actin signal. Statistical tests on

the last time point. **I)** Western blot showing an increase of cleaved PARP levels in HCC1954 treated with an HSPA5 inhibitor (HA15, 20 μ M, 24 hours). **H)** RT-qPCR showing an expression increase of UPR responsive genes (*ATF3*, *PPP1R15A*, and *DDIT3*) upon treatment of HCC1954 and SKBR3 cells with HA15 (20 μ M, 24 hours). **I)** HCC1954 cells treated with 20 μ M HA15 for 48h showed increased levels of the apoptosis marker cl-PARP, as assessed by western blot. **J)** Proliferation assay: treatment of HCC1954 and SKBR3 cells with HA15 (32 μ M and 10 μ M, respectively) dramatically reduce their proliferation potential. Left panels: representative pictures of crystal violet-staining; Right panels: quantification of the respective confluency. **K)** Assessment of the growth kinetics of HCC1954 cells treated with siUSP22 and/or HA15 (32 μ M): quantification of the confluence (normalized to day 0) over time by Celigo® measurements. Statistical tests were performed on the last time point. Statistical test: Student t-tests (**A**, **C**, **E**, **H**, and **J**). One-way Anova test (**K**). * p-val<0.05, *** p-val<0.005, ns= not significant. All experiments were performed in biological triplicates or more (specified where applicable). Error bars: standard error of the mean (SEM).

Discussion

Because of its reported association with tumor aggressiveness and progression of numerous cancers, USP22 has been the focus of increasing research efforts in recent years. As a subunit of the SAGA complex, the epigenetic function of USP22 via the deubiquitination of histone proteins has been extensively studied (23,24,45–48). However, as observed here and in previous studies, USP22 loss frequently does not result in significant changes to global H2Bub1 levels, suggesting USP22 to enact non-epigenetic oncogenic functions as well (22,48). Consistently, an increasing number of studies have uncovered novel deubiquitination targets of USP22 (10–21). In this way, USP22 can positively influence numerous oncogenic signaling cascades. For example, USP22 can promote breast and gastric cancer aggressiveness by stabilizing the proto-oncogene c-Myc (10) to reprogram cellular metabolism and stimulate mRNA and protein synthesis (49). Similarly, USP22 was also shown to promote hepatocellular cancer cell chemotherapy resistance, nasopharyngeal carcinoma progression, and gastric cancer tumorigenic properties by stimulating the PI3K/AKT- and the MAPK-signaling (50–52). Noticeably, both of these pathways also strongly positively influence metabolism, cell growth, and protein synthesis by inducing the activity of mTOR (53). In contrast, both AKT and MAPK signaling were unaffected in HER2⁺-BC in our study. Therefore, it appears that USP22 oncogenic functions are context-dependent, but frequently converge on the stimulation of anabolic pathways that have been associated with an increased ER stress load, including increased global protein synthesis, which requires increased capacity for protein folding (26,49). In

this context, the UPR-signaling can act as a negative feedback loop by inhibiting cap-dependent translation to restore protein homeostasis and protect against irreversible ER damage. However, how tumor cells avoid excessive UPR activation and downstream activation of p53-independent programmed cell death remains insufficiently understood. To date, investigations into the function of USP22 in breast cancer have been solely limited to *in vitro* studies and immunohistochemical staining of tumor samples and did not specifically investigate its relevance in HER2⁺-BC (10,18,54). In this study, we leveraged a previously uncharacterized genetic mouse model, human cell lines, and multiple publically available patient datasets to decipher the role of USP22 in HER2⁺-BC. Consistent with previous work in other breast cancer cell lines, loss of USP22 dramatically impaired tumorigenicity of HER2-driven mammary carcinoma cells both *in vivo* and *in vitro*. Interestingly, these effects were not related to a disruption of the oncogenic HER2-signaling. We recently reported a SAGA-related role for USP22 in supporting the protein chaperoning system by transcriptionally activating the expression of members of the HSP90 family in colorectal and breast cancer cells (24). In this study, we identified a novel function of USP22 supporting the protein chaperoning system by stabilizing the major ER-resident chaperone protein HSPA5. HSPA5 belongs to the glucose-regulated protein family supporting folding capacity and preventing the activation of stress sensor receptors in the ER (55,56). Interestingly, pronounced tumor supportive properties were described for HSPA5 in different cancer entities including BC *in vivo* and *in vitro* (55,57,58). We observed that impaired expression of USP22 sensitizes HER2-positive BC to the programmed cell death along the HSPA5/PERK/ATF4/ATF3-axis of the UPR (Fig. II.6). Interestingly, numerous recent studies reported a vulnerability of HER2⁺-BC to ER stress induction, suggesting this approach as an attractive alternative to specifically target this type of malignancies (25,27,29). Our work supports this notion and describes an important implication of HSPA5 in maintaining moderate UPR-signaling levels in USP22^{high} lesions. We, therefore, hypothesize that patients with USP22^{high} tumors may particularly benefit from therapies specifically stimulating the activity of this pathway, possibly in combination with inhibitors of USP22 activity. Recent efforts have been made to design potent HSPA5-specific small molecule inhibitors (59–63). The small-molecule inhibitor HA15, a thiazole benzenesulfonamide that specifically inhibits HSPA5 ATPase activity, was shown to activate the UPR-signaling in melanoma by disrupting its interaction with PERK, IRE1, and ATF6 and demonstrated to overcome BRAF therapy resistance of the cancer cells *in vitro* as well as in xenograft analyses (64). Our investigations further demonstrated that the anti-tumor properties of HSPA5 inhibition as well as small molecule-mediated PERK activation may also apply to the HER2⁺-BC. Interestingly, the toxicity of HSPA5 inhibitors seems to be

restricted to cancer cells as the tested compounds were well tolerated in murine xenograft models (65).

Collectively, our present work identifies a new pro-tumorigenic function of USP22 in the suppression of UPR signaling, revealing its global role in supporting the cellular protein chaperoning system and protecting tumor cells against proteostasis imbalance. It is therefore tempting to hypothesize that inhibition of USP22 activity could represent an innovative approach to target HER2+BC and that simultaneous pharmacologic stimulation of UPR-signaling could potentiate these effects.

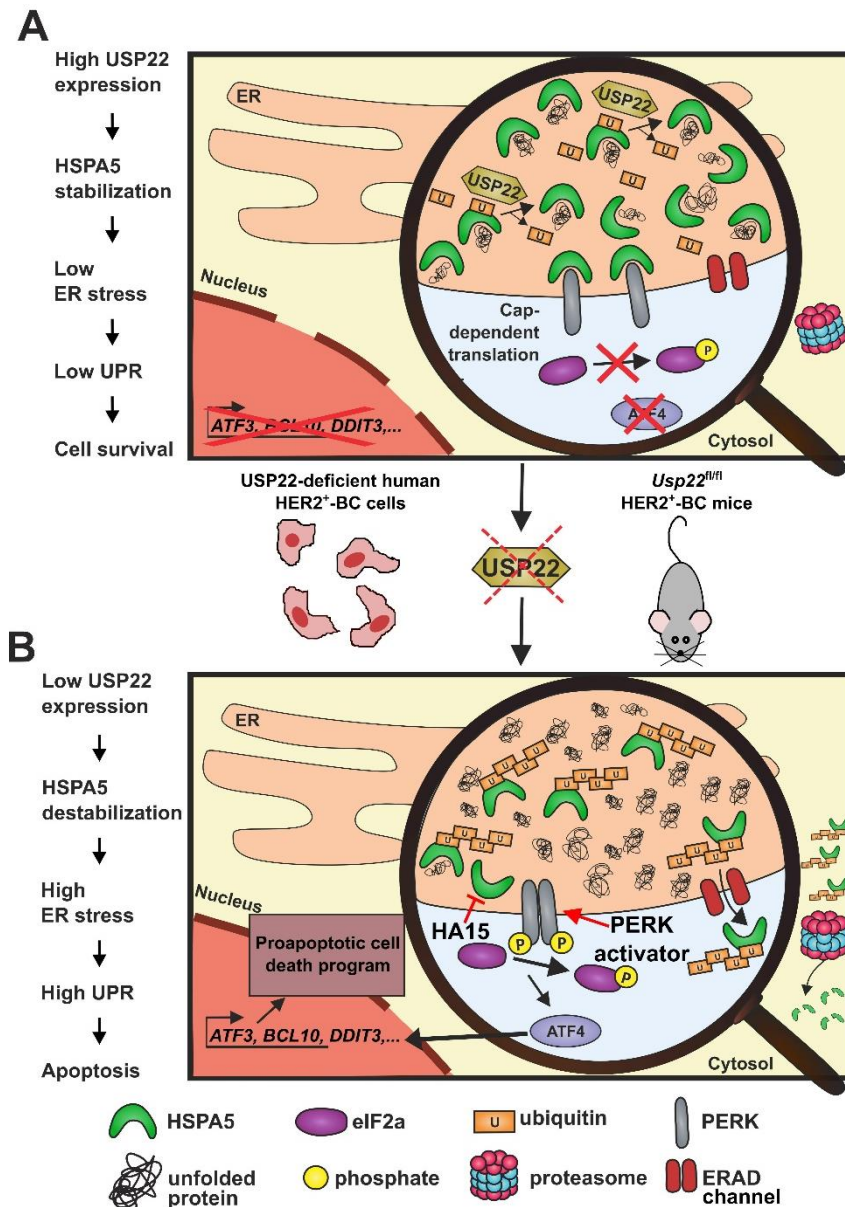


Fig.II.6: USP22 promotes HER2-driven mammary carcinoma aggressiveness by stabilizing HSPA5 and inhibiting the unfolded protein response. A) When highly expressed, USP22 stabilizes HSPA5 via its deubiquitinase activity, increasing thereby the

protein folding capacity in the ER of cancer cells and maintaining low levels of UPR signaling. **B)** At low USP22 levels or upon USP22 impairment, HSPA5 protein stability is decreased. As a consequence, unfolded proteins accumulate in the ER, leading to the stimulation of the UPR. Homodimerisation and autophosphorylation of PERK lead to the phosphorylation of eIF2a (p-eIF2a), inhibiting the cap-dependent translation and stimulating the synthesis of the ATF4 transcription factor that in turn activates the expression of important effectors of the UPR like ATF3. Prolonged activation of the PERK/ATF4/ATF3 axis robustly induces the programmed cell death in a p53-independent manner. Although no USP22-specific inhibitors are to date existing, several HSPA5-specific inhibitors (e.g HA15) or the PERK activator CTT have been developed. These inhibitors could help to simulate a USP22^{low/null} state in the tumor cells and substantially contribute to the development of new UPR-based anti-cancer therapeutic strategies

Materials and Methods

Animal handling and mouse model generation

Animals were housed under specific pathogen-free (SPF) conditions and in accordance with the animal welfare laws and regulations of the state of Lower-Saxony (LAVES, registration number #15/1754). For more details, please refer to the Supplementary Data.

Publically available datasets

Publically available data were extracted from the Kaplan-Meier plotter (30) (kmplot.com) and The Cancer Genome Atlas (TCGA, xenabrowser.net) platforms to examine the association of *USP22* and *HSPA5* expression with the progression-free interval (PFI), relapse-free survival (RFS) and distant metastasis-free survival (DMFS). Additionally, overall survival (OS) of HER2⁺-BC patients was assessed along on the expression of UPR-responsive genes. Please refer to the Supplementary Data for BC subtype classification parameters. Correlation of USP22 expression and UPR-responsive genes was performed on the "Tumor Breast (HER2) - Concha - 66 - fRMA - u133p2" dataset retrieved from the online R2-platform (<https://r2.amc.nl>).

Cell culture, transfections, and functional assays

HCC1954 (ATCC® CRL-2338™) and SKBR3 (ATCC® HTB-30™) cells were purchased from the American Type Culture Collection (ATCC) and cultivated in RPMI 1640 GlutaMAX (Gibco) and DMEM/F12 GlutaMAX (Gibco) supplemented with fetal bovine serum (Sigma-Aldrich) and 1x penicillin/streptavidin (Gibco), respectively (for more details about the used cell lines, please refer to Table S1). siRNA transfections were performed using Lipofectamine® RNAiMAX (Invitrogen) in OptiMEM GlutaMAX (Gibco) according to the

manufacturer's guidelines. A list of the siRNAs utilized in this study is provided in Table S2. Proliferation kinetics and tumorsphere numbers were recorded using a Celigo® S imaging cytometer (Nexcelom Bioscience LLC) or an IncuCyte® Live Cell Analysis System (Sartorius AG). Colony formation and trans-well migration assays were stained with crystal violet and scanned with an Epson Perfection V700 Photo. Detailed protocols for siRNA transfection and functional assays can be found in the Supplementary Data.

Immunofluorescence and immunohistochemical staining

Immunofluorescence: cells were reverse-transfected with siRNAs in 6-well plates with coverslips and grown for another 72 h. Cells were then washed with PBS, cross-linked with 4% paraformaldehyde in PBS, and permeabilized with 1% Triton X-100 in PBS for 10 min. Subsequently, coverslips were blocked for 1 h and incubated with the primary antibody overnight. Coverslips were washed and a secondary antibody was applied with DAPI for 1 h at room temperature. Coverslips were washed and mounted on microscope slides. The detailed protocol as well the list of antibodies used in this study are provided in the supplementary methods and Table S4, respectively.

Immunohistochemistry: a detailed protocol is provided in the supplementary methods. Briefly, 5 µm tissue sections were de-paraffinized in xylene and rehydrated using decreasing alcohol concentrations. Antigen retrieval and endogenous peroxidase block were performed in citric acid buffer (10 mM citric acid, pH 6, 0.1% Tween 20) and 3% H₂O₂ in PBS, respectively. Samples were then incubated in blocking solution (5% bovine serum albumin (BSA, Merk) and 1% donkey serum (Dianova GmbH) in PBS). Primary and secondary antibodies (see supplementary Table S4-5) were diluted in blocking solution and incubated in a dark humidified chamber. Biotinylated secondary antibodies (GE Healthcare, see supplementary Table S5) and ExtrAvidin-Peroxidase (Sigma-Aldrich) were diluted in PBS, and samples were incubated in a dark humid chamber. Staining was developed using 3,3'-diaminobenzidine-tetrahydrochloride (DAB; Roth) and counterstained using hematoxylin. Slides were dehydrated following the reverse order of the alcohol gradient and mounted with Histokitt (Carl Roth GmbH).

Microscopy

Immunohistochemistry (IHC) pictures were taken with a Zeiss Axio Scope A1. Brightfield images of cultured cells were taken with a Nikon Eclipse S100 inverted microscope and immunofluorescence pictures with a Zeiss LSM 510 Meta confocal microscope.

Apoptosis assay

Annexin V staining: 72 h post-transfection, adherent and floating cells were collected, washed twice with PBS and resuspended in binding buffer (10 mM HEPES, pH 7.4; 140 mM NaCl; 25 mM CaCl₂) at a concentration of 10⁵ cells in 100 µl. 5 µl Annexin V-FITC (Southern Biotech) and 1 µl propidium iodide (Sigma Aldrich) were added per sample, gently mixed, and incubated for 15 min at room temperature in the dark. 400 µl binding buffer was subsequently added to each sample. Analysis of the Annexin V staining was performed using a Guava EasyCyte Plus flow cytometer (Guava Technologies).

Protein stability assessment

Cycloheximide Chase Assay: siControl- and siUSP22-transfected HCC1954 cells were treated with 50 µM of cycloheximide (Sigma) at different time points (64, 66, 68 and 70 hours post-transfection) to achieve 8, 6, 4 and 2 hours treatment, respectively. The experiment was stopped at 72 hours post-transfection and proteins were harvested for later analysis via western blot.

Proteasome inhibition assay: 60 hours post-transfection, siControl- as well as siUSP22-transfected HCC1954 cells were treated with 20 nM bortezomib (Selleckchem) for 12 h. Control cells were treated with DMSO as a vehicle in all experiments. The experiment was stopped at 72 h post-transfection and proteins were harvested for later analysis via western blot.

Co-immunoprecipitation (CoIP) assay

CoIP was performed based on Wienken et al. (31). A detailed procedure is provided in the Supplementary Data.

RNA isolation and real-time quantitative PCR (RT-qPCR)

RNA isolation, cDNA synthesis, and RT-qPCR were performed as previously described (32,33). Detailed protocols are provided in Supplementary Data.

mRNA library preparation and data analysis

mRNA sequencing (mRNA-seq) libraries were generated from MMTV-*ErbB2* tumors with the TruSeq® RNA Library Prep Kit v2 (Illumina) according to the manufacturer's instructions and samples were sequenced (single-end 50 bp) on a HiSeq4000 (Illumina) at the NGS Integrative Genomics Core Unit (NIG) of the University Medical Center Göttingen (UMG). mRNA-seq data were then processed and analyzed in the Galaxy environment provided by the "Gesellschaft für Wissenschaftliche Datenverarbeitung mbH Göttingen" (GWDG).

Briefly, the first 11 nucleotides of the raw reads were trimmed (FASTQ Trimmer). Murine mRNA-seq data were mapped to the mm10 reference genome using RNA STAR (version 2.4.0d-2), and human mRNA-seq data were aligned to the hg19 reference genome using the TopHat Gapped-read mapper (version 2.1.1) (34,35). Read counts per gene were calculated with featureCounts. Finally, differential gene expression analysis and normalized counts were obtained using DESeq2 (36). To identify differentially regulated genes upon USP22 loss, we used a cut-off of $|\log_2 \text{fold change}| \geq 1$; $\text{FDR} < 0.05$ and $|\log_2 \text{fold change}| \geq 0.6$, $p\text{-value} < 0.05$ in murine tumors and HCC1954 cells, respectively. A detailed analysis workflow is available in Supplementary Data. Raw sequencing data are accessible at ArrayExpress (<https://www.ebi.ac.uk/arrayexpress/>) with the following accession number: E-MTAB-9331 (MMTV-*ErbB2* mouse model), E-MTAB-8256 (HCC1954).

Acknowledgments

We would like to thank S. Bolte, N. Molitor and the staff of the European Neuroscience Institute Göttingen for assistance in the animal handling administration, F. Alves (Translational Molecular Imaging, Max Planck Institute for Experimental Medicine, Göttingen) for access to the IncuCyte® Live Cell Analysis System (Sartorius AG). Also, we would especially like to thank Xin Wang and Ana Patricia Kutschat for providing precious feedback to this work. Moreover, we would like to thank the TCGA Research Network for the free access of patient-derived mRNA-seq and survival data (<https://www.cancer.gov/tcga>). This work was supported by funding from the Deutsche Krebshilfe to S.A.J. (111600).

Conflict of interest

E.P., A.D., R.G., S.F., U.B., Z.B.K., R.L.K., S.A.J., F.W. declare no conflict of interest.

Supplementary information is available at *Cell Death and Differentiation* website

References of Manuscript II

1. Voduc KD, Cheang MCU, Tyldesley S, Gelmon K, Nielsen TO, Kennecke H. Breast cancer subtypes and the risk of local and regional relapse. *J Clin Oncol*. 2010;
2. Harbeck N, Penault-Llorca F, Cortes J, Gnant M, Houssami N, Poortmans P, et al. Breast cancer. *Nat Rev Dis Prim*. 2019 Dec 1;5(1).
3. Kümler I, Tuxen MK, Nielsen DL. A systematic review of dual targeting in HER2-positive breast cancer. Vol. 40, *Cancer Treatment Reviews*. *Cancer Treat Rev*; 2014. p. 259–70.
4. Harbeck N. Advances in targeting HER2-positive breast cancer. Vol. 30, *Current Opinion in Obstetrics and Gynecology*. Lippincott Williams and Wilkins; 2018. p. 55–9.

5. Xu X, De Angelis C, Burke KA, Nardone A, Hu H, Qin L, et al. HER2 reactivation through acquisition of the HER2 L755S mutation as a mechanism of acquired resistance to HER2-targeted therapy in HER2+ breast cancer. *Clin Cancer Res.* 2017;23(17).
6. Glinsky G V., Berezovska O, Glinskii AB. Microarray analysis identifies a death-from-cancer signature predicting therapy failure in patients with multiple types of cancer. *J Clin Invest.* 2005;115(6):1503–21.
7. Koutelou E, Hirsch CL, Dent SYR. Multiple faces of the SAGA complex. Vol. 22, *Current Opinion in Cell Biology.* 2010. p. 374–82.
8. Tang P, Tse GM. Immunohistochemical surrogates for molecular classification of breast carcinoma: A 2015 update. In: *Archives of Pathology and Laboratory Medicine.* 2016.
9. Lang G, Bonnet J, Umlauf D, Karmodiya K, Koffler J, Stierle M, et al. The Tightly Controlled Deubiquitination Activity of the Human SAGA Complex Differentially Modifies Distinct Gene Regulatory Elements. *Mol Cell Biol.* 2011 Sep 15;31(18):3734–44.
10. Kim D, Hong A, Park HI, Shin WH, Yoo L, Jeon SJ, et al. Deubiquitinating enzyme USP22 positively regulates c-Myc stability and tumorigenic activity in mammalian and breast cancer cells. *J Cell Physiol.* 2017 Dec;232(12):3664–76.
11. Gennaro VJ, Stanek TJ, Peck AR, Sun Y, Wang F, Qie S, et al. Control of CCND1 ubiquitylation by the catalytic SAGA subunit USP22 is essential for cell cycle progression through G1 in cancer cells. *Proc Natl Acad Sci U S A.* 2018 Oct;115(40):E9298–307.
12. Lin Z, Yang H, Kong Q, Li J, Lee SM, Gao B, et al. USP22 Antagonizes p53 Transcriptional Activation by Deubiquitinating Sirt1 to Suppress Cell Apoptosis and Is Required for Mouse Embryonic Development. *Mol Cell.* 2012 May;46(4):484–94.
13. Zhang H, Han B, Lu H, Zhao Y, Chen X, Meng Q, et al. USP22 promotes resistance to EGFR-TKIs by preventing ubiquitination-mediated EGFR degradation in EGFR-mutant lung adenocarcinoma. *Cancer Lett.* 2018 Oct;433:186–98.
14. Lin Z, Tan C, Qiu Q, Kong S, Yang H, Zhao F, et al. Ubiquitin-specific protease 22 is a deubiquitinase of CCNB1. *Cell Discov.* 2015 Oct;1(1):1–16.
15. Xiao H, Tian Y, Yang Y, Hu F, Xie X, Mei J, et al. USP22 acts as an oncogene by regulating the stability of cyclooxygenase-2 in non-small cell lung cancer. *Biochem Biophys Res Commun.* 2015 May 2;460(3):703–8.
16. McCann JJ, Vasilevskaya IA, Neupane NP, Shafi AA, McNair C, Dylgjeri E, et al. USP22 functions as an oncogenic driver in prostate cancer by regulating cell proliferation and DNA repair. *Cancer Res.* 2020 Feb;80(3):430–43.
17. Zhou A, Lin K, Zhang S, Chen Y, Zhang N, Xue J, et al. Nuclear GSK3 β promotes tumorigenesis by phosphorylating KDM1A and inducing its deubiquitylation by USP22. *Nat Cell Biol.* 2016 Sep;18(9):954–66.
18. Wang S, Zhong X, Wang C, Luo H, Lin L, Sun H, et al. USP22 positively modulates ER α action via its deubiquitinase activity in breast cancer. *Cell Death Differ.* 2020;
19. Gao Y, Lin F, Xu P, Nie J, Chen Z, Su J, et al. USP22 is a positive regulator of NFATc2 on promoting IL2 expression. *FEBS Lett.* 2014 Mar;588(6):878–83.
20. Cai Z, Zhang MX, Tang Z, Zhang Q, Ye J, Xiong TC, et al. USP22 promotes IRF3 nuclear translocation and antiviral responses by deubiquitinating the importin protein KPNA2. *J Exp Med.* 2020 May;217(5).

21. Huang X, Zhang Q, Lou Y, Wang J, Zhao X, Wang L, et al. USP22 deubiquitinates CD274 to suppress anticancer immunity. *Cancer Immunol Res.* 2019;7(10):1580–90.
22. Kosinsky RL, Wegwitz F, Hellbach N, Dobbelstein M, Mansouri A, Vogel T, et al. Usp22 deficiency impairs intestinal epithelial lineage specification in vivo. *Oncotarget.* 2015;6(35):37906–18.
23. Kosinsky RL, Zerche M, Saul D, Wang X, Wohn L, Wegwitz F, et al. USP22 exerts tumor-suppressive functions in colorectal cancer by decreasing mTOR activity. *Cell Death Differ.* 2020 Apr 1;27(4):1328–40.
24. Kosinsky RL, Helms M, Zerche M, Wohn L, Dyas A, Prokakis E, et al. USP22-dependent HSP90AB1 expression promotes resistance to HSP90 inhibition in mammary and colorectal cancer. *Cell Death Dis.* 2019 Dec 1;10(12).
25. Martín-Pérez R, Palacios C, Yerbés R, Cano-González A, Iglesias-Serret D, Gil J, et al. Activated ERBB2/HER2 licenses sensitivity to apoptosis upon endoplasmic reticulum stress through a PERK-Dependent pathway. *Cancer Res.* 2014;74(6):1766–77.
26. Hetz C, Zhang K, Kaufman RJ. Mechanisms, regulation and functions of the unfolded protein response. *Nature Reviews Molecular Cell Biology.* Nature Research; 2020.
27. Baumann J, Wong J, Sun Y, Conklin DS. Palmitate-induced ER stress increases trastuzumab sensitivity in HER2/neu-positive breast cancer cells. *BMC Cancer.* 2016 Jul 27;16(1).
28. Komurov K, Tseng J Te, Muller M, Seviour EG, Moss TJ, Yang L, et al. The glucose-deprivation network counteracts lapatinib-induced toxicity in resistant ErbB2-positive breast cancer cells. *Mol Syst Biol.* 2012;8.
29. Darini C, Ghaddar N, Chabot C, Assaker G, Sabri S, Wang S, et al. An integrated stress response via PKR suppresses HER2+ cancers and improves trastuzumab therapy. *Nat Commun.* 2019 Dec;10(1).
30. Györfy B, Lanczky A, Eklund ACAC, Denkert C, Budczies J, Li Q, et al. An online survival analysis tool to rapidly assess the effect of 22,277 genes on breast cancer prognosis using microarray data of 1,809 patients. *Breast Cancer Res Treat.* 2010 Oct;123(3):725–31.
31. Wienken M, Dickmanns A, Nemajerova A, Kramer D, Najafova Z, Weiss M, et al. MDM2 Associates with Polycomb Repressor Complex 2 and Enhances Stemness-Promoting Chromatin Modifications Independent of p53. *Mol Cell.* 2016 Jan;61(1):68–83.
32. Prenzel T, Begus-Nahrmann Y, Kramer F, Hennion M, Hsu C, Gorsler T, et al. Estrogen-dependent gene transcription in human breast cancer cells relies upon proteasome-dependent monoubiquitination of histone H2B. *Cancer Res.* 2011;71(17):5739–53.
33. Mishra VK, Wegwitz F, Kosinsky RL, Sen M, Baumgartner R, Wulff T, et al. Histone deacetylase class-I inhibition promotes epithelial gene expression in pancreatic cancer cells in a BRD4-and MYC-dependent manner. *Nucleic Acids Res.* 2017;
34. Dobin A, Gingeras TR. Mapping RNA-seq Reads with STAR. *Curr Protoc Bioinforma.* 2015 Sep;51(1):11.14.1-11.14.19.
35. Trapnell C, Pachter L, Salzberg SL. TopHat: Discovering splice junctions with RNA-Seq. *Bioinformatics.* 2009;
36. Love MI, Huber W, Anders S. Moderated estimation of fold change and dispersion

- for RNA-seq data with DESeq2. *Genome Biol.* 2014;
37. Melo-Cardenas J, Xu Y, Wei J, Tan C, Kong S, Gao B, et al. USP22 deficiency leads to myeloid leukemia upon oncogenic Kras activation through a PU.1-dependent mechanism. *Blood.* 2018 Jul;132(4):423–34.
 38. Shubin A V., Demidyuk I V., Komissarov AA, Rafieva LM, Kostrov S V. Cytoplasmic vacuolization in cell death and survival. *Oncotarget.* 2016;7(34):55863–89.
 39. Pakos-Zebrucka K, Koryga I, Mnich K, Ljubic M, Samali A, Gorman AM. The integrated stress response. *EMBO Rep.* 2016;17(10):1374–95.
 40. Hayner JN, Shan J, Kilberg MS. Regulation of the ATF3 gene by a single promoter in response to amino acid availability and endoplasmic reticulum stress in human primary hepatocytes and hepatoma cells. *Biochim Biophys Acta - Gene Regul Mech.* 2018 Feb;1861(2):72–9.
 41. Brooks AC, Guo Y, Singh M, McCracken J, Xuan YT, Srivastava S, et al. Endoplasmic reticulum stress-dependent activation of ATF3 mediates the late phase of ischemic preconditioning. *Curr Ther Res - Clin Exp.* 2014 Dec;76:138–47.
 42. Ishizawa J, Kojima K, Chachad D, Ruvolo P, Ruvolo V, Jacamo RO, et al. ATF4 induction through an atypical integrated stress response to ONC201 triggers p53-independent apoptosis in hematological malignancies. *Sci Signal.* 2016 Feb;9(415).
 43. Iurlaro R, Muñoz-Pinedo C. Cell death induced by endoplasmic reticulum stress. Vol. 283, *FEBS Journal.* Blackwell Publishing Ltd; 2016. p. 2640–52.
 44. McConkey DJ. The integrated stress response and proteotoxicity in cancer therapy. Vol. 482, *Biochemical and Biophysical Research Communications.* Elsevier B.V.; 2017. p. 450–3.
 45. Wang L, Dent SYR. Functions of SAGA in development and disease. Vol. 6, *Epigenomics.* Future Medicine Ltd.; 2014. p. 329–39.
 46. Jeusset LMP, McManus KJ. Ubiquitin specific peptidase 22 regulates histone H2B mono-ubiquitination and exhibits both oncogenic and tumor suppressor roles in cancer. *Cancers (Basel).* 2017;9(12):1–17.
 47. Zhang XY, Varthi M, Sykes SM, Phillips C, Warzecha C, Zhu W, et al. The Putative Cancer Stem Cell Marker USP22 Is a Subunit of the Human SAGA Complex Required for Activated Transcription and Cell-Cycle Progression. *Mol Cell.* 2008 Jan;29(1):102–11.
 48. Atanassov BS, Mohan RD, Lan X, Kuang X, Lu Y, Lin K, et al. ATXN7L3 and ENY2 Coordinate Activity of Multiple H2B Deubiquitinases Important for Cellular Proliferation and Tumor Growth. *Mol Cell.* 2016 May 19;62(4):558–71.
 49. Zhang T, Li N, Sun C, Jin Y, Sheng X. MYC and the unfolded protein response in cancer: synthetic lethal partners in crime? *EMBO Mol Med.* 2020;12(5):1–12.
 50. Zhang J, Luo N, Tian Y, Li J, Yang X, Yin H, et al. USP22 knockdown enhanced chemosensitivity of hepatocellular carcinoma cells to 5-Fu by up-regulation of Smad4 and suppression of Akt. *Oncotarget.* 2017;8(15):24728–40.
 51. Ling S, Li J, Shan Q, Dai H, Lu D, Wen X, et al. USP22 mediates the multidrug resistance of hepatocellular carcinoma via the SIRT1/AKT/MRP1 signaling pathway. *Mol Oncol.* 2017;11(6):682–95.
 52. Lim CC, Xu JC, Chen TY, Xu JX, Chen WF, Hu JW, et al. Ubiquitin-specific peptide 22 acts as an oncogene in gastric cancer in a sevenless 1-dependent manner. *Cancer Cell Int.* 2020 Feb 10;20(1).
 53. Appenzeller-Herzog C, Hall MN. Bidirectional crosstalk between endoplasmic

- reticulum stress and mTOR signaling. Vol. 22, Trends in Cell Biology. Trends Cell Biol; 2012. p. 274–82.
54. Zhang Y, Yao L, Zhang X, Ji H, Wang L, Sun S, et al. Elevated expression of USP22 in correlation with poor prognosis in patients with invasive breast cancer. *J Cancer Res Clin Oncol.* 2011;137(8):1245–53.
 55. Ibrahim IM, Abdelmalek DH, Elfiky AA. GRP78: A cell's response to stress. *Life Sci.* 2019;226(April):156–63.
 56. Kopp MC, Larburu N, Durairaj V, Adams CJ, Ali MMU. UPR proteins IRE1 and PERK switch BiP from chaperone to ER stress sensor. *Nat Struct Mol Biol.* 2019 Nov 1;26(11):1053–62.
 57. Zhang LH, Zhang X. Roles of GRP78 in physiology and cancer. *J Cell Biochem.* 2010;110(6):1299–305.
 58. Yao X, Tu Y, Xu Y, Guo Y, Yao F, Zhang X. Endoplasmic reticulum stress confers 5-fluorouracil resistance in breast cancer cell via the GRP78/OCT4/lncRNA MIAT/AKT pathway. *Am J Cancer Res.* 2020;10(3):838–55.
 59. Schoenhacker-Alte B, Mohr T, Pirker C, Kryeziu K, Kuhn PS, Buck A, et al. Sensitivity towards the GRP78 inhibitor KP1339/IT-139 is characterized by apoptosis induction via caspase 8 upon disruption of ER homeostasis. *Cancer Lett.* 2017 Sep 28;404:79–88.
 60. Ruggiero C, Doghman-Bouguerra M, Ronco C, Benhida R, Rocchi S, Lalli E. The GRP78/BiP inhibitor HA15 synergizes with mitotane action against adrenocortical carcinoma cells through convergent activation of ER stress pathways. *Mol Cell Endocrinol.* 2018;474:57–64.
 61. Casas C. GRP78 at the centre of the stage in cancer and neuroprotection. *Front Neurosci.* 2017;11(APR):1–15.
 62. Yang GH, Li S, Pestka JJ. Down-regulation of the endoplasmic reticulum chaperone GRP78/BiP by vomitoxin (deoxynivalenol). *Toxicol Appl Pharmacol.* 2000 Feb 1;162(3):207–17.
 63. Bailly C, Waring MJ. Pharmacological effectors of GRP78 chaperone in cancers. Vol. 163, *Biochemical Pharmacology.* Elsevier Inc.; 2019. p. 269–78.
 64. Cerezo M, Lehraiki A, Millet A, Rouaud F, Plaisant M, Jaune E, et al. Compounds Triggering ER Stress Exert Anti-Melanoma Effects and Overcome BRAF Inhibitor Resistance. *Cancer Cell.* 2016;29(6):805–19.
 65. Millet A, Plaisant M, Ronco C, Cerezo M, Abbe P, Jaune E, et al. Discovery and Optimization of N-(4-(3-Aminophenyl)thiazol-2-yl)acetamide as a Novel Scaffold Active against Sensitive and Resistant Cancer Cells. *J Med Chem.* 2016 Sep 22;59(18):8276–92.

Supplements

Supplementary figures of Manuscript II

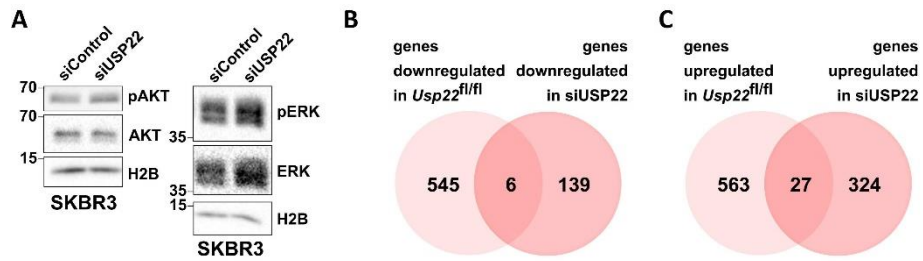


Fig.II.S1: Consequence of USP22-loss on HER2-signaling and gene expression of HER2⁺-BC cells. **A)** Representative western blot analysis of pERK, ERK, pAKT, and AKT in siControl- and siUSP22-treated SKBR3 cells. Experiments were performed in biological triplicates. **B-C)** Venn diagram of the mRNA-seq results showing a scarce overlap between downregulated (**B**) and upregulated (**C**) genes in the murine ($|\log_2$ fold change $|\geq 1$, FDR <0.05) and human ($|\log_2$ fold change $|\geq 0.6$, p-value <0.05) HER2⁺-BC models upon USP22-loss.

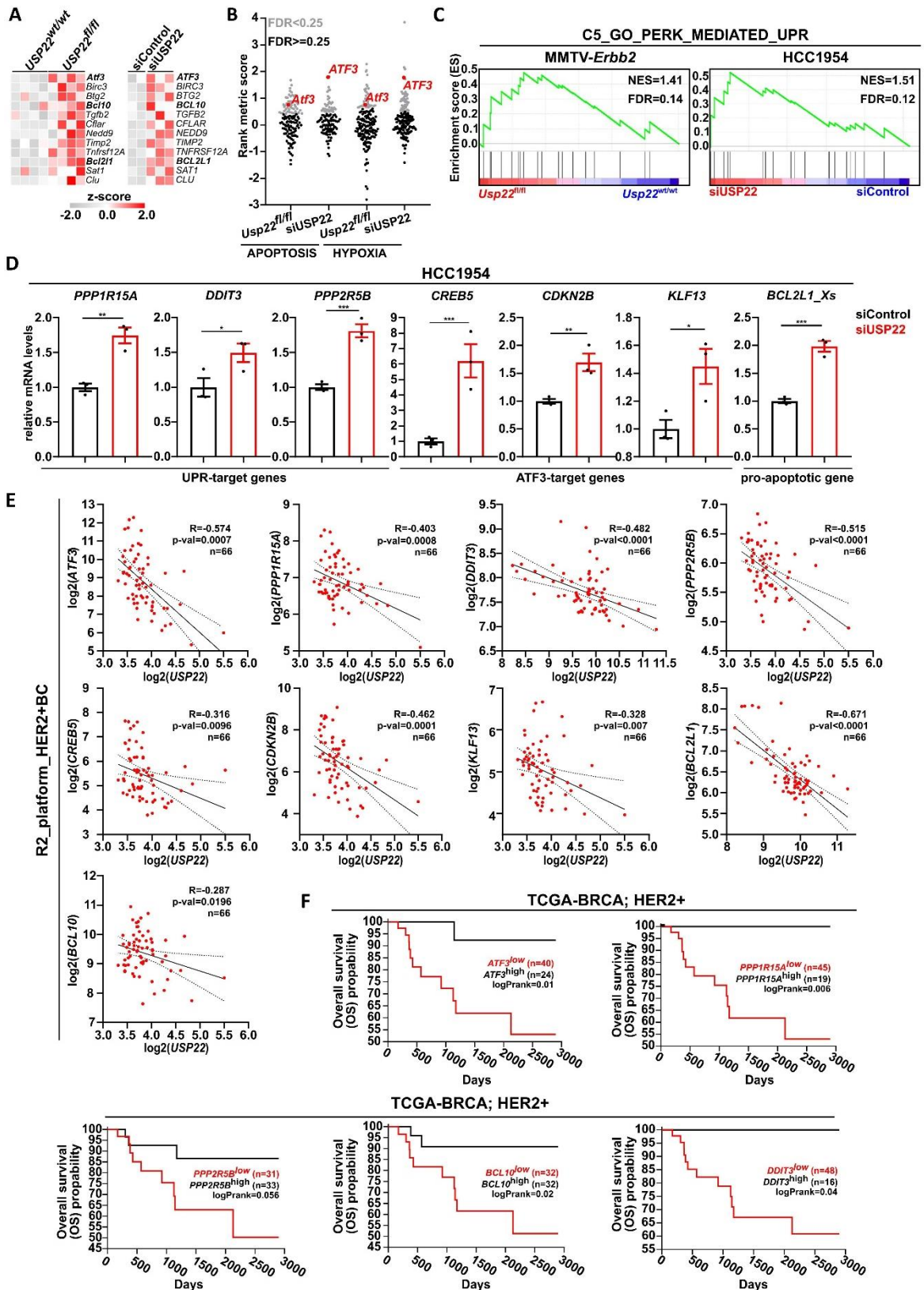


Fig.II.S2: USP22 loss increases the sensitivity of HER2⁺-BC to the unfolded protein response. A) Heatmap of GSEA results showing genes of the "HALLMARK_APOPTOSIS" signature commonly enriched in *Usp22*^{fl/fl} mice and siUSP22-treated HCC1954 cells. **B)** Scatter plot of GSEA results showing genes of the "HALLMARK_APOPTOSIS" and

"HALLMARK_HYPOXIA" gene sets enriched in *Usp22^{fl/fl}* mice and siUSP22-treated HCC1954 cells based on rank metric score. ATF3 (highlighted in red) was highly-ranked in all conditions. **C)** GSEA profile of the "GO_PERK_MEDIATED_UNFOLDED_PROTEIN_RESPONSE" gene set enriched in *Usp22^{fl/fl}* mice and siUSP22-treated HCC1954 cells. **D)** USP22 knockdown induces the expression of UPR- (*PPP1R15A*, *DDIT3*, *PPP2R5B*) and ATF3-responsive genes (*CREB5*, *CDKN2B*, *KLF13*) as well of the pro-apoptotic gene isoform *BCL2L1-Xs* in HCC1954 cells, as assessed by RT-qPCR. **E)** Correlation of *USP22* and UPR-responsive gene expression in HER2⁺-BC patients, provided as scatter-plots. Data were retrieved from the online R2-platform database (<https://r2.amc.nl>). Dotted lines: 95% confidence interval. **F)** Overall survival (OS) plots of low- and high-expressing *ATF3*, *PPP1R15A*, *DDIT3*, *PPP2R5B*, and *BCL10* HER2⁺-BC patients. TCGA-BRCA expression data retrieved from the online Xena browser (<https://xenabrowser.net>). NES: Normalized Enrichment Score.

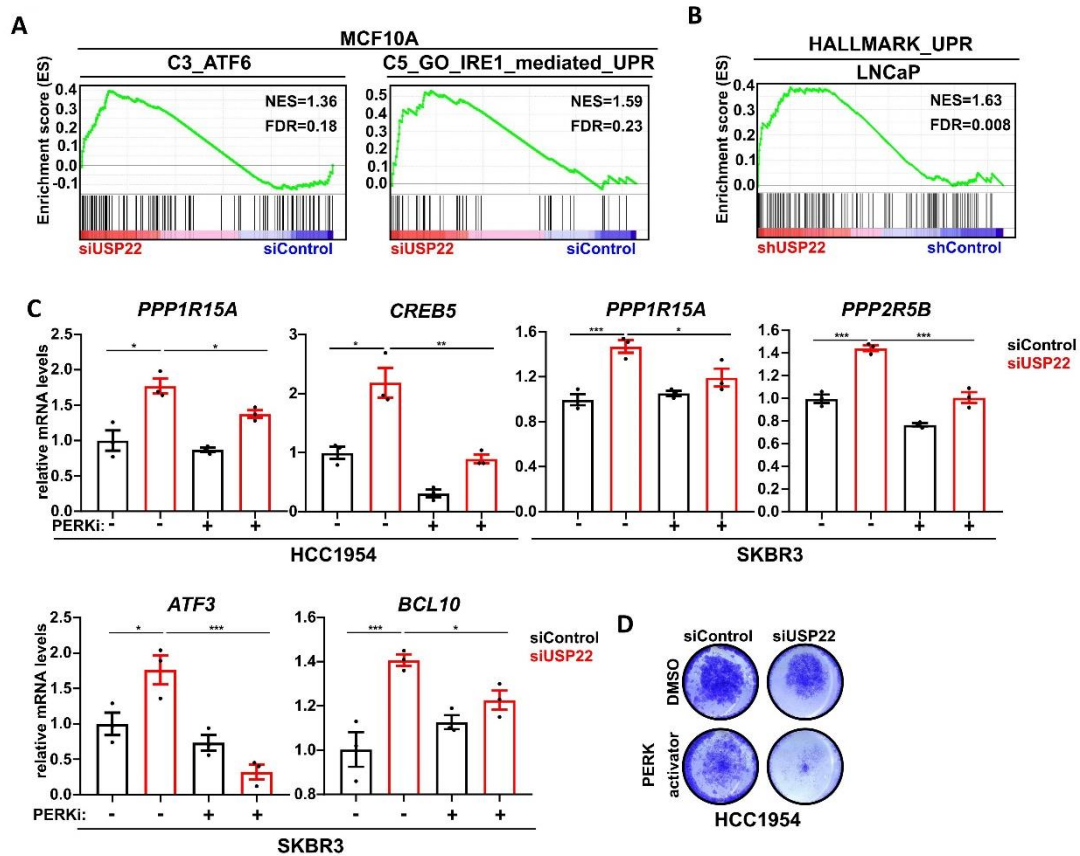


Fig.II.S3: USP22 loss increases the sensitivity of HER2⁺-BC to the unfolded protein response.

A) The "ATF6_Q6" and the "GO_IRE1_MEDIATED_UNFOLDED_PROTEIN_RESPONSE" gene signatures from the "regulatory target gene sets" and "GO gene sets", respectively, were enriched in MCF10A cells upon USP22 knockdown (accession number: E-MTAB-8247). **B)** GSEA profile of "HALLMARK_UNFOLDED_PROTEIN_RESPONSE" enriched in LNCaP cells upon shRNA

mediated USP22 silencing (accession number: GSE140164). **C)** Changes of *PPP1R15A*, *CREB5*, *PPP2R5B*, *ATF3*, and *BCL10* expression in HCC1954 and SKBR3 cells upon USP22 knockdown, with or without PERK inhibition (GSK2606414, 8 μ M, 24h). One-way Anova test. **D)** Representative crystal violet staining of a proliferation assay of siControl- and siUSP22-treated HCC1954 cells, without and with PERK activator (CCT020312, 2.5 μ M, continuous treatment). One-way Anova test. All experiments were performed in biological triplicates. * p-val<0.05, ** p-val<0.01, *** p-val<0.005. Error bars: standard error of the mean (SEM). NES: Normalized Enrichment Score.

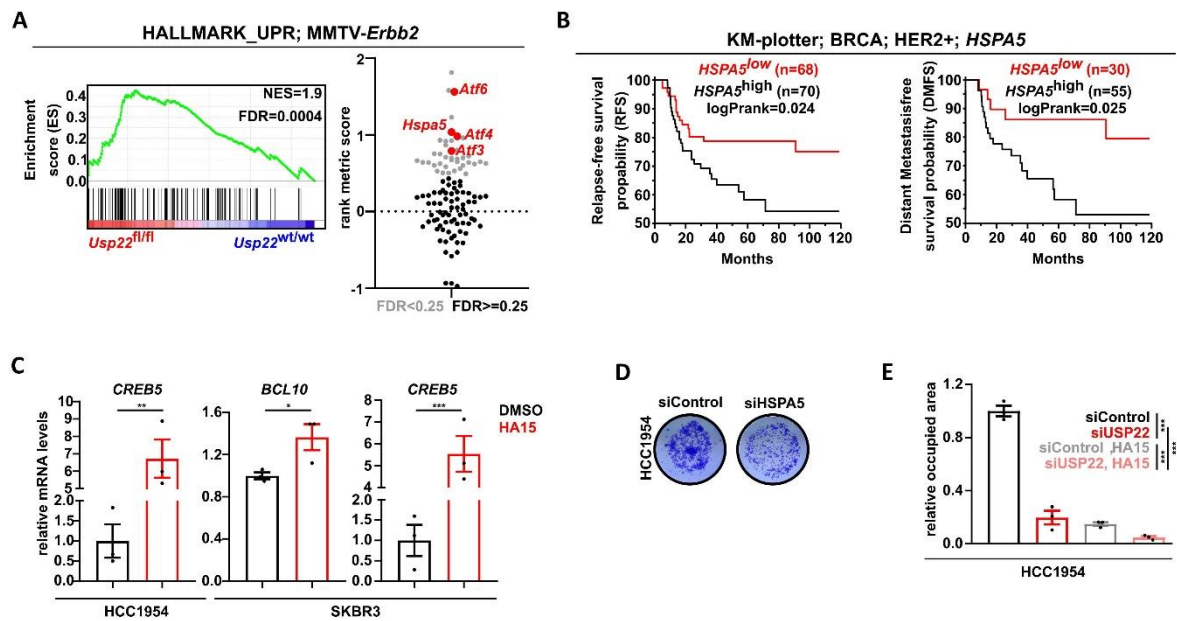


Fig.II.S4: USP22 stabilizes HSPA5 and suppresses UPR-induced apoptosis in HER2⁺-BC. **A)** GSEA profile of "HALLMARK_UNFOLDED_PROTEIN_RESPONSE" enriched in *Usp22*^{fl/fl} mice (left panel) and a respective scatter plot (right panel) of UPR-responsive genes (e.g *Hspa5*, *Atf6*, *Atf4*, *Atf3*) enriching for this gene set based on rank metric score. **B)** Relapse-free survival (RFS) and distant metastasis-free survival (DMFS) plot of low- and high-HSPA5 expressing HER2⁺-BC patients. Survival data were retrieved from KM-plotter (kmplot.com). log-rank test. **C)** RT-qPCR assessing *CREB5* and *BCL10* expression levels in vehicle- and HA15-treated HCC1954 and SKBR3 cells (20 μ M, 24 hours). Student t-test. **D)** Proliferation assay of siControl- and siHSPA5-treated HCC1954 cells. **E)** Relative occupied area of siControl- and siUSP22-treated HCC1954 cells, with or without HA15 (36 μ M continuous treatment). One-way Anova test. All experiments were performed in biological triplicates. * p-val<0.05, ** p-val<0.01, *** p-val<0.005. Error bars: standard error of the mean (SEM).

Supplementary Materials and Methods

Animal handling and mouse model generation

Animals were housed in the animal facility of the European Neuroscience Institute (ENI) of Göttingen under specific pathogen-free (SPF) conditions. The generation of mice harboring a conditional *Usp22* allele was previously described by our group (1). All mice had the FVB/N background. Specifically, the *Usp22*^{loxP} mice were crossed with MMTV-*Cre* and MMTV-*ErbB2* mice to allow co-expression of the Cre-recombinase and the rat *ErbB2* proto-oncogene in mammary epithelial cells (2,3). Tumor-bearing animals were monitored twice a week. Growing tumors were detected by palpating size and measured with a caliper. The measurements were performed in a blinded way by two independent investigators.

Histology of murine tumors

Paraffin-embedded murine tumors were deparaffinized in xylol for 20 min and rehydrated with subsequent incubations in 50% isopropanol/50% xylol, 100% isopropanol, 100%, 90%, and 70% ethanol, and finally, tap water for 5 min each. For hematoxylin and eosin (H&E) staining, nuclei were stained with hematoxylin solution (Carl Roth GmbH) for 1 min. Excess dye was removed using running tap water for 5 min. Counterstaining with eosin (Carl Roth GmbH) was performed for 5-10 min. For immunohistochemical staining (IHC), upon rehydration, antigen retrieval was performed by boiling slides in EDTA buffer (1 mM EDTA, pH 8, 0.1% Tween 20) or citric buffer (10 mM citric acid, pH 6, 0.1% Tween 20) for 10 min in a pressure cooker. After allowing tissue sections to cool slowly, endogenous peroxidase was inactivated with 3% hydrogen superoxide in PBS for 45 min and unspecific antigen binding was blocked with 5% bovine serum albumin (BSA, Merck) and 1% donkey serum (Dianova GmbH) in PBS (blocking solution) for 1 hour at room temperature in a humid chamber. Afterward, primary antibodies were diluted in blocking solution, and sections were incubated overnight in the humid chamber at 4 °C. Sections were next washed twice with 0.1% Tween 20 in PBS (PBS-T) and incubated with biotinylated secondary antibodies blocking solution (1:200 dilution) for 1 hour in the humid chamber at room temperature. After a wash step with PBS-T, Avidin-Peroxidase conjugate (Sigma-Aldrich) diluted in PBS (1:1000) was applied to the sections for 90 min at room temperature in the humid chamber. Finally, staining was developed using 3,3'-diaminobenzidine-tetrahydrochloride (DAB) with 1% hydrogen superoxide in PBS and counterstained using hematoxylin. Slides were washed under running tap water for 5 min and dehydrated in increasing concentrations of ethanol, isopropanol, xylol and mounted with Roti®-Histokitt mounting medium (Carl Roth

GmbH). Refer to Table S4-5 for antibodies, dilutions, and corresponding antigen retrieval buffers used in this study.

Analysis of publically available patient datasets

TCGA

The TCGA-derived BReast AdenoCarcinoma (BRCA) dataset was retrieved from the Xena browser (<https://xenabrowser.net>) (4) online platform to analyze the impact of *USP22* expression levels on the progression-free interval (PFI) of HER2⁺-BC patients (classified along the PAM50) using the normalized read cutoff of 11.71. To assess the overall survival of HER2⁺-BC patients, a cutoff of 9.21, 9.91, 8.42, 8.70, 8.89, 6.85, and 10.86 normalized reads counts was selected to discriminate low and high *ATF3*-, *PPP1R15A*-, *PPP2R5B*-, *DDIT3*-, *BCL10*-, *CREB5*- and *KLF13*-expressing patients, respectively. The results were finally plotted with GraphPad Prism v8.0.1.

Publically available normalized count tables were downloaded at the Genomic Data Commons (GDC) Data Portal (<https://portal.gdc.cancer.gov>). By selecting the top- (n=19, *USP22*^{high}) and bottom-30% (n=19, *USP22*^{low}) of *USP22*-expressing patients, we performed a Gene Set Enrichment Analysis (GSEA) to identify differentially enriched gene signatures (following specific settings: 1,000 permutations, type: gene set and a maximum size of sets of 1,000) (5).

R2 platform

Correlation of *USP22* expression with *ATF3*, *PPP1R15A*, *CREB5*, *DDIT3*, and *BCL2L1*, respectively, in HER2⁺-BC patients, we utilized the dataset "Tumor Breast (HER2) - Concha - 66 - fRMA - u133p2" publically available at the <https://hgserver1.amc.nl/cgi-bin/r2/main.cgi> website. The results were finally plotted with Graphpad Prism v8.0.1.

KM-plotter

To analyze the impact of *USP22* and *HSPA5* expression levels on the RFS and DMFS of HER2⁺-BC patients, the Affy IDs 200083 (for *USP22*) and 211936 (for *HSPA5*) dataset was retrieved from the online web tool KM-plotter (<https://kmplot.com>) using the following parameters: Split patients by "auto select best cutoff", intrinsic subtype "HER2⁺", patient cohort exclusion restrictions: 1) endocrine therapy: no, 2) chemotherapy: any (6).

RNA-seq data

Fastq files for siControl- and siUSP22-treated HCC1954 and MCF10A cells have been previously generated in our lab and accessible at ArrayExpress under the accession

number E-MTAB-8256 and E-MTAB-8247, respectively (<http://www.ebi.ac.uk/arrayexpress>). Fastq files derived from *Usp22*^{wt/wt} and *Usp22*^{fl/fl} tumors generated in this study are deposited at ArrayExpress under the accession number: E-MTAB-9331. Fastq files of shControl- and shUSP22-LNcAP cells (accession number GSE140164) were downloaded from Gene Expression Omnibus (GEO; <https://www.ncbi.nlm.nih.gov/geo/>).

Cell culture

HCC1954 and SKBR3 cells were purchased at the ATCC (following Table S1) and cultivated using the recommended medium supplemented with 10% fetal bovine serum (FBS) and 1% penicillin/streptomycin at 37°C and 5% CO₂.

siRNA transfections

Transfections were performed using Lipofectamine® RNAiMAX (Invitrogen) according to the manufacturer's guidelines. siGENOME SMARTpool siRNA (Dharmacon) are shown in Table S2.

Proliferation and colony formation assay

All experiments were performed in biological triplicates. The results were plotted with GraphPad Prism v8.0.1

HCC1954 cells:

Proliferation assay: 20,000 cells per well were seeded in a 24-well plate. 24 hours post-transfection, cell confluency was recorded every 12 hours over a period of 7 days using an IncuCyte® Live Cell Analysis System (Sartorius AG).

Clonogenic assay: 24 hours post-transfection, 500 cells were seeded in a 6-well. 15 days after seeding, colonies were washed with PBS, fixed with methanol for 10 min and stained with 1% crystal violet in 20% ethanol for 20 min. After a final wash in water, stained colonies were scanned using EPSON perfection V700 PHOTO scanner. The number of colonies was assessed using ImageJ.

SKBR3 cells:

Proliferation and clonogenic assay: 220,000 cells were reverse transfected in biological triplicates in a 6-well plate and re-transfected 96 hours after the first transfection. 24 hours later, 1,000 cells (for proliferation assay) and 500 cells (for colony formation assay) were seeded on a 96-well (adherent) and a 6-well plate, respectively. Proliferating cells were scanned every 2 days using a Celigo® S imaging cytometer (Nexcelom Bioscience LLC).

15 days after seeding, colonies were washed, fixed, stained, scanned, and analyzed as previously described.

HSPA5 inhibition: 20.000 and 220.000 HCC1954 or SKBR3 cells were seeded in 24-well (proliferation assay) and 6-well plates (protein or RNA extraction), respectively. The following day, the medium was replaced with fresh one supplemented with the HA15 inhibitor (Sigma Aldrich). For protein or RNA isolation, cells were harvested after 24 hours (20 μ M of HA15 inhibitor) of treatment. For proliferation assays, cells were grown for 5 days for HCC1954 cells and 10 days for SKBR3 cells (36 μ M in HCC1954 cells and 10 μ M in SKBR3 cells of HA15 inhibitor). Finally, plates were fixed, stained, scanned, and analyzed as previously described.

Pan-caspase inhibition: 20.000 HCC1954 cells were seeded in 24-well for proliferation assay. The following day, the medium was replaced with a fresh one including 80 μ M Z-VAD-FMK (Adooq). Cells were grown for 5 days. Finally, plates were fixed, stained, scanned, and analyzed as previously described.

PERK inhibition for rescue experiment as well for PERK activation: upon USP22 silencing, 20.000 and 220,000 HCC1954 cells were reverse transfected in a 24-well (proliferation assay) and 6-well plate (protein or RNA isolation), respectively. The medium was replaced with fresh one including 8 μ M PERK inhibitor (GSK2606414, MedChemExpress) or 2.5 μ M PERK activator (CCT020312, MedChemExpress) 24 hours after transfection for proliferation assay and 48 hrs after transfection for protein or RNA extraction. For protein and RNA isolation, cells were harvested 72 hours post-transfection while cells for proliferation assay were grown for 6 days.

Annexin V assay

Annexin V assay (modified from (7)): 220.000 HCC1954 cells were reverse transfected. At 72 hours post-transfection, cells (floating + adherent) were washed with PBS and resuspended in 1x Binding buffer (10 mM HEPES, 0.14 M NaCl, 2.5 mM CaCl₂ pH: 7.4) at a concentration of 10⁶ cells/ml. 100 μ l of the cell suspensions were transferred to sterile tubes, 5 μ l of Annexin V-FITC (Southern Biotech) and 1 μ l of propidium iodide (1mg/ml, Sigma Aldrich) was added in each sample and suspension was incubated for 15 min at room temperature in the dark. Finally, 400 μ l of 1x Binding buffer was added to each tube, and samples were analyzed using a Guava EasyCyte Plus flow cytometer from Guava Technologies. The results were finally plotted with Graphpad Prism v8.0.1.

Migration assay

Trans-well migration assay: 120,000 HCC1954 cells were reverse transfected in biological triplicates. The following day, cells were serum-starved for 8 hours and then collected and seeded on each trans-well inserts (Corning, 24-well insert, 8 μ m pore) while normally supplemented medium was added beneath the inserts. 48 hours after seeding, the inserts were washed with PBS, and cells that have not migrated through the membrane were removed with a cotton Q-tip. Migrated cells were then fixed with methanol for 10 min, stained with crystal violet, scanned, and analyzed as previously described (see method for proliferation assay). The results were finally plotted with Graphpad Prism v8.0.1.

Immunofluorescence microscopy

20,000 cells were reverse transfected on coverslips in biological triplicates in a 6-well plate as previously described. At 72 hours post-transfection, cells were washed with PBS and fixed with 4% paraformaldehyde in PBS for 20 min. Thereafter, cells were permeabilized with 1% Triton X-100 in PBS for 10 min, washed three times for 5 min with PBS, and blocked with blocking solution (3% BSA in PBS-T) for 1 hour in a humid chamber. The primary antibody was diluted in blocking solution and applied on the coverslips for overnight incubation in a dark humid chamber at 4°C. The following day, coverslips were washed three times with PBS-T and incubated with fluorophore-conjugated secondary antibodies and DAPI (1:1000 dilution) dissolved in blocking solution, for 1 hour in a dark humid chamber. Coverslips were washed three times with PBS-T. Finally, coverslips were mounted on microscope slides. Pictures were taken with a Zeiss LSM 510 Meta confocal microscope. Fluorescence intensity was quantified using ImageJ.

Fluorescence intensity quantification: photographed areas were processed in ImageJ. To quantify PCNA staining, the DAPI channel was utilized as a reference to determine cell nuclei regions. Finally, PCNA staining intensity was measured for every nucleus. The results were finally plotted with Graphpad Prism v8.0.1.

Coimmunoprecipitation (CoIP) assay

CoIP was performed according to a previous study (8). Specifically, cells were treated for 12 hours with 20 nM bortezomib, washed once with PBS and harvested with CoIP buffer (50 mM Tris-HCl, pH 7.7, 150 mM NaCl, 1% NP-40) supplemented with protease inhibitors (1 μ M activated orthovanadate, 10 mM β -glycerophosphate disodium salt hydrate, 10 mM Pefablock, 10 mM N-Ethylmaleimide, 1 mM Aprotinin/Leupeptinin, 1 μ M NaF, 1 μ M iodoacetic acid). After 10 min incubation on ice, cells were scraped and lysates were sonicated for three cycles, 5 min each using a Bioruptor (Diagenode). Sonicated lysates

were centrifuged at 13.000 rpm, 4°C for 15 min. Supernatants were collected and split into fresh tubes for immunoprecipitation for keeping input. 60 µl equilibrated sepharose beads (50%) were added for every coimmunoprecipitation and samples were rotated for 1 hour at 4 °C. Next, samples were centrifuged at 3.000 rpm for 4 min at 4°C, the supernatant was collected and antibodies were added. Afterward, samples were rotated overnight at 4 °C. The next day, 50 µl of precleared protein G beads (50%) were added and samples were rotated for 2 hours at 4 °C. At the next step, coimmunoprecipitated samples were centrifuged at 3.000 rpm for 2 min at 4°C and their respective pellet was collected and washed three times with CoIP buffer (supplemented with protease inhibitors) and centrifuged at 3000 rpm for 2 min at 4 °C. Finally, collected pellets were resuspended in 1:1 ratio with laemmli buffer, boiled at 95 °C for 5 min, and eluates were subsequently loaded for protein electrophoresis.

Protein isolation and western blot analyses

Radioimmunoprecipitation Assay Buffer (RIPA; 10 mM Tris-Cl pH 8, 1 mM EDTA, 1% v/v Triton X-100, 0.1% sodium deoxycholate, 0.1% SDS, 140 mM NaCl) supplemented with protease and phosphatase inhibitors was used (1 µM activated orthovanadate, 10 mM β-glycerophosphate disodium salt hydrate, 10 mM Pefablock, 10 mM N-Ethylmaleimide, 1 mM Aprotinin/Leupeptinin, 1µM NaF, 1 µM iodoacetic acid). Cells were washed once with PBS and 200 µl of RIPA buffer was added to each well (6 well plate). After 10 min incubation on ice, cells were scraped and lysates were sonicated for three cycles, 5 min each using a Bioruptor (Diagenode). Laemmli buffer (375 mM Tris/HCl, 10% SDS, 30% glycerol, 0.02% bromophenol blue, 9.3% DTT) was added to each lysate and cooked at 95°C for 5 min before protein separation with a 10 to 12% polyacrylamide gel. Proteins were transferred to nitrocellulose membrane (0.45 µm pore, Immobilon, Millipore), blocked with 5% skimmed milk in TBS-T for 1 hour and incubated with primary antibody overnight at 4°C. The day after, the membrane was washed with TBS-T, incubated 1 hour with secondary antibody at room temperature. After a final wash step, protein detection was achieved with the Millipore substrate in a BioRad ChemiDoc™ imager. Used primary antibodies are listed in Table S4-5 and S6.

RNA isolation and real-time quantitative PCR (RT-qPCR)

Briefly, cells were washed with PBS and lysed in 500 µl Qiazol (Qiagen). For RNA extraction from tissues, 50-100 mg frozen tissue was homogenized with 0.5-1 ml Qiazol with three cycles of 10-15 sec/2,000 rpm in a PowerLyzer24 (MoBio Laboratories). Lysates were then collected and RNA was extracted, as previously described(9,10). Reverse transcription of

1 µg RNA was performed using M-MuLV reverse transcriptase (NEB) with random primers according to the manufacturer's instructions. The expression of specific genes was finally estimated by quantitative real-time PCR using a CFX Connect™ Real-Time System (Bio-Rad). Gene expression levels were normalized relative to the *RPLP0* housekeeping gene. RT-PCR program: 1x 2 min-95 °C, 40x 10 sec-95 °C followed by 1x 30 sec-60 °C. Primers (Table S3) were designed using the online tool (<https://db-mml.sjtu.edu.cn/cgi-bin/primer3plus/primer3plus>) and were ordered from Sigma-Aldrich (Germany). The results were finally plotted with Graphpad Prism v8.0.1


Library preparation for mRNA next-generation sequencing

RNA sequencing libraries were generated with the TruSeq® RNA Library Prep Kit v2 (Illumina) according to the manufacturer's instructions. RNA library underwent amplification in a thermal cycler using the following program: 1 cycle of 37°C-30 min, 98°C-2 min, and 15 cycles of [98°C-30 sec, 1x 65 °C-30 sec, 1x 72 °C-60 sec] and one cycle of 72 °C-4 min. The quality and size of the libraries were examined using the high sensitivity DNA kit (Agilent) on the Agilent Bioanalyzer 2100. Finally, the concentration of the mRNA-libraries was estimated with a Qbit (Invitrogen), multiplexed in 2 nM pooled libraries and sequenced (single-end, 50 bp) on a HiSeq4000 (Illumina) at the NGS Integrative Genomics Core Unit (NIG) of the University Medical Center Göttingen (UMG).

Bioinformatic analysis of mRNA-sequencing data

Fastq files were uploaded and processed in the Galaxy environment (<https://galaxy.gwdg.de>). The quality of the sequencing data was assessed using FastQC (version 0.72)(11). Fastq files were trimmed for the first 11 bp using the FASTQ Trimmer tool (version 1.0.0) (11). Output data from the HCC1954 cell line were aligned to the human reference genome hg19 while for the MMTV-*ErbB2*-derived output data, the mouse reference genome mm10 was used (downloaded from www.ensembl.org) using the TopHat Gapped-read mapper (version 2.1.1) and RNA STAR (version 2.4.0d-2), respectively (12,13). Aligned reads were then assigned to the respective genomic features using featureCounts (version 1.4.6.p5) and, finally, DESeq2 (version 2.11.39) was used to identify significantly differentially regulated genes (14).

Matrix visualization of ATF3 gene signatures was created using the Morpheus tool (<https://software.broadinstitute.org/morpheus/>). Gene Set Enrichment Analyses (GSEA, v4.0.3) were performed with normalized counts of siControl/siUSP22 or *Usp22*^{wt/wt}/*Usp22*^{fl/fl} conditions using the following specific settings: 1,000 permutations, type: gene set and a maximum size of sets of 1,000) (5).



The volcano plot showing all UPR-associated signatures enriched in USP22 loss (Fig. II.4C) was performed using the Rstudio Desktop tool (v3.2.1, Bioconductor).

Supplementary Tables

Table S1: cell lines used in this study.

Human cell line	HCC1954	SKBR3
Tissue of origin	43 years old, female, mammary gland, adenocarcinoma	61 years old, female, ductal carcinoma
Morphology and growth properties	epithelial, monolayer, adherent	epithelial, monolayer, adherent
Supplier	ATCC	ATCC
Recommended medium	RPMI 1640. GlutaMAX™ (ThermoFisher Scientific)	DMEM/F12-Dulbecco's Modified Eagle's Medium: Nutrient Mixture F-12 (ThermoFisher Scientific)
HER2 status	+	+
ER/PR status	-/-	-/-
p53 status	mutated (Y136C)	mutated (R175H)

Table S2: siRNAs used in this study.

Gene	siRNA
Non-Targeting #5	UGGUUUACAUGUCGACUAA
<i>USP22</i>	#1 GGAGAAAGAUCACCUCGAA
	#2 CAAAGCAGCUCACUAUGAA
	#3 GGAAGAUCACCACGUAUGU
	#4 CCUUUAGUCUCAAGAGCGA
<i>HSPA5</i>	#1 CCACCAAGAUGCUGACAUU
	#2 GAAAGGAUGGUUAAUGAUG
	#3 CGACUCGAAUCCAAAGAU
	#4 CAGAUGAAGCUGUAGCGUA

Table S3: RT-PCR primers used in this study.

Gene name	Forward (5'-3')	Reverse (5'-3')	Species	Reference
<i>RPLP0</i>	GATTGGCTACCCAAC TGTTG	CAGGGGCAGCAGCCACAA A	Human	This study
<i>Rplp0</i>	GATTCGGGATATGCT GTTGG	GCCTGGAAGAAGGAGGTC TT	Mouse	This study
<i>USP22</i>	AGCCAAGGGTGTGG TCGCG	ACTGCCACCACGCCCGAAA G	Human	(15)
<i>Usp22</i>	TTCCAAGCCTTGCGC TGC	AACCGGCTGCACTCTTGC	Mouse	This study
<i>ATF3</i>	CGCTGGAATCAGTCA CTGTC	TTTCTCGTCGCCTCTTTTC	Human	This study
<i>Atf3</i>	GAGCGAAGACTGGAG CAAAA	TACCAGTGACCCAGGAGGT G	Human	This study
<i>PPP1R1 5A</i>	CTGGGTCTATCAGCC AGGAG	GGCCTTCAAGAAAGCACTT G	Human	This study
<i>BCL10</i>	AGGTCTGGACACCCT TGTTG	TGATCTGGAGAGGTTGTTC G	Human	This study
<i>Bcl10</i>	AAACTGGAGCACCTC AAAGG	GGGTGGTACATGACAGTG GA	Mouse	This study
<i>CREB5</i>	CAGCCATGCAGAAAG AATCA	CTTCCTACCACCTCGCTGA C	Human	This study
<i>PPP2R5 B</i>	GCAAACAGTGCAACC ACATC	AACTGCTTGTGCTCCGTCT T	Human	This study
<i>Casp3</i>	ATGGGAGCAAGTCAG TGGAC	CGTACCAGAGCGAGATGAC A	Mouse	This study
<i>BCL2L1 -xS</i>	GCAGTAAAGCAAGCG CTGAG	GTTCCACAAAAGTATCCTG TTCAAAG	Human	This study
<i>HSPA5</i>	CCCTGTCTTCTCAGC ATCAA	TTTCTGGACGGGCTTCATA G	Human	This study
<i>Hspa5</i>	TCAGCATCAAGCAAG GATTG	CATGGTAGAGCGGAACAG GT	Mouse	This study

Table S4: List of primary antibodies.

	WB (dilutions)	IHC (dilutions)	IF (dilutions)	IP (dilutions)	cat.number, company
HSC70	(1:100)				sc-1050, Santa Cruz
GAPDH	(1:2000)				OTI2D9, Origene
actin	(1:200)				sc-1616(1-19), Santa Cruz
HER2		(1:500,EDTA buffer)			2165, Cell Signaling
USP22	(1:200)			1 µg antibody per 1 mg of protein	sc-390585, Santa Cruz
Anti-HA				1 µg antibody per 1 mg of protein	CB051, Origene
H2Bub1		(1:100,EDTA buffer)			home-made
H2B	(1:1000)				ab52484, Abcam
PCNA			(1:50)		sc-56, Santa Cruz
PARP	(1:500)				9542, Cell Signaling
caspase-3	(1:500)	(1:200, citric buffer)			9662, Cell Signaling
cl-caspase		(1:200, citric buffer)			9661, Cell Signaling
p-ERK Y202/T204	(1:200)				sc-7383, Santa Cruz
ERK1	(1:200)				sc-94, Santa Cruz

p-AKT S473	(1:500)				736 E11, Cell Signaling
AKT	(1:500)				9272, Cell Signaling
ATF4	(1:200)				D4B8, Cell Signaling
ATF4		(1:100, citric buffer)			10835-1-ap, Proteintech
ATF3		(1:100, EDTA buffer)			NBP1-85816, Novus Bio
HSPA5	(1:500)	(1:200, EDTA buffer)			C50B12, Cell Signaling

Table S5: List of secondary antibodies.

	WB (Dilution)	IHC (Dilution)	IF (Dilution)	Cat.number, company
HRP-anti-rabbit IgG	(1:10.000)			211-032-171, Dianova
HRP-anti-mouse IgG	(1:10.000)			115-035-174, Dianova
HRP-anti-goat IgG	(1:5.000)			305-065-047, Dianova
Alexa 488-anti-mouse IgG			(1:400)	A-21202, Molecular Probes
biotin-anti-rabbit IgG		(1:200)		711-065-152, Dianova
biotin-anti-mouse IgG		(1:200)		711-065-150, Dianova

Supplementary References of Manuscript II

1. Xie W, Nagarajan S, Baumgart SJ, Kosinsky RL, Najafova Z, Kari V, et al. RNF40 regulates gene expression in an epigenetic context-dependent manner. *Genome Biol.* 2017;18(1):1–22.
2. Guy CT, Webster MA, Schaller M, Parsons TJ, Cardiff RD, Muller WJ. Expression of the neu protooncogene in the mammary epithelium of transgenic mice induces metastatic disease. *Proc Natl Acad Sci.* 1992;89(22):10578–82.
3. Wagner KU, Wall RJ, St-Onge L, Gruss P, Wynshaw-Boris A, Garrett L, et al. Cre-mediated gene deletion in the mammary gland. *Nucleic Acids Res.* 1997;
4. Goldman M, Craft B, Kamath A, Brooks A, Zhu J, Haussler D. The UCSC Xena Platform for cancer genomics data visualization and interpretation. *bioRxiv.* 2018;
5. Subramanian A, Tamayo P, Mootha VK, Mukherjee S, Ebert BL, Gillette MA, et al. Gene set enrichment analysis: A knowledge-based approach for interpreting genome-wide expression profiles. *Proc Natl Acad Sci U S A.* 2005 Oct;102(43):15545–50.
6. Györfy B, Lanczky A, Eklund ACAC, Denkert C, Budczies J, Li Q, et al. An online survival analysis tool to rapidly assess the effect of 22,277 genes on breast cancer prognosis using microarray data of 1,809 patients. *Breast Cancer Res Treat.* 2010 Oct;123(3):725–31.
7. Lakshmanan I, Batra S. Protocol for Apoptosis Assay by Flow Cytometry Using Annexin V Staining Method. *BIO-PROTOCOL.* 2013;3(6).
8. Wienken M, Dickmanns A, Nemajerova A, Kramer D, Najafova Z, Weiss M, et al. MDM2 Associates with Polycomb Repressor Complex 2 and Enhances Stemness-Promoting Chromatin Modifications Independent of p53. *Mol Cell.* 2016 Jan 7;61(1):68–83.
9. Prenzel T, Begus-Nahrman Y, Kramer F, Hennion M, Hsu C, Gorsler T, et al. Estrogen-dependent gene transcription in human breast cancer cells relies upon proteasome-dependent monoubiquitination of histone H2B. *Cancer Res.* 2011;71(17):5739–53.
10. Mishra VK, Wegwitz F, Kosinsky RL, Sen M, Baumgartner R, Wulff T, et al. Histone deacetylase class-I inhibition promotes epithelial gene expression in pancreatic cancer cells in a BRD4-and MYC-dependent manner. *Nucleic Acids Res.* 2017;
11. Blankenberg D, Gordon A, Von Kuster G, Coraor N, Taylor J, Nekrutenko A, et al. Manipulation of FASTQ data with galaxy. *Bioinformatics.* 2010 Jun 18;26(14):1783–5.
12. Trapnell C, Pachter L, Salzberg SL. TopHat: Discovering splice junctions with RNA-Seq. *Bioinformatics.* 2009;
13. Dobin A, Gingeras TR. Mapping RNA-seq Reads with STAR. *Curr Protoc Bioinforma.* 2015 Sep;51(1):11.14.1-11.14.19.
14. Love MI, Huber W, Anders S. Moderated estimation of fold change and dispersion for RNA-seq data with DESeq2. *Genome Biol.* 2014;
15. Kosinsky RL, Helms M, Zerche M, Wohn L, Dyas A, Prokakis E, et al. USP22-dependent HSP90AB1 expression promotes resistance to HSP90 inhibition in mammary and colorectal cancer. *Cell Death Dis.* 2019 Dec 1;10(12).

Author contribution

Author Full Name:	Specification of Contribution to the Manuscript:
Evangelos Prokakis	Study design, cell culture experiments and molecular analyses, mRNA-seq library preparation, histological analyses, preparation, drafting and revision of manuscript
Anna Dyas	Cell culture methods and molecular biology experiments, mRNA-seq library preparation, manuscript proof reading
Regina Grün	Cell culture methods and molecular biology experiments
Sonja Fritzsche	Cell culture methods and molecular biology experiments
Upasana Bedi	mRNA-seq library preparation
Zahra Kazerouni	Cell culture methods and molecular biology experiments
Robyn Kosinsky	Mouse experiments
Steven A. Johnsen	Study design and conception, preparation, drafting and revision of manuscript
Florian Wegwitz	Study design and conception, mouse experiments, preparation, drafting and revision of manuscript

5. General discussion

During the last decade, H2Bub1 has been an intensively studied hPTM in cancer research, by virtue of its important role in various tissue-specific differentiation programs and its documented gradual loss in cancer progression. Nonetheless, no previous report determined the biological consequence of H2Bub1 decrease or increase in a GEMM that mimics an oncogene-induced solid tumor like BC. To fill this gap, we genetically deleted RNF40 (*Rnf40^{wt/fl}* or *Rnf40^{fl/fl}*) or USP22 (*Usp22^{wt/fl}* or *Usp22^{fl/fl}*), which are the H2Bub1-specific E3 ligase and DUB, respectively, using a HER2⁺-BC-recapitulating mouse model. To substantiate our results, we took advantage of human HER2⁺ BC cell lines and publically available RNA-seq data.

Against our expectations, we found that RNF40 and USP22 do not play opposing functions but both support the tumorigenic phenotype of HER2⁺-BC. Specifically, RNF40 loss interfered with the H2Bub1/H3K4me3 *trans*-histone crosstalk, thereby, substantially impairing the gene expression and organization of the AC/FAK signaling cascade that impacted cell survival and motility features of HER2⁺-BC cells. Surprisingly, loss of USP22 did not elicit a global increase of H2Bub1, but rather compromised the protein stability of the ER-molecular chaperone HSPA5, leading to UPR-induced apoptotic cell death.

5.1. The first *in vivo* study, unraveling the impact of H2Bub1 loss on an oncogene-induced malignancy, using a conditional *RNF40* knockout approach

To date, the dichotomous role of H2Bub1 along with the respective catalytic complex RNF20-RNF40 in cancer has been extensively reported and studied in a broad spectrum of solid cancers (of colon, cervix, breast, brain, liver, lung, ovary, kidney, and prostate) as well in leukemia (see Table 2, chapter 2.6.6). The ambiguous role of the H2Bub1 in cancer biology has been so far studied, mainly using *in vitro* experimental approaches (see Table 2, chapter 2.6.6) or xenograft experiments with stable RNF20- or RNF40-knockdown cell clones as an *in vivo* approach (Duan et al. 2016; Gao et al. 2011; Hooda et al. 2019; Jing et al. 2020; Tarcic et al. 2017; Wang et al. 2013a). However the number of studies using a cancer GEMM to examine the role of H2Bub1 loss is, to date, scarce and only limited to Dextran Sulfate Sodium (DSS)-induced colitis-associated colorectal carcinoma (CRC) (Kosinsky et al. 2019a; Tarcic et al. 2016).

To further broaden our current knowledge about the role of the H2Bub1-epigenetic machinery *in vivo*, we utilized MMTV-*ErbB2* mice, a GEMM which adequately mimics HER2⁺-BC (Rennhack et al. 2019; Shackleton et al. 2006). Compared to the few GEMM-based studies focusing on the role of H2Bub1 loss in DSS-induced CRC (Kosinsky et al. 2019a; Tarcic et al. 2016), the rest *in vivo* H2Bub1-related studies rely on xenograft

experiments as a preclinical *in vivo* platform (Duan et al. 2016; Jing et al. 2020; Lee et al. 2017; Tarcic et al. 2017; Wang et al. 2013a). Although, xenograft studies, in general, are less time-consuming and less expensive compared to cancer GEMMs, the latter *in vivo* platform presents certain decisive features that more reliably recapitulate the human disease. Firstly, like all cancer-related GEMMs, MMTV-*ErbB2* mice are not immunodeficient, thereby, maintaining the tumor-to-immune system crosstalk, whereas the HER2-driven tumor bulk, to a great extent, mimics the tissue heterogeneity, like in human mammary carcinomas. Secondly, compared to the stably silenced human cell line clones (for xenograft use), the HER2-driven tumorigenesis program potentiates the expansion of a greater number of tumor clones, originating from the normal mammary epithelium, which satisfactorily follows the natural history of cancer disease (Becher and Holland 2006). Building on that, the greater (epi)genetic variety of these tumor clones can create a wide range of different cancer dependencies on the deleted gene-of-interest, mirroring a realistic differential response of various tumor clones to e.g. a hypothetical RNF40-specific inhibitor. Taken together, our study sets the basis for the role of H2Bub1 loss in HER2⁺-BC using a widely accepted GEMM for HER2⁺-BC. Moreover, future studies need to reconsider the use of GEMMs as preclinical *in vivo* platforms to more safely conclude the ambiguous role of H2Bub1 in cancer.

5.2. Why MMTV-*ErbB2* mice show a heterogeneous population of RNF40⁺ and RNF40⁻ tumor cells in an *Rnf40*^{fl/fl}-deficient state?

One of the surprising findings of our *in vivo* study was the heterogeneous population of RNF40-positive and -negative tumor cells in *Rnf40*^{fl/fl} HER2⁺ tumors. Consistent with the lack of a complete block of tumor progression, the existence of preserved RNF40⁺ BC cell clones may have been the leading cause of a suboptimal block of tumor growth, ensuing a slower but not eradicated growth kinetic of HER2-driven tumors in *Rnf40*^{fl/fl} mice. In the following paragraph, we will elaborately provide some representative study-examples which exclude the incomplete knockout of *Rnf40* in *Rnf40*^{fl/fl} tumors as a weakness of our *in vivo* study.

Indeed, previously published studies, focusing on the role of nodal BC-supportive genes in MMTV-*ErbB2* and MMTV-*PymT* (Polyomavirus T antigen) GEMMs, observed similar heterogeneous BC populations in a homozygous deletion state, such as for *Pak4* (Costa et al. 2019), *Myb* (Miao et al. 2011) and *Ptk2* (Lahlou et al. 2012). Specifically, the homozygous deletion of *Pak4* (MMTV-*PymT*; MMTV-*Cre*; *Pak4*^{fl/fl}) substantially reduced the tumorigenic phenotype of PymT-driven mammary tumors, however, heterogeneous subpopulations of PAK4⁺ and PAK4⁻ tumor cells emerged. Similar to their study, we speculate that the


"mosaic-like" RNF40 expression pattern in *Rnf40^{fl/fl}* tumors originates from the HER2-imposed positive selection and expansion of tumor clones, where *Cre* is not expressed or inactive, leading to an unsuccessful Cre-mediated knockout of *Rnf40^{fl/ox}*. Although we have not confirmed a heterogeneous Cre expression in *Rnf40^{fl/fl}* tumors, in the PAK4-related study, immunohistochemical (IHC) detection of Cre showed a "mosaic" Cre staining pattern, similar to PAK4 staining, in *Pak4^{fl/fl}* tumors, while observing a homogeneous Cre staining in wild-type tumors. Moreover, IHC of PyMT showed homogeneous staining in both mouse cohorts (similar to the HER2 staining in our study), strongly suggesting a stochastic and cell-specific suppression of *Cre* expression in *Pak4^{fl/fl}* tumors, which favored the oncogene-induced clonal expansion of PAK4-proficient tumor cells (Costa et al. 2019; Wegwitz et al. 2020).

To summarize, we believe our *in vivo* data substantially strengthen the essential role of RNF40 in HER2⁺-BC to the extent that rare RNF40/H2Bub1-expressing "escaper" cells are positively selected during HER2-driven tumor progression.

5.3. Understanding the context-dependent role of H2Bub1 in cancer disease

An increasing number of studies have improved the current knowledge about the H2Bub1-regulatory pathway in physiological and pathological conditions. The current chapter will provide us with some interesting interpretations regarding the opposing role of this hPTM in cancer progression.

As we have previously discussed (chapter 2.1.2), BC is a heterogeneous disease, comprising different molecular BC subtypes, characterized by a subtype-specific (epi)genetic landscape and a transcriptomic profile (Dawson et al. 2013; Gao et al. 2015; Garrido-Castro et al. 2019). Consistent with this knowledge, it is tempting to speculate that BC subtype-specific signaling cascades use the H2Bub1-machinery for different transcriptomic programs, that either support or suppress cancer progression. Building on this assumption, the H2Bub1-regulatory machinery may exert an executive role for a subtype-specific transcriptomic program that either supports or suppresses cancer aggressiveness. For example, the current study identified that the RNF40/H2Bub1-axis is indispensable for HER2⁺-BC *in vivo* and *in vitro* (Wegwitz et al. 2020), while impairing the same axis was shown to aggravate the tumorigenic phenotype in Lum A BC cells *in vitro* (Prenzel et al. 2011). Indeed, the ESR-transcriptomic program, that is potentiated by the RNF40/H2Bub1 axis, maintains a well-differentiated and less invasive phenotype in Lum A BC cells (Mak et al. 2013; Prenzel et al. 2011; Al Saleh et al. 2011). Accordingly, having on our disposal 52 Lum A primary tumor biopsies (compared to the limiting amount of 20 available HER2⁺ BC biopsies), that were matched with patient survival data, we confirmed



that RNF40^{high}, as well as H2Bub1^{high}-Lum A BC patients presented a better survival outcome (data not shown). Consistent with the contributory role of RNF40 in the ESR-driven transcription program (Prenzel et al. 2011), RNF40^{high}-patients present a low probability of distant metastasis in Lum A BC disease (kmplot.com, data not shown).

Given the opposing roles of the H2Bub1-catalyzing axis in a single BC entity, we do speculate that this bipolar behavior arises from the propensity of high-stage BC subtypes being more reliant on aggressive tumorigenic features, where the AC dynamics plays a quite important role (Desouza et al. 2012; Izdebska et al. 2018; Wang et al. 2012). Indeed, ROCK1 expression was associated with increased EMT in malignant types of BC whereas overexpression of ROCK1 in a normal mammary epithelial cell line significantly increased their stemness properties (Matsubara and Bissell 2016). Moreover, ROCK1 expression as well as F-actin have been correlated with HER2 expression, with advanced tumor stage, with decreased metastasis-free survival probability and inversely associated with ESR expression in BC (Kao et al. 2011; Tawab Osman et al. 2020). In concordance, using publically available data (kmplot.com), the current study showed that RNF40^{high}- as well as patients with high expression of all downstream AC-regulatory target genes display an increased probability of distant metastasis in HER2⁺-BC disease (Wegwitz et al. 2020). Accordingly, our study showed that RNF40 silencing or ROCK1 inhibition in HER2⁺-BC cells led to a cortical actin phenotype (Wegwitz et al. 2020) that resembles to the tumor-suppressive actin organization in non-invasive epithelial cells and Lum A BC cells at basal state (Lomakin et al. 2015; Padilla-Rodriguez et al. 2018).

Interestingly, no prognostic value was found for the expression of the RNF40-dependent AC-regulatory genes (*ROCK1*, *LIMK2*, *PFN2*) in Lum A BC (kmplot.com, data not shown). Concordantly, RNF40-depleted Lum A BC cells do not regulate the expression of the same AC-regulatory network (Prenzel et al. 2011) (data not shown). Moreover, and as previously mentioned, a past study has shown that the ESR-mediated transcription program in Lum A BC promotes the formation of tumor-suppressive cortical actin bundles, thereby, suppressing cell motility and local invasion (Padilla-Rodriguez et al. 2018). Additionally, ESR activity was shown to mediate an epithelial and well-differentiated phenotype, where RNF40 and H2Bub1 play a supportive role (Cristea and Polyak 2018; Mak et al. 2013; Prenzel et al. 2011; Al Saleh et al. 2011).

Collectively, the tumorigenic phenotype of Lum A BC subtype is not dependent on the RNF40/H2Bub1/ROCK1-driven AC organization due to the intrinsically suppressed invasive phenotype that is tightly imposed by the ESR-transcriptomic program (Cristea and Polyak 2018; Mak et al. 2013; Prenzel et al. 2011; Al Saleh et al. 2011). On the contrary, given the tendency of HER2-enriched BC and TNBC patients to develop distant metastasis (Masood


2016) and the integral role of the AC-dynamics during this process (Gandalovičová et al. 2017), our data portray a BC subtype-specific dependency on RNF40 and its downstream AC-regulatory network.

5.4. If H2Bub1 is a ubiquitous hPTM of active genes, why a fraction of genes is affected upon RNF40 loss?

Despite the presence of H2Bub1 in the gene-body of actively transcribed genes (Wegwitz et al. 2020), all H2Bub1-related studies (including ours) have shown a selective group of genes being affected upon loss of RNF20 or RNF40 (Cole et al. 2020; Jaaskelainen et al. 2012; Jing et al. 2020; Kosinsky et al. 2019a; Najafova et al. 2020; Prenzel et al. 2011; Schneider et al. 2019; Wang et al. 2013a; Wegwitz et al. 2020; Xie et al. 2017). Nevertheless, no study (including ours) has deciphered the mechanistic aspect of these RNF20- or RNF40-dependencies.

However, to date, only few studies have pictured the epigenetic landscape of RNF20- or RNF40-target genes, which may provide a better understanding of the RNF20- and RNF40-dependencies of specific genes. For example, the current as well as a past study from our group showed that the H2Bub1 occupancy of RNF40-dependent genes is considerably lower, compared to RNF40-independent genes (Wegwitz et al. 2020; Xie et al. 2017). According to the past study, Xie et al. demonstrated that RNF40-independent H2Bub1^{high}-genes were characterized by a high H3K27ac/H3K27me3 ratio and H3K4me3 intensity, compared to RNF40-dependent H2Bub1^{low}-genes (Xie et al. 2017). Concordantly, using publically available ChIP-seq tracks of gene-activating hPTMs (Franco et al. 2018; Malladi et al. 2016), our study uncovered lower levels of H3K79me2, H3K36me3, H3K9ac, and RNApol II in RNF40-dependent H2Bub1^{low}-genes, compared to RNF40-independent H2Bub1^{high}-genes, in HER2⁺-BC cells at basal state (Wegwitz et al. 2020). Consequently, both studies hypothesized that this independence may be attributed to the higher abundance of other gene-activating hPTMs that compensate for the loss of H2Bub1. On the contrary, concerning the RNF40-dependent H2Bub1^{low}-genes, we hypothesize that they are transcriptionally more vulnerable to H2Bub1 occupancy changes due to the moderate H2Bub1 occupancy, as well as of the rest transcription-activating hPTMs at basal state (Wegwitz et al. 2020; Xie et al. 2017). Unfortunately, though, there is so far no satisfactory and solid mechanistic explanation for the gene-specific dependencies on the RNApol II pausing-release mediated by the RNF20-RNF40/H2Bub1-axis.

As described in chapter 2.6.2, H2Bub1 and the H2Bub1-H3K4me3 *trans*-histone crosstalk are actively involved in the release of paused-RNApol II, hence, promoting transcriptional elongation (Chen et al. 2015; Fuchs et al. 2014; Laroche et al. 2012; Shchebet et al.



2012; Xie et al. 2017; Zhang et al. 2016). Nonetheless, H2Bub1 and its downstream *trans*-histone modifications, H3K4me3 and H3K79me2/3, are not the only hPTMs involved in transcriptional elongation. Also due to the greater abundance of some gene-activating hPTMs in RNF40-independent genes (Wegwitz et al. 2020; e.g H3K9ac), they may still sustain the transcription-elongating step, even in the absence of the H2Bub1-H3K4me3 *trans*-histone crosstalk.

Indeed, based on numerous studies in yeast and mammalian cells, it has been discovered that various chromosomal remodelers can recognize various gene-activating hPTMs, hence, directly promoting the chromatin openness to allow transcriptional processivity. For example, the SAGA complex-mediated H3K9ac [which is more abundant in RNF40-independent genes (Wegwitz et al. 2020)] becomes a docking site for the bromodomain region of SWItch/Sucrose Non-Fermentable (SWI/SNF) complex, which is a chromosome remodeler that promotes chromatin openness and gene activation (Swygert and Peterson 2014). Moreover, the INOitol-requiring mutant 80 (INO80) nucleosome remodeling complex is able to recognize acetylated residues of H4, via its bromodomain, to exchange H2A/H2B for H2A.Z/H2B dimers, leading to a more unstable nucleosome variant conferring a permissive chromatin state for the transcribing RNAPol II (Swygert and Peterson 2014). Moreover, our study did not take into account the DNA methylation status (in control and RNF40-deficient state) as well as the promoter-proximal CpG content of RNF40-dependent and -independent genes. CpG methylation, as a transcription-suppressive epigenetic mark, is able to control the local enrichment of other gene-(in)activating hPTMs (Cedar and Bergman 2009; Du et al. 2015). Therefore, we do hypothesize that RNF40-dependent genes are more enriched by CpG methylation, which may explain the moderate enrichment of H2Bub1 and of other transcription-activating hPTMs. Consistent with this idea, we, indeed, found that the GC and the C content of the promoter-proximal region (-50/+300 bp from the TSS) of RNF40-independent genes was significantly lower, compared to RNF40-dependent genes (data not shown). Therefore, we do suggest H2Bub1^{high}/RNF40-independent genes as less sensitive to the CpG methylation status and with a more transcriptionally permissive chromatin state compared to H2Bub1^{low}/RNF40-dependent genes.

To summarize, H2Bub1 is irrefutably a ubiquitous hPTM throughout actively transcribed genes (Wegwitz et al. 2020). However, besides H2Bub1, the abundance of additional gene-activating hPTMs that recruit chromosomal remodelers, as well as the promoter-proximal CpG methylation status or GC content, can greatly determine to which extent a gene is H2Bub1-dependent.

5.5. How RNF40/H2Bub1 loss and actin dynamics imbalance elicits programmed cell death in HER2⁺-BC?

To date, we know that the AC network sustains nodal functions in cancer biology, including cell motility, cell polarity, cytokinesis, and endocytosis (Suarez and Kovar 2016). Moreover, accumulating evidence highlights the AC dynamics being important to uphold signaling cascades that drive proliferation and resistance to programmed cell death (Desouza et al. 2012; Tavares et al. 2017).

In our study, we found that RNF40 epigenetically regulates, among other, the expression of ROCK1, thereby, suppressing the activity of cofilin (*in vitro* and *in vivo*) and sustaining the F-actin abundance (Wegwitz et al. 2020). As expected, ROCK1 inhibition (ROCKi) (Wegwitz et al. 2020), as well as cytochalasin D (an F-actin severing agent) treatment (data not shown), phenocopied the increased activity of cofilin (lower p-cofilin) leading to F-actin loss and increased apoptotic rate in RNF40-silenced HER2⁺-BC cells. In agreement, a series of studies using similar actin-modulatory compounds have shown that severing or stabilizing F-actin agents, dramatically impair the cell motility and viability of cancer cells (Desouza et al. 2012). For example, jasplakinolide, which is a potent F-actin stabilizing drug, resulted in apoptosis induction in various human cancer cell lines (Desouza et al. 2012). On the other hand, cytochalasin D or lantraculin A, compounds that bind to the barbed end (+) of F-actin or actin monomers, respectively, impeded actin polymerization, thereby eliciting a prominent apoptotic cell death in several cancer cell lines (Desouza et al. 2012). Concluding, unidirectional imbalance of the AC dynamics may impact all downstream cellular functions, such as cell motility and cell viability.

Despite our study did not provide a direct mechanistic link between F-actin impairment and the induction of the apoptotic cascade, the only known linking mechanism was given by Puthalakath et al., showing that the proapoptotic Bcl2-Modifying Factor (BMF) is released from the actin-associated myosin V upon cell detachment or cytochalasin D treatment, inducing the intrinsic apoptotic cascade (Puthalakath et al. 2001). However, it is widely known that the AC is inextricably linked to the FA structures and the kinase activity of FAK (Molecular Biology of the Cell, 6th edition, Garland Science, 2015; see chapter 2.3.2). As initially discussed in chapter 2.3.2, ROCK1-dependent actomyosin contraction leads to a retraction movement of the "trailing" edge of moving cells. The applied cytoskeletal tension on FA is a prerequisite not only for cell movement but also for the stabilization of FA complexes that activate, by autophosphorylation, the mechanosensitive FAK kinase (p-FAK) (Pasapera et al. 2010). Strikingly, a number of reports showed that FAK and its catalytic activity are indispensable for suppressing apoptosis in BC and that MMTV-*ErbB2* mice with BC-specific FAK knockout displayed improved disease-free survival, compared


to their control counterparts (Lahlou et al. 2012; McLean et al. 2005; Walker et al. 2016). Consequently, we speculated that the RNF40/H2Bub1/ROCK1 axis sustains cell viability via the FA-associated pro-survival FAK kinase. As such, we sought to solidify the involvement of FA imbalance and impaired FAK activity in RNF40-depleted HER2⁺-BC cells. Indeed, we observed that FAK-inhibited (FAKi) HER2⁺-BC cells lost their proliferative potential, which was compatible with the pronounced decrease of their FA complex size and decreased levels of p-FAK in RNF40-deficient, ROCKi- and FAKi-treated HER2⁺-BC cells. Finally, our data were substantiated by the significant enrichment of FA- along with AC- and H2Bub1-signatures in *RNF40*^{high}-expressing HER2⁺-BC patients (Wegwitz et al. 2020).

To conclude, the current study strongly proposes that RNF40/H2Bub1 is a tumor-supportive epigenetic axis that is crucial for the AC/FAK-sustained oncogenic features in HER2⁺-BC disease. Therefore, patients suffering from RNF40-dependent malignancies may profit from therapeutic schemes targeting the AC/FAK-axis.

5.6. The first conditional USP22 knockout BC model, pointing to a global H2Bub1-independent tumor-supportive mechanism

During the last fifteen years, USP22 has been shown to possess a strong tumor-supportive role in a plethora of malignancies, continuously confirming the position of this gene among the 11 prominent genes which constitute the "death-from-cancer" signature (Glinsky et al. 2005). Only a few studies reported a tumor-suppressive role of USP22 in CRC and leukemia (Kosinsky et al. 2020; Kosinsky et al. 2019b; Melo-Cardenas et al. 2018). The *in vivo* role of USP22 in cancer progression has been thoroughly elucidated using valuable mouse models that mimic prostate cancer, leukemia, and colorectal cancer (Kosinsky et al. 2020; McCann et al. 2020; Melo-Cardenas et al. 2018). However, to date, no combined *in vivo/in vitro* study has unraveled the biological consequence of H2Bub1 increase via USP22 loss in the leading cancer entity, worldwide, namely BC. For this reason, similar to the RNF40 project, we utilized a GEMM for HER2⁺-BC to shed light on the role of this H2Bub1-specific DUB.

Surprisingly, USP22-deficient HER2-driven mammary tumors (see Manuscript II) and HER2⁺-BC cells (data not shown) showed no apparent increase of H2Bub1. Although USP22 was reported to be an H2Bub1-specific DUB (Daniel et al. 2004; Jeusset and McManus 2017; Lang et al. 2011), we identified that USP22 loss was in certain cases not affecting the global H2Bub1 levels (Atanassov et al. 2016). Moreover, H2Bub1-specific DUBs, such as USP3 or USP44, were shown to play an equally decisive role on this hPTM (Bonnet et al. 2008). Therefore, future studies may consider identifying the biological



consequence of H2Bub1 increase in HER2⁺-BC via deleting one the abovementioned DUBs. In addition, loss of Enhancer Of Yellow 2 Transcription Factor Homolog (ENY2) or Ataxin 7 Like 3 (ATXN7L3) (the DUBm accessory subunits of the SAGA complex) was shown to substantially increase the total H2Bub1 levels in HEK293T cells (Atanassov et al. 2016), thereby, we suggest future studies to investigate the loss of ENY2 or ATXN7L3 in HER2⁺-BC.


Collectively, the current study provides the first conditional *Usp22* knockout mouse model in (HER2⁺)-BC, potentiating future research efforts to the design of USP22-specific inhibitors with therapeutic benefit for HER2⁺-BC patients.

5.7. Our study presents a so far undescribed role of USP22 in suppressing UPR, via stabilizing HSPA5 in HER2⁺-BC

Based on numerous studies, USP22, as the main catalytic DUBm of the SAGA complex, was thought to exclusively play an epigenetic function by deubiquitinating monoubiquitinated histone targets, including H2Aub1 and H2Bub1 (Daniel et al. 2004; Henry et al. 2003; Zhang et al. 2008; Zhao et al. 2008). However, during the last decade, accumulating evidence of non-histone targets, whose protein stability depends on the catalytic activity of USP22, undeniably broadens the pleiotropic functions of this DUB.

Our findings excluded a global H2Bub1-dependent involvement in the impaired phenotype upon USP22 loss. Therefore, we decided to look into each gene member of the proapoptotic signature that was strongly enriched upon USP22 loss. *ATF3* was a highly-ranked gene in the "HALLMARK_APOPTOSIS"-signature that was enriched in both USP22-deficient HER2⁺-BC models. *ATF3* has been characterized as a potent pro-apoptotic TF in several cancer entities (Ku and Cheng 2020), even in a p53-independent manner (Sharma et al. 2018). Given that at least 71% of human HER2⁺-BC patients (bioportal.org, data not shown) present a loss-of-function mutation in *TP53* (bioportal.org, data not shown), we reasoned that the observed apoptotic phenotype is largely dependent on a severe cellular, p53-independent stress response upon USP22 loss. In line, *ATF3* was shown to be a downstream gene target of the UPR in multiple reports (Brooks et al. 2014; Hayner et al. 2018; Sharma et al. 2018; Xu et al. 2012a). Indeed, we ascertained a PERK-mediated induction of the ATF4/ATF3/DDIT3 proapoptotic axis upon USP22 loss. Therefore, given that USP22 expression is inversely correlated with a UPR-transcriptomic signature in HER2⁺-BC and prostate cancer (Wegwitz et al. 2020), we conclude that USP22 is a potent suppressor of the UPR-mediated apoptotic cell death.

The proapoptotic role of UPR in HER2⁺-BC had been already known by two independent previous studies. For example, MMTV-*ErbB2* mice with a heterozygous knock-in S51A



mutation of the eIF2a led to an aggravated tumorigenic phenotype compared to the control cohort (Darini et al. 2019). In line, it was shown that IRE1A and ATF6 promote an apoptotic phenotype in response to palmitate-induced lipotoxicity, preferentially in HER2⁺-BC cells than other BC cell lines of Luminal A origin (Baumann et al. 2016). In alignment, and as it will be thoroughly discussed later, HER2-driven BC demonstrates a particularly heightened dependency on the ERAD-axis and the maintenance of ER homeostasis to counteract cytotoxic ER stress (Arora and Golemis 2015; Schulz et al. 2014a; Singh et al. 2015). Concluding, our findings point to a key-role of USP22 in suppressing the UPR activity at basal state in HER2⁺-BC.


In our study, we uncovered that HSPA5, the most abundant and nodal ER-molecular chaperone that actively suppresses all three UPR-mediators (PERK, IRE1, ATF6) (Molecular Biology of the Cell, 6th edition, Garland Science, 2015), is a binding partner of and stabilized by USP22 in HER2⁺-BC. This key-connection of USP22 loss to UPR induction was based on a very recent study from McCann et al. (McCann et al. 2020), examining the USP22-dependent ubiquitome (ubi-scan) in prostate cancer. Noteworthy, HSPA5 has been numerous times reported as a global tumor-supportive molecular chaperone in various cancer entities, including BC, whereas its expression associates with poor survival outcome in cancer patients (Casas 2017). The involvement of this chaperone in various cancer aspects such as proliferation, resistance to chemotherapeutics, aberrant vascularization and metastatic dissemination (Casas 2017), renders this molecular chaperone an ideal therapeutic target in USP22-dependent malignancies.

Collectively, we report that USP22 is the first acknowledged USP-member suppressing UPR via deubiquitinating/stabilizing HSPA5, thereby, promoting the tumorigenic phenotype of HER2⁺-BC.

5.8. USP22 plays multiple functions in protein homeostasis to prevent oncogene-induced PT

An extensive list of publications has shown that USP22 and HSPA5 are critical for the expression and stability of various tumor-supportive factors that sustain specific cancer hallmarks such as aberrant cell cycle, anabolic processes, protein quality control, and autophagy (Adams et al. 2019; Casas 2017; Cha-Molstad et al. 2016; Dong et al. 2008; Kim et al. 2017; Kosinsky et al. 2019b; Liang et al. 2014; McCann et al. 2020; Sussman et al. 2013; Wang and Dent 2014).

Moreover, and as mentioned in chapter 2.4, one additional cancer hallmark is the constant oncogene-driven PT (Guang et al. 2019; McConkey 2017). The current work complements USP22 with a cytoprotective role that counteracts the oncogene-driven (HER2 in this case)



PT via stabilizing HSPA5 and maintaining the ER-protein folding capacity in HER2⁺-BC. In our work, we provide evidence that USP22 deubiquitinates and stabilizes HSPA5 in HER2⁺-BC, a mammary malignancy which displays particularly increased cellular energetics and protein synthesis turnover, allowing fast-cycling cancer cells to cover their heightened anabolic needs (Arora and Golemis 2015; Schulz et al. 2014a; Singh et al. 2015). Accordingly, in the recent past, our research group has shown that USP22, as part of the SAGA complex, promotes the expression of heat-shock protein 90 Alpha family class B1 (*HSP90AB1*) (Kosinsky et al. 2019b). HSP90AB1 is a pivotal cytoplasmic chaperone that is frequently "hijacked" by cancer cells to promote the function and stability of numerous oncoproteins (Whitesell and Lindquist 2005). Moreover, USP22 and HSPA5 are able to support the autophagic pathway, thereby, relieving the oncogene-induced PT, as well as replenishing cancer cells with nutrients under starvation conditions (Dong and Cui 2018; Huang et al. 2018; Liang et al. 2014). In line, HER2-driven signaling was elegantly described to induce the cytoplasmic HSP90-based chaperone system, where USP22 is actively involved, to counteract the HER2-induced PT effect and balance the global protein turnover (Kosinsky et al. 2019b; Schulz et al. 2014b). Finally, a past study focusing on molecular vulnerabilities of HER2⁺-BC, identified that HER2/mTOR-driven PT, is tightly controlled by the ERAD-pathway as an adaptive response to excessive amounts of misfolded protein aggregates (Singh et al. 2015). Collectively, USP22 promotes the expression of two critical molecular chaperones as well as sustains the autophagic pathway, thereby, supporting two pivotal adaptive responses that ameliorate HER2-induced PT.

Moreover, USP22 was reported to promote the stability and activity of MYC, a well-known oncogene that, among other cancer hallmarks, similar to HER2, promotes protein synthesis and other anabolic processes (Chen et al. 2018). Additionally, based on the previously mentioned ubi-scan study (McCann et al. 2020), authors reported additional USP22 targets belonging to the translational machinery, such as the tRNA synthetase Alanine-tRNA Synthetase 1 (*AARS1*), the Glycyl-tRNA Synthetase 1 (*GARS1*), and the Eukaryotic Translation Elongation Factor 1 Delta (*EEF1D*). Therefore, USP22 is actively involved in mediating the global protein synthesis that is exacerbated in oncogene-induced malignancies.

Concluding, USP22 enacts a multilayered role, not only by mediating oncogene-induced protein synthesis (e.g via MYC), but also by simultaneously counterbalancing the accumulation of unfolded/misfolded proteins via the global protein control network (via HSPA5 and HSP90AB1) and the autophagic pathway, respectively.

6. Conclusion

Our work demonstrates that RNF40, the major E3 ligase of H2Bub1 is indispensable for the tumorigenic phenotype of HER2⁺-BC, via epigenetically controlling the AC/FAK-mediated cell survival and cell motility (Wegwitz et al. 2020). In addition, the current study was not able to confirm a global H2Bub1 increase upon USP22 loss. Nevertheless, similar to RNF40, we identified a novel, non-epigenetic and tumor-supportive involvement of USP22 in HER2⁺-BC, via stabilizing the major ER-chaperone HSPA5 and suppressing the PERK-mediated programmed cell death (2nd manuscript, under peer review process).

Central objective of the study was to leverage *in vivo* as well as *in vitro* experimental methods to decipher the biological impact of H2Bub1 loss or gain, via interfering with the expression of RNF40 and USP22, respectively, in a GEMM for HER2⁺-BC. To date, most of the studies examining the role of H2Bub1 in a cancer, rely on *in vitro* cancer models which partially mimic the (epi)genetic heterogeneity, and completely lack the histologic complexity and the cancer-to-microenvironment crosstalk that is present in growing tumor bulks. Therefore, we do believe that our preclinical work sets the basis for future studies to design novel RNF40- and USP22-specific inhibitors with promising therapeutic response in HER2⁺-BC patients.

With regard to the RNF40-related study, we showed that HER2-driven BC uses the RNF40/H2Bub1/H3K4me3-axis to promote transcriptomic programs sustaining one of its most aggressive tumorigenic features, namely, the AC dynamics that supports, among other, cell motility and downstream pro-survival pathways (Cabrita et al. 2011; Desouza et al. 2012; Foerster et al. 2014; Nersesian et al. 2018; Stehn et al. 2013; Wegwitz et al. 2020). In line, the involvement of the RNF40/H2Bub1-axis in controlling AC strengthens a growing body of evidence demonstrating the impact of epigenetic alterations on the AC dynamics in multiple cancers, including melanoma, colon, and breast cancer (Ding et al. 2015; Koroknai et al. 2020; Mielnicki et al. 1999; Zacharopoulou et al. 2018). Collectively, given the strong entanglement of epigenetic aberrations in controlling various other cancer hallmarks (Darwiche 2020), we suggest that the discovery of cancer (sub)type-specific epigenetic vulnerabilities/dependencies will broaden or open novel avenues in the therapeutic management of this malady.

On the other hand, MMTV-*ErbB2* mice with genetic loss of *Usp22* demonstrated, as expected, an impacted tumorigenic phenotype *in vivo* and *in vitro*. The most striking finding of this study was a global H2Bub1-independent involvement of USP22 in the observed phenotype. After performing a combined RNA-seq approach in USP22-proficient and -deficient HER2⁺-BC (*in vivo* and *in vitro*), we finally unraveled that USP22 suppresses the UPR by deubiquitinating and stabilizing HSPA5, the major ER-chaperone. Therefore, our

work not only displays a novel role of USP22 in the ER-associated chaperoning machinery, but substantially updates our current knowledge of the multilayered function of this DUB in protein synthesis, autophagy and protein folding.

Taken together, our work paves the way for using potent RNF20/RNF40-specific inhibitors as a single therapeutic scheme or combined with currently available ROCK1- or FAK-specific inhibitors to provide a synergistic therapeutic benefit for HER2⁺-BC patients. Finally, we suggest that future USP22-specific inhibitors, as a standalone therapy or in combination with molecular chaperone-specific inhibitors (HSPA5, HSP90AB1), will also provide synergistic effects to annihilate major adaptive and pro-survival responses in oncogene-induced aggressive malignancies, including HER2⁺-BC.

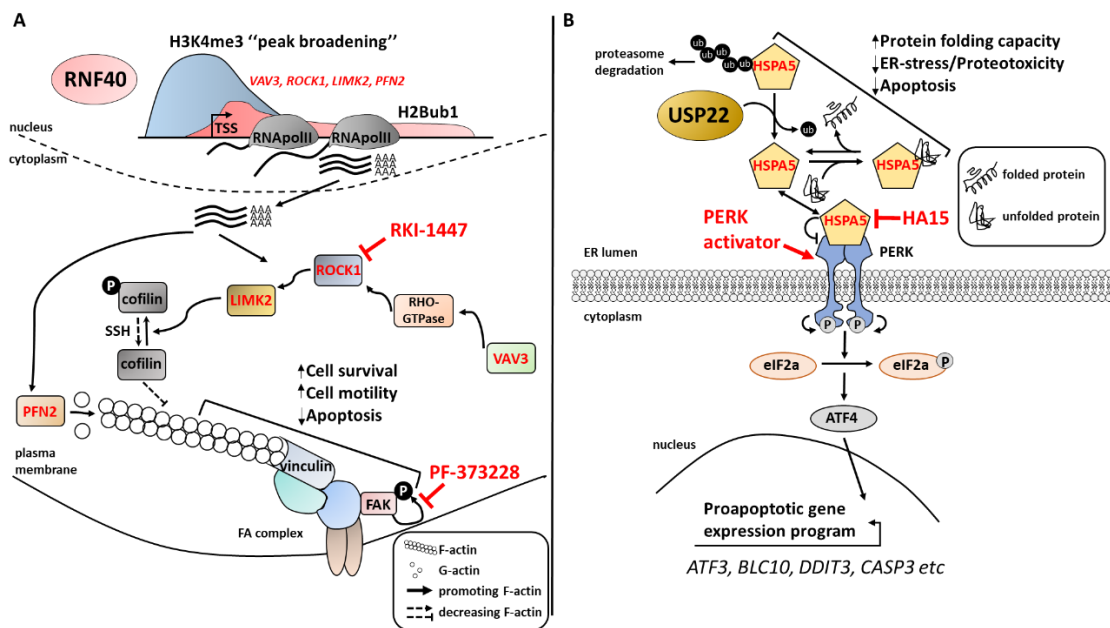


Fig.16: RNF40 and USP22 are indispensable for the tumorigenic behavior of HER2⁺-BC. **A)** RNF40, via the H2Bub1-H3K4me3 *trans*-histone crosstalk, sustains the expression of critical components of the AC-regulatory, thereby preserving the FAK-driven pathway that is essential for cell survival and motility in HER2⁺-BC. Therefore, future enzymatic RNF40-specific inhibitors as a single therapy or in combination with currently available ROCK1- or FAK-inhibitors (e.g RKI-1447, PF-373228) may provide a therapeutic window for patients suffering from RNF40-dependent HER2⁺-BC. **B)** USP22 exerts a decisive tumor-supportive role by deubiquitinating and stabilizing the ER-chaperone HSPA5, thereby suppressing the apoptotic cascade elicited by the PERK/ATF4/ATF3-cascade in HER2⁺-BC. Concluding, future USP22-specific inhibitors or, particularly, in combination with currently available HSPA5 inhibitors (e.g HA15) or PERK activators may provide a synergistic effect against the critical ER-protein quality circuit that sustain oncogene-dependent malignancies (like HER2⁺-BC).

7. References

- Adams CJ, Kopp MC, Larburu N, Nowak PR, Ali MMU. Structure and molecular mechanism of ER stress signaling by the unfolded protein response signal activator IRE1. *Front. Mol. Biosci. Frontiers Media S.A.*; 2019.
- Ao N, Liu Y, Feng H, Bian X, Li Z, Gu B, et al. Ubiquitin-specific peptidase USP22 negatively regulates the STAT signaling pathway by deubiquitinating SIRT1. *Cell. Physiol. Biochem. Cell Physiol Biochem Press*; 2014;33(6):1863–75.
- Arora S, Golemis EA. A new strategy to ERADicate HER2-positive breast tumors? . *Sci. Signal. Sci Signal*; 2015. p. fs11.
- Atanassov BS, Dent SYR. USP22 regulates cell proliferation by deubiquitinating the transcriptional regulator FBP1. *EMBO Rep. EMBO Rep*; 2011 Sep;12(9):924–30.
- Atanassov BS, Evrard YA, Multani AS, Zhang Z, Tora L, Devys D, et al. Gcn5 and SAGA Regulate Shelterin Protein Turnover and Telomere Maintenance. *Mol. Cell . Cell Press*; 2009 Aug 14;35(3):352–64.
- Atanassov BS, Koutelou E, Dent SY. The role of deubiquitinating enzymes in chromatin regulation. *FEBS Lett. John Wiley & Sons, Ltd*; 2011 Jul 7 <http://doi.wiley.com/10.1016/j.febslet.2010.10.042>
- Atanassov BS, Mohan RD, Lan X, Kuang X, Lu Y, Lin K, et al. ATXN7L3 and ENY2 Coordinate Activity of Multiple H2B Deubiquitinases Important for Cellular Proliferation and Tumor Growth. *Mol. Cell. Elsevier Inc.*; 2016;62(4):558–71.
- Baedke J. The epigenetic landscape in the course of time: Conrad Hal Waddington's methodological impact on the life sciences. *Stud. Hist. Philos. Sci. Part C Stud. Hist. Philos. Biol. Biomed. Sci. Stud Hist Philos Biol Biomed Sci*; 2013 Dec;44(4):756–73.
- Baum M. The changing face of breast cancer - Past, present and future perspectives . *Breast Cancer Res. Treat. Springer*; 2002. p. 1–5.
- Baumann J, Wong J, Sun Y, Conklin DS. Palmitate-induced ER stress increases trastuzumab sensitivity in HER2/neu-positive breast cancer cells. *BMC Cancer. BioMed Central Ltd.*; 2016 Jul;16(1).
- Beard JR, Officer AM, Cassels AK. The world report on ageing and health . *Gerontologist. Gerontological Society of America*; 2016
- Becher OJ, Holland EC. Genetically engineered models have advantages over xenografts for preclinical studies . *Cancer Res. Cancer Res*; 2006. p. 3355–8.
- Berns K, Horlings HM, Hennessy BT, Madiredjo M, Hijmans EM, Beelen K, et al. A Functional Genetic Approach Identifies the PI3K Pathway as a Major Determinant of Trastuzumab Resistance in Breast Cancer. *Cancer Cell . Cancer Cell*; 2007 Oct 16
- Bi M, Naczki C, Koritzinsky M, Fels D, Blais J, Hu N, et al. ER stress-regulated translation increases tolerance to extreme hypoxia and promotes tumor growth. *EMBO J. . EMBO J*; 2005 Oct 5;24(19):3470–81.
- Blackwell KL, Burstein HJ, Storniolo AM, Rugo H, Sledge G, Koehler M, et al. Randomized study of lapatinib alone or in combination with trastuzumab in women with ErbB2-positive, trastuzumab-refractory metastatic breast cancer. *J. Clin. Oncol. J Clin Oncol*; 2010 Mar 1;28(7):1124–30.
- Bombonati A, Sgroi DC. The molecular pathology of breast cancer progression. *J. Pathol. . 2011;223(November 2010):307–17.*
- Bonnet J, Romier C, Tora L, Devys D. Zinc-finger UBPs: regulators of deubiquitylation. *Trends Biochem. Sci. Trends Biochem Sci*; 2008 Aug;33(8):369–75.

- Bowman EA, Kelly WG. RNA Polymerase II transcription elongation and Pol II CTD Ser2 phosphorylation: A tail of two kinases . Nucl. (United States). Landes Bioscience; 2014.
- Bradner JE, Hnisz D, Young RA. Transcriptional Addiction in Cancer . Cell. Cell Press; 2017. p. 629–43.
- Bray F, Ferlay J, Soerjomataram I, Siegel RL, Torre LA, Jemal A. Global cancer statistics 2018: GLOBOCAN estimates of incidence and mortality worldwide for 36 cancers in 185 countries. CA. Cancer J. Clin. 2018 Nov;68(6):394–424.
- Bright MD, Itzhak DN, Wardell CP, Morgan GJ, Davies FE. Cleavage of BLOC1S1 mRNA by IRE1 Is Sequence Specific, Temporally Separate from XBP1 Splicing, and Dispensable for Cell Viability under Acute Endoplasmic Reticulum Stress . Mol. Cell. Biol. American Society for Microbiology; 2015 Jun 15;35(12):2186–202.
- Brooks AC, Guo Y, Singh M, McCracken J, Xuan YT, Srivastava S, et al. Endoplasmic reticulum stress-dependent activation of ATF3 mediates the late phase of ischemic preconditioning. Curr. Ther. Res. - Clin. Exp. Excerpta Medica Inc.; 2014 Dec 1;76:138–47.
- Burris HA. Dual Kinase Inhibition in the Treatment of Breast Cancer: Initial Experience with the EGFR/ErbB-2 Inhibitor Lapatinib. Oncologist . Wiley; 2004 Jun 3;9(S3):10–5.
- Burstein HJ, Sun Y, Dirix LY, Jiang Z, Paridaens R, Tan AR, et al. Neratinib, an irreversible ErbB receptor tyrosine kinase inhibitor, in patients with advanced ErbB2-positive breast cancer. J. Clin. Oncol. J Clin Oncol; 2010 Mar 10;28(8):1301–7.
- Byrne KM, Monsefi N, Dawson JC, Degasperis A, Bukowski-Wills JC, Volinsky N, et al. Bistability in the Rac1, PAK, and RhoA Signaling Network Drives Actin Cytoskeleton Dynamics and Cell Motility Switches. Cell Syst. Cell Press; 2016 Jan 27;2(1):38–48.
- Cabrita MA, Jones LM, Quizi JL, Sabourin LA, McKay BC, Addison CL. Focal adhesion kinase inhibitors are potent anti-angiogenic agents. Mol. Oncol. 2011;
- Cai Z, Zhang MX, Tang Z, Zhang Q, Ye J, Xiong TC, et al. USP22 promotes IRF3 nuclear translocation and antiviral responses by deubiquitinating the importin protein KPNA2. J. Exp. Med. NLM (Medline); 2020 May 4;217(5).
- Callahan R, Hurvitz S. Human epidermal growth factor receptor-2-positive breast cancer: current management of early, advanced, and recurrent disease. Curr. Opin. Obstet. Gynecol. . 2011 Feb;23(1):37–43.
- Callis J. The Ubiquitination Machinery of the Ubiquitin System. Arab. B. . BioOne; 2014 Jan;12:e0174.
- Capelan M, Pugliano L, De Azambuja E, Bozovic I, Saini KS, Sotiriou C, et al. Pertuzumab: New hope for patients with HER2-positive breast cancer . Ann. Oncol. Ann Oncol; 2013. p. 273–82.
- Casás-Selves M, Degregori J. How Cancer Shapes Evolution and How Evolution Shapes Cancer . Evol. Educ. Outreach. BioMed Central Ltd.; 2011. p. 624–34.
- Casas C. GRP78 at the centre of the stage in cancer and neuroprotection . Front. Neurosci. Frontiers Research Foundation; 2017.
- Castellano E, Downward J. RAS Interaction with PI3K: More Than Just Another Effector Pathway. Genes Cancer. 2011;
- Cedar H, Bergman Y. Linking DNA methylation and histone modification: Patterns and paradigms . Nat. Rev. Genet. Nat Rev Genet; 2009. p. 295–304.
- Cha-Molstad H, Yu JE, Lee SH, Kim JG, Sung KS, Hwang J, et al. Modulation of SQSTM1/p62 activity by N-terminal arginylation of the endoplasmic reticulum chaperone

- HSPA5/GRP78/BiP. Autophagy. Taylor and Francis Inc.; 2016 Jan 1;12(2):426–8.
- Chan A, Delalogue S, Holmes FA, Moy B, Iwata H, Harvey VJ, et al. Neratinib after trastuzumab-based adjuvant therapy in patients with HER2-positive breast cancer (ExteNET): A multicentre, randomised, double-blind, placebo-controlled, phase 3 trial. *Lancet Oncol.* Lancet Publishing Group; 2016 Mar 1;17(3):367–77.
 - Chandarlapaty S, Sakr RA, Giri D, Patil S, Heguy A, Morrow M, et al. Frequent mutational activation of the PI3K-AKT pathway in trastuzumab-resistant breast cancer. *Clin. Cancer Res.* Clin Cancer Res; 2012 Dec 15;18(24):6784–91.
 - Chandrasekharan MB, Huang F, Sun ZW. Ubiquitination of histone H2B regulates chromatin dynamics by enhancing nucleosome stability. *Proc. Natl. Acad. Sci. U. S. A.* . Proc Natl Acad Sci U S A; 2009 Sep 29;106(39):16686–91.
 - Chen H, Bernstein BW, Bamburg JR. Regulating actin-filament dynamics in vivo . *Trends Biochem. Sci.* Trends Biochem Sci; 2000. p. 19–23.
 - Chen H, Liu H, Qing G. Targeting oncogenic Myc as a strategy for cancer treatment . *Signal Transduct. Target. Ther.* Springer Nature; 2018.
 - Chen K, Chen Z, Wu D, Zhang L, Lin X, Su J, et al. Broad H3K4me3 is associated with increased transcription elongation and enhancer activity at tumor-suppressor genes. *Nat. Genet.* 2015 Oct 24;47(10):1149–57.
 - Chen R, Liu M, Li H, Xue Y, Ramey WN, He N, et al. PP2B and PP1 α cooperatively disrupt 7SK snRNP to release P-TEFb for transcription in response to Ca²⁺ signaling. *Genes Dev.* Genes Dev; 2008 May 15;22(10):1356–68.
 - Chen S, Jing Y, Kang X, Yang L, Wang DL, Zhang W, et al. Histone H2B monoubiquitination is a critical epigenetic switch for the regulation of autophagy. *Nucleic Acids Res.* Nucleic Acids Res; 2017 Feb 17;45(3):1144–58.
 - Chen X, Iliopoulos D, Zhang Q, Tang Q, Greenblatt MB, Hatziapostolou M, et al. XBP1 promotes triple-negative breast cancer by controlling the HIF1 α pathway. *Nature* . Nature Publishing Group; 2014;508(1):103–7.
 - Chen Y, Zhu WG. Biological function and regulation of histone and non-histone lysine methylation in response to DNA damage. *Acta Biochim. Biophys. Sin. (Shanghai).* Oxford University Press; 2016. p. 603–16.
 - Chin LS, Vavalle JP, Li A. Staring, a novel E3 ubiquitin-protein ligase that targets syntaxin 1 for degradation. *J. Biol. Chem.* J Biol Chem; 2002 Sep 20;277(38):35071–9.
 - Chiu LY, Gong F, Miller KM. Bromodomain proteins: Repairing DNA damage within chromatin . *Philos. Trans. R. Soc. B Biol. Sci.* Royal Society Publishing; 2017.
 - Citron F, Fabris L. Targeting epigenetic dependencies in solid tumors: Evolutionary landscape beyond germ layers origin . *Cancers (Basel).* MDPI AG; 2020
 - Cole AJ, Clifton-Bligh R, Marsh DJ. Histone H2B monoubiquitination: Roles to play in human malignancy. *Endocr. Relat. Cancer.* 2015;22(1):T19–33.
 - Cole AJ, Dickson KA, Liddle C, Stirzaker C, Shah JS, Clifton-Bligh R, et al. Ubiquitin chromatin remodelling after DNA damage is associated with the expression of key cancer genes and pathways. *Cell. Mol. Life Sci.* . Springer; 2020;
 - Core L, Adelman K. Promoter-proximal pausing of RNA polymerase II: A nexus of gene regulation . *Genes Dev.* Cold Spring Harbor Laboratory Press; 2019. p. 960–82.
 - Cortez JT, Montauti E, Shifrut E, Gatchalian J, Zhang Y, Shaked O, et al. CRISPR screen in regulatory T cells reveals modulators of Foxp3. *Nature* . Nature Research; 2020 Jun 18;582(7812):416–20.

- Costa TDF, Zhuang T, Lorent J, Turco E, Olofsson H, Masia-Balague M, et al. PAK4 suppresses RELB to prevent senescence-like growth arrest in breast cancer. *Nat. Commun.* Nature Publishing Group; 2019 Dec 1;10(1).
- Cramer P. Organization and regulation of gene transcription. *Nature* . Nature Publishing Group; 2019a Sep 5;573(7772):45–54.
- Cramer P. Eukaryotic Transcription Turns 50 . *Cell.* Cell Press; 2019b. p. 808–12.
- Cristea S, Polyak K. Dissecting the mammary gland one cell at a time . *Nat. Commun.* Nature Publishing Group; 2018.
- Cullinan SB, Zhang D, Hannink M, Arvisais E, Kaufman RJ, Diehl JA. Nrf2 Is a Direct PERK Substrate and Effector of PERK-Dependent Cell Survival. *Mol. Cell. Biol.* . American Society for Microbiology; 2003 Oct 15;23(20):7198–209.
- Dadey DYA, Kapoor V, Khudanyan A, Thotala D, Hallahan DE. PERK regulates glioblastoma sensitivity to ER stress although promoting radiation resistance. *Mol. Cancer Res.* . American Association for Cancer Research Inc.; 2018 Oct 1;16(10):1447–53.
- Dai H, Shen K, Yang Y, Su X, Luo Y, Jiang Y, et al. PUM1 knockdown prevents tumor progression by activating the PERK/eIF2/ATF4 signaling pathway in pancreatic adenocarcinoma cells. *Cell Death Dis.* . Nature Publishing Group; 2019 Aug 1;10(8).
- Daneshmand S, Quek ML, Lin E, Lee C, Cote RJ, Hawes D, et al. Glucose-regulated protein GRP78 is up-regulated in prostate cancer and correlates with recurrence and survival. *Hum. Pathol.* . Hum Pathol; 2007 Oct;38(10):1547–52.
- Daniel JA, Torok MS, Sun ZW, Schieltz D, Allis CD, Yates JR, et al. Deubiquitination of Histone H2B by a Yeast Acetyltransferase Complex Regulates Transcription. *J. Biol. Chem.* . J Biol Chem; 2004 Jan 16;279(3):1867–71.
- Darini C, Ghaddar N, Chabot C, Assaker G, Sabri S, Wang S, et al. An integrated stress response via PKR suppresses HER2+ cancers and improves trastuzumab therapy. *Nat. Commun.* . Nature Publishing Group; 2019 Dec 1;10(1).
- Darwiche N. Epigenetic mechanisms and the hallmarks of cancer: an intimate affair. *Am. J. Cancer Res.* Am J Cancer Res; 2020;10(7):1954–78.
- Davie JR, Xu W, Delcuve GP. Histone H3K4 trimethylation: Dynamic interplay with pre-mRNA splicing1 . *Biochem. Cell Biol.* National Research Council of Canada; 2015. p. 1–11.
- Dawood S, Broglio K, Buzdar AU, Hortobagyi GN, Giordano SH. Prognosis of women with metastatic breast cancer by HER2 status and trastuzumab treatment: An institutional-based review. *J. Clin. Oncol.* American Society of Clinical Oncology; 2010 Jan 1;28(1):92–8.
- Dawson SJ, Rueda OM, Aparicio S, Caldas C. A new genome-driven integrated classification of breast cancer and its implications . *EMBO J.* EMBO J; 2013. p. 617–28.
- Desouza M, Gunning PW, Stehn JR. The actin cytoskeleton as a sensor and mediator of apoptosis. *Bioarchitecture.* 2012 May 20;2(3):75–87.
- Dickson KA, Cole AJ, Gill AJ, Clarkson A, Gard GB, Chou A, et al. The RING finger domain E3 ubiquitin ligases BRCA1 and the RNF20/RNF40 complex in global loss of the chromatin mark histone H2B monoubiquitination (H2Bub1) in cell line models and primary high-grade serous ovarian cancer. *Hum. Mol. Genet.* 2016;
- Ding W, Fan XL, Xu X, Huang JZ, Xu SH, Geng Q, et al. Epigenetic Silencing of ITGA2 by MiR-373 promotes cell migration in breast cancer. *PLoS One* . Public Library of Science; 2015 Aug 10;10(8).

- Dong D, Ni M, Li J, Xiong S, Ye W, Virrey JJ, et al. Critical role of the stress chaperone GRP78/BiP in tumor proliferation, survival, and tumor angiogenesis in transgene-induced mammary tumor development. *Cancer Res.* Cancer Res; 2008 Jan 15;68(2):498–505.
- Dong Z, Cui H. The Autophagy-Lysosomal Pathways and Their Emerging Roles in Modulating Proteostasis in Tumors. *Cells* . MDPI AG; 2018 Dec 20;8(1):4.
- Donzé O, Jagus R, Koromilas AE, Hershey JWB, Sonenberg N. Abrogation of translation initiation factor eIF-2 phosphorylation causes malignant transformation of NIH 3T3 cells. *EMBO J.* . Wiley-VCH Verlag; 1995;14(15):3828–34.
- Dou S, Yao YD, Yang XZ, Sun TM, Mao CQ, Song EW, et al. Anti-Her2 single-chain antibody mediated DNMTs-siRNA delivery for targeted breast cancer therapy. *J. Control. Release* . J Control Release; 2012 Aug 10;161(3):875–83.
- Du J, Johnson LM, Jacobsen SE, Patel DJ. DNA methylation pathways and their crosstalk with histone methylation. *Nat. Rev. Mol. Cell Biol.* Nature Publishing Group; 2015 Aug 21;16(9):519–32.
- Duan Y, Huo D, Gao J, Wu H, Ye Z, Liu Z, et al. Ubiquitin ligase RNF20/40 facilitates spindle assembly and promotes breast carcinogenesis through stabilizing motor protein Eg5. *Nat. Commun.* Nature Publishing Group; 2016 Aug 25;7.
- Dupont C, Armant DR, Brenner CA. Epigenetics: Definition, mechanisms and clinical perspective . *Semin. Reprod. Med.* Semin Reprod Med; 2009. p. 351–7.
- Eckhardt M, Zhang W, Gross AM, Von Dollen J, Johnson JR, Franks-Skiba KE, et al. Multiple routes to oncogenesis are promoted by the human papillomavirus–host protein network. *Cancer Discov.* American Association for Cancer Research Inc.; 2018 Nov 1;8(11):1474–89.
- Evangelista FM, Maglott-Roth A, Stierle M, Brino L, Soutoglou E, Tora L. Transcription and mRNA export machineries SAGA and TREX-2 maintain monoubiquitinated H2B balance required for DNA repair. *J. Cell Biol.* . Rockefeller University Press; 2018;217(10):3382–97.
- Fagnocchi L, Mazzoleni S, Zippo A. Integration of signaling pathways with the epigenetic machinery in the maintenance of stem cells. *Stem Cells Int.* 2016.
- Fernandez PM, Tabbara SO, Jacobs LK, Manning FCR, Tsangaris TN, Schwartz AM, et al. Overexpression of the glucose-regulated stress gene GRP78 in malignant but not benign human breast lesions. *Breast Cancer Res. Treat.* Breast Cancer Res Treat; 200;59(1):15–26.
- Fierz B, Chatterjee C, McGinty RK, Bar-Dagan M, Raleigh DP, Muir TW. Histone H2B ubiquitylation disrupts local and higher-order chromatin compaction. *Nat. Chem. Biol.* . Nature Publishing Group; 2011;7(2):113–9.
- Flavahan WA, Gaskell E, Bernstein BE. Epigenetic plasticity and the hallmarks of cancer . *Science.* American Association for the Advancement of Science; 2017.
- Fleming AB, Kao CF, Hillyer C, Pikaart M, Osley MA. H2B Ubiquitylation Plays a Role in Nucleosome Dynamics during Transcription Elongation. *Mol. Cell.* 2008;
- Flis S, Gnyszka A, Misiewicz-Krzemińska I, Splawiński J. Decytidine enhances cytotoxicity induced by oxaliplatin and 5-fluorouracil in the colorectal cancer cell line Colo-205. *Cancer Cell Int.* . Cancer Cell Int; 2009 Apr 27;9.
- Foerster F, Braig S, Moser C, Kubisch R, Busse J, Wagner E, et al. Targeting the actin cytoskeleton: Selective antitumor action via trapping PKC ϵ . *Cell Death Dis.* Nature Publishing Group; 2014;5(8).

- Foglizzo M, Middleton AJ, Day CL. Structure and Function of the RING Domains of RNF20 and RNF40, Dimeric E3 Ligases that Monoubiquitylate Histone H2B. *J. Mol. Biol.* . Academic Press; 2016 Oct 9;428(20):4073–86.
- Franco HL, Nagari A, Malladi VS, Li WW, Xi Y, Richardson D, et al. Enhancer transcription reveals subtype-specific gene expression programs controlling breast cancer pathogenesis. *Genome Res.* 2018 Feb;28(2):159–70.
- Freedman RA, Gelman RS, Wefel JS, Melisko ME, Hess KR, Connolly RM, et al. Translational breast cancer research consortium (TBCRC) 022: A phase II trial of neratinib for patients with human epidermal growth factor receptor 2-positive breast cancer and brain metastases. *J. Clin. Oncol.* . American Society of Clinical Oncology; 2016 Mar 20;34(9):945–52.
- Frías-Lasserre D, Villagra CA. The importance of ncRNAs as epigenetic mechanisms in phenotypic variation and organic evolution . *Front. Microbiol.* Frontiers Media S.A.; 2017.
- Fuchs G, Hollander D, Voichek Y, Ast G, Oren M. Cotranscriptional histone H2B monoubiquitylation is tightly coupled with RNA polymerase II elongation rate. *Genome Res.* . Cold Spring Harbor Laboratory Press; 2014 Oct 1;24(10):1572–83.
- Galehdar Z, Swan P, Fuerth B, Callaghan SM, Park DS, Cregan SP. Neuronal apoptosis induced by endoplasmic reticulum stress is regulated by ATF4-CHOP-mediated induction of the Bcl-2 homology 3-only member PUMA. *J. Neurosci.* . J Neurosci; 2010 Dec 15;30(50):16938–48.
- Gallego LD, Schneider M, Mittal C, Romanauska A, Gudino Carrillo RM, Schubert T, et al. Phase separation directs ubiquitination of gene-body nucleosomes. *Nature* . Nature Research; 2020 Mar 26;579(7800):592–7.
- Gallego LD, Steger MG, Polyansky AA, Schubert T, Zagrovic B, Zheng N, et al. Structural mechanism for the recognition and ubiquitination of a single nucleosome residue by Rad6-Bre1. *Proc. Natl. Acad. Sci. U. S. A.* . National Academy of Sciences; 2016 Sep 20;113(38):10553–8.
- Galluzzi L, Vitale I, Aaronson SA, Abrams JM, Adam D, Agostinis P, et al. Molecular mechanisms of cell death: Recommendations of the Nomenclature Committee on Cell Death 2018 . *Cell Death Differ.* Nature Publishing Group; 2018. p. 486–541.
- Gandalovičová A, Rosel D, Fernandes M, Veselý P, Heneberg P, Čermák V, et al. Migrastatics—Anti-metastatic and Anti-invasion Drugs: Promises and Challenges . *Trends in Cancer.* Cell Press; 2017. p. 391–406.
- Gao Y, Jones A, Fasching PA, Ruebner M, Beckmann MW, Widschwendter M, et al. The integrative epigenomic-transcriptomic landscape of ER positive breast cancer. *Clin. Epigenetics* . Springer Verlag; 2015 Dec 9;7(1).
- Gao Y, Lin F, Xu P, Nie J, Chen Z, Su J, et al. USP22 is a positive regulator of NFATc2 on promoting IL2 expression. *FEBS Lett.* FEBS Lett; 2014 Mar 18;588(6):878–83.
- Gao Z, Xu MS, Barnett TL, Xu CW. Resveratrol induces cellular senescence with attenuated mono-ubiquitination of histone H2B in glioma cells. *Biochem. Biophys. Res. Commun. Biochem Biophys Res Commun*; 2011 Apr 8;407(2):271–6.
- García-Oliver E, García-Molinero V, Rodríguez-Navarro S. mRNA export and gene expression: The SAGA-TREX-2 connection . *Biochim. Biophys. Acta - Gene Regul. Mech.* Biochim Biophys Acta; 2012. p. 555–65.
- Gardner RG, Nelson ZW, Gottschling DE. Ubp10/Dot4p Regulates the Persistence of Ubiquitinated Histone H2B: Distinct Roles in Telomeric Silencing and General Chromatin. *Mol. Cell. Biol.* American Society for Microbiology; 2005 Jul;25(14):6123–39.

- Garrido-Castro AC, Lin NU, Polyak K. Insights into molecular classifications of triple-negative breast cancer: Improving patient selection for treatment . *Cancer Discov.* American Association for Cancer Research Inc.; 2019. p. 176–98.
- Garrido Castro P, Van Roon EHJ, Pinhanços SS, Trentin L, Schneider P, Kerstjens M, et al. The HDAC inhibitor panobinostat (LBH589) exerts in vivo anti-leukaemic activity against MLL-rearranged acute lymphoblastic leukaemia and involves the RNF20/RNF40/WAC-H2B ubiquitination axis. *Leukemia* . Nature Publishing Group; 2018 Feb 1;32(2):323–31.
- Gates LA, Shi J, Rohira AD, Feng Q, Zhu B, Bedford MT, et al. Acetylation on histone H3 lysine 9 mediates a switch from transcription initiation to elongation. *J. Biol. Chem.* . American Society for Biochemistry and Molecular Biology Inc.; 2017 Sep 1;292(35):14456–72.
- Gennaro VJ, Stanek TJ, Peck AR, Sun Y, Wang F, Qie S, et al. Control of CCND1 ubiquitylation by the catalytic SAGA subunit USP22 is essential for cell cycle progression through G1 in cancer cells. *Proc. Natl. Acad. Sci. U. S. A.* . National Academy of Sciences; 2018 Oct 2;115(40):E9298–307.
- Glinsky G V., Berezovska O, Glinskii AB. Microarray analysis identifies a death-from-cancer signature predicting therapy failure in patients with multiple types of cancer. *J. Clin. Invest.* 2005 Jun;115(6):1503–21.
- Goel S, Wang Q, Watt AC, Tolaney SM, Dillon DA, Li W, et al. Overcoming Therapeutic Resistance in HER2-Positive Breast Cancers with CDK4/6 Inhibitors. *Cancer Cell.* Cell Press; 2016 Mar 14;29(3):255–69.
- Goldstein LJ, Zhao F, Wang M, Swaby RF, Sparano JA, Meropol NJ, et al. A Phase I/II study of suberoylanilide hydroxamic acid (SAHA) in combination with trastuzumab (Herceptin) in patients with advanced metastatic and/or local chest wall recurrent HER2-amplified breast cancer: a trial of the ECOG-ACRIN Cancer Research Group (E1104). *Breast Cancer Res. Treat.* . Springer New York LLC; 2017 Sep 1;165(2):375–82.
- Gomes NP, Bjerke G, Llorente B, Szostek SA, Emerson BM, Espinosa JM. Gene-specific requirement for P-TEFb activity and RNA polymerase II phosphorylation within the p53 transcriptional program. *Genes Dev.* . Genes Dev; 2006 Mar ;20(5):601–12.
- Gómez-Schiavon M, Buchler NE. Epigenetic switching as a strategy for quick adaptation while attenuating biochemical noise. *PLoS Comput. Biol.* Public Library of Science; 2019;15(10).
- Gong Z, Liu J, Xie X, Xu X, Wu P, Li H, et al. Identification of potential target genes of USP22 via ChiP-seq and RNA-seq analysis in HeLa cells. *Genet. Mol. Biol.* . Brazilian Journal of Genetics; 2018 Apr 1;41(2):488–95.
- Greber BJ, Nogales E. The Structures of Eukaryotic Transcription Pre-initiation Complexes and Their Functional Implications. *Subcell. Biochem.* Springer; 2019. p. 143–92.
- Guang MHZ, Kavanagh EL, Dunne LP, Dowling P, Zhang L, Lindsay S, et al. Targeting proteotoxic stress in cancer: A review of the role that protein quality control pathways play in oncogenesis . *Cancers (Basel).* MDPI AG; 2019.
- Gutierrez C, Schiff R. HER2: Biology, detection, and clinical implications. *Arch. Pathol. Lab. Med.* . Arch Pathol Lab Med; 2011 Jan;135(1):55–62.
- Hahn MA, Dickson KA, Jackson S, Clarkson A, Gill AJ, Marsh DJ. The tumor suppressor CDC73 interacts with the ring finger proteins RNF20 and RNF40 and is required for the maintenance of histone 2B monoubiquitination. *Hum. Mol. Genet.* 2012;

- Halazonetis TD, Gorgoulis VG, Bartek J. An oncogene-induced DNA damage model for cancer development . *Science* (80-.). *Science*; 2008. p. 1352–5.
- Halperin L, Jung J, Michalak M. The many functions of the endoplasmic reticulum chaperones and folding enzymes . *IUBMB Life*. Blackwell Publishing Ltd; 2014. p. 318–26.
- Han SJ, Guo QQ, Wang T, Wang YX, Zhang YX, Liu F, et al. Prognostic significance of interactions between er alpha and ER beta and lymph node status in breast cancer cases. *Asian Pacific J. Cancer Prev. . Asian Pacific Journal of Cancer Prevention*; 2013;14(10):6081–4.
- Hanahan D, Weinberg RA. Hallmarks of cancer: The next generation . *Cell*. *Cell*; 2011. p. 646–74.
- Harbeck N, Penault-Llorca F, Cortes J, Gnant M, Houssami N, Poortmans P, et al. Breast cancer. *Nat. Rev. Dis. Prim. Nature Publishing Group*; 2019 Dec 1;5(1):1–31.
- Harding HP, Zhang Y, Bertolotti A, Zeng H, Ron D. Perk is essential for translational regulation and cell survival during the unfolded protein response. *Mol. Cell . Cell Press*; 2000;5(5):897–904.
- Hayner JN, Shan J, Kilberg MS. Regulation of the ATF3 gene by a single promoter in response to amino acid availability and endoplasmic reticulum stress in human primary hepatocytes and hepatoma cells. *Biochim. Biophys. Acta - Gene Regul. Mech. Elsevier B.V.*; 2018 Feb 1;1861(2):72–9.
- Henry KW, Wyce A, Lo WS, Duggan LJ, Emre NCT, Kao CF, et al. Transcriptional activation via sequential histone H2B ubiquitylation and deubiquitylation, mediated by SAGA-associated Ubp8. *Genes Dev. . Genes Dev*; 2003 Nov 1;17(21):2648–63.
- Hillary RF, Fitzgerald U. A lifetime of stress: ATF6 in development and homeostasis . *J. Biomed. Sci. BioMed Central Ltd.*; 2018.
- Hodge RG, Ridley AJ. Regulating Rho GTPases and their regulators . *Nat. Rev. Mol. Cell Biol. Nature Publishing Group*; 2016. p. 496–510.
- Holt MT, David Y, Pollock S, Tang Z, Jeon J, Kim J, et al. Identification of a functional hotspot on ubiquitin required for stimulation of methyltransferase activity on chromatin. *Proc. Natl. Acad. Sci. U. S. A. . National Academy of Sciences*; 2015 Aug 18;112(33):10365–70.
- Holubekova V, Mendelova A, Jasek K, Mersakova S, Zubor P, Lasabova Z. Epigenetic regulation by DNA methylation and miRNA molecules in cancer . *Futur. Oncol. Future Medicine Ltd.*; 2017 p. 2217–22.
- Hong A, Lee JE, Chung KC. Ubiquitin-specific protease 22 (USP22) positively regulates RCAN1 protein levels through RCAN1 de-ubiquitination. *J. Cell. Physiol. . Wiley-Liss Inc.*; 2015 Jul 1;230(7):1651–60.
- Hooda J, Novak M, Salomon MP, Matsuba C, Ramos RI, MacDuffie E, et al. Early loss of histone H2B monoubiquitylation alters chromatin accessibility and activates key immune pathways that facilitate progression of ovarian cancer. *Cancer Res. American Association for Cancer Research Inc.*; 2019 Feb 15;79(4):760–72.
- Hsieh FK, Kulaeva OI, Patel SS, Dyer PN, Luger K, Reinberg D, et al. Histone chaperone FACT action during transcription through chromatin by RNA polymerase II. *Proc. Natl. Acad. Sci. U. S. A. . Proc Natl Acad Sci U S A*; 2013 May 7;110(19):7654–9.
- Hu R, Warri A, Jin L, Zwart A, Riggins RB, Fang H-B, et al. NF- κ B Signaling Is Required for XBP1 (Unspliced and Spliced)-Mediated Effects on Antiestrogen Responsiveness and Cell Fate Decisions in Breast Cancer. *Mol. Cell. Biol. . American Society for*

- Microbiology; 2015 Jan 15;35(2):379–90.
- Huang L, Hu C, Li H, Cao H, Wu X, Wang R, et al. MicroRNA-29c Increases the Chemosensitivity of Pancreatic Cancer Cells by Inhibiting USP22 Mediated Autophagy. *Cell. Physiol. Biochem.* . S. Karger AG; 2018 Jun 1;47(2):747–58.
 - Huang X, Zhang Q, Lou Y, Wang J, Zhao X, Wang L, et al. USP22 deubiquitinates CD274 to suppress anticancer immunity. *Cancer Immunol. Res. American Association for Cancer Research Inc.*; 2019;7(10):1580–90.
 - Hurvitz SA, Dirix L, Kocsis J, Bianchi G V., Lu J, Vinholes J, et al. Phase II randomized study of trastuzumab emtansine versus trastuzumab plus docetaxel in patients with human epidermal growth factor receptor 2-positive metastatic breast cancer. *J. Clin. Oncol.* . American Society of Clinical Oncology; 2013 Mar 1;31(9):1157–63.
 - Hwang WW, Venkatasubrahmanyam S, Ianculescu AG, Tong A, Boone C, Madhani HD. A conserved RING finger protein required for histone H2B monoubiquitination and cell size control. *Mol. Cell . Cell Press*; 2003 Jan 1;11(1):261–6.
 - In S, Kim YI, Lee JE, Kim J. RNF20/40-mediated eEF1B δ L monoubiquitylation stimulates transcription of heat shock-responsive genes. *Nucleic Acids Res. Oxford University Press*; 2019 Apr 1;47(6):2840–55.
 - Ishino Y, Hayashi Y, Naruse M, Tomita K, Sanbo M, Fuchigami T, et al. Bre1a, a histone H2B ubiquitin ligase, regulates the cell cycle and differentiation of neural precursor cells. *J. Neurosci. J Neurosci*; 2014;34(8):3067–78.
 - Izdebska M, Zielińska W, Grzanka D, Gagat M. The Role of Actin Dynamics and Actin-Binding Proteins Expression in Epithelial-to-Mesenchymal Transition and Its Association with Cancer Progression and Evaluation of Possible Therapeutic Targets . *Biomed Res. Int. Hindawi Limited*; 2018.
 - J L, X X, P W, J X. [Ubiquitin specific peptidase 22 regulates the transcription activity of mitogen-activated protein kinase kinase 6 gene]. *Zhong Nan Da Xue Xue Bao. Yi Xue Ban . Zhong Nan Da Xue Xue Bao Yi Xue Ban*; 2019;44(2).
 - Jaaskelainen T, Makkonen H, Visakorpi T, Kim J, Roeder RG, Palvimo JJ, et al. Histone H2B ubiquitin ligases RNF20 and RNF40 in androgen signaling and prostate cancer cell growth. *Mol. Cell. Endocrinol.* 2012 Mar 5;350(1):87–98.
 - Jeon MY, Min K jin, Woo SM, Seo SU, Choi YH, Kim SH, et al. Maritoclax enhances TRAIL-induced apoptosis via CHOP-mediated upregulation of DR5 and miR-708-mediated downregulation of cFLIP. *Molecules . MDPI AG*; 2018 Nov 20;23(11).
 - Jeon YG, Lee JH, Ji Y, Sohn JH, Lee D, Kim DW, et al. RNF20 functions as a transcriptional coactivator for PPAR γ by promoting ncor1 degradation in adipocytes. *Diabetes . American Diabetes Association Inc.*; 2020 Jan 1;69(1):20–34.
 - Jeusset LMP, McManus KJ. Ubiquitin specific peptidase 22 regulates histone H2B mono-ubiquitination and exhibits both oncogenic and tumor suppressor roles in cancer. *Cancers (Basel). MDPI AG*; 2017.
 - Ji AL, Li T, Zu G, Feng DC, Li Y, Wang GZ, et al. Ubiquitin-specific protease 22 enhances intestinal cell proliferation and tissue regeneration after intestinal ischemia reperfusion injury. *World J. Gastroenterol.* . Baishideng Publishing Group Co., Limited; 2019 Feb 21;25(7):824–36.
 - Jiang H-Y, Wek SA, McGrath BC, Lu D, Hai T, Harding HP, et al. Activating Transcription Factor 3 Is Integral to the Eukaryotic Initiation Factor 2 Kinase Stress Response. *Mol. Cell. Biol. American Society for Microbiology*; 2004 Feb 1;24(3):1365–77.
 - Jing YY, Cai FF, Zhang L, Han J, Yang L, Tang F, et al. Epigenetic regulation of the

Warburg effect by H2B monoubiquitination. *Cell Death Differ.* Springer Nature; 2020 May 1;27(5):1660–76.

- Jo HJ, Yang JW, Park JH, Choi ES, Lim CS, Lee S, et al. Endoplasmic reticulum stress increases DUSP5 expression via PERK-CHOP pathway, leading to hepatocyte death. *Int. J. Mol. Sci.* MDPI AG; 2019 Sep 1;20(18).
- Johnsen SA. The enigmatic role of H2Bub1 in cancer. *FEBS Lett.* Federation of European Biochemical Societies; 2012;586(11):1592–601.
- Johnston S, Pippen J, Pivot X, Lichinitser M, Sadeghi S, Dieras V, et al. Lapatinib combined with letrozole versus letrozole and placebo as first-line therapy for postmenopausal hormone receptor - Positive metastatic breast cancer. *J. Clin. Oncol.* . J Clin Oncol; 2009 Nov 20;27(33):5538–46.
- Kao KJ, Chang KM, Hsu HC, Huang AT. Correlation of microarray-based breast cancer molecular subtypes and clinical outcomes: Implications for treatment optimization. *BMC Cancer* . BMC Cancer; 2011 Apr 18;11.
- Kari V, Shchebet A, Neumann H, Johnsen SA. The H2B ubiquitin ligase RNF40 cooperates with SUPT16H to induce dynamic changes in chromatin structure during DNA double-strand break repair. *Cell Cycle.* Taylor and Francis Inc.; 2011 Oct 31;10(20):3495–504.
- Karpiuk O, Najafova Z, Kramer F, Hennion M, Galonska C, Konig A, et al. The Histone H2B Monoubiquitination Regulatory Pathway Is Required for Differentiation of Multipotent Stem Cells. *Mol. Cell.* 2012 Jun 8;46(5):705–13.
- Kaufman B, Mackey JR, Clemens MR, Bapsy PP, Vaid A, Wardley A, et al. Trastuzumab plus anastrozole versus anastrozole alone for the treatment of postmenopausal women with human epidermal growth factor receptor 2-positive, hormone receptor-positive metastatic breast cancer: Results from the randomized phase III TAnDEM study. *J. Clin. Oncol.* . J Clin Oncol; 2009 Nov 20;27(33):5529–37.
- Khan DH, Gonzalez C, Tailor N, Hamedani MK, Leygue E, Davie JR. Dynamic Histone Acetylation of H3K4me3 Nucleosome Regulates MCL1 Pre-mRNA Splicing. *J. Cell. Physiol.* . Wiley-Liss Inc.; 2016 Oct 1;231(10):2196–204.
- Kim D, Hong A, Park HI, Shin WH, Yoo L, Jeon SJ, et al. Deubiquitinating enzyme USP22 positively regulates c-Myc stability and tumorigenic activity in mammalian and breast cancer cells. *J. Cell. Physiol.* Wiley-Liss Inc.; 2017 Dec 1;232(12):3664–76.
- Kim J, Roeder RG. Direct Bre1-Paf1 complex interactions and RING finger-independent Bre1-Rad6 interactions mediate histone H2B ubiquitylation in yeast. *J. Biol. Chem.* . J Biol Chem; 2009 Jul 31;284(31):20582–92.
- Kim TH, Yang YM, Han CY, Koo JH, Oh H, Kim SS, et al. Gα12 ablation exacerbates liver steatosis and obesity by suppressing USP22/SIRT1-regulated mitochondrial respiration. *J. Clin. Invest.* . American Society for Clinical Investigation; 2018a Dec 3;128(12):5587–602.
- Kim TW, Lee SY, Kim M, Cheon C, Ko SG. Kaempferol induces autophagic cell death via IRE1-JNK-CHOP pathway and inhibition of G9a in gastric cancer cells. *Cell Death Dis.* . Nature Publishing Group; 2018b Sep 1;9(9). A
- Kirmizis A, Santos-Rosa H, Penkett CJ, Singer MA, Vermeulen M, Mann M, et al. Arginine methylation at histone H3R2 controls deposition of H3K4 trimethylation. *Nature* . Nature Publishing Group; 2007 Oct 18;449(7164):928–32.
- Kobayashi T, Iwamoto Y, Takashima K, Isomura A, Kosodo Y, Kawakami K, et al. Deubiquitinating enzymes regulate Hes1 stability and neuronal differentiation . *FEBS J.*

- Blackwell Publishing Ltd; 2015. p. 2475–87.
- Kolber MA, Hill P. Vincristine potentiates cytochalasin B-induced DNA fragmentation in vitro. *Cancer Chemother. Pharmacol.* . Springer-Verlag; 1992 Jul;30(4):286–90.
 - Kopp MC, Larburu N, Durairaj V, Adams CJ, Ali MMU. UPR proteins IRE1 and PERK switch BiP from chaperone to ER stress sensor. *Nat. Struct. Mol. Biol.* Springer US; 2019;26(11):1053–62.
 - Kornberg RD. Mediator and the mechanism of transcriptional activation . *Trends Biochem. Sci.* Trends Biochem Sci; 2005. p. 235–9.
 - Koroknai V, Szász I, Hernandez-Vargas H, Fernandez-Jimenez N, Cuenin C, Herceg Z, et al. DNA hypermethylation is associated with invasive phenotype of malignant melanoma. *Exp. Dermatol.* . Blackwell Publishing Ltd; 2020 Jan 1;29(1):39–50.
 - Kosinsky RL, Chua RL, Qui M, Saul D, Mehlich D, Ströbel P, et al. Loss of rnf40 decreases nf-kb activity in colorectal cancer cells and reduces colitis burden in mice. *J. Crohn's Colitis* . Oxford University Press; 2019a Mar 26;13(3):362–73.
 - Kosinsky RL, Helms M, Zerche M, Wohn L, Dyas A, Prokakis E, et al. USP22-dependent HSP90AB1 expression promotes resistance to HSP90 inhibition in mammary and colorectal cancer. *Cell Death Dis.* Springer Nature; 2019b Dec 1;10(12).
 - Kosinsky RL, Wegwitz F, Hellbach N, Dobbelstein M, Mansouri A, Vogel T, et al. Usp22 deficiency impairs intestinal epithelial lineage specification in vivo. 2015a;22(35).
 - Kosinsky RL, Wegwitz F, Hellbach N, Dobbelstein M, Mansouri A, Vogel T, et al. Usp22 deficiency impairs intestinal epithelial lineage specification in vivo. *Oncotarget* . Impact Journals LLC; 2015b;6(35):37906–18.
 - Kosinsky RL, Zerche M, Saul D, Wang X, Wohn L, Wegwitz F, et al. USP22 exerts tumor-suppressive functions in colorectal cancer by decreasing mTOR activity. *Cell Death Differ.* Springer Nature; 2020 Apr;27(4):1328–40.
 - Koutelou E, Wang L, Schibler AC, Chao HP, Kuang X, Lin K, et al. USP22 controls multiple signaling pathways that are essential for vasculature formation in the mouse placenta. *Dev.* . Company of Biologists Ltd; 2019 Feb 1;146(4).
 - Ku HC, Cheng CF. Master Regulator Activating Transcription Factor 3 (ATF3) in Metabolic Homeostasis and Cancer . *Front. Endocrinol. (Lausanne).* Frontiers Media S.A.; 2020.
 - Kümper S, Mardakheh FK, McCarthy A, Yeo M, Stamp GW, Paul A, et al. Rho-associated kinase (ROCK) function is essential for cell cycle progression, senescence and tumorigenesis. *Elife* . eLife Sciences Publications, Ltd; 2016 Jan 14;5.
 - Lahlou H, Sanguin-Gendreau V, Frame MC, Muller WJ. Focal adhesion kinase contributes to proliferative potential of ErbB2 mammary tumour cells but is dispensable for ErbB2 mammary tumour induction in vivo. *Breast Cancer Res.* . Breast Cancer Res; 2012 Feb 28;14(1).
 - Lai CY, Hsieh MC, Ho YC, Wang HH, Chou D, Wen YC, et al. Spinal RNF20-mediated histone H2B monoubiquitylation regulates mGluR5 transcription for neuropathic allodynia. *J. Neurosci.* Society for Neuroscience; 2018 Oct 24;38(43):9160–74.
 - Lam FC, Kong YW, Huang Q, Vu Han TL, Maffa AD, Kasper EM, et al. BRD4 prevents the accumulation of R-loops and protects against transcription–replication collision events and DNA damage. *Nat. Commun.* . Nature Research; 2020 Dec 1;11(1).
 - Lambert JM, Chari RVJ. Ado-trastuzumab emtansine (T-DM1): An antibody-drug conjugate (ADC) for HER2-positive breast cancer. *J. Med. Chem.* . American Chemical Society; 2014;57(16):6949–64.

- Lan X, Atanassov BS, Li W, Zhang Y, Florens L, Mohan RD, et al. USP44 Is an Integral Component of N-CoR that Contributes to Gene Repression by Deubiquitinating Histone H2B. *Cell Rep. Elsevier B.V.*; 2016 Nov 22;17(9):2382–93.
- Lane J, Martin TA, Watkins G, Mansel RE, Jiang WG. The expression and prognostic value of ROCK I and ROCK II and their role in human breast cancer. *Int. J. Oncol. . Spandidos Publications*; 2008 Sep 1;33(3):585–93.
- Lang G, Bonnet J, Umlauf D, Karmodiya K, Koffler J, Stierle M, et al. The Tightly Controlled Deubiquitination Activity of the Human SAGA Complex Differentially Modifies Distinct Gene Regulatory Elements. *Mol. Cell. Biol. American Society for Microbiology*; 2011 Sep;31(18):3734–44.
- Längst G, Manelyte L. Chromatin remodelers: From function to dysfunction . *Genes (Basel). MDPI AG*; 2015. p. 299–324.
- Laroche S, Amat R, Glover-Cutter K, Sansó M, Zhang C, Allen JJ, et al. Cyclin-dependent kinase control of the initiation-to-elongation switch of RNA polymerase II. *Nat. Struct. Mol. Biol. . Nat Struct Mol Biol*; 2012 Nov;19(11):1108–15.
- Lee E, Nichols P, Spicer D, Groshen S, Yu MC, Lee AS. GRP78 as a novel predictor of responsiveness to chemotherapy in breast cancer. *Cancer Res. . Cancer Res*; 2006 Aug 15;66(16):7849–53.
- Lee JH, Jeon YG, Lee K-H, Lee HW, Park J, Jang H, et al. RNF20 Suppresses Tumorigenesis by Inhibiting the SREBP1c-PTTG1 Axis in Kidney Cancer. *Mol. Cell. Biol.* 2017;
- Lee JH, Lee GY, Jang H, Choe SS, Koo SH, Kim JB. Ring finger protein20 regulates hepatic lipid metabolism through protein kinase A-dependent sterol regulatory element binding protein1c degradation. *Hepatology . John Wiley and Sons Inc.*; 2014;60(3):844–57.
- Lei Y, Wang S, Ren B, Wang J, Chen J, Lu J, et al. CHOP favors endoplasmic reticulum stress-induced apoptosis in hepatocellular carcinoma cells via inhibition of autophagy. *PLoS One . Public Library of Science*; 2017 Aug 1;12(8).
- Li C, Irrazabal T, So CC, Berru M, Du L, Lam E, et al. The H2B deubiquitinase Usp22 promotes antibody class switch recombination by facilitating non-homologous end joining. *Nat. Commun. . Nature Publishing Group*; 2018 Dec 1;9(1).
- Liang JX, Ning Z, Gao W, Ling J, Wang AM, Luo HF, et al. Ubiquitin-specific protease 22-induced autophagy is correlated with poor prognosis of pancreatic cancer. *Oncol. Rep. . Spandidos Publications*; 2014 Dec 1;32(6):2726–34.
- Liang Q, Xia W, Li W, Jiao J. RNF20 controls astrocytic differentiation through epigenetic regulation of STAT3 in the developing brain. *Cell Death Differ. Nature Publishing Group*; 2018 Feb 1;25(2):294–306.
- Liang X, Tao C, Pan J, Zhang L, Liu L, Zhao Y, et al. Rnf20 deficiency in adipocyte impairs adipose tissue development and thermogenesis. *Protein Cell . Higher Education Press*; 2020
- Lim CC, Xu JC, Chen TY, Xu JX, Chen WF, Hu JW, et al. Ubiquitin-specific peptide 22 acts as an oncogene in gastric cancer in a son of sevenless 1-dependent manner. *Cancer Cell Int. . BioMed Central Ltd.*; 2020 Feb 10;20(1).
- Lin NU. Better treatments needed for breast cancer brain metastases . *Lancet Oncol. Lancet Publishing Group*; 2015. p. 1583–4.
- Lin Y, Zheng Y. Approaches of targeting Rho GTPases in cancer drug discovery . *Expert Opin. Drug Discov. Taylor and Francis Ltd*; 2015. p. 991–1010.

- Lin Z, Tan C, Qiu Q, Kong S, Yang H, Zhao F, et al. Ubiquitin-specific protease 22 is a deubiquitinase of CCNB1. *Cell Discov.* . Nature Publishing Groups; 2015 Oct 13;1.
- Ling S, Li J, Shan Q, Dai H, Lu D, Wen X, et al. USP22 mediates the multidrug resistance of hepatocellular carcinoma via the SIRT1/AKT/MRP1 signaling pathway. *Mol. Oncol.* 2017;11(6):682–95.
- Liu S, Goldstein RH, Scepanisky EM, Rosenblatt M. Inhibition of Rho-associated kinase signaling prevents breast cancer metastasis to human bone. *Cancer Res.* . Cancer Res; 2009 Nov 15;69(22):8742–51.
- Lo HW, Hsu SC, Hung MC. EGFR signaling pathway in breast cancers: From traditional signal transduction to direct nuclear translocalization. *Breast Cancer Res. Treat.* 2006. p. 211–8.
- Lomakin AJ, Lee KC, Han SJ, Bui DA, Davidson M, Mogilner A, et al. Competition for actin between two distinct F-actin networks defines a bistable switch for cell polarization. *Nat. Cell Biol.* . Nature Publishing Group; 2015 Nov 1;17(11):1435–45.
- Lu Y, Chan YT, Tan HY, Li S, Wang N, Feng Y. Epigenetic regulation in human cancer: The potential role of epi-drug in cancer therapy . *Mol. Cancer.* BioMed Central Ltd.; 2020.
- Luo S, Baumeister P, Yang S, Abcouwer SF, Lee AS. Induction of Grp78/BiP by translational block: Activation of the Grp78 promoter by ATF4 through an upstream ATF/CRE site independent of the endoplasmic reticulum stress elements. *J. Biol. Chem.* . J Biol Chem; 2003 Sep 26;278(39):37375–85.
- Luo W, Johnson AW, Bentley DL. The role of Rat1 in coupling mRNA 3'-end processing to transcription termination: Implications for a unified allosteric-torpedo model. *Genes Dev.* . Genes Dev; 2006 Apr 15;20(8):954–65.
- Lyu X, Zhang M, Li G, Cai Y, Li G, Qiao Q. Interleukin-6 production mediated by the IRE1-XBP1 pathway confers radioresistance in human papillomavirus-negative oropharyngeal carcinoma. *Cancer Sci.* Blackwell Publishing Ltd; 2019;110(8):2471–84.
- Ma B, Zhang H, Wang Y, Zhao A, Zhu Z, Bao X, et al. Corosolic acid, a natural triterpenoid, induces ER stress-dependent apoptosis in human castration resistant prostate cancer cells via activation of IRE-1/JNK, PERK/CHOP and TRIB3. *J. Exp. Clin. Cancer Res.* . BioMed Central Ltd.; 2018 Sep 3;37(1).
- Ma Y, Fu HL, Wang Z, Huang H, Ni J, Song J, et al. USP22 maintains gastric cancer stem cell stemness and promotes gastric cancer progression by stabilizing BMI1 protein. *Oncotarget* . Impact Journals LLC; 2017;8(20):33329–42.
- Mak P, Chang C, Pursell B, Mercurio AM. Estrogen receptor β sustains epithelial differentiation by regulating prolyl hydroxylase 2 transcription. *Proc. Natl. Acad. Sci. U. S. A.* . Proc Natl Acad Sci U S A; 2013 Mar 19;110(12):4708–13.
- Malladi S, Macalinao DG, Jin X, He L, Basnet H, Zou Y, et al. Metastatic Latency and Immune Evasion through Autocrine Inhibition of WNT. *Cell.* 2016 Mar 24;165(1):45–60.
- Marciniak SJ, Yun CY, Oyadomari S, Novoa I, Zhang Y, Jungreis R, et al. CHOP induces death by promoting protein synthesis and oxidation in the stressed endoplasmic reticulum. *Genes Dev.* Genes Dev; 2004 Dec 15;18(24):3066–77.
- Marfella CGA, Imbalzano AN. The Chd family of chromatin remodelers. *Mutat. Res. - Fundam. Mol. Mech. Mutagen.* . Mutat Res; 2007 May 1;618(1–2):30–40.
- Marsh DJ, Dickson KA. Writing histone monoubiquitination in human malignancy—The role of RING finger E3 ubiquitin ligases . *Genes (Basel).* MDPI AG; 2019
- Marsh DJ, Ma Y, Dickson K-A. Histone Monoubiquitination in Chromatin Remodelling: Focus on the Histone H2B Interactome and Cancer. *Cancers (Basel).* Multidisciplinary

- Digital Publishing Institute; 2020 Nov 20;12(11):3462.
- Maruyama T, Farina A, Dey A, Cheong J, Bermudez VP, Tamura T, et al. A Mammalian Bromodomain Protein, Brd4, Interacts with Replication Factor C and Inhibits Progression to S Phase. *Mol. Cell. Biol.* American Society for Microbiology; 2002 Sep 15;22(18):6509–20.
 - Masood S. Breast cancer subtypes: Morphologic and biologic characterization. *Women's Heal. . Future Medicine Ltd.*; 2016 Jan 1;12(1):103–19.
 - Matsubara M, Bissell MJ. Inhibitors of Rho kinase (ROCK) signaling revert the malignant phenotype of breast cancer cells in 3D context. *Oncotarget . Impact Journals LLC*; 2016 May 31;7(22):31602–22.
 - Maupin-Furlow J. Proteasomes and protein conjugation across domains of life . *Nat. Rev. Microbiol.* Nat Rev Microbiol; 2012. p. 100–11.
 - Mbonye UR, Gokulrangan G, Datt M, Dobrowolski C, Cooper M, Chance MR, et al. Phosphorylation of CDK9 at Ser175 Enhances HIV Transcription and Is a Marker of Activated P-TEFb in CD4+ T Lymphocytes. *PLoS Pathog. . PLoS Pathog*; 2013 May;9(5).
 - McCann JJ, Vasilevskaya IA, Neupane NP, Shafi AA, McNair C, Dylgjeri E, et al. USP22 functions as an oncogenic driver in prostate cancer by regulating cell proliferation and DNA repair. *Cancer Res.* American Association for Cancer Research Inc.; 2020 Feb 1;80(3):430–43.
 - McConkey DJ. The integrated stress response and proteotoxicity in cancer therapy. *Biochem. Biophys. Res. Commun.* Elsevier B.V.; 2017. p. 450–3.
 - McLean GW, Carragher NO, Avizienyte E, Evans J, Brunton VG, Frame MC. The role of focal-adhesion kinase in cancer - A new therapeutic opportunity . *Nat. Rev. Cancer.* Nat Rev Cancer; 2005. p. 505–15.
 - Melling N, Grimm N, Simon R, Stahl P, Bokemeyer C, Terracciano L, et al. Loss of H2Bub1 Expression is Linked to Poor Prognosis in Nodal Negative Colorectal Cancers. *Pathol. Oncol. Res. . Springer Netherlands*; 2016 Jan 1;22(1):95–102.
 - Melo-Cardenas J, Xu Y, Wei J, Tan C, Kong S, Gao B, et al. USP22 deficiency leads to myeloid leukemia upon oncogenic Kras activation through a PU.1-dependent mechanism. *Blood . American Society of Hematology*; 2018 Jul 26;132(4):423–34.
 - Melo-Cardenas J, Zhang Y, Zhang DD, Fang D. Ubiquitin-specific peptidase 22 functions and its involvement in disease. *Oncotarget . Impact Journals LLC*; 2016;7(28):44848–56.
 - Meric-Bernstam F, Johnson AM, Ileana Dumbrava EE, Raghav K, Balaji K, Bhatt M, et al. Advances in HER2-targeted therapy: Novel agents and opportunities beyond breast and gastric cancer . *Clin. Cancer Res.* American Association for Cancer Research Inc.; 2019. p. 2033–41.
 - Mevissen TET, Komander D. Mechanisms of deubiquitinase specificity and regulation . *Annu. Rev. Biochem.* Annual Reviews Inc.; 2017. p. 159–92.
 - Miao RY, Drabsch Y, Cross RS, Cheasley D, Carpinteri S, Pereira L, et al. MYB is essential for mammary tumorigenesis. *Cancer Res. . Cancer Res*; 2011 Nov 15;71(22):7029–37.
 - Mielnicki LM, Ying AM, Head KL, Asch HL, Asch BB. Epigenetic regulation of gelsolin expression in human breast cancer cells. *Exp. Cell Res. . Academic Press Inc.*; 1999 May 25;249(1):161–76.
 - Minsky N, Shema E, Field Y, Schuster M, Segal E, Oren M. Monoubiquitinated H2B is

- associated with the transcribed region of highly expressed genes in human cells. *Nat. Cell Biol.* 2008a Apr 16;10(4):483–8.
- Minsky N, Shema E, Field Y, Schuster M, Segal E, Oren M. Monoubiquitinated H2B is associated with the transcribed region of highly expressed genes in human cells. *Nat. Cell Biol.* . *Nat Cell Biol*; 2008b;10(4):483–8.
 - Minuti G, Cappuzzo F, Duchnowska R, Jassem J, Fabi A, O'Brien T, et al. Increased MET and HGF gene copy numbers are associated with trastuzumab failure in HER2-positive metastatic breast cancer. *Br. J. Cancer* . *Br J Cancer*; 2012 Aug 21;107(5):793–9.
 - Miranda Furtado CL, Dos Santos Luciano MC, Silva Santos R Da, Furtado GP, Moraes MO, Pessoa C. *Epidrugs: targeting epigenetic marks in cancer treatment* . Epigenetics. Taylor and Francis Inc.; 2019. p. 1164–76.
 - Moon KJ, Mochizuki K, Zhou M, Jeong HS, Brady JN, Ozato K. The bromodomain protein Brd4 is a positive regulatory component of P-TEFb and stimulates RNA polymerase II-dependent transcription. *Mol. Cell* . *Mol Cell*; 2005 Aug 19;19(4):523–34.
 - Müller J, Cacace AM, Lyons WE, McGill CB, Morrison DK. Identification of B-KSR1, a Novel Brain-Specific Isoform of KSR1 That Functions in Neuronal Signaling. *Mol. Cell. Biol.* American Society for Microbiology; 2000 Aug 1;20(15):5529–39.
 - Nagarajan S, Hossain T, Alawi M, Najafova Z, Indenbirken D, Bedi U, et al. Bromodomain Protein BRD4 Is Required for Estrogen Receptor-Dependent Enhancer Activation and Gene Transcription. *Cell Rep.* Elsevier; 2014 Jul 24;8(2):460–9.
 - Nagata Y, Lan KH, Zhou X, Tan M, Esteva FJ, Sahin AA, et al. PTEN activation contributes to tumor inhibition by trastuzumab, and loss of PTEN predicts trastuzumab resistance in patients. *Cancer Cell* . *Cancer Cell*; 2004 Aug;6(2):117–27.
 - Nahta R, Yuan LXH, Zhang B, Kobayashi R, Esteva FJ. Insulin-like growth factor-I receptor/human epidermal growth factor receptor 2 heterodimerization contributes to trastuzumab resistance of breast cancer cells. *Cancer Res.* . *Cancer Res*; 2005 Dec 1;65(23):11118–28.
 - Najafova Z, Liu P, Wegwitz F, Ahmad M, Tamon L, Kosinsky RL, et al. RNF40 exerts stage-dependent functions in differentiating osteoblasts and is essential for bone cell crosstalk. *Cell Death Differ.* Springer Nature; 2020;
 - Nakanishi S, Jung SL, Gardner KE, Gardner JM, Takahashi YH, Chandrasekharan MB, et al. Histone H2BK123 monoubiquitination is the critical determinant for H3K4 and H3K79 trimethylation by COMPASS and Dot1. *J. Cell Biol.* *J Cell Biol*; 2009 Aug 10;186(3):371–7.
 - Nardi IK, Stark JM, Larsen A, Salgia R, Raz DJ. USP22 interacts with PALB2 and promotes chemotherapy resistance via homologous recombination of DNA double-strand breaks. *Mol. Cancer Res.* . American Association for Cancer Research Inc.; 2020;18(3):424–35.
 - Nelson MH, Dolder CR. Lapatinib: a novel dual tyrosine kinase inhibitor with activity in solid tumors. *Ann. Pharmacother.* 2006 Feb;40(2):261–9.
 - Nersesian S, Williams R, Newsted D, Shah K, Young S, Evans PA, et al. Effects of Modulating Actin Dynamics on HER2 Cancer Cell Motility and Metastasis. *Sci. Rep.* 2018 Nov 22;8(1):17243.
 - Nimnual AS, Taylor LJ, Bar-Sagi D. Redox-dependent downregulation of Rho by Rac. *Nat. Cell Biol.* . *Nat Cell Biol*; 2003 Mar 1;5(3):236–41.
 - Ohtani K, Dimmeler S. Epigenetic regulation of cardiovascular differentiation. *Cardiovasc. Res.* . *Cardiovasc Res*; 2011 Jun 1;90(3):404–12.

- Oza J, Ganguly B, Kulkarni A, Ginja V, Yao M, Ganesan S. A novel role of chromodomain protein CBX8 in DNA damage response. *J. Biol. Chem. American Society for Biochemistry and Molecular Biology Inc.*; 2016 Oct 28;291(44):22881–93.
- Padilla-Rodriguez M, Parker SS, Adams DG, Westerling T, Puleo JI, Watson AW, et al. The actin cytoskeletal architecture of estrogen receptor positive breast cancer cells suppresses invasion. *Nat. Commun. . Nature Publishing Group*; 2018 Dec 1;9(1).
- Pakos-Zebrucka K, Koryga I, Mnich K, Lujic M, Samali A, Gorman AM. The integrated stress response. *EMBO Rep. EMBO*; 2016 Oct;17(10):1374–95.
- Palomer S, Diaz-Lagares Á, Viñas G, Setien F, Ferreira HJ, Oliveras G, et al. Epigenetic silencing of TGFBI confers resistance to trastuzumab in human breast cancer. *Breast Cancer Res. . BioMed Central Ltd.*; 2019 Jul 5;21(1).
- Pan Y, An N, Deng X, Zhang Q, Du X. RNF220 promotes the proliferation of leukaemic cells and reduces the degradation of the Cyclin D1 protein through USP22. *Blood Cells, Mol. Dis. . Academic Press Inc.*; 2021 Feb 1;86.
- Pasapera AM, Schneider IC, Rericha E, Schlaepfer DD, Waterman CM. Myosin II activity regulates vinculin recruitment to focal adhesions through FAK-mediated paxillin phosphorylation. *J. Cell Biol. J Cell Biol*; 2010 Mar 22;188(6):877–90.
- Patel RA, Forinash KD, Pireddu R, Sun Y, Sun N, Martin MP, et al. RKI-1447 is a potent inhibitor of the Rho-associated ROCK kinases with anti-invasive and antitumor activities in breast cancer. *Cancer Res.* 2012 Oct 1;72(19):5025–34.
- Pernas S, Tolaney SM. HER2-positive breast cancer: new therapeutic frontiers and overcoming resistance . *Ther. Adv. Med. Oncol. SAGE Publications Inc.*; 2019.
- Perou CM, Sørlie T, Eisen MB, van de Rijn M, Jeffrey SS, Rees C a, et al. Molecular portraits of human breast tumours. *Nature.* 2000;406(6797):747–52.
- Pinto AC, Ades F, de Azambuja E, Piccart-Gebhart M. Trastuzumab for patients with HER2 positive breast cancer: Delivery, duration and combination therapies. *Breast . Churchill Livingstone*; 2013 Aug 1;22(S2).
- Pirngruber J, Shchebet A, Schreiber L, Shema E, Minsky N, Chapman RD, et al. CDK9 directs H2B monoubiquitination and controls replication-dependent histone mRNA 3'-end processing. *EMBO Rep.* 2009 Aug 3;10(8):894–900.
- Pollock NI, Grandis JR. HER2 as a therapeutic target in head and neck squamous cell carcinoma . *Clin. Cancer Res. American Association for Cancer Research Inc.*; 2015. p. 526–33.
- Polyak K. Breast cancer: Origins and evolution . *J. Clin. Invest. American Society for Clinical Investigation*; 2007. p. 3155–63.
- Pontrello CG, Ethell IM. Accelerators, Brakes, and Gears of Actin Dynamics in Dendritic Spines. *Open Neurosci. J. . Bentham Science Publishers Ltd.*; 2009 Dec 1;3(2):67–86.
- Prenzel T, Begus-Nahrmann Y, Kramer F, Hennion M, Hsu C, Gorsler T, et al. Estrogen-dependent gene transcription in human breast cancer cells relies upon proteasome-dependent monoubiquitination of histone H2B. *Cancer Res.* 2011;71(17):5739–53.
- Prudnikova TY, Rawat SJ, Chernoff J. Molecular pathways: Targeting the kinase effectors of RHO-family GTPases. *Clin. Cancer Res.* 2015;
- Puthalakath H, O'Reilly LA, Gunn P, Lee L, Kelly PN, Huntington ND, et al. ER Stress Triggers Apoptosis by Activating BH3-Only Protein Bim. *Cell . Cell*; 2007 Jun 29;129(7):1337–49.
- Puthalakath H, Villunger A, O'Reilly LA, Beaumont JG, Coultas L, Cheney RE, et al. Bmf:

A proapoptotic BH3-only protein regulated by interaction with the myosin V actin motor complex, activated by anoikis. *Science* (80-). . *Science*; 2001 Sep 7;293(5536):1829–32.

- Qiu GZ, Mao XY, Ma Y, Gao XC, Wang Z, Jin MZ, et al. Ubiquitin-specific protease 22 acts as an oncoprotein to maintain glioma malignancy through deubiquitinating B cell-specific Moloney murine leukemia virus integration site 1 for stabilization. *Cancer Sci.* . Blackwell Publishing Ltd; 2018 Jul 1;109(7):2199–210.
- Ramachandran S, Haddad D, Li C, Le MX, Ling AK, So CC, et al. The SAGA Deubiquitination Module Promotes DNA Repair and Class Switch Recombination through ATM and DNAPK-Mediated γ H2AX Formation. *Cell Rep.* Elsevier B.V.; 2016 May 17;15(7):1554–65.
- Ranganathan AC, Ojha S, Kourtidis A, Conklin DS, Aguirre-Ghiso JA. Dual function of pancreatic endoplasmic reticulum kinase in tumor cell growth arrest and survival. *Cancer Res.* . *Cancer Res*; 2008 May 1;68(9):3260–8.
- Rani A, Stebbing J, Giamas G, Murphy J. Endocrine resistance in hormone receptor positive breast cancer—from mechanism to therapy . *Front. Endocrinol. (Lausanne).* Frontiers Media S.A.; 2019. p. 245.
- Reavis HD, Drapkin R. The tubal epigenome – An emerging target for ovarian cancer . *Pharmacol. Ther.* Elsevier Inc.; 2020.
- Rennhack JP, To B, Swiatnicki M, Dulak C, Ogradzinski MP, Zhang Y, et al. Integrated analyses of murine breast cancer models reveal critical parallels with human disease. *Nat. Commun.* . Nature Publishing Group; 2019 Dec 1;10(1).
- Robson A, Makova SZ, Barish S, Zaidi S, Mehta S, Drozd J, et al. Histone H2B monoubiquitination regulates heart development via epigenetic control of cilia motility. *Proc. Natl. Acad. Sci. U. S. A.* . National Academy of Sciences; 2019;116(28):14049–54.
- Robzyk K, Recht J, Osley MA. Rad6-dependent ubiquitination of histone H2B in yeast. *Science* (80-). *Science*; 2000 Jan 21;287(5452):501–4.
- Rohini M, Haritha Menon A, Selvamurugan N. Role of activating transcription factor 3 and its interacting proteins under physiological and pathological conditions . *Int. J. Biol. Macromol.* Elsevier B.V.; 2018. p. 310–7.
- Rubin; H. Etymology of Epigenetics. *Science* (80-). American Association for the Advancement of Science (AAAS); 2001 Dec 21;294(5551):2477c – 2478.
- Rye IH, Trinh A, Sætersdal AB, Nebdal D, Lingjærde OC, Almendro V, et al. Intratumor heterogeneity defines treatment-resistant HER2+ breast tumors. *Mol. Oncol.* . John Wiley and Sons Ltd.; 2018 Nov 1;12(11):1838–55.
- Salaroglio IC, Panada E, Moiso E, Buondonno I, Provero P, Rubinstein M, et al. PERK induces resistance to cell death elicited by endoplasmic reticulum stress and chemotherapy. *Mol. Cancer* . BioMed Central Ltd.; 2017 May 12;16(1).
- Al Saleh S, Al Mulla F, Luqmani YA. Estrogen receptor silencing induces epithelial to mesenchymal transition in human breast cancer cells. *PLoS One* . *PLoS One*; 2011;6(6).
- Sanchez R, Zhou MM. The role of human bromodomains in chromatin biology and gene transcription . *Curr. Opin. Drug Discov. Dev.* NIH Public Access; 2009. p. 659–65.
- Sander EE, Ten Klooster JP, Van Delft S, Van Der Kammen RA, Collard JG. Rac downregulates Rho activity: Reciprocal balance between both GTPases determines cellular morphology and migratory behavior. *J. Cell Biol.* . *J Cell Biol*; 1999 Nov 29;147(5):1009–21.
- Sansó M, Lee KM, Viladevall L, Jacques PÉ, Pagé V, Nagy S, et al. A Positive Feedback

- Loop Links Opposing Functions of P-TEFb/Cdk9 and Histone H2B Ubiquitylation to Regulate Transcript Elongation in Fission Yeast. *PLoS Genet.* . *PLoS Genet*; 2012 Aug;8(8).
- Schewe DM, Aguirre-Ghiso JA. ATF6 α -Rheb-mTOR signaling promotes survival of dormant tumor cells in vivo. *Proc. Natl. Acad. Sci. U. S. A.* . *Proc Natl Acad Sci U S A*; 2008 Jul 29;105(30):10519–24.
 - Schneeweiss A, Chia S, Hickish T, Harvey V, Eniu A, Hegg R, et al. Pertuzumab plus trastuzumab in combination with standard neoadjuvant anthracycline-containing and anthracycline-free chemotherapy regimens in patients with HER2-positive early breast cancer: A randomized phase II cardiac safety study (TRYPHAENA). *Ann. Oncol.* . *Ann Oncol*; 2013 Sep;24(9):2278–84.
 - Schneider D, Chua RL, Molitor N, Feda H, Maria RE, Prokakis E, et al. The E3 ubiquitin ligase RNF40 suppresses apoptosis in colorectal cancer cells. *Clin. Epigenetics.* 2019 Jul 2;11(1):98.
 - Schulz R, Streller F, Scheel AH, Rüschoff J, Reinert M-C, Dobbelstein M, et al. HER2/ErbB2 activates HSF1 and thereby controls HSP90 clients including MIF in HER2-overexpressing breast cancer. *Cell Death Dis.* 2014a;5:e980.
 - Schulz R, Streller F, Scheel AH, Rüschoff J, Reinert MC, Dobbelstein M, et al. HER2/ErbB2 activates HSF1 and thereby controls HSP90 clients including MIF in HER2-overexpressing breast cancer. *Cell Death Dis.* . *Cell Death Dis*; 2014b Jan;5(1).
 - Segala G, Bennesch MA, Pandey DP, Hulo N, Picard D. Monoubiquitination of Histone H2B Blocks Eviction of Histone Variant H2A.Z from Inducible Enhancers. *Mol. Cell . Cell Press*; 2016 Oct 20;64(2):334–46.
 - Sen R, Lahudkar S, Durairaj G, Bhaumik SR. Functional analysis of Bre1p, an E3 ligase for histone H2B ubiquitylation, in regulation of RNA polymerase II association with active genes and transcription in vivo. *J. Biol. Chem.* . *J Biol Chem*; 2013 Apr 5;288(14):9619–33.
 - Sequeira SJ, Ranganathan AC, Adam AP, Iglesias B V., Farias EF, Aguirre-Ghiso JA. Inhibition of proliferation by PERK regulates mammary acinar morphogenesis and tumor formation. *PLoS One* . *PLoS One*; 2007 Jul 18;2(7).
 - Serra V, Scaltriti M, Prudkin L, Eichhorn PJ, Ibrahim YH, Chandralapaty S, et al. PI3K inhibition results in enhanced HER signaling and acquired ERK dependency in HER2-overexpressing breast cancer. *Oncogene* . 2011;30(22):2547–57.
 - Sethi G, Shanmugam MK, Arfuso F, Kumar AP. Role of RNF20 in cancer development and progression – a comprehensive review . *Biosci. Rep. Portland Press Ltd*; 2018.
 - Shackleton M, Vaillant F, Simpson KJ, Stingl J, Smyth GK, Asselin-Labat ML, et al. Generation of a functional mammary gland from a single stem cell. *Nature* . 2006;439(7072):84–8.
 - Shao J, Zhang H, Wang Z. Coronin 1c and F-actin promote metastasis of breast cancer. *Med. Sci. Monit.* . *International Scientific Information, Inc.*; 2018 Aug 28;24:5980–7.
 - Shao W, Ding Z, Zheng ZZ, Shen JJ, Shen YX, Pu J, et al. Prp5-Spt8/Spt3 interaction mediates a reciprocal coupling between splicing and transcription. *Nucleic Acids Res.* . *NLM (Medline)*; 2020 Jun 19;48(11):5799–813.
 - Sharma K, Vu TT, Cook W, Naseri M, Zhan K, Nakajima W, et al. p53-independent Noxa induction by cisplatin is regulated by ATF3/ATF4 in head and neck squamous cell carcinoma cells. *Mol. Oncol. John Wiley and Sons Ltd.*; 2018 Jun 1;12(6):788–98.
 - Shchebet A, Karpiuk O, Kremmer E, Eick D, Johnsen SA. Phosphorylation by cyclin-

- dependent kinase-9 controls ubiquitin-conjugating enzyme-2A function. *Cell Cycle*. 2012;11(11):2122–7.
- Shema E, Kim J, Roeder RG, Oren M. RNF20 Inhibits TFIIIS-Facilitated Transcriptional Elongation to Suppress Pro-oncogenic Gene Expression. *Mol. Cell*. Mol Cell; 2011 May 20;42(4):477–88.
 - Shen H, Laird PW. Interplay between the cancer genome and epigenome . *Cell*. Cell; 2013 p. 38–55.
 - Shi JX, Wang QJ, Li H, Huang Q. Silencing of USP22 suppresses high glucose-induced apoptosis, ROS production and inflammation in podocytes. *Mol. Biosyst.* . Royal Society of Chemistry; 2016;12(5):1445–56.
 - Shilatifard A. Chromatin modifications by methylation and ubiquitination: Implications in the regulation of gene expression . *Annu. Rev. Biochem.* Annu Rev Biochem; 2006. p. 243–69.
 - Shilatifard A. The COMPASS Family of Histone H3K4 Methylases: Mechanisms of Regulation in Development and Disease Pathogenesis. *Annu. Rev. Biochem.* 2012;
 - Shuda M, Kondoh N, Imazeki N, Tanaka K, Okada T, Mori K, et al. Activation of the ATF6, XBP1 and grp78 genes in human hepatocellular carcinoma: A possible involvement of the ER stress pathway in hepatocarcinogenesis. *J. Hepatol.* Elsevier; 2003 May 1;38(5):605–14.
 - Simó-Riudalbas L, Esteller M. Targeting the histone orthography of cancer: Drugs for writers, erasers and readers . *Br. J. Pharmacol.* John Wiley and Sons Inc.; 2015. p. 2716–32.
 - Sims AH, Howell A, Howell SJ, Clarke RB. Origins of breast cancer subtypes and therapeutic implications . *Nat. Clin. Pract. Oncol.* Nat Clin Pract Oncol; 2007. p. 516–25.
 - Singh N, Joshi R, Komurov K. HER2-mTOR signaling-driven breast cancer cells require ER-associated degradation to survive. *Sci. Signal.* . American Association for the Advancement of Science; 2015 May 26;8(378).
 - Skinner MK. Role of epigenetics in developmental biology and transgenerational inheritance . *Birth Defects Res. Part C - Embryo Today Rev.* NIH Public Access; 2011. p. 51–5.
 - Slamon DJ, Leyland-Jones B, Shak S, Fuchs H, Paton V, Bajamonde A, et al. Use of Chemotherapy plus a Monoclonal Antibody against HER2 for Metastatic Breast Cancer That Overexpresses HER2. *N. Engl. J. Med.* . New England Journal of Medicine (NEJM/MMS); 2001 Mar 15;344(11):783–92.
 - Song YH, Ahn SH. A bre1-associated protein, large 1 (Lge1), promotes h2b ubiquitylation during the early stages of transcription elongation. *J. Biol. Chem.* J Biol Chem; 2010 Jan 22;285(4):2361–7.
 - Spector NL, Blackwell KL. Understanding the mechanisms behind trastuzumab therapy for human epidermal growth factor receptor 2-positive breast cancer . *J. Clin. Oncol.* J Clin Oncol; 2009. p. 5838–47.
 - Stehn JR, Haass NK, Bonello T, Desouza M, Kottyan G, Treutlein H, et al. A novel class of anticancer compounds targets the actin cytoskeleton in tumor cells. *Cancer Res.* . Cancer Res; 2013 Aug 15;73(16):5169–82.
 - Suarez C, Kovar DR. Internetwork competition for monomers governs actin cytoskeleton organization . *Nat. Rev. Mol. Cell Biol.* Nature Publishing Group; 2016. p. 799–810.
 - Sun Z-WW, Allis CD. Ubiquitination of histone H2B regulates H3 methylation and gene silencing in yeast. *Nature*. 2002 Jul 23;418(6893):104–8.

- Sussman RT, Stanek TJ, Estes P, Gearhart JD, Knudsen KE, McMahon SB. The epigenetic modifier ubiquitin-specific protease 22 (USP22) regulates embryonic stem cell differentiation via transcriptional repression of sex-determining region Y-box 2 (SOX2). *J. Biol. Chem.* . *J Biol Chem*; 2013 Aug 16;288(33):24234–46.
- Swygart SG, Peterson CL. Chromatin dynamics: Interplay between remodeling enzymes and histone modifications . *Biochim. Biophys. Acta - Gene Regul. Mech.* Elsevier; 2014. p. 728–36.
- Tam AB, Koong AC, Niwa M. Ire1 has distinct catalytic mechanisms for XBP1/HAC1 splicing and RIDD. *Cell Rep.* . Elsevier B.V.; 2014;9(3):850–8.
- Taneja P, Frazier DP, Kendig RD, Maglic D, Sugiyama T, Kai F, et al. MMTV mouse models and the diagnostic values of MMTV-like sequences in human breast cancer. *Expert Rev. Mol. Diagn.* 2009.
- Tarcic O, Granit RZ, Pateras IS, Masury H, Maly B, Zwang Y, et al. RNF20 Links Histone H2B Ubiquitylation with Inflammation and Inflammation-Associated Cancer. *Cell Rep.* 2016 Feb 16;24(6):694–704.
- Tarcic O, Granit RZ, Pateras IS, Masury H, Maly B, Zwang Y, et al. RNF20 and histone H2B ubiquitylation exert opposing effects in Basal-Like versus luminal breast cancer. *Cell Death Differ.* 2017 Apr 3;24(4):694–704.
- Tavares S, Vieira AF, Taubenberger AV, Araújo M, Martins NP, Brás-Pereira C, et al. Actin stress fiber organization promotes cell stiffening and proliferation of pre-invasive breast cancer cells. *Nat. Commun.* 2017 Aug 16;8(1):15237.
- Tawab Osman N, Khalaf M, Ibraheem S. Assessment of CIP2A and ROCK-I expression and their prognostic value in breast cancer. *Pol. J. Pathol. NLM (Medline)*; 2020;71(2):87–98.
- Teves SS, Weber CM, Henikoff S. Transcribing through the nucleosome . *Trends Biochem. Sci.* Elsevier Ltd; 2014. p. 577–86.
- Torii S, Yamamoto T, Tsuchiya Y, Nishida E. ERK MAP kinase in G cell cycle progression and cancer. *Cancer Sci.* 2006;
- Trendowski M, Yu G, Wong V, Acquafondata C, Christen T, Fondy TP. The real deal: Using cytochalasin B in sonodynamic therapy to preferentially damage leukemia cells. *Anticancer Res. International Institute of Anticancer Research*; 2014 May 1;34(5):2195–202.
- Turco E, Gallego LD, Schneider M, Köhler A. Monoubiquitination of histone H2B is intrinsic to the Bre1 RING domain-Rad6 interaction and augmented by a second Rad6-binding site on Bre1. *J. Biol. Chem. American Society for Biochemistry and Molecular Biology Inc.*; 2015 Feb 27;290(9):5298–310.
- Valencia-Sánchez MI, De Ioannes P, Wang M, Vasilyev N, Chen R, Nudler E, et al. Structural Basis of Dot1L Stimulation by Histone H2B Lysine 120 Ubiquitination. *Mol. Cell.* 2019 Jun 6;74(5):1010-1019.e6.
- van Vugt JJFA, Ranes M, Campsteijn C, Logie C. The ins and outs of ATP-dependent chromatin remodeling in budding yeast: Biophysical and proteomic perspectives . *Biochim. Biophys. Acta - Gene Struct. Expr. Biochim Biophys Acta*; 2007. p. 153–71.
- Wade AK, Liu Y, Bethea MM, Toren E, Tse HM, Hunter CS. LIM-domain transcription complexes interact with ring-finger ubiquitin ligases and thereby impact islet-cell function. *J. Biol. Chem.* . *American Society for Biochemistry and Molecular Biology Inc.*; 2019 Aug 2;294(31):11728–40.
- Walker S, Foster F, Wood A, Owens T, Brennan K, Streuli CH, et al. Oncogenic activation

- of FAK drives apoptosis suppression in a 3D-culture model of breast cancer initiation. *Oncotarget*. 2016 Oct 25;7(43):70336–52.
- Wang A, Ning Z, Lu C, Gao W, Liang J, Yan Q, et al. USP22 induces cisplatin resistance in lung adenocarcinoma by regulating γ H2AX-mediated DNA damage repair and Ku70/bax-mediated apoptosis. *Front. Pharmacol.* . Frontiers Research Foundation; 2017 May 17;8(MAY).
 - Wang E, Kawaoka S, Yu M, Shi J, Ni T, Yang W, et al. Histone H2B ubiquitin ligase RNF20 is required for MLL-rearranged leukemia. *Proc. Natl. Acad. Sci. U. S. A.* . *Proc Natl Acad Sci U S A*; 2013a Mar 5;110(10):3901–6.
 - Wang J, Xu B. Targeted therapeutic options and future perspectives for her2-positive breast cancer . *Signal Transduct. Target. Ther.* Springer Nature; 2019.
 - Wang L, Dent SYR. Functions of SAGA in development and disease . *Epigenomics.* Future Medicine Ltd.; 2014. p. 329–39.
 - Wang S, Huang J, Lyu H, Lee CK, Tan J, Wang J, et al. Functional cooperation of miR-125a, miR-125b, and miR-205 in entinostat-induced downregulation of erbB2/erbB3 and apoptosis in breast cancer cells. *Cell Death Dis.* *Cell Death Dis*; 2013b Mar;4(3).
 - Wang S, Zhong X, Wang C, Luo H, Lin L, Sun H, et al. USP22 positively modulates ER α action via its deubiquitinase activity in breast cancer. *Cell Death Differ.* Springer Nature; 2020a Nov 1;27(11):3131–45.
 - Wang Y, George SP, Srinivasan K, Patnaik S, Khurana S. Actin reorganization as the molecular basis for the regulation of apoptosis in gastrointestinal epithelial cells. *Cell Death Differ.* *Cell Death Differ*; 2012 Sep;19(9):1514–24.
 - Wang Y, Sun Q, Mu N, Sun X, Wang Y, Fan S, et al. The deubiquitinase USP22 regulates PD-L1 degradation in human cancer cells. *Cell Commun. Signal.* BioMed Central; 2020b Jul 14;18(1).
 - Wang Y, Yang L, Zhang X, Cui W, Liu Y, Sun Q, et al. Epigenetic regulation of ferroptosis by H2B monoubiquitination and p53. *EMBO Rep.* EMBO; 2019a Jul;20(7).
 - Wang Z, Sun L, Liang S, Liu Z chao, Zhao Z yi, Yang J, et al. GPER stabilizes F-actin cytoskeleton and activates TAZ via PLC β -PKC and Rho/ROCK-LIMK-Cofilin pathway. *Biochem. Biophys. Res. Commun.* . Elsevier B.V.; 2019b Aug 27;516(3):976–82.
 - Wang Z, Zhu L, Guo T, Wang Y, Yang J. Decreased H2B monoubiquitination and overexpression of ubiquitin-specific protease enzyme 22 in malignant colon carcinoma. *Hum. Pathol.* W.B. Saunders; 2015 Jul 1;46(7):1006–14.
 - Wegwitz F, Prokakis E, Pejkovska A, Kosinsky RL, Glatzel M, Pantel K, et al. The histone H2B ubiquitin ligase RNF40 is required for HER2-driven mammary tumorigenesis. *Cell Death Dis.* Springer Nature; 2020 Oct 1;11(10).
 - Whitesell L, Lindquist SL. HSP90 and the chaperoning of cancer. *Nat. Rev. Cancer* . 2005;5(10):761–72.
 - Winkler DD, Luger K. The histone chaperone FACT: Structural insights and mechanisms for nucleosome reorganization . *J. Biol. Chem.* *J Biol Chem*; 2011. p. 18369–74.
 - Wood A, Krogan NJ, Dover J, Schneider J, Heidt J, Boateng MA, et al. Bre1, an E3 ubiquitin ligase required for recruitment and substrate selection of Rad6 at a promoter. *Mol. Cell* . Cell Press; 2003 Jan 1;11(1):267–74.
 - Worden EJ, Hoffmann NA, Hicks CW, Wolberger C. Mechanism of Cross-talk between H2B Ubiquitination and H3 Methylation by Dot1L. *Cell* . Cell Press; 2019 Mar 7;176(6):1490-1501.e12.
 - Wortel IMN, van der Meer LT, Kilberg MS, van Leeuwen FN. Surviving Stress:

Modulation of ATF4-Mediated Stress Responses in Normal and Malignant Cells . Trends Endocrinol. Metab. Elsevier Inc.; 2017. p. 794–806.

- Wozniak GG, Strahl BD. Catalysis-dependent stabilization of Bre1 fine-tunes histone H2B ubiquitylation to regulate gene transcription. *Genes Dev.* Cold Spring Harbor Laboratory Press; 2014;28(15):1647–52.
- Wu CH, Yamaguchi Y, Benjamin LR, Horvat-Gordon M, Washinsky J, Enerly E, et al. NELF and DSIF cause promoter proximal pausing on the hsp70 promoter in Drosophila. *Genes Dev.* Cold Spring Harbor Laboratory Press; 2003 Jun 1;17(11):1402–14.
- Wu MY, Lin CY, Tseng HY, Hsu FM, Chen PY, Kao CF. H2B ubiquitylation and the histone chaperone Asf1 cooperatively mediate the formation and maintenance of heterochromatin silencing. *Nucleic Acids Res.* . Nucleic Acids Res; 2017a Aug 21;45(14):8225–38.
- Wu Z, Liu J, Zhang Q Di, Lv DK, Wu NF, Zhou JQ. Rad6-Bre1-mediated H2B ubiquitination regulates telomere replication by promoting telomere-end resection. *Nucleic Acids Res.* Oxford University Press; 2017b;45(6):3308–22.
- Wüst HM, Wegener A, Fröb F, Hartwig AC, Wegwitz F, Kari V, et al. Egr2-guided histone H2B monoubiquitination is required for peripheral nervous system myelination. *Nucleic Acids Res.* . NLM (Medline); 2020 Sep 18;48(16):8959–76.
- Xiao H, Tian Y, Yang Y, Hu F, Xie X, Mei J, et al. USP22 acts as an oncogene by regulating the stability of cyclooxygenase-2 in non-small cell lung cancer. *Biochem. Biophys. Res. Commun.* Academic Press Inc.; 2015 May 2;460(3):703–8.
- Xie W, Mieke M, Laufer S, Johnsen SA. The H2B ubiquitin-protein ligase RNF40 is required for somatic cell reprogramming. *Cell Death Dis.* Springer Nature; 2020 Apr;11(4).
- Xie W, Nagarajan S, Baumgart SJ, Kosinsky RL, Najafova Z, Kari V, et al. RNF40 regulates gene expression in an epigenetic context-dependent manner. *Genome Biol.* . BioMed Central Ltd.; 2017 Feb 16;18(1).
- Xie Y, Liu C, Qin Y, Chen J, Fang J. Knockdown of IRE1 α suppresses metastatic potential of colon cancer cells through inhibiting FN1-Src/FAK-GTPases signaling. *Int. J. Biochem. Cell Biol.* . Elsevier Ltd; 2019 Sep 1;114.
- Xiong H, Li B, He J, Zeng Y, Zhang Y, He F. lncRNA HULC promotes the growth of hepatocellular carcinoma cells via stabilizing COX-2 protein. *Biochem. Biophys. Res. Commun.* . Elsevier B.V.; 2017a Aug 26;490(3):693–9.
- Xiong H, Ni Z, He J, Jiang S, Li X, He J, et al. lncRNA HULC triggers autophagy via stabilizing Sirt1 and attenuates the chemosensitivity of HCC cells . *Oncogene.* Nature Publishing Group; 2017b. p. 3528–40.
- Xu G, Cai J, Wang L, Jiang L, Huang J, Hu R, et al. MicroRNA-30e-5p suppresses non-small cell lung cancer tumorigenesis by regulating USP22-mediated Sirt1/JAK/STAT3 signaling. *Exp. Cell Res.* Elsevier Inc.; 2018 Jan 15;362(2):268–78.
- Xu G, Jaffrey SR. The new landscape of protein ubiquitination. *Nat. Biotechnol.* Nat Biotechnol; 2011 Dec;29(12):1098–100.
- Xu L, Su L, Liu X. PKC δ regulates death receptor 5 expression induced by PS-341 through ATF4-ATF3/CHOP axis in human lung cancer cells. *Mol. Cancer Ther.* 2012a Oct;11(10):2174–82.
- Xu N, Lao Y, Zhang Y, Gillespie DA. Akt: A double-edged sword in cell proliferation and genome stability. *J. Oncol.* 2012b.
- Xu Z, Song Z, Li G, Tu H, Liu W, Liu Y, et al. H2B ubiquitination regulates meiotic

- recombination by promoting chromatin relaxation. *Nucleic Acids Res.* . Oxford University Press; 2016;44(20):9681–97.
- Yang Z, Yik JHN, Chen R, He N, Moon KJ, Ozato K, et al. Recruitment of P-TEFb for stimulation of transcriptional elongation by the bromodomain protein Brd4. *Mol. Cell . Mol Cell*; 2005 Aug 19;19(4):535–45.
 - Yap KL, Zhou MM. Structure and mechanisms of lysine methylation recognition by the chromodomain in gene transcription. *Biochemistry . Biochemistry*; 2011 Mar 29;50(12):1966–80.
 - Ye J, Kumanova M, Hart LS, Sloane K, Zhang H, De Panis DN, et al. The GCN2-ATF4 pathway is critical for tumour cell survival and proliferation in response to nutrient deprivation. *EMBO J. . EMBO J*; 2010 Jun 16;29(12):2082–96.
 - Yoneda T, Imaizumi K, Oono K, Yui D, Gomi F, Katayama T, et al. Activation of Caspase-12, an Endoplasmic Reticulum (ER) Resident Caspase, through Tumor Necrosis Factor Receptor-associated Factor 2-dependent Mechanism in Response to the ER Stress. *J. Biol. Chem. American Society for Biochemistry and Molecular Biology Inc.*; 2001 Apr 27;276(17):13935–40.
 - Yu L, Chen W, Tang Q, Ji KY. Micheliolide inhibits liver cancer cell growth via inducing apoptosis and perturbing actin cytoskeleton. *Cancer Manag. Res. Dove Medical Press Ltd*; 2019;11:9203–12.
 - Zacharopoulou N, Tsapara A, Kallergi G, Schmid E, Alkahtani S, Alarifi S, et al. The Epigenetic Factor KDM2B Regulates EMT and Small GTPases in Colon Tumor Cells. *Cell. Physiol. Biochem. . S. Karger AG*; 2018 Jun 1;47(1):368–77.
 - Zhang F, Yu X. WAC, a Functional Partner of RNF20/40, Regulates Histone H2B Ubiquitination and Gene Transcription. *Mol. Cell . Mol Cell*; 2011 Feb 18;41(4):384–97.
 - Zhang H, Han B, Lu H, Zhao Y, Chen X, Meng Q, et al. USP22 promotes resistance to EGFR-TKIs by preventing ubiquitination-mediated EGFR degradation in EGFR-mutant lung adenocarcinoma. *Cancer Lett. Elsevier Ireland Ltd*; 2018 Oct 1;433:186–98.
 - Zhang K, Wang J, Tong TR, Wu X, Nelson R, Yuan Y-CC, et al. Loss of H2B monoubiquitination is associated with poor-differentiation and enhanced malignancy of lung adenocarcinoma. *Int. J. Cancer. 2017 Aug 15*;141(4):766–77.
 - Zhang XY, Pfeiffer HK, Thorne AW, McMahan SB. USP22, an hSAGA subunit and potential cancer stem cell marker, reverses the polycomb-catalyzed ubiquitylation of histone H2A. *Cell Cycle . Taylor and Francis Inc.*; 2008 Jun 1;7(11):1522–4.
 - Zhang Y, Wang Y, Gao B, Sun Y, Cao L, Genardi SM, et al. USP22 controls iNKT immunity through MED1 suppression of histone H2A monoubiquitination. *J. Exp. Med. . Rockefeller University Press*; 2020 May 4;217(5).
 - Zhang Z, Shi L, Dawany N, Kelsen J, Petri MA, Sullivan KE. H3K4 tri-methylation breadth at transcription start sites impacts the transcriptome of systemic lupus erythematosus. *Clin. Epigenetics . Springer Verlag*; 2016 Feb 2;8(1):1–13.
 - Zhao Y, Lang G, Ito S, Bonnet J, Metzger E, Sawatsubashi S, et al. A TFTC/STAGA Module Mediates Histone H2A and H2B Deubiquitination, Coactivates Nuclear Receptors, and Counteracts Heterochromatin Silencing. *Mol. Cell . Cell Press*; 2008 Jan 18;29(1):92–101.
 - Zheng S, Li D, Lu Z, Liu G, Wang M, Xing P, et al. Bre1-dependent H2B ubiquitination promotes homologous recombination by stimulating histone eviction at DNA breaks. *Nucleic Acids Res. Oxford University Press*; 2018a;46(21):11326–39.
 - Zheng X, Chen K, Liu X, Pan Y, Liu H. High RNF40 expression indicates poor prognosis

of hepatocellular carcinoma. *Int. J. Clin. Exp. Pathol.* *Int J Clin Exp Pathol*; 2018b;11(5):2901–6.

- Zhou A, Lin K, Zhang S, Chen Y, Zhang N, Xue J, et al. Nuclear GSK3 β promotes tumorigenesis by phosphorylating KDM1A and inducing its deubiquitylation by USP22. *Nat. Cell Biol.* . Nature Publishing Group; 2016 Sep 1;18(9):954–66.
- Zhou J, Li J, Serafim RB, Ketchum S, Ferreira CG, Liu JC, et al. Human CHD1 is required for early DNA-damage signaling and is uniquely regulated by its N terminus. *Nucleic Acids Res.* Oxford University Press; 2018;46(8):3891–905.
- Zhou Q, Yik JHN. The Yin and Yang of P-TEFb regulation: implications for human immunodeficiency virus gene expression and global control of cell growth and differentiation. *Microbiol. Mol. Biol. Rev.* 2006 Sep 1;70(3):646–59.
- Zoghbi HY, Beaudet AL. Epigenetics and human disease. Cold Spring Harb. Perspect. Biol. . Cold Spring Harbor Laboratory Press; 2016 Feb 1;8(2):1–28.
- Zou W, Bai Y, Wang X, Cheng K, Sun H, Zhang G, et al. PERK-Phosphorylated eIF2 α Pathway Suppresses Tumor Metastasis Through Downregulating Expression of Programmed Death Ligand 1 and CXCL5 in Triple-Negative Breast Cancer. *Cancer Biother. Radiopharm.* . Mary Ann Liebert Inc.; 2017 Oct 1;32(8):282–7.

8. Referenced books


1. GENES, 8th edition, B. Lewin, 2004; Pearson Prentice Hall; 2004
2. Molecular Biology of the Cell 6th edition; Bruce Alberts, Alexander Johnson, Julian Lewis, David Morgan, Martin Raff, Keith Roberts, Peter Walter; Garland Science; 2015
3. Genetics, Histone Code; Zainab Shahid, Brittany Simpson, Kathleen H. Miao, Gurdeep Singh; 2020
4. Mukherjee, S. (2010), 6th edition; The emperor of all maladies: A biography of cancer. New York: Scribner.
5. Cytoskeleton-Structure, Dynamics, Function and Disease, Zhang, Xuan et al. 2017
6. Henry, D. (2018). Aristotle on Epigenesis: Two Senses of Epigenesis. In A. Falcon & D. Lefebvre (Eds.), *Aristotle's Generation of Animals: A Critical Guide* (Cambridge Critical Guides, pp. 89-107). Cambridge: Cambridge University Press. doi:10.1017/9781316459386.007

Acknowledgements

Being research-wise involved in the field of cancer and, generally, in life science, was not very far from my first wish as a kid, becoming a medical doctor. Nevertheless, I never regretted following Biology, even when I got an acceptance letter from the Heinrich-Heine Medical School of Düsseldorf, and that was proven later as a right choice for me. The years in college together with Garyfallia were peaceful, pleasant and without intensively thinking about my future steps, until I got this phone call from my parents, hearing that my beloved uncle (being my "second father") passed away from a long-standing stomach cancer at the age of 56. This sudden and heart-breaking moment, though, pushed me to rapidly finish all my duties with college and the military duties within 1.5 year and to apply for several Master Programs in Germany and the Netherlands for one single purpose: to understand cancer and help people that suffer from this malady.

The Master Program of Molecular Medicine was the only tempting choice and, actually, it is Matthias, the first person in Germany who first contacted me, interviewed me and brought me in Göttingen in 2015. Therefore, the least I can do is to deeply thank this brilliant person for helping me to fulfill my dreams, as well as constantly supporting me during the TAC meetings. Of course, it would have been a miss not to mention my experience with Matthias, easily commanding some ancient greek words like *apoptosis* using the right ancient punctuation system during his lectures and harnessing the Greek Mythology. Very importantly, I would like to thank him a lot for sharing any consumables or machines that were important for our work and providing us with the needed lab space during this last year. My impression is that not all people in his position would have been so prompt to help us in the way he did.

For the next person, that I want to express my deep gratitude, I will never be confident enough to find the right words. In September 2016, Florian welcomed me as a rotation student that was feeling insecure and with low self-confidence to even handle a pipette. Knowing that the proposed, at that time, project was extremely interesting and which turned to what you have read, I would say that any proposed project under Florian's supervision would have been the same amusing journey. Besides being a "Doktorvater" for me, Florian has been constantly a priceless companionship and due to his wisecracking sense of humor, his omnipresent good mood (at least 99% of the days in a year) in the lab environment, automatically makes him a must-have fellow in science. Possibly, one of the reasons I have to thank Florian is the fact that he showed me how to think in a scientific manner and how to objectively judge and make use of scientific findings, including mine. Most importantly, I think that Florian changed me in certain aspects as a person and truly treated me as good as a protective older brother of mine. Although I haven't even reached



half of the reasons to thank you, Florian, I just end this sentence by saying that it is a great luck knowing you.


The next person I should express my gratitude is to Steve, not only because he was the one involved in ensuring the financial coverage of my PhD position, but because he believed in my enthusiasm to pursue a PhD for such a promising project. Moreover, the frequently scheduled journal clubs and meetings, that were not discontinued even when he moved to US, were unique to get-to-know cutting-edge research through his eyes and his dexterous way of thinking. Although he moved from Göttingen in the middle of my PhD, I deeply appreciate the fact that in critical times he was always there when needed.

An important part of having a successful PhD is not only to prove yourself fruitful and make soon or later publications, but to be surrounded by great people that show their true face through understanding, courage and sharing altogether unforgettable moments. Iga, it would have been a miss not to mention you and thank you for all your kindness and the good times we shared together for 3 years next to each other. Also, I want to deeply thank you for being patient with my constant ups or downs during the hard times I have been through and, of course, for visiting me on Paros. You, Julia and Mati should always know that there is an open door for you there.

Ana, Xin, Milu and Zeynab, I don't know how my PhD would have been without you guys. Similar to Iga's case, a happy PhD is meant to be only with happy, joyful people surrounding you. Your solid and essential help in many parts during my PhD was priceless. Actually, I could not think that people from different corners of the globe with a different mentality and personality were able to complement each other so well. From the time we used to be minimum 15 people at least in the lab until we are finally only a handful of us now, it was one of the greatest lab experiences I can hardly see coming again in the future. Of course, you should know that my home in Greece is always open to you and I really wish we arrange a reunion in any site of the globe you want.

Furthermore, I would like to thank all past members of this super-international Johnsen Lab Group. Especially, I want to say special thanks to Feda-mou who is so good at singing old greek songs from 50s and 60s that even me cannot harness the lyrics as well as she does. I really miss her since she moved with Steve to US. I wish she becomes a successful and acknowledged scientist and a great Group Leader.

In addition, I want to express my gratitude to all of the rest co-authors that contributed to these two very exciting works with decisive translational impact. My special thanks to the lab rotation students of mine and Florian's: Anastasija, Regina, Sonja, Anna and Zahra. Finally, I want to thank all the co-authors which I personally never met such as Dr. Upasana Bedi, Prof. Harriet Wikman and Prof. Markus Glatzel.



Moreover, I would like to give special thanks to sci-hub website which literally removed all possible barriers to access to tons of published studies that were central to my work (<https://www.sci-hub.ren/>).

Finally, I would like to thank mine and Garyfallia's parents, her brother who is currently serving his military duty, as well as my brother and sister for being continuously "there", being encouraging all these years, standing by and cheering me up. Coming to the end and as a final "scene" of this work, I want to say that I am so blessed knowing Garyfallia since middle school, sharing all good and bad times with her through high school, college, my military service, my master and the PhD. It is such a rare thing to find your soulmate and I feel so lucky being part of her life.

Evangelos Prokakis, November 28th, 2020

Curriculum vitae

Full name: Evangelos Prokakis

Date of birth: 08 April 1991, Athens, Greece

Current residence address: Ludwig Prandtl Str. 54, 37077, Göttingen

e-mail: eprokak@gwdg.de

Tel.: +49 0 174 9739073

Skype: vaggos352

Education Background

04.2018-present

University Medical Center Göttingen, Georg-August-University of Göttingen (Göttingen, Germany)

Ph. D program: Molecular Medicine, Medical School of Göttingen, Georg-August University, Germany

Department of General-, Visceral- and Pediatric Surgery, Medical School of Göttingen, Georg-August University, Germany

Supervisor: Dr. rer. nat. Florian Wegwitz

10.2017-03.2018

University Medical Center Göttingen, Georg-August-University of Göttingen (Göttingen, Germany)

Scientific assistant, Department of General-, Visceral- and Pediatric Surgery, Medical School of Göttingen, Georg-August University

10.2015-08.2017

MSc Program: Molecular Medicine, Medical School of Göttingen, Georg-August University, Germany

Master Thesis: Department of General-, Visceral- and Pediatric Surgery, Medical School of Göttingen, Georg-August University, Germany (01.2017-07.2017)

Supervisor: Dr. rer. nat. Florian Wegwitz

09.2009-03.2015

**BSc in Biology, Faculty of Biology, School of Science, Aristotle University of
Thessaloniki, Greece**

BSc Thesis: Department of Genetics, Developmental and Molecular Biology

Research/Work Experience

10.2016-present

- Understanding the epigenetic basis of aggressive breast cancer, with major interest in the H2B monoubiquitination (H2Bub1) machinery in HER2-driven mammary carcinoma (HER2⁺-BC). (Medical School of Göttingen, Georg-August University, Germany)
 - Animal handling (certified by FELASA), mammosphere formation, Cell culture, functional cell-based assays, western blotting, RT-PCR, flow cytometry, immunohistochemistry, bright-field and fluorescence microscopy, DNA fiber assay, molecular cloning, analysis of publically-available RNA- and ChIP-seq data, RNA- and ChIP-library preparation and deep analysis of raw data

05.2016-06.2016

- Lab rotation on Molecular Pneumonology Lab (under the supervision of Dr. Muriel Lize). (Medical School of Göttingen, Georg-August University, Germany)
 - Animal handling and trachea dissection to study the role of microRNA-34 and -449 in cigarette-smoke- and naphthalene-induced Chronic obstructive pulmonary disease (COPD) in mice.
 - Western blotting, RT-PCR, immunofluorescence, immunohistochemistry

03.2014-12.2014

- 88th Military Brigade of the Greek Army, Laboratory of Microbiological Diagnostics, Greek Army, Lemnos, Greece
 - Blood, urine sampling from military personnel and molecular diagnostics

09.2013-01.2014

- Research on the role of Apolipoprotein A1 (ApoA1) and the viral core protein of Hepatitis C virus (HCV) in replication in hepatocellular carcinoma (HCC). (Department of Genetics, Molecular Biology and Biotechnology, Faculty of Biology, Aristotle University of Thessaloniki, Greece)

- Western blotting, bibliographic research

07.2013-08.2013

- Genotyping of high- and low-risk Human papillomavirus (HPV) strains. (Anti-Cancer Theageneio Hospital, Thessaloniki, Greece).
 - Large-scale HPV-genotype screening of cervix specimens from human patients

Research Interests

Tumor cells rely on dysregulated epigenetic mechanism predisposing them to cellular transformation, thereby leading to transcription programs which potentiate sustained proliferation, cell survival and metastasis. I am strongly interested in unravelling decisive epigenetic dependencies, and, particularly, in the role of global H2B monoubiquitination homeostasis governed by RNF40 (the writer) and USP22 (the eraser) in malignant types of breast cancer. Particularly, I am very intrigued, as well, by the non-epigenetic involvement of this factors in breast carcinogenesis.

Publications

- ❖ Wegwitz F[#], **Prokakis E[#]**, Pejkovska A, Kosinsky RL, Glatzel M, Pantel K, Wikman H, Johnsen SA. **The histone H2B ubiquitin ligase RNF40 is required for HER2-driven mammary tumorigenesis.** Cell Death Dis. 2020 Oct 17;11(10):873. doi: 10.1038/s41419-020-03081-w. PMID: 33070155; PMCID: PMC7568723.
- ❖ Kosinsky RL[#], Helms M, Zerche M, Wohn L, Dyas A, **Prokakis E**, Kazerouni ZB, Bedi U, Wegwitz F, Johnsen SA. **USP22-dependent HSP90AB1 expression promotes resistance to HSP90 inhibition in mammary and colorectal cancer.** Cell Death Dis. 2019 Dec 4;10(12):911. doi: 10.1038/s41419-019-2141-9. PMID: 31801945; PMCID: PMC6892875.
- ❖ Schneider D[#], Chua RL, Molitor N, Hamdan FH, Rettenmeier EM, **Prokakis E**, Mishra VK, Kari V, Wegwitz F, Johnsen SA, Kosinsky RL. **The E3 ubiquitin ligase RNF40 suppresses apoptosis in colorectal cancer cells.** Clin Epigenetics. 2019 Jul 2;11(1):98. doi: 10.1186/s13148-019-0698-x. PMID: 31266541; PMCID: PMC6604314.

1st (co)author